

**ASSESSING THE EFFICACY AND PROBABLE MOLECULAR
MECHANISM OF ONCOLYTIC MEASLES VIRUS-INDUCED CELL
DEATH IN CULTURED NASOPHARYNGEAL CARCINOMA CELLS**

By

LOOI HONG KEAT

A thesis submitted to the Department of Pre-Clinical Sciences,

M. Kandiah Faculty of Medicine and Health Sciences,

Universiti Tunku Abdul Rahman,

in partial fulfilment of the requirements for the degree of

Doctor of Philosophy (Medical Science)

May 2024

© 2024 Looi Hong Keat. All rights reserved.

This thesis is submitted in partial fulfilment of the requirements for the degree of Doctor of Philosophy (Medical Science) at Universiti Tunku Abdul Rahman (UTAR). This thesis represents the work of the author, except where due acknowledgment has been made in the text. No part of this thesis may be reproduced, stored, or transmitted in any form or by any means, whether electronic, mechanical, photocopying, recording, or otherwise, without the prior written permission of the author or UTAR, in accordance with UTAR's Intellectual Property Policy.

ABSTRACT

ASSESSING THE EFFICACY AND PROBABLE MOLECULAR MECHANISM OF ONCOLYTIC MEASLES VIRUS-INDUCED CELL DEATH IN CULTURED NASOPHARYNGEAL CARCINOMA CELLS

Looi Hong Keat

Nasopharyngeal carcinoma (NPC) is often diagnosed at advanced stages and radiotherapy, the existing first-line treatment for NPC, often results in diverse functional defects around the head and neck region. Oncolytic measles virus (oMV) has shown potential as a new and gentle cancer therapeutics. However, their efficacy against NPC has yet to be explored.

The present study aimed to assess the in-vitro efficacy of oMV in killing NPC with and without resistance to chemo- or radiotherapy and to elucidate the molecular mechanism involved in the oMV-induced cell killing. The infectivity and killing of NPC cells following infection with oMV were monitored by microscopy and quantitated by flow cytometry and cell viability assay. Differentially expressed peptides were quantitated using the iTRAQ-based assay.

All NPC cell lines tested expressed CD46 and were efficiently infected by oMV. Infected NPC cells form syncytium at 24-hours post-infection, and cell loss was prominent at 48-hours post-infection. Proteomic analysis revealed that infected cells did not undergo apoptotic nor necrotic cell death pathway. However, HMGB1 and Rab GTPase 11a were found to be increased. HMGB1

functions as a damage-associated molecular pattern molecule that reportedly led to tumour cell killing via immune cell-mediated immunogenic cell death. Interestingly, both HMGB1 and Rab11a, a key molecule in endocytic trafficking, were reportedly involved in autophagy-associated active release of HMGB1 via exosome.

Taken together, it is postulated that in this study, active release of HMGB1 could be mediated by autophagy induced by oMV infection, oMV-C, and -N proteins, leading to the formation of HMGB1-autophagy protein complexes followed by trafficking by Rab GTPases to host cell membrane, and consequently lead to extracellular release by exosome. Rab11a upregulation suggests that oMV-induced HMGB1 active release may involve Rab11a-dependant secretory pathway and HMGB1 plays can play a mediatory role in promoting autophagosome formation and enhances oMV-induced autophagic flux.

(295 words)

Keywords: oncolytic measles virus; nasopharyngeal carcinoma; oncolytic virotherapy; immunogenic cell death; measles-induced oncolysis

Subject Area: RZ409.7-999 Miscellaneous systems and treatments

ACKNOWLEDGEMENT

I want to take this opportunity to extend my heartfelt gratitude to Professor Dr Ngeow Yun Fong for her boundless generosity, invaluable and timely advice, and unwavering selflessness. Her proactive guidance has been instrumental in the successful completion of my seven-year-long doctoral journey. Without her mentorship and support, navigating the intricacies of my doctoral project would have been an immense challenge.

I am also thankful to my esteemed supervisor, Associate Professor Dr. Ong Hooi Tin, for her continuous support, insightful guidance, and meticulous reviews throughout my candidature.

In remembrance of my late friend, Mr. Chew Eng How, whose memory I hold dear, and Dr. Kuan Chee Sian, whose wisdom continues to inspire me, I am reminded of their pivotal roles in influencing my decision to pursue a doctoral degree. Their generosity in sharing knowledge and providing unwavering inspiration has equipped me with the essential resources to navigate complex scientific challenges and delve into in-depth technicalities during my doctoral studies.

I extend my special thanks to Associate Professor Dr. Chang Li-Yen and Associate Professor Kiew Lik Voon from Universiti Malaya for their invaluable guidance, meticulous reviews, and advice during the process of crafting our project and publication manuscripts. Additionally, I am deeply appreciative of the insights and troubleshooting advice provided by Dr. Lin Qingsong and Mr. Lim Teck Kwang from the Singapore Mass Spectrometry Lab (SingMass),

which greatly contributed to refining the iTRAQ proteomics methodology central to my research. This study was supported by the Malaysian Ministry of Higher Education under the Fundamental Research Grant Scheme programme and minor funding by the National Cancer Council (MAKNA).

Lastly, I extend my heartfelt appreciation to Professor Dr Ngeow Yun Fong, Ms Shirley Liew, the late Mr Sunny Chow, Mr Jimmy Shio, Mr Chow Yeng Keet, and my family members for their unwavering support and encouragement. Beyond my immediate family, their benevolence, steadfast support, and motivational presence have been my pillars of strength throughout this seven-year journey of perseverance and growth.

DECLARATION

I, LOOI HONG KEAT, hereby declare that the thesis is based on my original work except for quotations and citations which have been duly acknowledged. I also declare that it has not been previously or concurrently submitted for any other degree at UTAR or any other institution.

LOOI HONG KEAT

Date: 17th May 2024

TABLE OF CONTENTS

	Page
ABSTRACT	iii
ACKNOWLEDGEMENT	v
DECLARATION	vii
TABLE OF CONTENTS	viii
LIST OF TABLES	xii
LIST OF FIGURES	xiv
LIST OF ABBREVIATIONS	xvii
CHAPTER	
1.0 INTRODUCTION	1
2.0 LITERATURE REVIEW	6
2.1 Epidemiology of NPC	6
2.2 Risk factors of NPC	11
2.3 Clinical management of NPC	12
2.4 Post-chemotherapy and -radiotherapy outcome	13
2.5 Oncolytic measles virus as onco-therapeutics	16
2.5.1 Safety and development of oncolytic measles virus	17
2.5.2 Onco-selectivity for cell infection by oncolytic measles virus	19
2.5.3 Measles virus cytopathic effect as naturally efficient means of infection and lateral viral dissemination	21
2.5.4 Oncolytic measles virus in clinical trials	22
2.5.5 Potential application of oncolytic measles virus in NPC	24
2.6 Cell death pathways induced by cancer therapies	26

2.7	iTRAQ quantitative proteomics for the understanding of cell death induced by the oncolytic measles virus	32
2.8	Bioinformatics analysis for better understanding of protein-to-protein interaction	35
3.0	MATERIALS AND METHODOLOGY	37
3.1	Overview of methodology	37
3.2	Establishing radio- and chemo-resistant NPC cell line	39
3.2.1	Cell viability assay and cell density optimization	41
3.2.1.1	Cell density optimization	41
3.2.1.2	Evaluation of initial inhibitory concentration for cisplatin treatment	42
3.2.1.3	Assessing cell resistance to gamma-irradiation treatment	43
3.2.1.4	Assessing cell resistance to cisplatin treatment	44
3.2.2	Establishment of chemo- and radio-resistant NPC cell line	45
3.3	Upscaling and titration of oncolytic measles virus stock	46
3.3.1	Measles-GFP-NIS propagation	46
3.3.2	Viral titration with Reed-Muench algorithm	48
3.4	NPC cells infection studies	49
3.4.1	Expression of oncolytic measles virus attachment protein	49
3.4.2	Infection efficacy study	50
3.4.3	Monitoring syncytia spread and efficacy of cell killing in NPCs	51
3.5	iTRAQ quantitative proteomics with bioinformatics analysis	52
3.5.1	C666-1 cell infection and protein extraction	52
3.5.2	Protein quantitation	52
3.5.3	Protein preparation and iTRAQ labelling	52
3.5.4	Protein identification, relative quantitation, and bioinformatics analysis	54

4.0	RESULTS AND DISCUSSION	57
4.1	Part 1: Evaluation of oncolytic measles virus infectivity in untreated, CR-, and RR-NPC	57
4.1.1	NPC cell lines exhibiting more than 2-fold resistance to radiation and cisplatin cytotoxicity are considered resistant cell lines	57
4.1.2	Measles-GFP-NIS infects all NPC cell lines tested and was not affected by acquired resistance to cisplatin or gamma-radiation	59
4.1.3	Measles-GFP-NIS effectively spread horizontally <i>in vitro</i> , and shrinkage of infected bodies were observed at 60 hours post-infection	65
4.1.4	Conclusion	79
4.2	Part 2: Evaluation of cell death mechanism induced by Measles-GFP-NIS in NPC cell model	80
4.2.1	164 genes identified with PeptideShaker tools were differentially regulated throughout 24-, 36-, and 48-hours post-infection	80
4.2.2	Gene Ontology (GO): cell death-associated DAPs downregulated at 24-hours p.i. but were both up- and downregulated at 48-hours p.i.	82
4.2.3	KEGG: pathways not related to regulated cell death were differentially regulated at 48-hours p.i.	86
4.2.4	DAP matches protein complexes with protein production and metabolism function	87
4.2.5	Review of possible anti-cancer effect induced by oncolytic measles virus	93
4.2.5.1	Recent research publication shows that measles virus does not cause direct death of infected cells	94
4.2.5.2	Indirect tumour cell clearance or killing after oMV infection	95
4.2.5.3	Possible mode of active extracellular release of HMGB1 from C666-1 cells infected with Measles-GFP-NIS	102
4.2.6	Conclusion	105

5.0 CONCLUSION	107
5.1 Conclusion	107
5.2 Limitation of study	109
5.3 Future studies	110
REFERENCES	113
APPENDICES	131

LIST OF TABLES

Table	Page
3.1 Details and description of cell lines used in this study.	40
3.2 iTRAQ labelling details for quantitative proteomics study	53
3.3 Liquid chromatography parameters for iTRAQ-tagged peptide sample separation.	54
3.4 Mass spectrometry parameters for iTRAQ-tagged peptide ionization and peptide sequencing.	54
4.1 All NPC cell line treated with repeated cycles of cisplatin treatment exhibit \geq 2-fold change of resistance towards cisplatin.	59
4.2 GO Biological Processes annotation of downregulated and upregulated genes at (A) 24-hours, (B) 36-hours, and (C) 48-hours post-infection.	82
4.3 Different DAPs related to cell death processes were (A) upregulated and (B) downregulated at 48-hours post-infection.	85
4.4 KEGG analysis showing that pathways related to cellular metabolism and biosynthesis but not regulated cell death were (A) upregulated and (B) downregulated at 48-hours post-infection.	87
4.5 Upregulated DAP MCODE clusters validated with CORUM database.	90

4.6	Downregulated DAP MCODE cluster validated with CORUM database.	92
4.7	Relative abundance of HMGB1 and XPO1 proteins in two biological replicates (R1 and R2).	101
4.8	Only Rab11a protein shows upregulation at 24- and 36- hour post-infection.	104

LIST OF FIGURES

Figure		Page
1.1	A comprehensive summary of oncolytic viruses of current research interest alongside advantages and disadvantages in the clinical application (Lin et al., 2023).	2
2.1	Southeast Asia countries are the top 8 countries with the highest reported NPC incidences, both sexes, out of 185 countries worldwide (Ferlay et al., 2024).	7
2.2	Malaysia and other Southeast Asia countries reported high WASR, indicating a concerning high risk of NPC among 185 countries that reported more than 1,000 cases of NPC in 2022 (Ferlay et al., 2024).	8
2.3	Lineage map of oncolytic measles virus developed by Russell and co-workers (Myers et al., 2007).	18
2.4	(A) Recommended nomenclature by Nomenclature Committee on Cell Death (NCCD) and (B) common classification of regulated cell death mechanisms used to define various cell death events (Galluzzi et al., 2018; Yan et al., 2020).	28
2.5	The difference in isotopic mass in reporter group of each iTRAQ 8-plex tags allows identification and quantification of protein sample (Pierce et al., 2008).	34
3.1	Overview of study methodology.	38

4.1	Only CNE-2 and C666-1 cells were resistant to gamma-radiation after completing a cumulative dose of 60-Gy and were considered radio-resistant (RR) NPCs.	58
4.2	CD46 were consistently expressed on untreated, chemo- and radio-resistant NPC cells.	60
4.3	Representative images showing infected (A) CNE-1, (B) CNE-2, (C) C666-1, and (D) HONE-1 cells expressing GFP observed under fluorescence microscope at 100x magnification.	63
4.4	CR- and RR-NPC showed a higher percentage of GFP-positive cells counted with FACS Canto II flow cytometer, suggesting treated cells are more susceptible to Measles-GFP-NIS infection.	64
4.5	The spread of Measles-GFP-NIS infection throughout NPC cells between 36-hours p.i and 60-hours p.i., followed by shrinkage of infected bodies observable at the 60-hours timepoint (Figure 4.6) shows a successful oncolytic event.	75
4.6	Representative fluorescence images showing typical shrinkage of cellular bodies (black arrowhead) in infected (A) CNE-2 and (B) C666-1 observed prominently at 60-hour post-infection.	77
4.7	CR- and RR-NPC cells exhibit a notable increase in the proportion of dead cells following MV-GFP-NIS	78

	infection compared to untreated cells, indicating enhanced susceptibility to infection-induced cell death.	
4.8	Low overlapping of DAPs between two biological replicates (R1 and R2) at 24-, 36-, and 48-hours post-infection.	81
4.9	Upregulated DAPs cluster identified with MCODE cut-off score ≥ 6.0 .	89
4.1	Downregulated DAPs cluster identified with MCODE cut-off score ≥ 6.0 .	91
4.11	Illustration summarizing hypothetical molecular pathway involving Measles-GFP-NIS infection from inducing nuclear-to-cytoplasm translocation of HMGB1 to autophagy-dependent active release of HMGB1 via extracellular vesicle.	106

LIST OF ABBREVIATIONS

AJCC	American Joint Committee on Cancer
Atg12	Autophagy related 12 protein
Atg14	Autophagy related 14 protein
Atg5	Autophagy related 5 protein
Atg7	Autophagy related 7 protein
ATP	adenosine triphosphate
BCA	bicinchoninic acid
BSA	bovine serum albumin
CD150/SLAM	Signalling Lymphocyte Activation Molecule
CD21/CR2	Complement Receptor 2 protein
CD46	cluster of differentiation 46 also known as Membrane Cofactor Protein
CORUM	the comprehensive resource of mammalian protein complexes database
DAP	differentially abundance protein
DEG	differentially expressed gene
DMSO	dimethyl sulfoxide
EBV	Epstein-Barr virus
eGFP	enhanced green fluorescence protein
ESCRT	endosomal sorting complexes required for transport
FIP	fusion inhibitory peptide
FunCat	Functional Catalogue
GAPDH	glyceraldehyde 3-phosphate dehydrogenase gene

GFP	green fluorescence protein
GO	Gene Ontology annotation database
Gorasp2	golgi reassembly stacking protein 2
GTPase	guanidine triphosphate hydrolase enzyme
Gy	Gray, unit of dosage for radioactive radiation for radiotherapy
HMGB1	high mobility group box 1
IARC	International Agency for Research on Cancer
ICD	immunogenic cell death
IM	infectious mononucleosis
IMRT	intensity modulated radiotherapy
IRGM	Immunity Related GTPase M
iTRAQ	isobaric Tags for Relative and Absolute Quantitation
KEGG	Kyoto Encyclopedia of Genes and Genomes
LMP1	EBV's Latent Membrane Protein-1 gene
MAPK	mitogen-activated protein kinase
MCODE	Molecular Complex Detection algorithm
Measles-GFP-NIS	genetically modified vaccine strain measles virus of Edmonston lineage (MV-Edm) possessing green fluorescence protein and sodium iodide symporter gene
MTT	methylthiazol tetrazolium
MV-Edm	Edmonston lineage of vaccine strain measles virus
NIS	sodium iodide symporter
NMHC-IIA	non-muscle myosin heavy chain IIA
NPC	nasopharyngeal carcinoma

oMV	oncolytic Measles virus or genetically modified vaccine strain measles virus of Edmonston lineage (MV-Edm)
p.i.	post-infection
PI3K	phosphatidylinositol 3-kinase
Rab27a	Ras-related protein Rab-27A
Rab8a	Ras-Related Protein Rab-8A
RAS	family of oncogenes encoding GDP/GTP-binding protein
RIPK1	receptor-interacting protein kinase 1
RNP	ribonucleoprotein
ROS	reactive oxygen species
SCX	strong cation exchange
TP53	tumour protein p53
U87MG	glioblastoma cell line
WASR	Worldwide age-standardized rate
WHO	World Health Organization
XPO1	Exportin 1
IC ₅₀	inhibitory concentration at 50 % of cell population
TCID ₅₀	50% tissue culture infectious dose


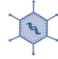






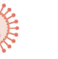

CHAPTER 1

INTRODUCTION

Oncolytic viruses (OV) demonstrated tumour-selective anti-cancer capability with tolerable and resolvable side effects, unlike chemo- and radiotherapy which give rise to long-lasting side effects and do not promise full recovery (Cao et al., 2020). Since the earliest record of oncolytic capacity exhibited by wild-type influenza virus in causing remission of leukaemia, eight human pathogenic viruses (Herpes-, Adeno-, Vaccinia, Reo-, Coxsackie-, Polio, Measles, and Vesicular stomatitis virus) and apathogenic viruses (Seneca valley and Newcastle disease virus) had been genetically modified to enhanced potency against cancer cells while ensuring apathogenicity in the human host (Lin et al., 2023). The safety and applicability of oncolytic viruses have been tested in clinical trials on various tumours, such as glioblastoma, hepatocarcinoma, melanoma, glioma, and pancreatic adenocarcinoma, breast cancer, colorectal cancers, leukaemia and many more (Cao et al., 2020; Lin et al., 2023). Four oncolytic virus products were clinically approved for selected cancer treatment, namely Rigvir (picornavirus), Oncorine (adenovirus), T-VEC (herpesvirus) and DELYTACT (herpesvirus) for treatment of melanoma, head and neck cancer, metastatic melanoma, and malignant glioma and primary brain cancer, respectively (Rahman and McFadden, 2021).

Lin and co-workers reviewed and discussed in detail promising oncolytic viruses that are of clinical interest (Figure 1.1). Herpesvirus and Adenoviruses were the most extensively studied due to the viral capacity to accept large fragments or several smaller fragments of transgene in the former and the ease of producing high titres of recombinant viral progenies in the latter

(Lin et al., 2023). Both OV_s also produce the most complete responses (Herpesvirus: 64 and Adenovirus: 34) among all the oncolytic viruses of interest (Macedo et al., 2020). Despite the high success rate, clinical trials utilizing oncolytic herpesviruses are mostly limited to melanoma (436 out of a total of 1,000 melanoma patients), primarily due to the ease of patient recruitment and treatment administration via the intra-tumoral route (Macedo et al., 2020). Oncolytic adenoviruses have been evaluated in wider ranges of solid tumours, including glioblastoma, head and neck carcinoma, colorectal, prostate, ovarian and melanoma; but most trials were done via intra-tumoral administration (Mantwill et al., 2021). Intra-tumoral administration (78 patients) of OV yields the most complete responses compared to the intravenous route (7 patients), highlighting that the success and efficacy of currently most successful OV_s are subject to limited to intra-tumoral accessible cancers (Macedo et al., 2020).

	Herpesvirus	Adenovirus	Vaccinia virus	Reovirus	Coxsackievirus	Seneca Valley virus	Poliovirus	Measles virus	Newcastle disease virus	Vesicular stomatitis virus
Model										
Genome	dsDNA 150 kb	dsDNA 36 kb	dsDNA 190 kb	dsRNA123 kb	ss(+)RNA 28 kb	ss(+)RNA 7 kb	ss(-)RNA 7.5 kb	ss(-)RNA 16 kb	ss(-)RNA 15 kb	ss(-)RNA 11 kb
Capsid symmetry	Icosahedral	Icosahedral	Complex	Icosahedral	Icosahedral	Icosahedral	Icosahedral	Icosahedral	Helical	Helical
Virion	Enveloped	Naked	Complex coats	Naked	Naked	Naked	Naked	Enveloped	Enveloped	Enveloped
Replication site	Nucleus and cytoplasm	Nucleus and cytoplasm	Cytoplasm	Cytoplasm	Cytoplasm	Cytoplasm	Cytoplasm	Cytoplasm	Cytoplasm	Cytoplasm
Methods of entry	HVEM, nectin-1, nectin 2	CAR, CD46	Receptor-mediated endocytosis	JAM-A	CAR/ICAM1/DAF	Endocytosis	CD155	SLAM, CD46	Sialic acid	LDLR
Blood-brain barrier penetration	-	-	-	+	-	+	+	-	+	-
Advantages	Large genome to insert large fragments and multiple transgenes; drug to shut-off	Feasibility of manufacturing; high viral titers; ease of genome manipulation; inherently potent lytic activity	Fast, efficient spreading virus; high-speed life cycle; up to 40kd large gene fragment insertion; enough knowledge due to smallpox	Good adaptability for intravenous injection; displaying no dose-limiting toxicity	Good adaptability for intravenous injection	Nonpathogenic in human	Clinical trial experience	Clinical trial experience	Nonpathogenic in human	High-speed life cycle; nonpathogenic in human
Disadvantages	Pathogenicity; ubiquitous nAbs	Extensive tissue tropism	Pathogenicity	Rarely gene-editing	Pathogenicity; ubiquitous nAbs	Clinical trials were not entirely satisfactory	Highly pathogenic in neurons of the human	Pathogenicity	Rarely gene-editing	Clinical trials were not entirely satisfactory; rarely gene-editing

dsDNA double-stranded DNA, dsRNA double-stranded RNA, ssRNA single-stranded RNA, HVEM herpesvirus entry mediator, CAR coxsackie adenovirus receptor, JAM-A junctional adhesion molecule A, ICAM1 intercellular adhesion molecule 1, DAF decay-accelerating factor, SLAM signaling lymphocytic activation molecule, LDLR low-density lipoprotein receptor, nAbs neutralizing antibodies

Figure 1.1: A comprehensive summary of oncolytic viruses of current research interest alongside advantages and disadvantages in the clinical application (Lin et al., 2023).

Clinical utility of oMV has been demonstrated in a handful of clinical trials to treat ovarian cancer, mesothelioma, glioblastoma multiforme, breast cancer, nerve sheath tumour, bladder, and head and neck cancers, although not as extensively studied as oncolytic herpes- and adenoviruses (Engeland and Ungerechts, 2021). oMV had demonstrated a high degree of versatility compared to other oncolytic viruses, owing primarily to its natural tropism to two constitutively expressed proteins, CD46 and CD150, and secondly to genetical recombination with human sodium iodide symporter gene that functions to uptake and accumulate radio-iodide in infected tumour cells (Russell et al., 2014; Engeland and Ungerechts, 2021). CD150 (also known as Signalling Lymphocytic Activation Molecule or SLAM) and CD46 are specifically and constitutively expressed in lymphocytic and non-lymphocytic nucleated human cells, respectively (Engeland and Ungerechts, 2021).

The natural tropism towards CD46 and CD150 allows oMV to theoretically target any solid and selected population of haematological tumours as long as both surface proteins are not abrogated or downregulated in the process of carcinogenesis. CD46 is known to be upregulated in solid tumours as a deterrent to avoid attack by complement and CD150 expression has been reported in cutaneous T-cell lymphoma and B-cell malignancies (M Elvington et al., 2020; Gordiienko et al., 2019). A third cell surface protein that oMV can utilize for infection, nectin-4, is an adherent junction protein of lung epithelial cells (Mühlebach et al., 2011). Unlike CD46 and CD150, nectin-4 is only expressed in gastrointestinal, skin, urogenital, and lymphoid organs, but the expression seems to be maintained or upregulated throughout carcinogenesis into respective malignant counterparts (Bouleftour et al., 2022).

This means oMV do not require additional scientific effort and cost for genetic modification to adapt and “re-target” the viruses towards selected tumours based on tumour-specific cell surface proteins that other oncolytic viruses require to achieve oncostelectivity (Lin et al., 2023). The constant improvement over the years made the oncolytic measles virus (oMV) one of the promising therapeutic candidates capable of targeting both solid and hematologic tumours, through oMV’s natural tropism to haematocyte-specific CD150, while least affected by existing anti-measles immunity among patients who were recipient of measles vaccine (Muñoz-Aliá et al., 2021; Engeland and Ungerechts, 2021). Clinical trials demonstrated that oMV successfully target and resolve multiple myeloma localized at difficult-to-reach region in the brain (Engeland and Ungerechts, 2021; Russell et al., 2014). Therefore, oMV could be a suitable therapeutic candidate that can target and kill a broad spectrum of tumours with minimal anatomical restriction.

Nasopharyngeal carcinoma (NPC) is the fifth most common cancer among Malaysians as reported between year 2012 to 2016 (A. Azizah et al., 2019). It is often diagnosed late due to the anatomically sheltered location of the nasopharynx (Ren et al., 2017; A. Azizah et al., 2019). It is more prevalent in the Chinese population which makes up one of the major ethnic groups in Asian countries (Mak et al., 2015; Wei et al., 2017; Chiang et al., 2016; MahdaviFar et al., 2016; A. Azizah et al., 2019). Mainstream treatment for all stages of NPC involves either standalone or a combination of chemo- and radiotherapy which often causes various forms of long-lasting therapeutic toxicities and side effects resulting from off-target damages to the nervous system, delicate muscle skeletal structures and organs in the proximity of the

nasopharyngeal site (Ministry of Health Malaysia, 2016; McDowell et al., 2020). Moreover, existing surgical intervention is highly invasive and difficult to perform because of the restrictive spaces accessing the nasopharynx from the nasal or buccal cavity (Xi Ding et al., 2021). A less damaging cancer treatment is desirable, and the oncolytic measles virus could be an ideal vector for NPC treatment.

To date, oMV has not been tested in NPC cells. Moreover, the exact mechanism of oncolytic measles cell killing had not been extensively studied and recent findings suggested the involvement of the non-apoptotic pathway instead of the widely accepted apoptotic pathway (M. Xia et al., 2014; Zhao et al., 2013; Rudak et al., 2021). Therefore, this study's main objective is to determine the overall *in vitro* effectiveness of oMV in treating NPC cells using a quantitative global proteomics pipeline. To achieve this, the research focuses on specific objectives: firstly, to evaluate the capacity of oMV to induce cell death in nasopharyngeal carcinoma cells cultured; secondly, to analyse their efficacy in inducing cell death in the context of radio-resistant and chemo-resistant NPC; thirdly, to investigate the virus-induced alterations in protein expression resulting in cell death; and finally, to elucidate the underlying mechanisms of cell death in virus-infected cells using proteomic analysis. By addressing these specific objectives, this study seeks to enhance our understanding of the potential therapeutic mechanisms of oMV in treating NPC.

CHAPTER 2

LITERATURE REVIEW

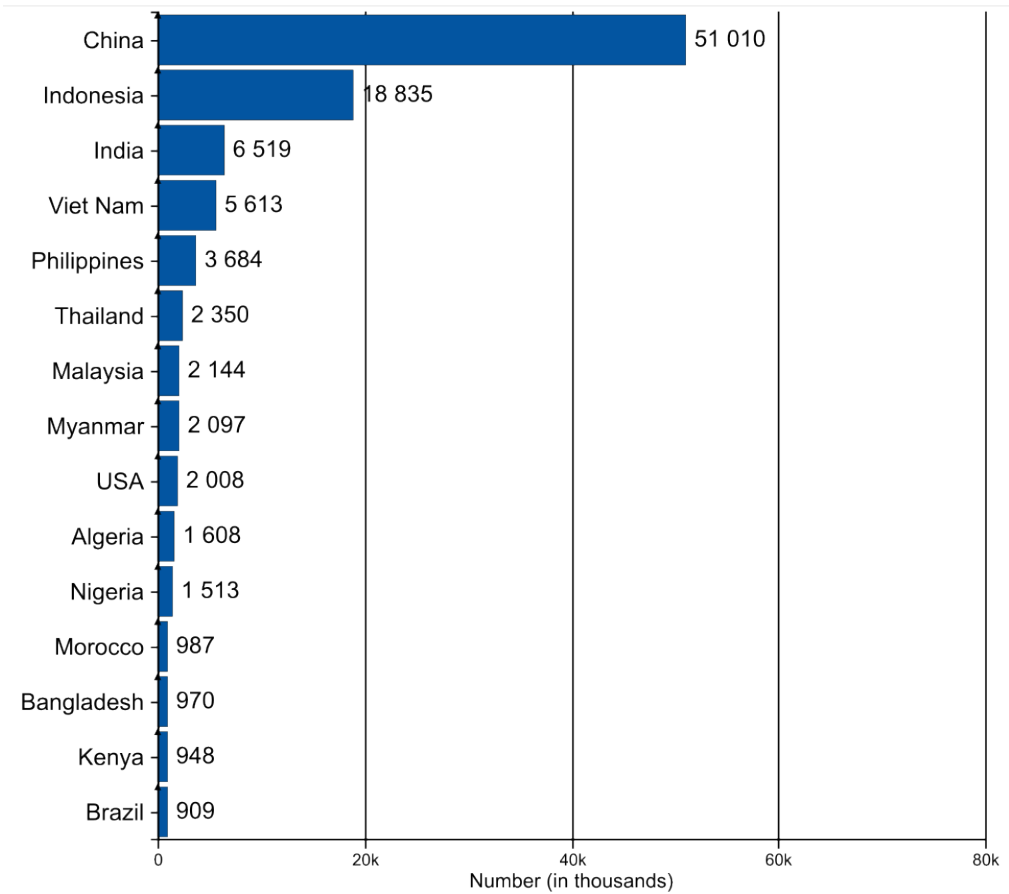
2.1 Epidemiology of NPC

NPC is the predominant tumour diagnosed in patients with cancer of the nasopharynx, constituting about 90% of reported cases worldwide (Lee et al., 2016; Perez et al., 1969; Chang and Adami, 2006). According to the latest epidemiology data from Global Cancer Observatory (GLOBOCAN) collected for the year 2022 by the International Agency for Research on Cancer (IARC) from 185 countries, China, the country with the largest Chinese population, contributed to the highest number, 51,010, of NPC cases (both sexes), followed by Indonesia (18,835), India (6,519), Vietnam (5,613), Philippines (3,684), Thailand (2,350), Malaysia (2,144), and Myanmar (2,097), United States of America (2,008), and Algeria (1,608) at the tenth place among the Top 10 countries with highest reported NPC incidences (Figure 2.1) (Ferlay et al., 2024).

Absolute numbers, Incidence, Both sexes, in 2022

Nasopharynx

Countries (Top 15)



Cancer TODAY | IARC- <https://gco.iarc.who.int/today>

Data version :Globocan 2022

© All Rights Reserved 2024

Figure 2.1: Southeast Asia countries are the top 8 countries with the highest reported NPC incidences, both sexes, out of 185 countries worldwide (Ferlay et al., 2024).

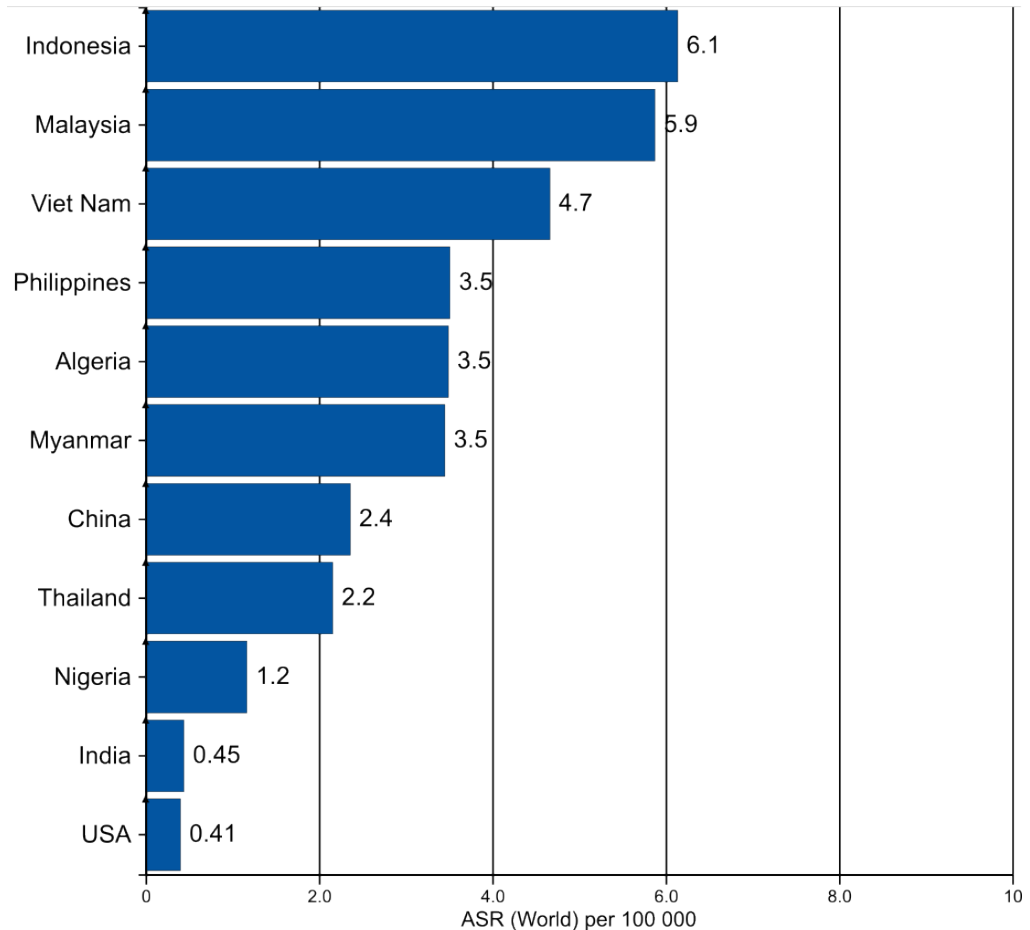
Despite the high reported incidences, the worldwide age-standardized rate (WASR) of NPC in China was relatively low, at 2.4 per 100,000 population (Figure 2.2). Looking at countries with more than 1,000 reported incidences of NPC, Indonesia (6.1), Malaysia (5.9), and Vietnam (4.7) were the top three countries with relatively high WASR. Philippines (3.5), Algeria (3.5) and Myanmar (3.5) were relatively moderate, though still higher than China (2.4),

Thailand (2.2) and Nigeria (1.2). Lastly, India (0.45) and the United States of America (0.41) were the lowest.

Age-Standardized Rate (World) per 100 000, Incidence, Both sexes, in 2022

Nasopharynx

Algeria - Myanmar - China - India - Indonesia - Malaysia - Nigeria - Philippines - Viet Nam - Thailand - United States of America



Cancer TODAY | IARC- <https://gco.iarc.who.int/today>

Data version :Globocan 2022

© All Rights Reserved 2024

Figure 2.2: Malaysia and other Southeast Asia countries reported high WASR, indicating a concerning high risk of NPC among 185 countries that reported more than 1,000 cases of NPC in 2022 (Ferlay et al., 2024).

NPC had unequal prevalence distribution across geographical regions. In China, despite constituting mainly of Chinese population, the southern region reported higher incidences of NPC (Wong et al., 2021; Tian et al., 2020). In other countries, NPC affects different ethnicities in different proportions and

has shown uneven geographical distribution as well. To date, only a limited number of epidemiological studies have been performed in Southeast Asia countries and India, mostly dating back to before 2010 with some in the 1990s. Natives in Indonesia, the Philippines, and Thailand have reportedly higher incidences of NPC than pure Chinese or Chinese-descent populations (Sarmiento and Mejia, 2014; West et al., 1993; Ekburanawat et al., 2010; Adham et al., 2012). In Indonesia, a study on 1,173 NPC patient data collected from 2007 to 2011 showed that Javanese (32 %) has a 2.9 times higher incidence than Chinese (11 %) and was the major ethnic among natives affected by NPC, followed by Sudanese (19 %), Batak (10 %), Betawi (8 %), Lampung (3 %), and lastly Minangkabau (2 %) (Adham et al., 2012). Less than 10 % of NPC patients were Chinese in the Philippines (7.3 %, N=104) and Thailand (5.5 %, N=327) (Ekburanawat et al., 2010; West et al., 1993). No epidemiological study on NPC in Vietnam could be found on PubMed or online repositories. In India, NPC reportedly had a higher prevalence among natives, the Mongoloid population, in the northeast India region (Roy Chattopadhyay et al., 2017). A sub-tribe of the Naga tribe known as the Tangkhul tribe had the highest incidences of NPC within the Manipur state (Kataki et al., 2011; Roy Chattopadhyay et al., 2017).

In Malaysia, the Chinese population throughout the country and natives of East Malaysia, the Bidayuh and Iban tribes, were reported to have high incidences of NPC (Wong et al., 2023; Linton et al., 2021; Yeo et al., 2018; A. M. Azizah et al., 2019). NPC is reportedly affecting males two to three times more than females (Tan et al., 2018; Xie et al., 2013). Malaysian males were three times more likely than females (ASR 6.4 in males versus 2.2 in females,

per 100,000 population) to get NPC and Chinese males have the highest ASR (11.0 per 100,000 population) compared to the males of Malay (3.3 per 100,000 population), Indian (1.1 per 100,000 population) and other ethnicities (9.9 per 100,000 population).

According to the World Health Organization's (WHO) Classification of head and neck tumours, NPC is classified into three histopathology categories of squamous cell carcinoma, as follows (El-Naggar et al., 2017; Wei et al., 2011; Wang et al., 2013; Rueda Domínguez et al., 2022):

WHO Grade 1: keratinizing

WHO Grade 2: non-keratinizing differentiated

WHO Grade 3: non-keratinizing undifferentiated

Not graded: Basaloid

Non-keratinizing NPC, especially the undifferentiated subtype, is predominant in areas with moderate to high NPC incidence while keratinizing NPC is more prevalent in areas with low NPC incidence (Chang et al., 2021; Wei et al., 2011). Basaloid NPC, not graded by WHO, is very rare and is described in available literature as poorly differentiated (80.4%) and undifferentiated (11.8%) neoplasms (Unsal et al., 2019; Rueda Domínguez et al., 2022). For these morphologically variable neoplasms, WHO histologic grading had not been useful for predicting prognosis (Wang et al., 2016). To date, the prognosis and treatment of NPC are based on tumour, node, and metastasis (TNM) staging guidelines proposed by the American Joint Committee on Cancer (AJCC) (Farias et al., 2003; Bossi et al., 2021; Wang and Kang, 2021; Chen et al., 2021). NPC accounts for about 70 % of malignancies at the nasopharynx, 20 %

lymphomas, and the remainder 10 % as other types of tumours of the nasopharynx (Stoffey, 2012).

Non-keratinizing NPC has been highly correlated to EBV infection (Tsao et al., 2017; Anon, 2016b). In contrast, keratinizing NPC is not associated with EBV but is correlated with smoking (Anon, 2016a; Rueda Domínguez et al., 2022). Non-keratinizing NPC accounts for about 80 % of all reported NPC cases while keratinizing NPC accounts for most of the remainder 20 % (Lee et al., 2012).

2.2 Risk factors of NPC

Historically, the aetiology of NPC is mainly attributed to smoking or the intake of carcinogens via the intake of salt-preserved food (Tsang et al., 2019). In the past decade, molecular evidence revealed the involvement of oncogenic Epstein-Barr virus (EBV) in the carcinogenesis of NPC (Chan, 2014; Young and Dawson, 2014; Huang et al., 2018; Ferrari et al., 2012). Nevertheless, while EBV is a strong driver of NPC carcinogenesis, genetic susceptibility (Class I MHC gene mutation, affecting mainly the Chinese) and other regulatory gene mutations (PI3K/MAPK, TP53, RAS) also contribute to the development of NPC (Chen et al., 2019). Other etiological factors such as dietary consumption of salt-preserved food, carcinogen exposure from contaminated food consumption and environmental sources are still widely acknowledged although less well understood and lacking strong evidence to substantiate the hypotheses derived from various correlation studies (H. M. Lee et al., 2019; Yuan et al., 2000; Yu et al., 1988). One theory from early correlation studies suggests that

salt preservation produces carcinogenic nitrosamine (Secretan et al., 2009; Zou et al., 1994; Jia et al., 2010). A recent study detected nitrosamine contamination above the USDA permissible level (10 µg/kg cure meat) in more than 68 % of salted fish tested (H. M. Lee et al., 2019; Qiu et al., 2017). Contradictorily, Barrett et al. (2019) reported a low correlation of salted fish intake among adults with the risk of developing NPC (Barrett et al., 2019). A different *in vitro* study also demonstrated that carcinogen found in some food and herbs, such as phorbol ester or butyrate, could reactivate dormant EBV to undergo the viral lytic life cycle, a phenomenon that had been extensively proven to drive carcinogenesis of latently infected cells (Fang et al., 2012; Tsang et al., 2019). To date, only molecular evidence from genetic studies has substantially described the dynamics of NPC development, which often revolves around EBV, and host mutation-associated etiological factors rather than carcinogen-associated factors emphasized in correlation studies (Tsang et al., 2019; Chen et al., 2019; Wah et al., 2014).

2.3 Clinical management of NPC

The existing recommended treatment regimens for NPC in Malaysia are radiotherapy alone for Stage I disease, concurrent chemoradiotherapy for Stage II, III, IVA and IVB disease, and palliative treatment with chemotherapy or/and radiotherapy for distant metastasis stage (Stage IVC) (Ministry of Health Malaysia, 2016). The selection of a suitable treatment regimen for recurrent NPC depends on the localization of the disease. For local recurrence, nasopharyngectomy or radiotherapy or brachytherapy is recommended. For

regional disease, neck dissection, radiotherapy and chemotherapy are recommended.

The use of intensity-modulated radiotherapy (IMRT) and platinum-based chemotherapeutic agents is recommended for NPC treatment (Ministry of Health Malaysia, 2016). Clinical trials are only recommended for recurrence involving distant sites where no other existing treatment works, while palliative chemo- and radiotherapy can be considered for patients with suitable health and functionality conditions. Similar to the Malaysian guideline, guidelines from European countries recommend radiotherapy alone for Stage I disease. However, European guidelines recommend concurrent chemoradiotherapy for Stage II up to IVA disease, unlike the Malaysian guideline which includes the IVB stage of the disease (Bossi et al., 2021). Various countries treat NPC with similar treatment dosages; where Stage I NPC is given a cumulative irradiation dose of 60 – 70 Gy with a rate of 2 Gy dosage per treatment and 100 mg/m² of cisplatin is administered for a regimen that requires chemotherapy (Simo et al., 2016; Chan et al., 2010; Pastor et al., 2018; Gooi et al., 2017).

2.4 Post-chemotherapy and -radiotherapy outcome

Although IMRT significantly enhanced the precision of radiotherapy while reducing irradiation damage to the normal healthy cells within proximity of the tumour site, off-target irradiation is still inevitable (Qu et al., 2015; Ghosh et al., 2016). The dose of irradiation exposure to the healthy spinal cord and brainstem was reportedly reduced by up to 22 % compared to two-dimensional radiotherapy. Still, each site was inevitably exposed to an estimate of 43.6 Gy

and 52.8 Gy of irradiation, respectively, with IMRT (Qu et al., 2015). An estimated dose of 50 Gy and above to the spinal cord is sufficient to cause myelopathy (Jerrold T. Bushberg, 2020). In the study by Ding et al. (2019), NPC patients exhibited Grade 3 toxicities associated with haematotoxicity (39%, n=58/149), skin reaction (11%, n=16/149), and mucous-related adverse effects (37%, n=55/149) among those treated with different combinations of chemo- and IMRT. Most NPC survivors had to live with various forms of functional impairment caused by irradiation damage to normal cells and structures in the vicinity of the tumour (Hong et al., 2015; Tsai et al., 2014; Jerrold T. Bushberg, 2020). Some studies reported a high proportion of survivors affected by functional impairments (adverse decline in hearing, 51.67 %, and swallowing difficulty, 52.38 %, n=192) and some showed otherwise (serious dry mouth, 23.51 %, sore mouth, 10.71 %, adverse decline in hearing, 28.87 %, n= 336) with the duration of NPC survival studied ranging from 2 years up to 38 years (Hong et al., 2015). Dry mouth, sore mouth, and difficulty in hearing were reportedly the common functional impairments observed across various studies (Hong et al., 2015; Leong et al., 2020). However, various functional impairments and problems have been reported with varying proportions across different studies. For instance, neuropathy, osteoradionecrosis, and feeling ill were reported in lower proportion while fatigue, insomnia, and sense impairment were reportedly affecting an average to high proportion of NPC survivors (Pan et al., 2017; Leong et al., 2020; Ho et al., 2017; Tsai et al., 2014). It may take up to 10 years for impairment to the ear to recover to a state of minimal functional disturbance (Young, 2019). In addition, NPC patients undergoing concurrent chemoradiotherapy had to cope with side effects caused

by platinum-based chemotherapy drugs, which may include toxicity to organs such as the kidney, gastrointestinal tract, liver, and nervous system, damage to the inner ear, disrupted bone marrow function and blood production, and potential damage to heart muscles or the rhythmic state (Oun, Yvonne E Moussa, et al., 2018). Therefore, the existing treatment regimens for nasopharyngeal carcinoma are comparable to a double-edged sword where survivors must cope with various forms of long-lasting side effects that persist up to decades after recovery from the disease in exchange for survival.

To date, radiotherapy alone and radio-chemotherapy demonstrated high effectiveness in treating NPC, with 87.0 % to 89.4 % success in early-stage NPC and 69 % to 81 % success in advanced NPC, respectively (Niu et al., 2022; Blanchard et al., 2015). However, it was reported that up to 21 % of early-stage and 10 % of advanced-stage NPC survivors develop recurrence or metastasis after combination treatment of radio-chemotherapy (Guan et al., 2020; A. W. M. Lee et al., 2019). The standard treatment for recurrent NPC after radio-chemotherapy is multidrug chemotherapy, which reported results in between 15 – 48 % treatment responses with progression-free survival around 5 months (4, 4.47, and 5 months) up to 14 months, depending on combinations of chemotherapy drugs (Perri et al., 2019; Guan et al., 2020). Re-irradiation as second-line treatment for recurrent NPC reportedly results in 41 % of patients with 5-years overall survival, which is a much better outcome than chemotherapy, but the overall grade 5 toxicity was reported in 33 % of survivors, leading up to potentially 40 % of mortality among survivor (Perri et al., 2019).

It is evident that chemo- and radiotherapy, even in combination, are losing effectiveness in treating advanced, recurrent, and metastatic NPC, not to

forget the post-treatment side effects that accompany both treatments. Growing evidence shows how cellular signalling and molecular responses contribute to the resistance towards various chemotherapeutic drugs and radiotherapy, suggesting that tumour cells would be capable of adapting to any new chemical-based drugs or radiation intervention, resulting in treatment resistance and unlikely for NPC survivors to be free from long-term side effects of newer version of treatments (S. Li et al., 2017; Guo et al., 2021; Ma et al., 2018; Tu et al., 2015; Zhang et al., 2007; Zuo et al., 2010; Zhang et al., 2014). Therefore, a “gentler” cancer treatment, or at least causes less persistent side effects, yet effective is desirable. For treatment of NPC which is surrounded by delicate nervous system, muscle and skeletal structure, and lymphoid organs of nasopharynx, a less destructive cancer treatment would be favourable.

2.5 Oncolytic measles virus as onco-therapeutics

The idea of using a conditionally replicating and apathogenic recombinant virus to selectively kill cancer cells was first demonstrated by Martuza and co-workers in 1991 (Martuza et al., 1991). The study was motivated by the fact that glioblastoma patients have very low survival rates, with high chances of recurrence, and are resistant to existing treatment regimens, which are chemotherapy, radiotherapy, and surgical intervention. Martuza and co-workers demonstrated that a human herpes simplex virus 1 (HSV-1) mutant with thymidine kinase gene (*thk*) deletion was able to replicate and completely kill glioma cells without pathogenically burdening the host mouse. Thereon, various recombinant viruses were designed specifically to target different types of tumour cells (Driever and Rabkin, 2001).

2.5.1 Safety and development of oncolytic measles virus

Oncolytic measles virus (oMV), or genetically engineered variants of vaccine strain measles virus of Edmonston lineage (MV-Edm), is one of the oncolytic viruses of interest (Myers et al., 2007). Key factors that make MV-Edm a suitable oncolytic vector candidate is its inherent safety, broad-spectrum tropism, tumour selectivity for oncolysis, and efficacy of viral transduction. The attenuated MV-Edm vaccine strain lineage (Figure 2.3) has a long safety record with no reports of the vaccine strain reverting to the pathogenic phenotype over the past decades of measles vaccination (Msaouel et al., 2012). Moreover, vaccinated individuals achieve lifelong immunity against the measles virus. Based on an estimation from the WHO, worldwide coverage of one dose of measles vaccine among 1-year-old children had achieved a high annual record of 73 % coverage in the year 1995 with a gradual increment to 84 % in the year 2010, and a sustained record of 84 % to 85 % between 2010 to 2015. WHO further estimated an increment of second-dose measles vaccine coverage from 15 % in the year 2000 to 67 % in the year 2017 (Dabbagh et al., 2018). Therefore, more than 73 % of adults worldwide are estimated to possess immune protection against measles virus to date and vaccine strain measles virus would be one of the safest oncolytic virus candidates for further development.

The wild-type strain of measles virus was first isolated from a child named Edmonston by John Franklin Enders and Thomas Chalmers Peebles in 1954. Wild-type strain was attenuated after extensive passages in human and avian cell cultures, giving rise to vaccine strains, Seed A and Seed B, which serve as the core genetic backbone to produce the measles vaccine (Rota et al., 1994). Various strains of oncolytic measles viruses were developed from Seed B through a series of genetic modifications by Russell and co-workers (Myers et al., 2007).

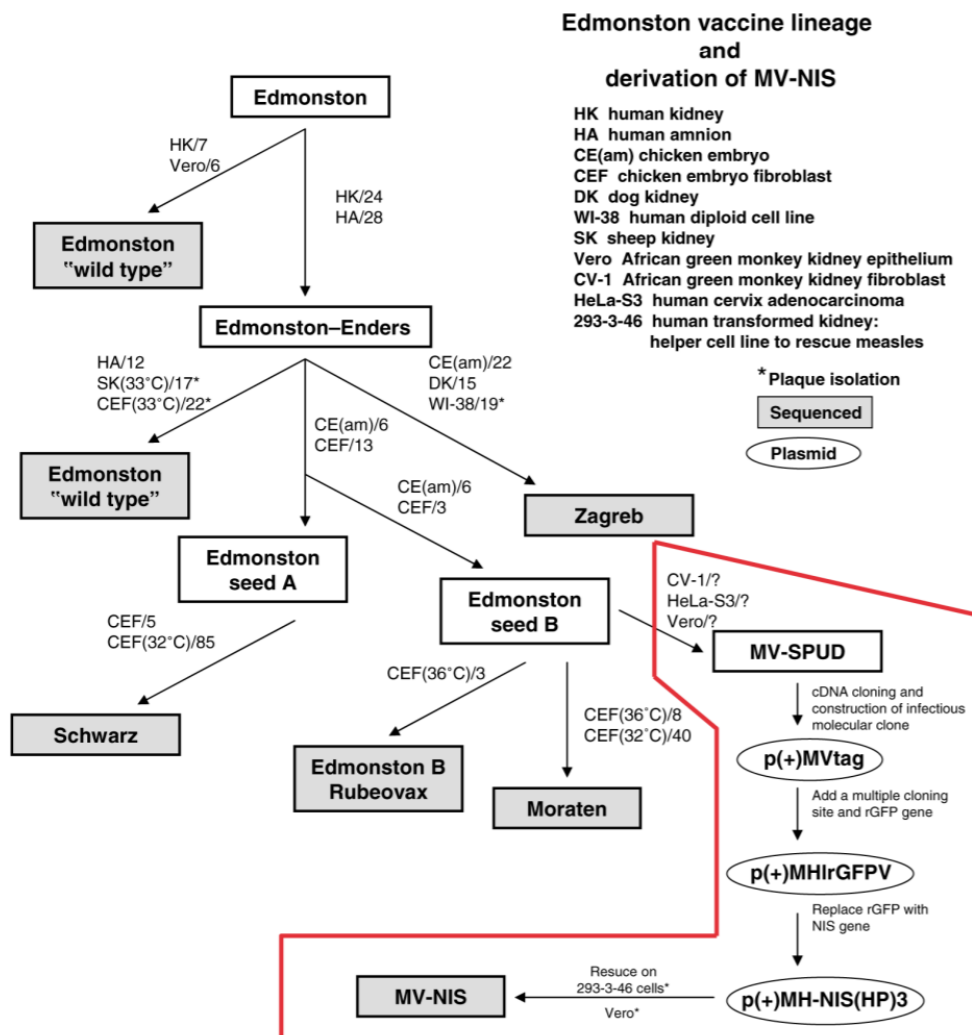


Figure 2.3: Lineage map of oncolytic measles virus developed by Russell and co-workers (Myers et al., 2007).

2.5.2 Onco-selectivity for cell infection by oncolytic measles virus

The fundamental process of MV oncolysis requires infection of target cells followed by viral-induced cancer cell killing. MV-Edm demonstrated tropisms towards three human cell surface proteins, two of which were natural targets inherited from wild-type measles virus (CD150/SLAM and nectin-4) and the last target (CD46) was a resulting mutation acquired from viral attenuation. Wild-type measles virus naturally targets CD150/SLAM and nectin-4 to initiate infection and establish pathogenesis in human lymphocyte and epithelial cells (Shingai et al., 2005; Tatsuo et al., 2000; Liu et al., 2014). CD150, also known as a signalling lymphocytic activation molecule (SLAM), is specifically expressed in T-lymphocyte, B-lymphocyte, and dendritic cells (Wang et al., 2001). Nectin-4 is a cell adhesion molecule that is naturally enriched in embryonic and placental tissue. However, recent studies revealed overexpression of nectin-4 in various cancers but not in normal cells and this protein became a suitable candidate for tumour-selective therapy (Chatterjee et al., 2021; Reches et al., 2020). MV-Edm acquired tropism towards CD46 due to asparagine to tyrosine substitution at amino acid position 481 within the viral H-gene during the extensive passaging in avian cell culture (Rota et al., 1994; Hsu et al., 1998; Schneider et al., 2002). CD46 is a membrane cofactor protein that inactivates the C3b complement protein and prevents activation of the complement system from causing damage to the host cell (Liszewski et al., 1991; Dunkelberger and Song, 2010). Contrary to CD150/SLAM, CD46 is expressed in nucleated human cells except in erythrocytes (Frecha et al., 2008).

Overexpression of CD46 has been observed across various malignancies, mainly carcinomas, to evade killing by the immune complement system

(Maciejczyk et al., 2011; Boisgerault et al., 2013; Peng et al., 2004; Johnstone et al., 1993; Michelle Elvington et al., 2020). CD150/SLAM expression in haematological cancer varies, with high expression reported in cutaneous T-cell lymphoma, and low expression or none in malignancy of B-cell origin (Gordiienko et al., 2019). Nectin-4 was reportedly overexpressed in solid tumours, such as gastrointestinal malignancy, lung, hepatocarcinoma, ovarian and breast cancer (Boulefour et al., 2022). Taken together, MV-Edm is a compatible vector to target solid and haematological malignancies expressing CD46, CD150/SLAM, and nectin-4.

The onco-selectivity of MV-Edm depends on two elements:

1. the dysfunctionality of target cell activation and response to Type 1 interferon in response to viral infection, in turn allowing MV-Edm to replicate (Engeland and Ungerechts, 2021; Heinzerling et al., 2005) and
2. threshold expression level of CD46 on the host cell surface (Anderson et al., 2004).

MV-Edm generally infects cells expressing CD46 indiscriminately. However, cells expressing high levels of CD46 are predestined to viral-induced cell death while cells expressing low levels of CD46 are minimally affected (Anderson et al., 2004). Only cells expressing high CD46 undergo cytopathic effects unique to measles virus infection while equally infected normal cells were spared and avoided cell death (Anderson et al., 2004). Moreover, a recent study demonstrated that the differential expression of interferon- β (IFN- β) could modulate the tumour cell killing capacity of MV-Edm, with high expression causing cellular resistance to the viral-induced oncolysis (Aref et al., 2020).

Newer variants, based on the MV-Edm genetic backbone, are only capable of partially suppressing interferon- α (IFN- α) and - β expression (Haralambieva et al., 2007). Therefore, dysfunctional Type I interferon response could be the underlying reason MV-Edm display selective killing of tumours expressing CD46 exceeding a certain threshold even though there is evidence of indiscriminate and equal infection of CD46-positive normal and tumour cells (Anderson et al., 2004). In normal cells, CD46 expression is low but interferon expression is intact albeit partially suppressed by MV-Edm infection, but in the case of tumour cells, IFN- β could be highly suppressed since Type I interferon signalling pathways are known to be dysregulated via downregulation of interferon receptor in the tumour microenvironment (Cho et al., 2020).

2.5.3 Measles virus cytopathic effect as naturally efficient means of infection and lateral viral dissemination

MV-Edm can efficiently infect targeted cells due to two important features unique to the Paramyxoviridae genera. First, the measles viral particle enters the host cell by fusion between the lipid membrane of the viral envelope and the lipid bilayer of host cell, owing to collective and sequential interaction between complementary binding of viral haemagglutinin (H) protein to host cell surface protein (CD46, CD150, or nectin-4) and the consequential fusion of both entities triggered by viral fusion (F) protein (Stern et al., 1995; Liu et al., 2014). Second, successful infection induces expression of viral H- and F-protein on the surface of the infected host cells that drives indiscriminate intercellular fusion between infected and adjacent host cells to form a large multinucleated body known as syncytium (Griffin et al., 2012). The latter event also confers

additional dissemination advantage compared to viruses that are solely dependent on the expression of viral progenies to disseminate secondary infection. In the context of oncolysis, it is theoretically possible for MV-Edm to spread to underlying layers of tumour cells, which may otherwise be inaccessible directly by intercellular infiltration. Therefore, the dual mean of viral dissemination, via cell-to-cell fusion and viral egress, of Paramyxoviruses improves the efficiency of tumour cell eradication both locally and in the distal part of the human body. As low as 0.5 multiplicity of infection (MOI) was sufficient to drive cells expressing a high level of CD46 to start intercellular fusion and pre-destined the infected cells to death in vitro (Anderson et al., 2004).

2.5.4 Oncolytic measles virus in clinical trials

To date, various variants of oncolytic measles virus based on MV-Edm origin have been designed and tested in various clinical trials (Msaouel et al., 2017). Clinical trials successfully demonstrated the safety of administering a dose of MV-Edm as high as 10^9 TCID₅₀ titre via intrapleural, intratumorally, or intravenous route. Even though no dose-limiting toxicity had been reported across various trials, a high titre of MV-Edm is crucial for successful treatment and the production of such a high titre of pure viral particle remains a challenge (Bah et al., 2020). Moreover, the efficacy of virotherapy is hampered by existing immunity in patients who have a history of receiving the measles virus vaccine (Engeland and Ungerechts, 2021). Nevertheless, an immune-suppressed patient does benefit the most from virotherapy and thus immune suppression remains a logical albeit not favourable option to maximize the potential of oncolytic

measles virotherapy (Russell et al., 2014). Although the sample size of successes is small, owing to a small population of patients who are eligible for clinical trials, complete regression of tumours was reported in some trials (Msaouel et al., 2017; Pidelaserra-Martí and Engeland, 2020). Despite its potential as a potent cancer treatment regimen, the number of successful cancer remission due to measles virotherapy treatment is still far lower than existing radio- and chemotherapy (Engeland and Ungerechts, 2021; Mailankody et al., 2015). Out of thirty-two patients in Clinical Trial NCT00450814, only one patient achieved complete remission of multiple myeloma with administration of oncolytic measles virus (Packiriswamy et al., 2020). Chemotherapy had reportedly achieved up to 80 % complete remission of multiple myeloma with the possibility of recurrence anticipated (Mailankody et al., 2015; Landgren et al., 2016). In rarer cases where radiotherapy is required as a palliative intervention for multiple myeloma patients, the reported success rate was 76.4% among 55 patients assessed (Talamo et al., 2015). Hence, measles virotherapy is not feasible for primary cancer treatment for the general population and requires further improvement to enhance its potency. Comparing therapy-associated side effects, MV-Edm causes manageable and short-term resolvable adverse effects while those of radiotherapy and chemotherapy are long-lasting and may cause functional impairment, more so in cancer of the head and neck which are situated closer to the neural system and are denser with anatomical structures and delicate organs (Maltser et al., 2017; Pidelaserra-Martí and Engeland, 2020; Oun, Yvonne E. Moussa, et al., 2018; Hong et al., 2015).

2.5.5 Potential application of oncolytic measles virus in NPC

Non-tumorous tissue protein expression data from The Human Protein Atlas (<https://www.proteinatlas.org/>) revealed prominent expression of nectin-4 protein (ENSG00000143217-NECTIN4) in urogenital, skin, hematopoietic, and gastrointestinal organs, while CD46 protein (ENSG00000117335-CD46) was prominent across all human organs except the eyes and skin (Digre and Lindskog, 2023). Nectin-4 protein overexpression was documented in various solid tumours, such as lung, breast, pancreatic, colorectal, urothelial, ovarian, and more recently in head and neck squamous cell carcinoma (HNSCC) (Sanders et al., 2022; Liu et al., 2021). Similarly, CD46 overexpression was documented in breast, ovarian, hepatocellular carcinoma, multiple myeloma, and HNSCC (Ravindranath and Shuler, 2006; Michelle Elvington et al., 2020). Carcinogenesis did not seem to downregulate both proteins but elevated both proteins' expression, presumably for pro-survival needs, especially with the CD46 proteins (Michelle Elvington et al., 2020).

Current knowledge regarding nectin-4 and CD46 expression in NPC tissues is limited, with no documented study investigating their differential expression. Overexpression of either or both proteins, as observed in other HNSCC, could render NPC susceptible to oMV infection and subsequent oncolysis. An earlier *in vitro* study had shown oMV was able to infect and kill HNSCC cell lines (Zaoui et al., 2012). This study aims to investigate the potential for oMV to infect and eliminate NPC cells by exploiting the presence or overexpression of these established entry receptors.

Section 2.5.2 discussed how defective Type 1 interferon activity and response in host cells contribute to the onco-selectivity of oMV. EBV-

associated NPC exhibits a well-documented deficiency in IFN- β activity due to the collective suppressor effects mounted by gene products of EBV, the Zta, LMP1, and BFRF1 proteins (Bentz et al., 2012; Wong et al., 2017; Wang et al., 2020). Additionally, the LMP1 protein can suppress the activation of IFN- α via the degradation of the RIG-I protein, further disrupting the interferon signalling pathway (Xu et al., 2018; Onomoto et al., 2021). IFN- β therapy has shown significant tumour suppression capacity in NPC, multiple sclerosis, and triple-negative breast cancer with or without combination with existing cancer therapy, demonstrating the necessity of NPC to suppress Type 1 interferon response for survival (Makowska et al., 2018; Severa et al., 2020; Doherty et al., 2017; Buehrlen et al., 2012).

In the Section 2.5.1, the safety properties of oMV as therapeutics, with a primary focus on safety with high dose administration of the virus in humans, resolvable mild flu-like side effects, and the genetic makeup of oMV originating from the vaccine strain. These properties highlight that oMV offers a potentially wide extent of beneficial potential, from serving as a simple MV vaccine, if the oncotherapy outcome is not satisfactory, to successful cancer remission and all with minimal resolvable side effects.

Taken together, there is a high possibility that EBV-associated NPC is naturally primed by EBV gene products and oncogenesis to be defective in interferon activity and still express nectin-4 and/or CD46, if not upregulated, respectively. Hypothetically, both conditions are sufficient for oMV to effectively infect NPC cells, propagate within the tumour cells, and eventually kill the infected cells. The lack of documented evidence on nectin-4 and CD46

expression in NPC provides us with an invaluable opportunity to fill the gaps of knowledge while testing oMV as a potential new alternative to treat NPC.

2.6 Cell death pathways induced by cancer therapies

The earliest mechanism of cell death, apoptosis, was morphologically described by Kerr et. al. in 1972 (Kerr et al., 1972;). In earlier days, mechanisms of cell death were morphologically classified into three types: apoptosis, necrosis, and autophagy (Green and Llambi, 2015). These three types are still relevant to date and remain the mainstream events driving natural death (apoptosis), death due to physical injury (necrosis) and degradation of intracellular components of normal non-transformed cells and clearance of cellular remains (Green and Llambi, 2015). Over the past five decades, various forms of cell deaths were described based on molecular involvement on top of visually descriptive morphological changes (D'Arcy, 2019; Yan et al., 2020). Advancements in biomolecular techniques revealed more cell death mechanisms since the year 2000, which are solely identifiable based on the expression of specific genes or gene products leading to cell death through biomolecular investigation (Nirmala and Lopus, 2019). These new generations of cell death mechanisms are further complicated by the fact that a proportion of these mechanisms shares morphological features close to necrosis, yet each mechanism undergoes a systematic molecular interaction typical of a programmed pathway, namely NETosis, necroptosis, methuosis, and pyroptosis (Nirmala and Lopus, 2019; Yan et al., 2020). The Nomenclature Committee on Cell Death (NCCD) compiled and recommended the nomenclature of all the known mechanisms of cell death in 2018 (Galluzzi et al., 2018). While NCCD

acknowledges all mechanisms of cell death as “regulated cell death” (Figure 2.4A) and does not divide the mechanisms into sub-grouping, researchers may still refer to known mechanisms according to non-programmed and programmed modalities, whereby the latter group is further subdivided into two categories of programmed apoptotic and programmed non-apoptotic mechanisms (Yan et al., 2020). According to this classification (Figure 2.4B), the non-programmed group consists solely of necrosis (Yan et al., 2020). The programmed apoptotic group consist of apoptosis and anoikis; while the programmed non-apoptotic group consists of autophagy and all the new generation of cell death mechanisms: entosis, methuosis, paraptosis, mitoptosis, parthanatos, ferroptosis, pyroptosis, NETosis, and necroptosis (Yan et al., 2020).

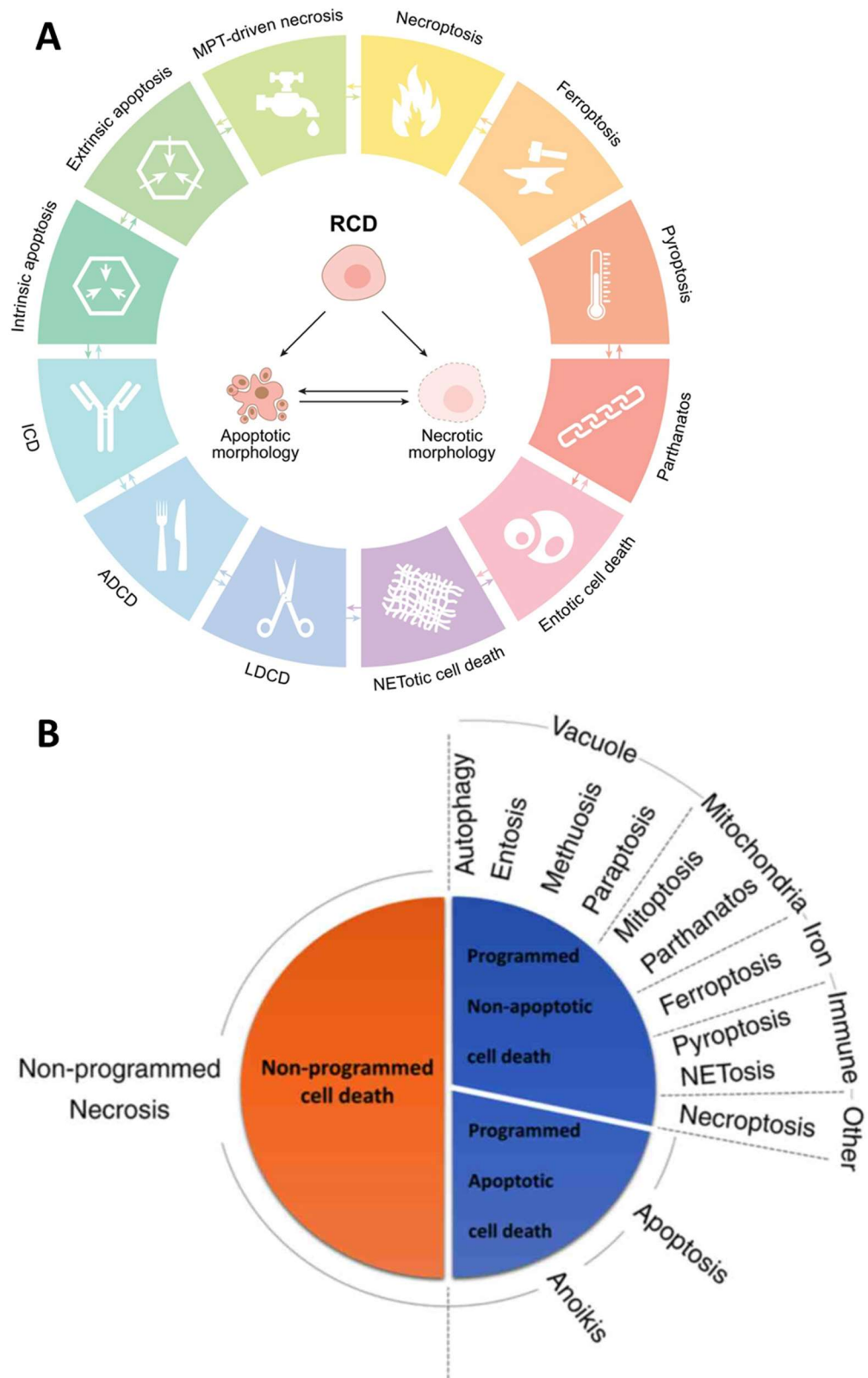


Figure 2.4: (A) Recommended nomenclature by Nomenclature Committee on Cell Death (NCCD) and (B) common classification of regulated cell death mechanisms used to define various cell death events (Galluzzi et al., 2018; Yan et al., 2020).

Despite the extensive understanding of various mechanisms of cell death as independent phenomena, the biological events from the point of the trigger until the definitive death of tumorous cells due to therapeutic intervention remain complicated and elusive (Adjemian et al., 2020). Apoptosis is generally accepted as the main mechanism of cell death induced by radiotherapy (Baskar and Itahana, 2017; Li et al., 2017). However, radiotherapy may not be killing tumour cells via a single independent pathway but could involve several mechanisms, occurring in parallel, such as mitotic catastrophe, senescence, immunogenic cell deaths, methuosis, and iron-dependent cell death, as evidenced by the detection of the representative biological marker within the same culture tested (Baskar and Itahana, 2017; Adjemian et al., 2020). Each cell in the tested tissue could be undergoing one mechanism of cell death, but collectively, radiotherapy may not be inducing specifically one pathway of cell death. Radiotherapy has been reported to kill tumour cells based on cell types, such as killing solid tumours via mitotic catastrophe or haematological malignancies via apoptosis (Sia et al., 2020). Other factors that dictate the consequential mechanism of cell death include the functional status of genes that regulate the cell death pathway, intercellular interaction within the tumour microenvironment, and intracellular molecular interaction and signalling (Sia et al., 2020; Hotchkiss et al., 2009). Chemotherapeutic drugs are selected, designed, and administered with the expectation to induce apoptosis pathways to kill tumour cells (Hannun, 1997; Pan et al., 2016). Unlike radiotherapy, chemotherapy drug has not been reported to induce other mechanisms of cell death, except for immunogenic cell death which is elicited by selected drugs, such as anthracyclines (doxorubicin, idarubicin, and epirubicin),

cyclophosphamide, oxaliplatin, mitoxantrone and bortezomib (Gebremeskel and Johnston, 2015; Vanmeerbeek et al., 2020).

In the context of virotherapy, wild-type measles virus was known to induce apoptosis in cell lines and agranulocytes (Esolen et al., 1995; Pignata et al., 1998). Vaccine strain MV, Hu-191, induces DNA double-stranded break (TUNEL assay) and necrosis (Haematoxylin and Eosin staining) in infected Lewis Lung Carcinoma (LLC) cell line in a dose-dependent manner (Zhao et al., 2013). MV-Edm induces caspase-3-dependent apoptosis in cervical cancer cell lines (Wang et al., 2015). MV-Edm demonstrated contradictory outcome in non-small cell lung cancer cell lines, whereby autophagy was induced, which in turn suppresses caspase-dependent apoptosis in favour of viral replication, and lead to necrotic death of the cells (Mao Xia et al., 2014). A different study using the HeLa cell line showed agreement with the finding by Xia et al. (2014) where autophagy, which corresponds to the formation of syncytia, is induced in cells infected with either wild-type (G954-MeV) or MV-Edm for the same pro-replicative reason (Richetta et al., 2013). The same study also discovers that vaccine strains but not wild-type strains, can induce an additional, CD46-dependent, early wave of autophagy that was observed at 1.5 hours after infection (Richetta et al., 2013). Richetta et al. (2013) did not investigate whether the end outcome of their study resulted in apoptotic or necrotic death of infected cells but their experiments using pan-caspase apoptosis inhibitor, Z-VAD, suggests that the observed autophagy could be a means to delay apoptosis of host cell in favour of increasing measles virus particle production. Based on the collective molecular evidence thus far, it seems that both wild-type and vaccine-strain measles virus induces apoptotic cell death in tumour cell lines,

with vaccine-strain measles conferring pro-replicative advantage over wild-type measles virus with delayed cell death due to sustained autophagy in the form of two sequential waves of autophagy induction. However, the mitophagy-regulated necrotic cell death outlined by Xia et al. (2014) and the dose-dependent increment of necrotic cells from histopathological observation by Zhao et al. (2013) could not be simply dismissed. Not to dismiss, the histopathological observation may present a more holistic and realistic endpoint overview than molecular-based in vitro evidence which are more often offer deeper insight but constrained to a single pathway at a time.

In the past decades, accumulating evidence suggests immunogenic cell death (ICD) as a potential new modality in cancer treatment (Gebremeskel and Johnston, 2015; Vanmeerbeek et al., 2020; Donnelly et al., 2013). Unlike the mechanisms of regulated cell death, which involve intracellular molecular interplay from the point of the trigger until the eventual death of cells, ICD is a post-cell death event that involves induction and antigen-priming of dendritic cells with a tumour-specific antigen which in turn prime and stimulate cytotoxic T lymphocyte to target and kill intact tumour cells (Zhou et al., 2019). Several immunogenic molecules, generally known as damage-associated molecular patterns (DAMPs), released from dead cells recruit and stimulate the maturation of dendritic cells for the removal of dead tumour cells. Upon priming with tumour-specific antigen from the dead tumour cell, dendritic cells in turn present tumour cell antigen and stimulate T lymphocytes for targeted killing on tumour cells. Therefore, ICD could be seen as a tumour vaccination event that boosts the effectiveness of cancer therapy. Necrotic cell death (necrosis, necroptosis, or pyroptosis), selected chemotherapy drugs, chemicals, and

oncolytic measles virus have been shown able to induce ICD response (Zhou et al., 2019; Gebremeskel and Johnston, 2015; Vanmeerbeek et al., 2020; Nicolas Boisgerault, 2015; Donnelly et al., 2013).

2.7 iTRAQ quantitative proteomics for the understanding of cell death induced by the oncolytic measles virus

Mass spectrometry has been the mainstream methodology for acquiring in-depth and comprehensive molecular data for the predictive modelling of cellular microenvironments in the field of biochemistry and chemistry (Urban, 2016). The greatest advantage of mass spectrometry in proteomics lies in its capability to identify proteins in a high-throughput manner by leveraging on experimentally curated peptide sequences publicly available in electronic repositories, resulting in an extensive amount of data available for cellular microenvironment modelling and subsequent inference validation (Wang and Wilson, 2013). Technological advancement over the past two decades has improved mass spectrometry beyond the scope of an efficient tool for protein identification. To date, mass spectrometry proteomics can perform relative quantitation that allows researchers to interrogate differential gene expression based on different treatment groups or across time under specific stimulation (Ankney et al., 2016).

Relative quantitation with mass spectrometry is generally performed in two branches of methodology, either incorporating chemical tags or a label-free method (Ankney et al., 2016). The chemical tag method, also known as a label-based method, utilizes a set of molecules with similar molecular weight but

isotopically different mass to chemically label peptides in each sample, pool labelled sample and relative quantitation with tandem mass spectrometry can be performed in one analysis (Anand et al., 2017). Label-free method, lacking the multiplexing capacity, requires each sample to be analysed by mass spectrometry independently and relative quantification must be done *in silico* (Anand et al., 2017). The chemical tag method is more expensive taking into consideration the procurement cost of the tag reagents, but it is cost worthy since tagged samples can be multiplexed, owing to the design of the chemical tags that makes it possible for differential separation of independent samples within a mixture based on mass spectrometry signals, and simplify sample preparation protocol. The label-free method is less expensive but relatively more cumbersome due to the inability to multiplex sample and each sample had to be prepared separately (Anand et al., 2017). Notably, while the label-free method is more cumbersome, this method is not restrained by the number of samples for mass spectrometry analysis. In comparison, the variation of chemical tags is often limited in number and only able to differentially label up to a definite number of samples due to the limitation in chemical tag design. Therefore, depending on the experimental design and level of expertise available for any proteomics study, each method has its pros and cons.

In recent years, isobaric tag for relative and absolute quantitation (iTRAQ) has been widely adopted in various mass spectrometry-based quantitative proteomics and phosphoproteomics studies to model molecular interactions and identify molecular markers contributing to disease progression and development or contribute to treatment responses and disease suppression (He et al., 2019; Singh et al., 2021; Zhao et al., 2021). iTRAQ is designed with

4 and 8 variations of tags where each variant possesses physically the same molecular weight (Figure 2.5). Each variant of the tag is distinguishable by different mass-to-charge ratios after ionization detected by mass spectrometry (Bachor et al., 2019). This electronic mean of differentiation is only possible due to various combination of isotopic nitrogen and carbon molecule in iTRAQ chemistry that results in the same net molecular weight but produces different charges state upon ionization (Wiese et al., 2007; Pierce et al., 2008).

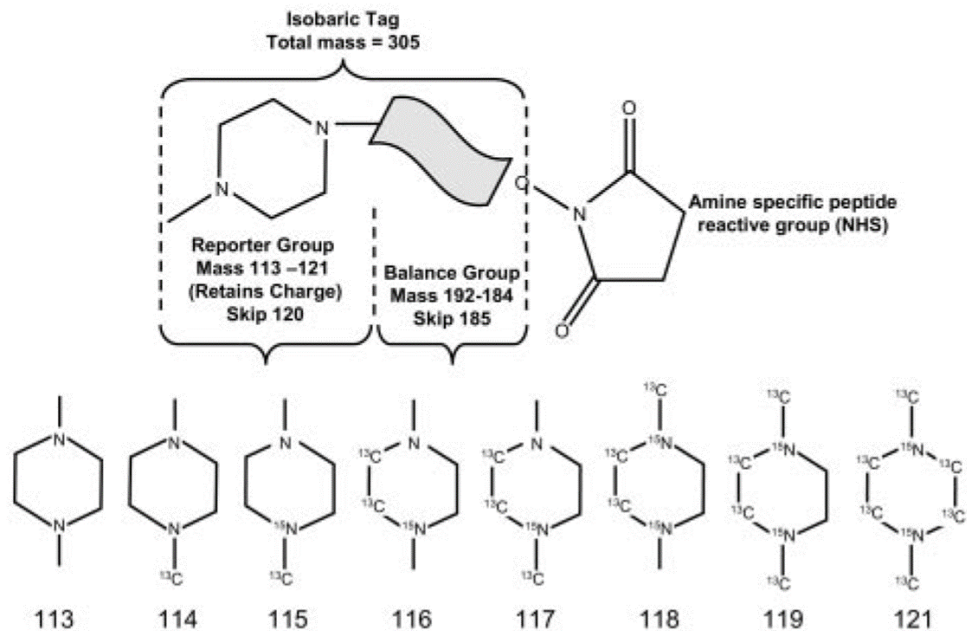


Figure 2.5: The difference in isotopic mass in reporter group of each iTRAQ 8-plex tags allows identification and quantification of protein sample (Pierce et al., 2008).

The exact cell-killing mechanism induced by the oncolytic measles virus has not been elucidated. Although the oncolytic virus had been commonly accepted to kill infected tumour cells via apoptosis, Xia et al. (2014) had shown necrosis could take place instead of apoptosis (Richetta et al., 2013; Mao Xia et

al., 2014). Notably, there are two primary distinctive differences between both studies. Firstly, Richetta et al. (2013) tested on the HeLa cell line, while Xia et al. (2014) tested on a non-small cell lung cancer (NSCLC) cell line. Deregulation of molecular signalling within tumour cells is driven by distinctive mutation and oncogenic factors specific to cell types, causing a type of tumour cells to a variable that results in molecular signalling beyond the expected and known pathway (Giancotti, 2014). Secondly, Richetta et al. (2013) showed that apoptosis is an event that follows viral-induced pro-replicative autophagy, while Xia et al. (2014) showed that mitophagy abrogated caspase-mediated apoptosis and redirected NSCLC towards necrotic death. Despite the contrasting findings from both studies, evidence from both studies was derived from the interrogation of a handful of biomarkers within selected cell death pathways. Both studies lack comprehensive details on other participating biomarkers, expression changes over time of these unknown yet relevant biomarkers, and relevant secondary signalling pathways that are also affected by the expression of viral gene products. Henceforth, this project attempts to elucidate the mode of NPC cell killing after infection with Measles-GFP-NIS, a variant of the oncolytic measles virus, via protein expression analysis in combination with bioinformatics.

2.8 Bioinformatics analysis for better understanding of protein-to-protein interaction

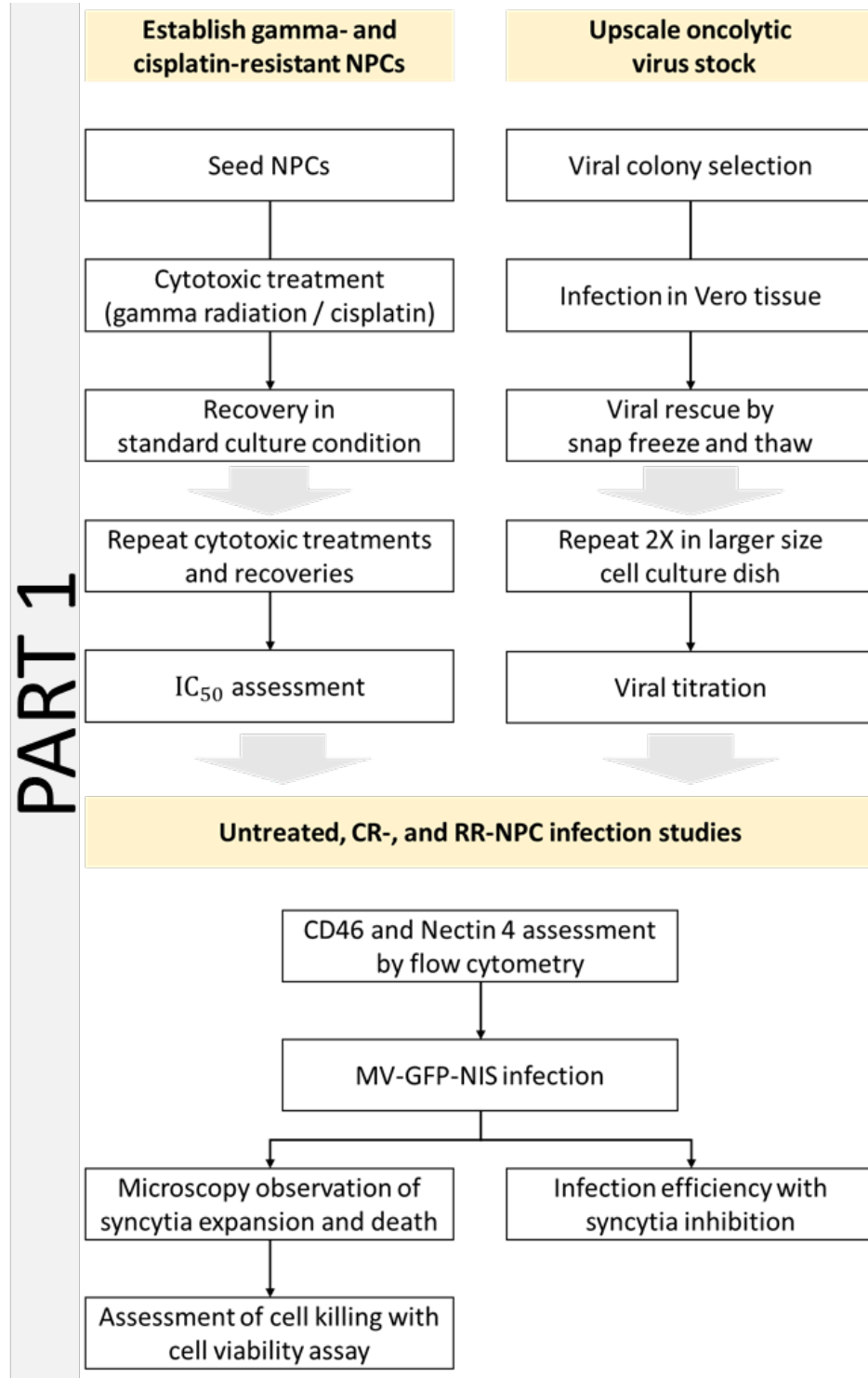
An integrated approach combining proteomics data with bioinformatics analysis has been the popular approach to understanding the interactions between proteins of interest in biological responses (Schmidt et al., 2014). To

date, bioinformatics analysis has evolved beyond the functional annotation of gene-related data, which was the pioneering effort in biological information aggregation, to the identification of key genes or proteins that may play regulatory roles in biological pathways that affect the progression of diseases or treatment outcomes (Li and Zhan, 2019; Kit et al., 2018). With the combined use of bioinformatics databases, topological algorithms, and analysis software, it is possible to shortlist identified proteins that could be serving dedicated functions or play key regulatory roles when the expressed proteins collectively form a protein complex (Li and Zhan, 2019). By utilizing software such as Cytoscape that is technically designed and tuned for network analysis, researchers can effectively and efficiently understand the protein-to-protein interaction or gene-to-gene relationship to generate inferences for further investigation and understanding of the complicated interplay between the pathological entity and its host microenvironment (Menon and Elengoe, 2020). In this thesis, this powerful software was used to assist in elucidating the potential cell death pathway that is induced by oMV in the NPC cell line.

CHAPTER 3

MATERIALS AND METHODOLOGY

3.1 Overview of methodology



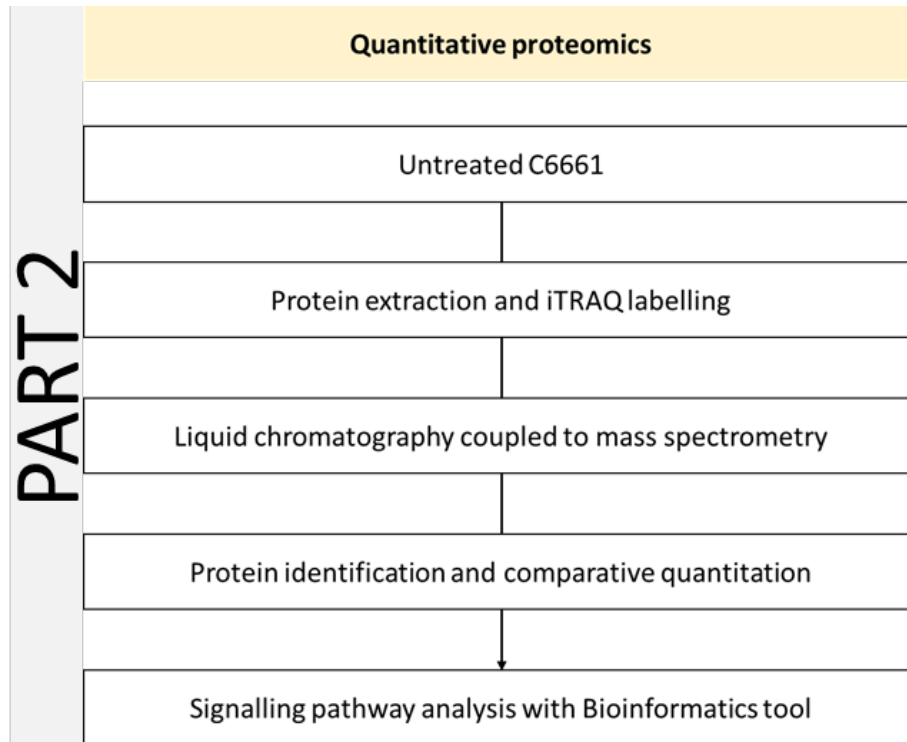


Figure 3.1: Overview of study methodology.

The methodology for this project comprises two parts. The first part involves establishing therapeutic resistant NPC cell lines and evaluating the therapeutic potential of oMV on NPC. NPC cell lines resistant to gamma radiation and cisplatin were established through repeated cycles of cytotoxic treatment and recovery. Cell surface receptors utilized by oncolytic measles virus to infect cells, CD46 and nectin-4, were quantified by flow cytometry (Dörig et al., 1993; Noyce and Richardson, 2012). On the other hand, Measles-GFP-NIS was grown in Vero cell culture and upscaled in three successive cultures from a 6-well plate to a 15 cm cell culture dish to achieve the titre required for infection. Once the virus stock was prepared, untreated and resistant cells were seeded at optimal density for Measles-GFP-NIS infection. Several

parameters were observed and quantified to validate the progression of infection and document the efficacy of infection and cell killing.

In the second part, untreated C666-1 cells were infected with Measles-GFP-NIS and cultured for mass spectrometry proteomics analysis. At 24-, 36-, and 48-hours post-infection (p.i.), infected cell cultures were harvested, and total proteins were extracted from each culture. Proteins were then prepared and labelled with an iTRAQ tag (SCIEX, USA) according to the manufacturer's protocol. iTRAQ-labelled samples were analysed with mass spectrometry. The resulting mass spectrometry data was analysed using PeptideShaker protein identification and quantification software. Protein annotation, function, interaction, and signalling pathway analysis were performed using STRING DB and Cytoscape bioinformatics tools.

3.2 Establishing radio- and chemo-resistant NPC cell line

Untreated CNE-1, CNE-2, HONE-1, and C666-1 cell lines (Table 3.1) were treated with repeated cycles of either cisplatin or gamma-radiation, followed by a recovery period, until surviving cells achieved more than two-fold tolerance towards the tested cytotoxic elements. The level of tolerance towards both cytotoxic elements was tested using a tetrazolium-based cell viability assay. NPC cell lines were a kind gift from Associate Professor Dr. Yap Lee Fah from the University Malaya Medical Centre.

Table 3.1: Details and description of cell lines used in this study.

Cell line	Cell line description*	Maintenance media	References
CNE-1	Well-differentiated squamous cell carcinoma	DMEM with 10% FBS	Zeng 1978
CNE-2	Poorly differentiated epithelial carcinoma	RPMI with 10% FBS	Sizhong et al. 1983
C666-1	Undifferentiated carcinoma, derived from xenografted NPC, EBV positive, metastatic in mouse model	RPMI with 10% FBS	Cheung et al. 1999; Smith, Merritt et al. 2011
HONE-1	Poorly differentiated squamous cell carcinoma, derived from biopsy specimen	RPMI with 10% FBS	Glaser et al. 1989
Vero	Spontaneously immortalized, derived from green African monkey kidney cell	DMEM with 5% FBS	Commercially available

* Information retrieved from <https://www.expasy.org/>.

3.2.1 Cell viability assay and cell density optimisation

Methyl thiazol tetrazolium-based cell viability assays, conventional MTT (Nacalai Tesque, Japan) or Cell Counting Reagent SF (Nacalai Tesque, Japan), were used to measure several parameters:

1. Cell density optimization for chemotherapy and Measles-GFP-NIS infection studies.
2. Evaluate the initial inhibitory concentration of cisplatin for chemotherapy treatment.
3. Cell viability after chemotherapy, radiotherapy, and Measles-GFP-NIS infection.

3.2.1.1 Cell density optimisation

Owing to the different growth rates of NPC cell lines, the cell density of each cell line was optimised before the initiation of the cisplatin treatment and Measles-GFP-NIS infection to ensure:

1. the cell count is high enough to increase the survival chance of cells after cisplatin treatment, and
2. the cell culture medium can last 48 hours of cisplatin treatment without becoming acidic (phenolphthalein indicator changes to yellow) to minimize cell death due to the acidity of the medium
3. the seeding density is optimal for Measles-GFP-NIS-induced cell-to-cell fusion

Each NPC cell line was seeded into a 96-well plate to achieve between 1,000 to 10,000 cells in a 100 μ L cell culture medium. After 24 hours post-seeding,

another 100 μL cell culture medium was added to each well to imitate the actual cisplatin treatment workflow. Cell cultures were allowed to incubate for 48 hours under standard cell culture conditions (37 $^{\circ}\text{C}$ with 5% CO_2) after which the cell culture medium was replaced with 90 μL fresh medium and 10 μL of Cell Counting Reagent SF (Nacalai Tesque, Japan) was added into each well for additional 2 hours incubation. The absorbance at 450 nm in each well was collected with Infinite 200 Pro culture plate spectrophotometer (TECAN, Switzerland). Data was tabulated in fraction of viability for presentation and analysis.

3.2.1.2 Evaluation of initial inhibitory concentration for cisplatin treatment

Untreated NPC cells were treated with increasing concentrations of cisplatin followed by a cell viability assay to identify suitable concentrations to initiate cisplatin treatments to induce cisplatin resistance in NPC cells.

In brief, untreated NPC cells were seeded with optimal density (Section 3.2.1.1) in 100 μL cell culture media into a 96-well plate for 24 hours of incubation at standard cell culture conditions. After 24 hours of incubation, 100 μL of fresh cell culture medium containing cisplatin were added to create 0, 2, 4, 8, and 16 $\mu\text{g}/\text{mL}$ final concentration in 200 μL of cell culture medium containing cisplatin. The cells were incubated under cell culture conditions and away from light for 48 hours after the addition of cisplatin-containing media. The cell viability after exposure to 48 hours of cisplatin was performed using Cell Counting Reagent SF (Nacalai Tesque, Japan) according to the

manufacturer's protocol with 2 hours of incubation after addition of the reagent (Section 3.2.1.1). The assessment was repeated three times and data was tabulated as the fraction of viable cells for data analysis. Data was analysed using GraphPad Prism four parameters log (inhibitor) vs response non-linear regression to calculate the inhibitory concentration of 50 % population (IC₅₀) as concentration reference to start the first cisplatin treatment.

The serial dilution was prepared by diluting the main stock of 200 µg/mL (w/v) cisplatin (Sigma-Aldrich) with cell culture media. To prepare the main stock, 400 µg of cisplatin powder was weighed and dissolved in 0.9% saline followed by sterilization by filtration through a 0.2 µM syringe filter. The main stock was kept for 28 days at 4 °C away from light until use (Karbownik et al., 2012).

3.2.1.3 Assessing cell resistance to gamma-irradiation treatment

To assess NPC cell resistance to gamma-irradiation treatment, a cell viability assay was performed periodically and after NPC cells achieved cumulative 60-Gy irradiation. NPC cells that survived primary gamma-irradiation treatment (treated cells) were allowed to recover to 90 % confluence before being sub-cultured to assess cell resistance to gamma-irradiation using cell viability assay.

In brief, treated cells were exposed to a series of increasing doses of 2-, 4-, 8-, 16-, to 32-Gy gamma irradiation. After irradiation, treated cells were returned to incubation under standard cell culture conditions for 48 hours before the extent of cell death was assessed. Conventional MTT assay was used as a

more cost-saving methodology in place of Cell Counting Reagent SF to accommodate the usage of a 60 mm cell culture dish to evaluate the cell viability of gamma-irradiated cells. Briefly, MTT was added into the cell culture at a 1:10 ratio and the culture was further incubated for another 2 hours. After incubation, the insoluble MTT was dissolved with 1 mL of dimethyl sulfoxide (DMSO), and absorbance at 570 nm was measured with an Infinite 200 Pro-96-wells plate UV-Vis spectrophotometer (TECAN, Switzerland). The assessment was repeated twice, with three technical replicates in each repeat, and data was tabulated as the fraction of survival for data presentation.

3.2.1.4 Assessing cell resistance to cisplatin treatment

Cell resistance to cisplatin treatment was assessed by subjecting cisplatin-treated cells to a serial dilution of increasing cisplatin concentration. In brief, cisplatin-treated cells were seeded with optimal density (Section 3.2.1.1) in 100 μ L cell culture media into a 96-well plate for 24 hours of incubation at standard cell culture conditions. After 24 hours of incubation, 100 μ L of fresh cell culture medium containing cisplatin were added to create 0, 2, 4, 8, 16, and 32 μ g/mL final concentration in 200 μ L of cell culture medium containing cisplatin. The cells were incubated under cell culture conditions and away from light for 48 hours after the addition of cisplatin-containing media. The cell viability after exposure to 48 hours of cisplatin was performed as described in Section 3.2.1.2 above. The quantitation was repeated three times and data was tabulated as the fraction of viable cells for data presentation. Data was analysed using GraphPad Prism four parameters log (inhibitor) vs response regression to

calculate IC_{50} for each treated NPC cell and increment of IC_{50} value across cycle of cisplatin treatments was assessed achieving resistance against cisplatin.

The serial dilution was prepared by diluting the main stock of 400 $\mu\text{g}/\text{mL}$ (w/v) cisplatin (Sigma-Aldrich) with cell culture media. The cisplatin stock solution was prepared according to the methodology in Section 3.2.1.2, except with 400 μg cisplatin powder instead.

3.2.2 Establishment of chemo- and radio-resistant NPC cell line

NPC cell lines used in this study (Table 3.1) were kind gifts from Associate Professor Dr Yap Lee Fah from the University Malaya Medical Centre. The Vero cell was a kind gift from Associate Professor Dr Kenny Voon Gah Leong from the University of Nottingham. All cells were incubated at 37 °C with 5 % CO_2 . To establish chemo- and radio-resistant NPC cell lines, untreated NPC (CNE-1, CNE-2, HONE-1, and C666-1) cells were seeded in T25 cell culture flasks 24 hours before treatment.

To establish radio-resistant NPCs, cells were irradiated with 2-Gy gamma radiation using a Gammacell 3000 irradiator with a radiation source from Caesium137 (Theratronics, Canada). Irradiated cell cultures were returned to incubators to recover under standard cell culture conditions. After 24 hours, the cell culture medium was replaced with fresh medium, then followed by further incubation to allow irradiated cells to recover and grow. The treatment was repeated until all NPC cell lines achieved a cumulative dose of 60-Gy treatment.

To establish chemo-resistant cells, the cell viability assay was performed on untreated NPCs to get the initial inhibitory concentration (IC) for cisplatin according to Section 3.2.1.2. Based on the initial data, NPC was treated with a cisplatin concentration that kills 10% of the cell population (IC₁₀) for 48 hours and then the cell cultures were allowed to recover in a drug-free fresh medium. The cycles of cytotoxic treatment and recovery were repeated with gradual increment in cisplatin concentration to IC₂₅, IC₅₀, and lastly IC₇₅. Changes in cisplatin resistance was assessed with cell viability assay according to Section 3.2.1.4 every 3 to 5 cycles of treatment. Treated NPCs that exhibited more than two-fold change of IC₅₀ when compared to their respective untreated NPC were deemed resistant (Han et al., 2014; Barr et al., 2013).

3.3 Upscaling and titration of oncolytic measles virus stock

3.3.1 Measles-GFP-NIS propagation

Commercially procured Measles-GFP-NIS (Imanis Life Sciences, USA) were upscaled to higher titres in three phases.

In Phase 1, Vero cells were seeded in a 6-well plate with DMEM culture medium supplemented with 5 % FBS and incubated at standard cell culture conditions for 24 hours before infection. The cell culture medium was discarded and 10 µL of Measles-GFP-NIS viral stock resuspended into 200 µL OptiMEM was overlaid onto the Vero cells for 3 hours under standard cell culture conditions. At the end of the infection, fresh DMEM was added, and infected cells were further incubated in standard cell culture conditions for up to 24 hours for clonal selection of syncytia. The syncytia developed were scrapped using

pipette tips, resuspended into 200 μ L OptiMEM and overlaid onto Vero cells for 3 hours under standard cell culture conditions for Phase 1 viral propagation. Fresh DMEM was added, and infected cells were incubated further up to 36 hours. Once the syncytia covered more than 90 % of Vero cell culture, the culture medium was discarded, and all infected cells were scrapped and concentrated into a small volume of OptiMEM. The collection of infected cells was snap-frozen and thawed three times between liquid nitrogen and a 37 $^{\circ}$ C water bath to lyse the Vero cells and to recover the viral particles. Cell debris was spun down with 4000 rpm centrifugation and discarded. The supernatant was recovered as the Phase 1 viral stock. The procedures for Phase 1 were repeated in a 100 mm cell culture dish to prepare viral stock with a higher viral load.

The procedure in Phase 1 was repeated but performed in a bigger cell culture dish to scale up viral progeny yield for Phase 3 infection. In brief, Vero cells were seeded in a 100 mm culture dish for 24 hours before infection. 20 μ L of viral stock recovered in Phase 1 was diluted to 1 mL with OptiMEM to inoculate Vero cells in a 100 mm cell culture dish for infection. Same as Phase 1, the infected cell culture was incubated for 3 hours for infection, top-up with fresh DMEM media, incubated for up to 36 hours, syncytia harvested, viral progenies rescued by three cycles of snap freeze-thawing, and collection of debris-free supernatant containing viral progenies. 10 μ L of Phase 2 viral stock was used for titration according to the Reed-Muench method as described in Section 3.3.2 to calculate the multiplicity of infection (MOI) for Phase 3 viral propagation.

Like Phase 2, the procedure in Phase 1 was repeated, but in multiple 150 mm cell culture dishes and seeded Vero cells were inoculated with 0.02 MOI viral suspension recovered in Phase 2, to get a final working viral stock with high viral titre for infection studies. In brief, Vero cells were seeded in more than five 150 mm cell culture dishes and incubated overnight under standard cell culture conditions. Seeded cells were inoculated with 2 mL of viral suspension adjusted to a multiplicity of infection (MOI) of 0.02 for infection. The infected cell culture was incubated for 3 hours for infection, top-up with fresh DMEM media, and incubated for up to 36 hours accordingly. Syncytia in all culture dishes were harvested and pooled into a 50 mL centrifuge tube, and viral progenies were rescued by three cycles of snap freeze-thawing, and collection of debris-free supernatant containing viral progenies accordingly. 10 μ L of Phase 3 viral stock was titrated with the Reed-Muench method according to Section 3.3.2 to calculate the viral titre for downstream infection experiments. Viral stock with the highest titre was used for infection studies.

3.3.2 Viral titration with Reed-Muench algorithm

In brief, 10 μ L of viral particle suspension was serially 10-fold diluted up to 10^7 dilution. For assessment at each dilution factor, 8 wells of 96-well plate were seeded with Vero cells 24 hours before viral inoculation. 50 μ L of diluted viral suspensions were inoculated into each of 8 wells of Vero cell culture according to the respective dilution factor. The infected plate was incubated under standard cell culture conditions for 5 days and the number of wells with visible syncytia for each dilution factor was recorded for calculation using the Reed-Muench method (Lei et al., 2021). The TCID₅₀ for the rescued

Measles-GFP-NIS virus stock used for the infection study was $4.74 \times 10^6 \text{ ml}^{-1}$.

3.4 NPC cells infection studies

Before investigating the infectivity of Measles-GFP-NIS in the untreated and treated NPC cells, the cell surface protein, CD46 and nectin-4, which act as viral attachment proteins were quantitated with flow cytometry for correlation in subsequent infection studies.

Two different infection studies were performed; first, to assess the infection efficacy of Measles-GFP-NIS and second, to monitor the extent of syncytia spread and efficacy of cell killing in untreated, RR-, and CR-NPCs. NPC cells were seeded in a cell culture medium and incubated under standard cell culture conditions for 24 hours before infection.

3.4.1 Expression of oncolytic measles virus attachment protein

Untreated, cisplatin-resistant (CR), and radio-resistant (RR) NPC were stained with anti-human-CD46 (1:10, BD Biosciences, USA) and -nectin-4 (1:100, R&D System, USA) antibody for 30 minutes away from light and in ice. IgG2a, k (1:10, BD Biosciences, USA) and IgG2b (1:100, R&D Systems, USA) antibodies were used as an isotype control for CD46 and nectin-4 detection, respectively. Antibody-stained cells were measured with FITC channel (CD46 and IgG2a, channel voltage: 260) and APC channel (nectin-4 and IgG2b, channel voltage: 475) with a gating population of 10,000 cells. The expression of both proteins was measured using the FACS Canto II (BD Biosciences, USA)

flow cytometer and assessed as the difference in Mean Fluorescence Index (Δ MFI) calculated with the following equation:

$$\Delta\text{MFI} = \text{FITC or APC positive MFI} - \text{Isotype control MFI}$$

3.4.2 Infection efficacy study

An infection efficacy study was performed under the influence of Fusion Inhibitor Peptide (FIP) (Bachem, Switzerland) to inhibit intercellular fusogenic activity for accurate measurement of NPC cells infected by Measles-GFP-NIS. In brief, NPC cells seeded into a 6-well plate were inoculated with viral particles in OptiMEM at MOI of 1.0 and incubated under standard cell culture conditions for 1 hour. At the end of incubation, 20 $\mu\text{g}/\text{mL}$ FIP was added, and the cells were further incubated. At 48-hours post-infection, cells were observed under ZEISS Axio Observer.A1 inverted microscope in brightfield and fluorescence setting to capture cell images at 100 x magnification before quantitative measurement using a flow cytometer. Mock infection was done with the same protocol, except with only OptiMEM media, without introducing Measles-GFP-NIS. Infected NPC cells were harvested with 0.25% trypsin (GE Healthcare Life Sciences, USA) and the number of infected cells expressing the enhanced green fluorescence protein (GFP) signal was measured using a FITC channel (voltage: 150) with a FACSCanto II flow cytometer (BD Biosciences, USA). Data was analysed with FlowJo version 10.6.2 software and the number of GFP-positive cells measured was recorded as the number of infected cells. Data were collected from two biological replicates for each NPC cells and one-way

ANOVA with Welch's t-test was performed using GraphPad Prism 9 to compare the statistical significance between the treated and untreated groups.

3.4.3 Monitoring syncytia spread and efficacy of cell killing in NPCs

NPC cells seeded into 12-well plates were inoculated with 0.2 MOI of viral particles in OptiMEM suspension and incubated for 1 hour under standard cell culture conditions. Cell culture medium was added to infected cells and syncytia development was monitored and recorded at 24-, 36-, 48-, and 60-hours post-infection under fluorescence and brightfield microscopes. Microscopy images were captured and GFP fluorescence images were overlaid using ImageJ software. Mock infection was done using the same protocol, except with only OptiMEM media, without introducing Measles-GFP-NIS, before the 1-hour incubation. To assess the efficacy of NPC cell killing, the experiment was scaled down and repeated in a 96-well plate. Cell viability assay was performed at 60-hours post-infection to measure the fraction of viable cells and data was presented as a fraction of dead cells with the following formula:

$$1.0 - \frac{A_{570nm} (MV - GFP - NIS \text{ infected})}{A_{570nm} (Mock \text{ infected control})}$$

One-way ANOVA with Welch's t-test was performed with GraphPad Prism 9 software to test the statistical significance between the treated and untreated groups.

3.5 iTRAQ quantitative proteomics with bioinformatics analysis

3.5.1 C666-1 cell infection and protein extraction

C666-1 cells were seeded into four 100 mm cell culture dishes for 24 hours before infection with 0.2 MOI of viral particles in OptiMEM for 1 hour under standard cell culture conditions. Cell culture medium was added to infected C666-1 cells, and the dishes were incubated further for cell and syncytia development. At 24-, 36-, and 48-hours post-infection, one dish of infected cells was scrapped, and cellular protein was extracted with RIPA lysis buffer (Merck, Germany) supplemented with protease and phosphatase inhibitor cocktail (Nacalai Tesque, Japan). The fourth dish was harvested, and proteins were extracted as the mock-infected control. The experiment was repeated once, and the second set of proteins was extracted as the biological replicate. Extracted proteins were stored at -20 °C.

3.5.2 Protein quantitation

Extracted proteins were quantified using the bicinchoninic acid (BCA) quantitation kit (Nacalai Tesque, Japan) according to the manufacturer's protocol and bovine serum albumin (BSA) was used as a reference to create a standard curve for quantitation. Absorbance at 562 nm was measured using a TECAN Infinite 200 Pro 96-wells plate UV-Vis spectrophotometer.

3.5.3 Protein preparation and iTRAQ labelling

100 µg of proteins extracted from the mock-infected and each infection timepoint were denatured, reduced, and alkylated according to the iTRAQ

labelling kit protocol (Table 3.2). Proteins were cleaned and precipitated with the methanol/chloroform method followed by Trypsin/Lys-C protease cocktail (Promega, USA) protein digestion according to the manufacturer’s protocol (Shahinuzzaman et al., 2020). iTRAQ labelling of peptides and sample multiplexing were done according to the manufacturer’s protocol. iTRAQ labelled and multiplexed peptides were cleaned up using a handheld strong cation exchange (SCX) clean-up kit (SCIEX, USA). Peptides were then fractionated into eight fractions using a Pierce™ High pH Reversed-Phase Peptide Fractionation Kit (Thermo Fischer Scientific, USA) and each fraction was analysed with Agilent 1200 C18 HPLC-Chip coupled to Agilent 6550 iFunnel Q-TOF liquid chromatography mass spectrometer at the LCMS Laboratory in Jeffrey Cheah School of Medicine and Health Sciences, Monash University, Malaysia. The liquid chromatography mass spectrometry analysis was run with the parameters described in Table 3.3 and Table 3.4.

Table 3.2: iTRAQ labelling details for quantitative proteomics study

	iTRAQ tag	C666-1 p.i. protein extraction timepoint
Biological replicate 1	113	Mock infected
	114	24-hours
	115	36-hours
	116	48-hours
Biological replicate 2	117	Mock infected
	118	24-hours
	119	36-hours
	121	48-hours

Table 3.3: Liquid chromatography parameters for iTRAQ-tagged peptide sample separation.

Column	: Agilent Large Capacity Chip, 300 Å, C18, 160nL enrichment column & 75 µm x 150 mm analytical column (P/N: G4240-62010)		
Flow rate	: 4 µL/min from Agilent 1200 Series Capillary pump and 0.5 µL/min from Agilent 1200 Series Nano Pump		
Solvents	: A - Water with 0.1% formic acid B - 90% Acetonitrile in water with 0.1% formic acid		
Autosampler temperature	: 4 °C	Injection volume	: 1 µL

Sample analysis gradient with Agilent 1200 Series nanoflow LC pump as follows:

Time (min)	Solvent B (%)
Initial	5
40	70
50	70

Stop time: 50
Post run: 8 minutes
Total run time: 63 minutes

Table 3.4: Mass spectrometry parameters for iTRAQ-tagged peptide ionization and peptide sequencing.

Ion polarity	: Positive
Capillary voltage (V _{cap})	: 1900 V
Fragmentor voltage	: 360 V
Gas temperature	: 325 °C
Drying gas flow	: 5.0 l/MIN
Collision energy	: Use slope, 3.7 V / (100Da) offset 2.5 V
Reference masses	: Positive polarity – 299.294457 and 1221.990637

Data acquisition : Spectra acquired in aMSMS mode

		MS	MS/MS
Mass range (m/z)	Min	110	50
	Max	3000	3000
Acquisition rate (spectra/s)		2	4
Time (ms/spectrum)		500	250

3.5.4 Protein identification, relative quantitation, and bioinformatics analysis

Protein identification and relative quantification were performed using the PeptideShaker's SearchGUI version 4.1.24 tool with human protein sequences input from Swiss-Prot repositories (Farag et al., 2021; Vaudel et al., 2015). Parent and fragment mass tolerance of 0.1 Da, 1 % false discovery rate

(FDR) for peptide spectral match (PSM) and 1 % FDR for protein matching were used for protein identification. Relative quantitation was performed with the PeptideShaker Reporter tool. Proteins with iTRAQ \log_2 fold change ratio (\log_2FC) more than 0.58 and less than -0.58, or equivalent to FC ratio of 1.5 or -1.5, were considered as differentially expressed genes (DEG) or abundant protein (DAP). Data imputation was performed on proteins that lacked quantitative data by recording the missing value as $\log_2FC = 0$ to represent no change of expression for downstream analysis and interpretation (Aguilan et al., 2020).

Protein-to-protein interaction information among identified proteins was mined using the STRING database (<https://string-db.org/>) and visualized with Cytoscape bioinformatic tools (Shannon et al., 2003). A confidence factor of 0.4 and prediction without text mining was set as analysis parameters in the STRING database. Data acquired from the STRING database were imported into Cytoscape software for hub gene analysis and pathway visualization. Identified proteins were screened for proteins related to cell death with functional annotation from Gene Ontology (GO) Biological Processes (<http://geneontology.org/>) and Kyoto Encyclopedia of Genes and Genomes (KEGG) database (<https://www.genome.jp/kegg/>). MCODE plugin was used to identify clusters of genes that form a dense interaction edge (Bader and Hogue, 2003). MCODE analysis was performed with the following parameters: node score cutoff = 0.2, K-core = 2, Max depth = 100, Degree cutoff = 2 and with haircut. Identified gene clusters were validated with annotation from an experimentally curated comprehensive resource of mammalian protein complexes database, CORUM, using the gProfiler plugin (Giurgiu et al., 2019).

Functional Catalogue (FunCat) annotations available in the CORUM database were utilized to summarize the function of the protein complexes that match proteins shortlisted by the MCODE tool (Ruepp et al., 2004).

CHAPTER 4

RESULTS AND DISCUSSION

4.1 Part 1: Evaluation of oncolytic measles virus infectivity in untreated, CR-, and RR-NPC

4.1.1 NPC cell lines exhibiting more than 2-fold resistance to radiation and cisplatin cytotoxicity are considered resistant cell lines

Radiation and cisplatin-resistant NPC cell lines were established by repeated cycles of gamma radiation or cisplatin treatment followed by recovery in standard cell culture media. Different cells respond to the treatment differently.

In the gamma-irradiated group, all NPC cell lines were equally treated with 2-Gy gamma irradiation up to a total of 32 cycles of treatment. The cumulative dose of 60-Gy was chosen as the treatment limit because it is the standard radiation dose applied in radiotherapy treatment for NPC (A. Azizah et al., 2019). Of the four cell lines, only CNE-2 and C666-1 cell lines showed tolerance towards radiation after a cumulative treatment of 60-Gy (Figure 4.1). Therefore, only CNE-2 and C666-1 cell lines that survived the 32 cycles of radiation treatments are deemed as radiation-resistant cells (RR-NPC) for a downstream experiment in this study.

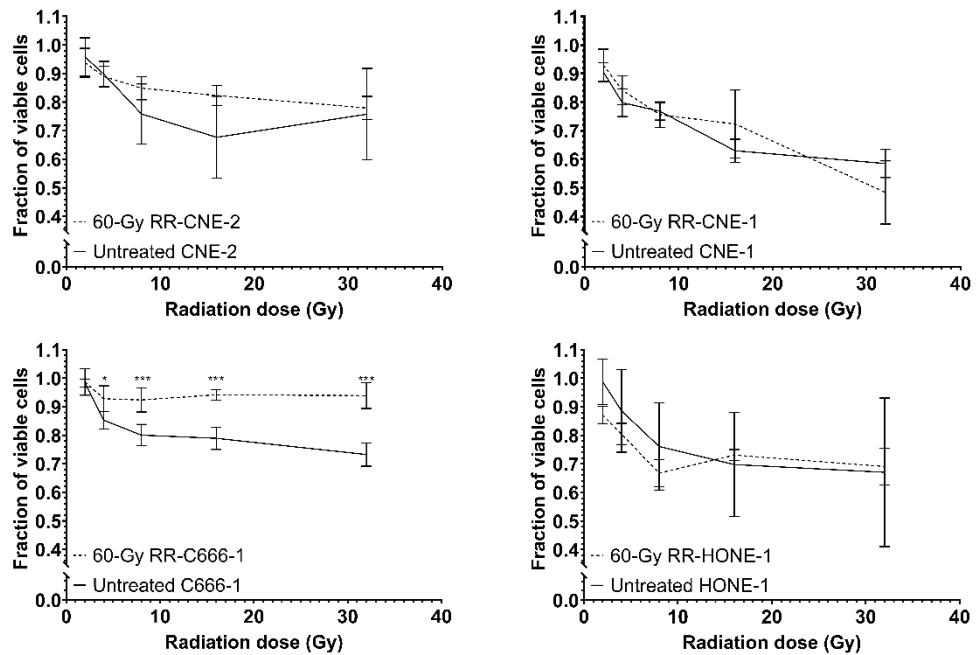


Figure 4.1: Only CNE-2 and C666-1 cells were resistant to gamma-radiation after completing a cumulative dose of 60-Gy and were considered radio-resistant (RR) NPCs.

Putative RR cells were exposed to a series of increasing doses of gamma irradiation, 2-, 4-, 8-, 16-, and 32-Gy, before being assessed with cell viability assay to evaluate the extent of resistance toward gamma irradiation. Data were collected from two biological repeats with three technical replicates in each repeat. P-value ≤ 0.05 (*) and < 0.001 (***)

In the cisplatin-treated group, all NPC cell lines tested achieved more than 2-fold resistance, evaluated as more than 2-fold change in the final IC_{50} compared to the initial IC_{50} evaluated at Cycle 0 (Table 4.1). Therefore, all surviving NPC cells treated with cisplatin are deemed cisplatin-resistant cells (CR-NPC).

Table 4.1: All NPC cell lines treated with repeated cycles of cisplatin treatment exhibit ≥ 2 -fold change of resistance towards cisplatin.

Treatment group	Average IC50 ($\mu\text{g/mL}$)			
	CNE-1	CNE-2	C666-1	HONE-1
Untreated	3.27 ± 1.05	5.08 ± 0.30	5.22 ± 1.26	3.93 ± 1.57
Resistant	14.44 ± 1.03	12.73 ± 3.70	14.04 ± 0.90	10.16 ± 0.12
Fold increment	4.42	2.51	2.69	2.59

4.1.2 Measles-GFP-NIS infects all NPC cell lines tested and was not affected by acquired resistance to cisplatin or gamma-radiation

Variants of the oncolytic measles virus derived from the MV-Edm lineage are known to infect cells via CD46 and nectin-4 (Engeland and Ungerechts, 2021). The expression of CD46 and nectin-4 protein on untreated, RR- and CR-NPC cells was evaluated using flow cytometry. CD46 was found to be consistently expressed on the NPC cell lines. Repeated exposure to radiation treatment did not affect the expression (Figure 4.2). The expression of nectin-4 cell surface protein in these cell lines was, however, negligible (Appendix A). Therefore, Measles-GFP-NIS can infect NPCs by anchoring to CD46. To investigate the efficacy of Measles-GFP-NIS infection, the untreated-, CR-, and RR-NPCs were infected with Measles-GFP-NIS and cultured in a medium containing 20 $\mu\text{g/mL}$ of FIP. Measles viruses are known to cause cell-to-cell fusion to form a large multinuclear body known as syncytium for viral replication (Herschke et al., 2007). The addition of FIP in the culture medium inhibited cell-to-cell fusion and infected cells expressed GFP for quantitative

measurement using flow cytometry (Bovier et al., 2021). Figure 4.3 shows that CR- and RR-NPC were more susceptible to Measles-GFP-NIS infection.

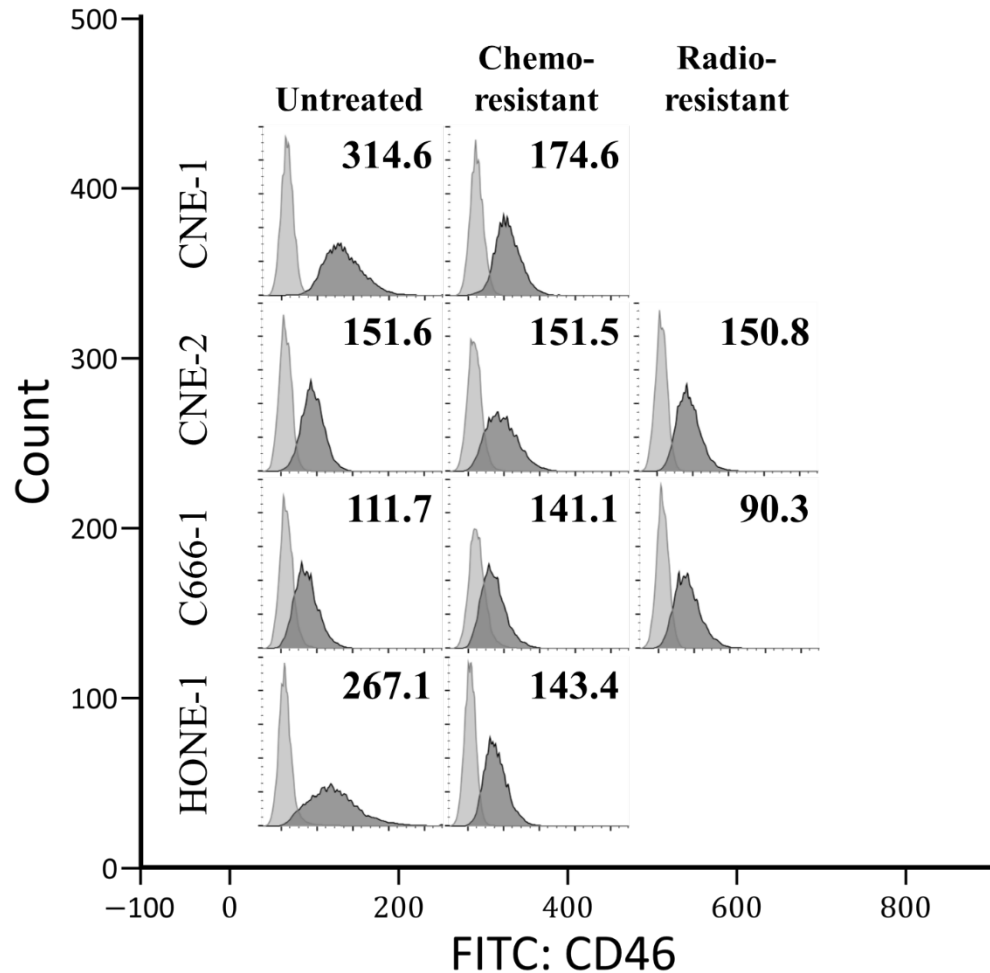
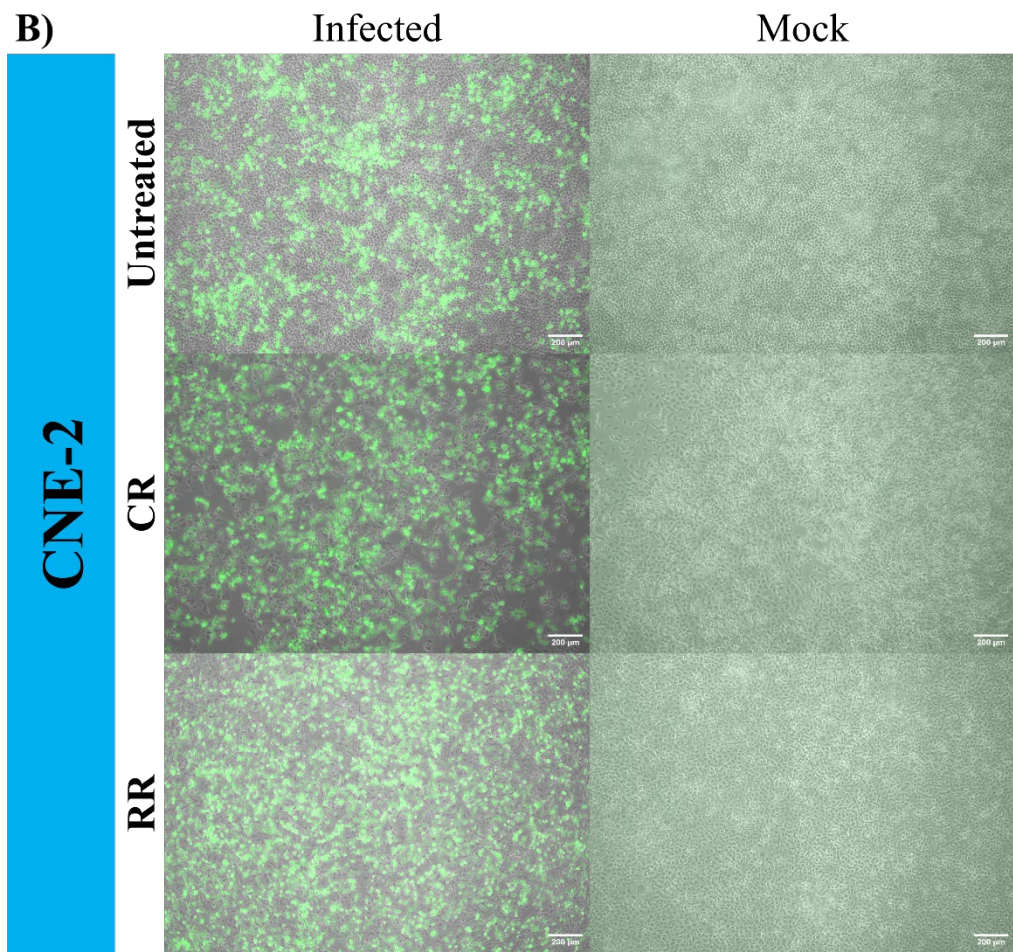
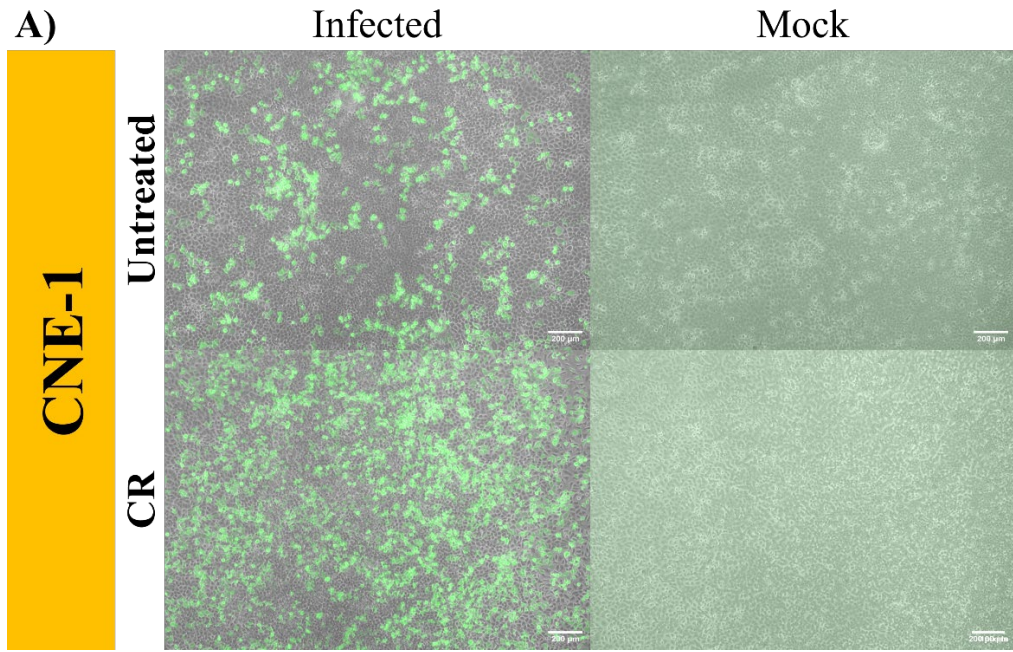


Figure 4.2: CD46 was consistently expressed on untreated, chemo-, and radio-resistant NPC cells.

Number inset represent the mean fluorescence index (MFI) shift of CD46 (dark grey tone) from IgG2A isotype control (light grey tone) quantitated among 10,000 cell population per analysis. Data were collected from single set of sample analysis per biological replicate, and a total of two biological replicates were performed (Appendix A).



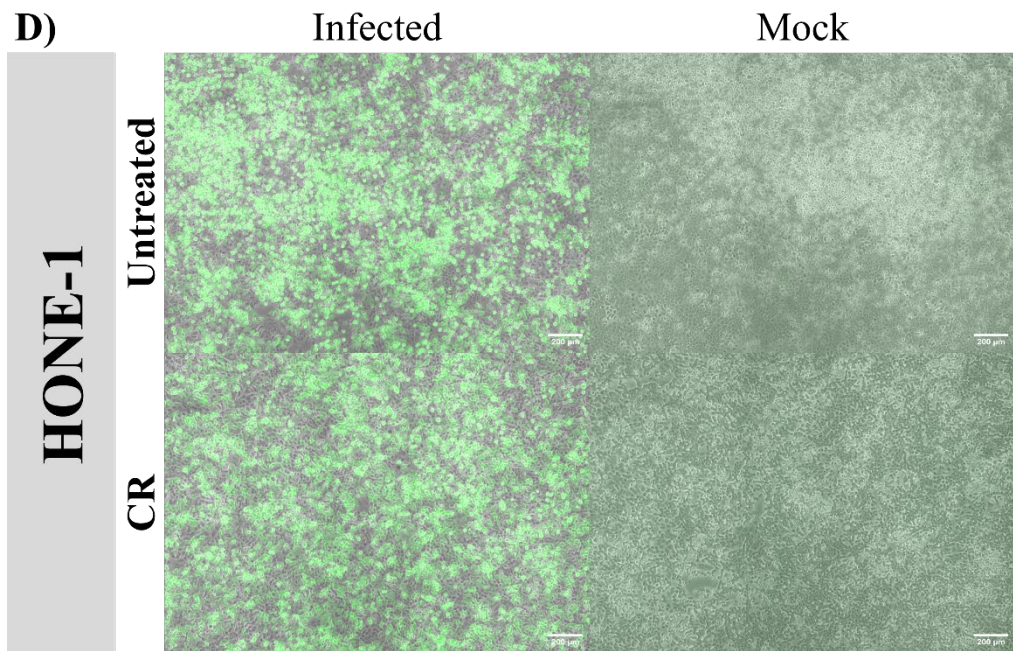
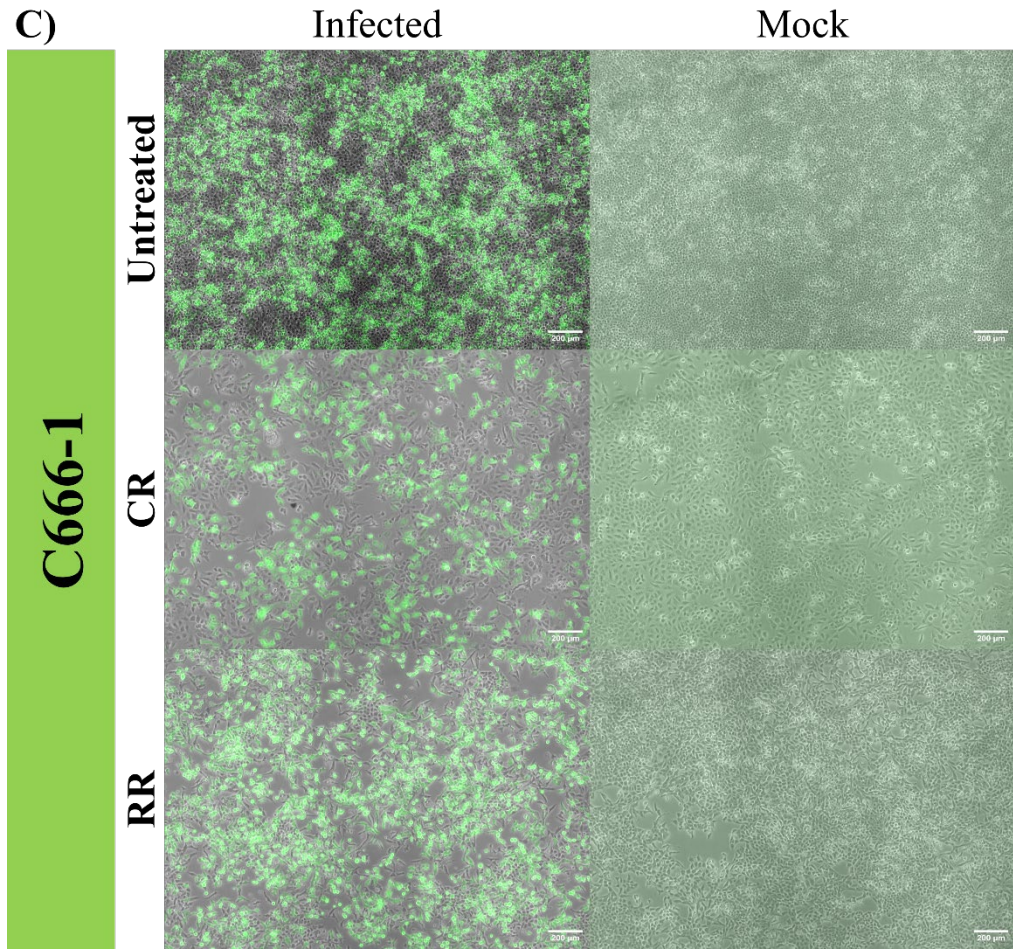


Figure 4.3: Representative images showing infected (A) CNE-1, (B) CNE-2, (C) C666-1, and (D) HONE-1 cells expressing GFP observed under fluorescence microscope at 100x magnification.

Infected NPCs were cultured in a cell culture medium supplemented with 20 µg/mL FIP to inhibit syncytia formation. CR – chemo-resistant; RR – radioresistant. Line inset represent 200 µm scale bar.

Figure 4.4 shows that resistance to cisplatin and gamma radiation did not inhibit Measles-GFP-NIS infection of NPC cells in-vitro and the viral infection was efficient, albeit statistically not significant. RR- (55%) and CR-CNE-2 (56%) show a higher number of infected cells compared to untreated-CNE-2 (34%). Similarly, RR- (58%) and CR-C666-1 (39%) also show a higher number of infected cells compared to untreated-C666-1 (30%). CR-CNE-1 and CR-HONE-1 also show a higher number of infected cells compared to their respective untreated counterparts. The outcome suggests that radiation exposure may sensitise cells to viral infection (Figure 4.4). This data agrees with data from other studies that both ionizing radiation and chemotherapy could sensitize tumour cells, which in turn, enhances the oncolytic capacity of the subsequent oncolytic virotherapy in adjuvant cancer therapy (Liu et al., 2007; Harrington et al., 2010; Advani et al., 2006).

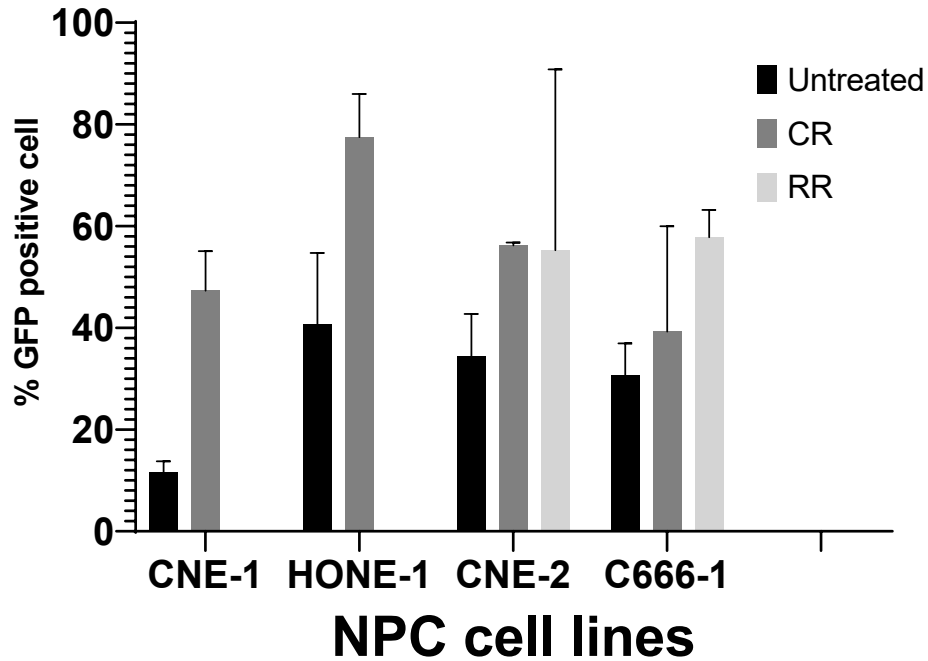


Figure 4.4: CR- and RR-NPC showed a higher percentage of GFP-positive cells counted with FACS Canto II flow cytometer, suggesting treated cells are more susceptible to Measles-GFP-NIS infection.

Two biological replicate measurements were taken for each NPC cell. No statistically significant changes in the infectivity (One-way ANOVA with Welch's t test). CR – chemo-resistant; RR – radio-resistant.

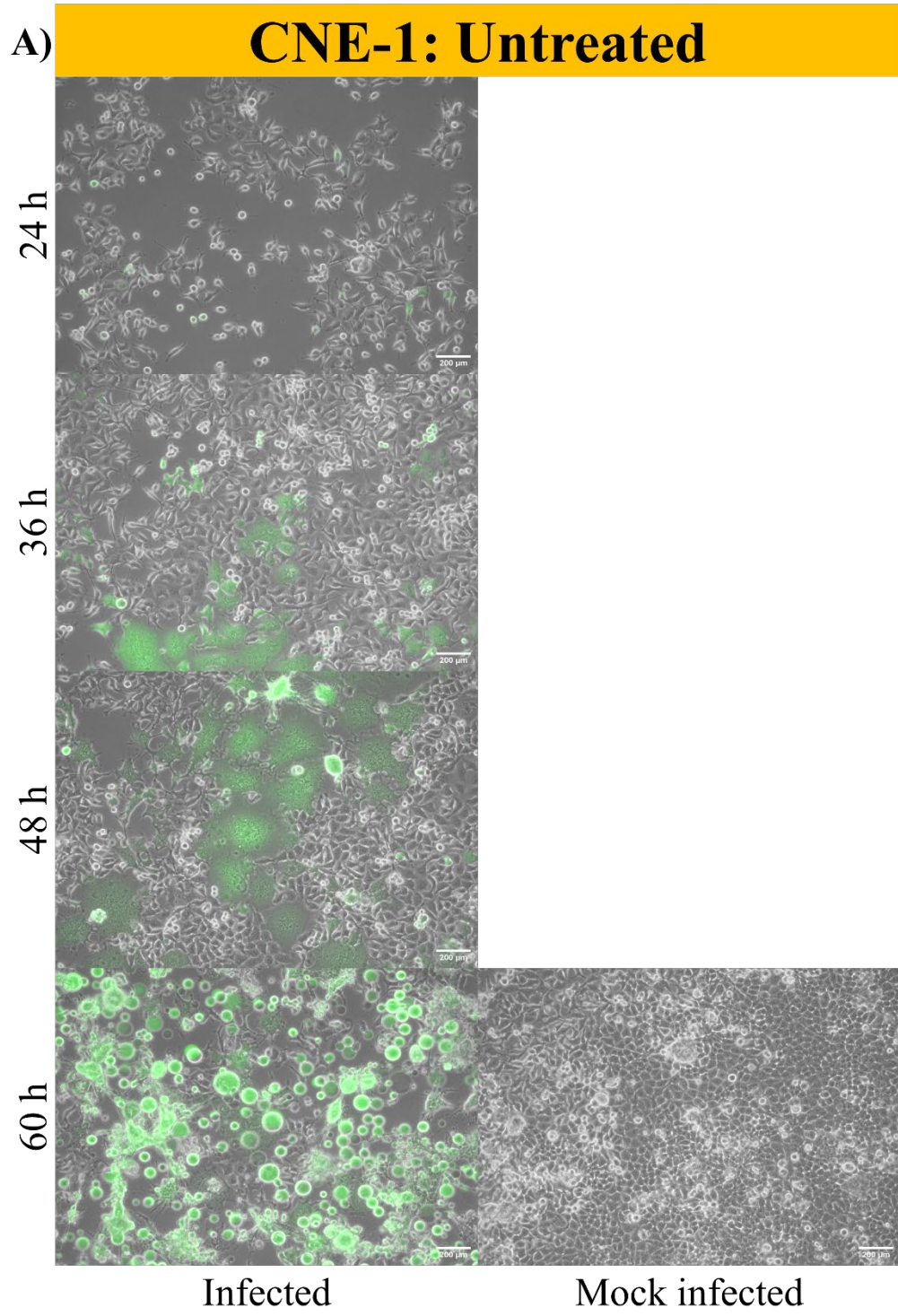
Untreated CNE-1 and HONE-1 showed a bigger shift in CD46 fluorescence signal compared to other NPCs (Figure 4.2). However, untreated CNE-1 and HONE-1 did not produce a higher number of GFP-positive cells (Figure 4.4). On the contrary, CR- and RR-NPC showed a higher GFP-positive cell count than the untreated NPC. This data demonstrated that infectivity of Measles-GFP-NIS is not linearly dependent on the level of CD46 expression and could be cell type-specific. This result agrees with the previous report where a threshold level of CD46 expression is required for effective infection of MV-Edm (Anderson et al., 2004). In addition, intracellular factors could affect the efficacy of measles virotherapy. For example, cytotoxic treatment might have

caused a certain extent of intracellular changes in response to the toxic or damaging elements within the cells which, in turn, sensitized the cells towards Measles-GFP-NIS infectivity (Liu et al., 2007; Harrington et al., 2010; Advani et al., 2006).

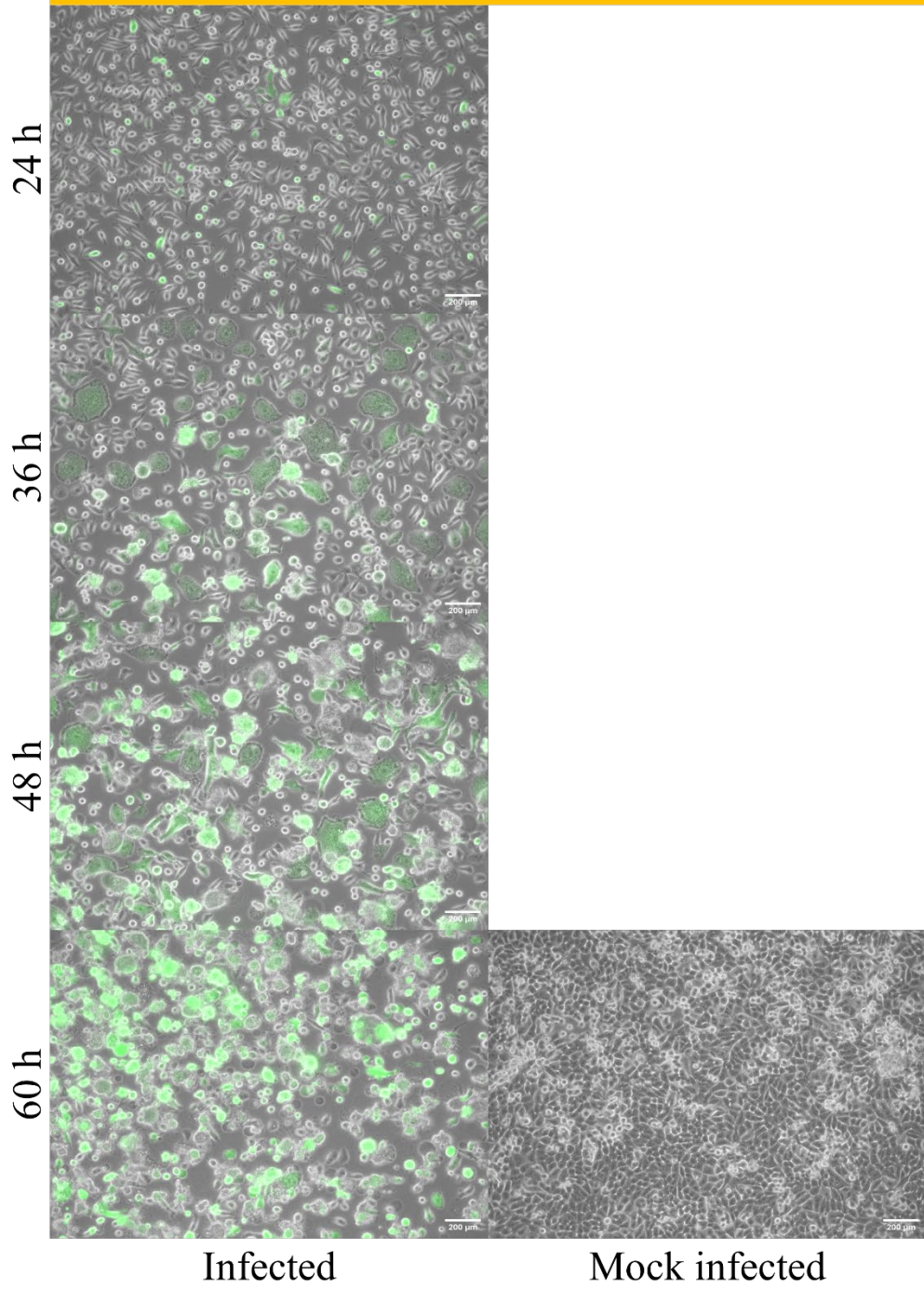
4.1.3 Measles-GFP-NIS effectively spread horizontally in vitro, and shrinkage of infected bodies was observed at 60-hours post-infection

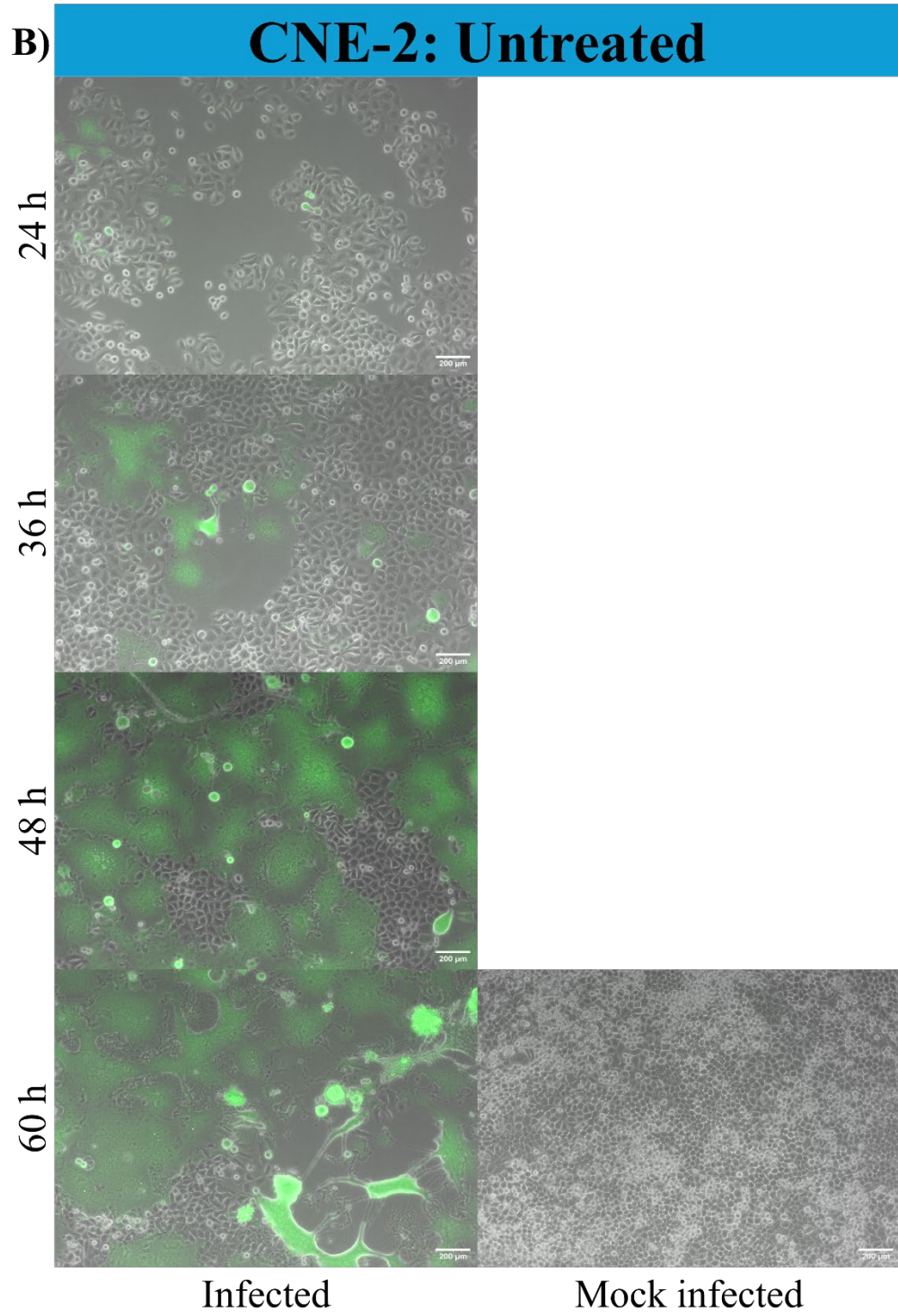
Following the demonstration that Measles-GFP-NIS were able to infect all NPCs, the in vitro suppression of NPC cells by the cytopathic effect of Measles-GFP-NIS was evaluated with microscopic monitoring at 24-, 36-, 48-, and 60-hours post-infection.

The fluorescence microscopy data in Figure 4.5 showed that Measles-GFP-NIS successfully spread horizontally via cell-to-cell fusion after 24 hours of infection. At 60-hours post-infection, more empty spaces were observed compared to other time points, suggesting that cells were lost at this time point because of Measles-GFP-NIS infection whereas the mock-infected control at 60-hours post-infection remained confluent. Upon close inspection, cellular bodies that appeared shrunken or abnormally compressed with elongated protrusions were prominently observed at 60-hours post-infection (Figure 4.6). These shrunken bodies were considered a consequence of apoptotic events after the measles virus infection (Lal and Rajala, 2019; Bhaskar et al., 2011).

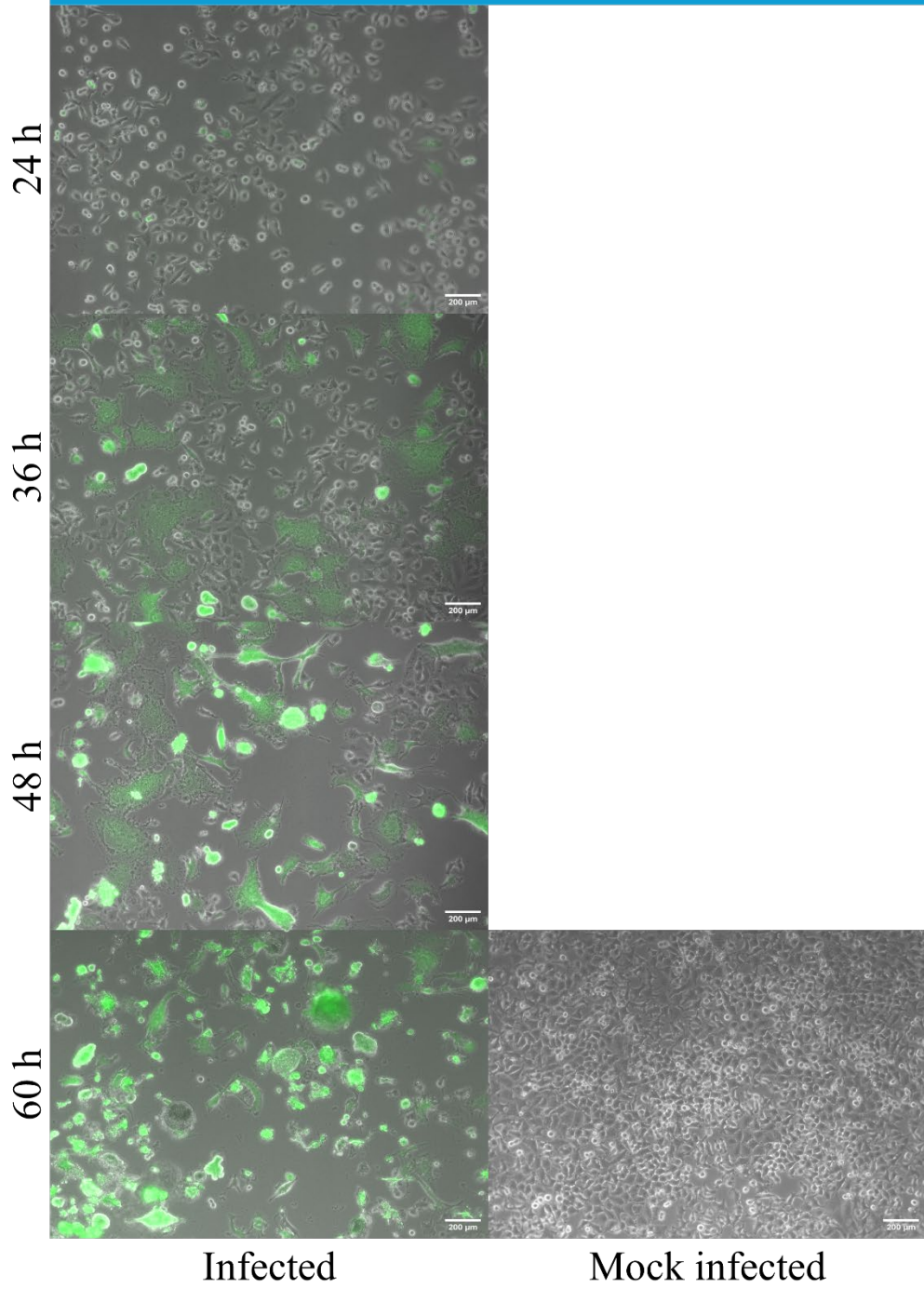


CNE-1: CR

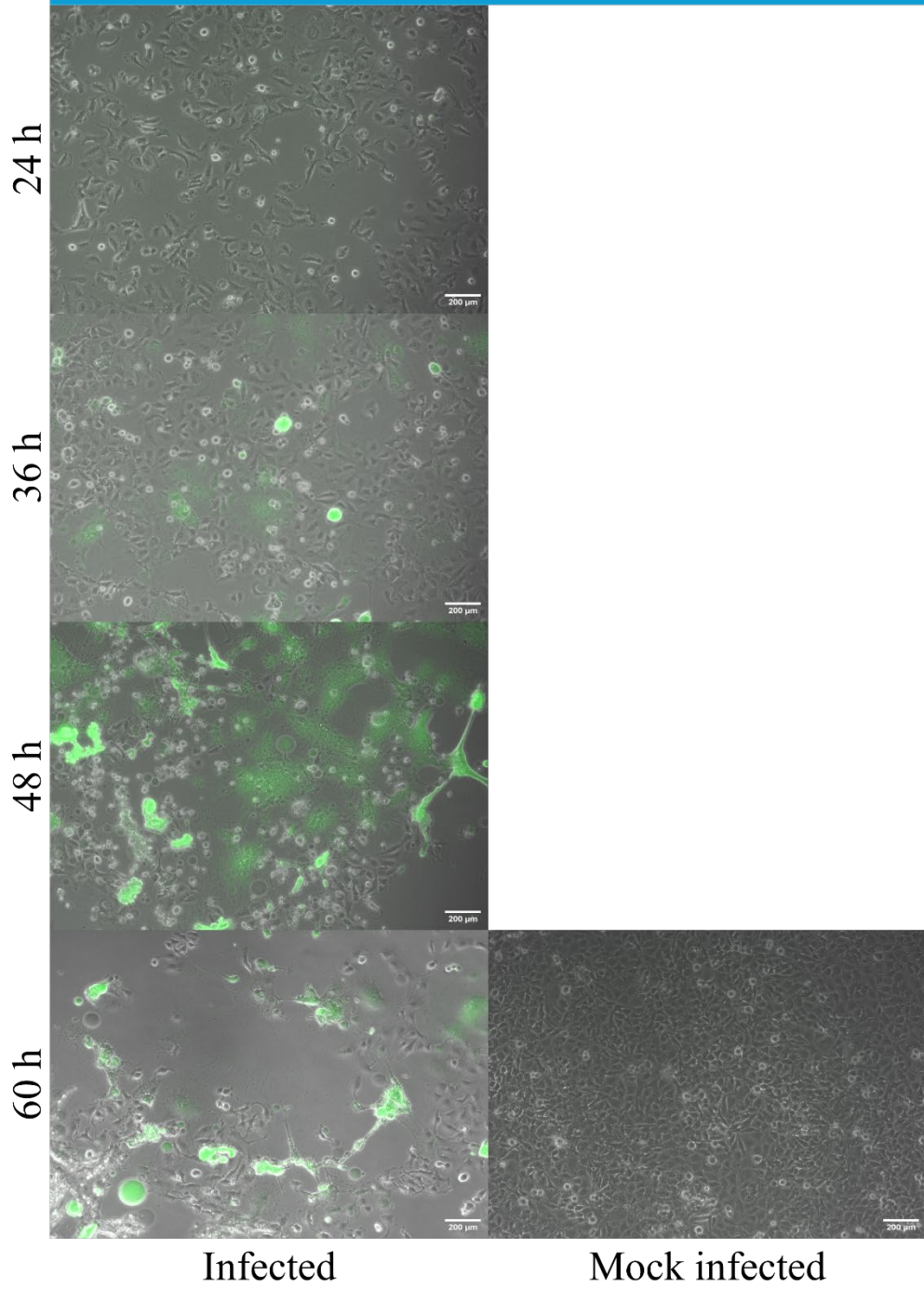


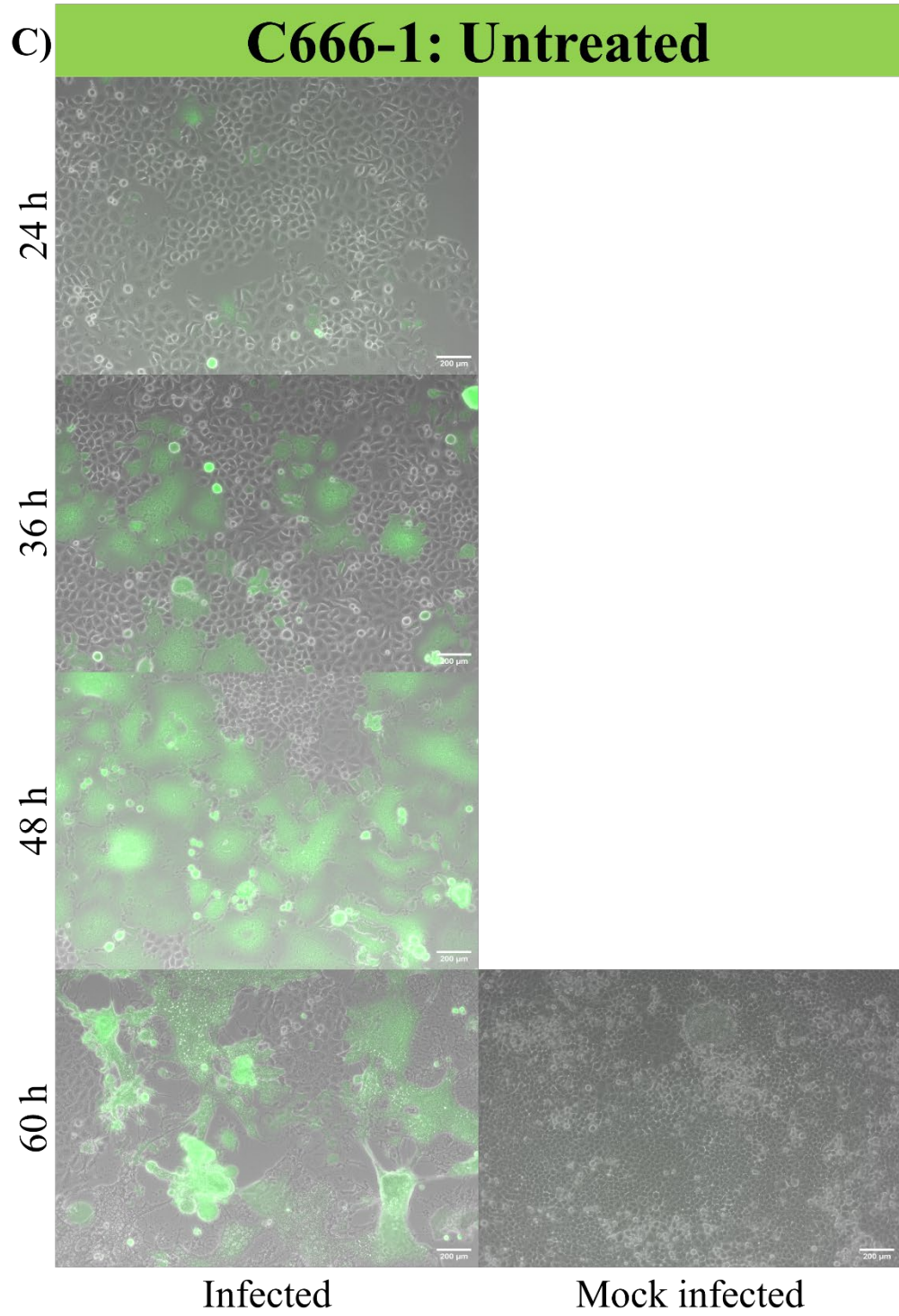


CNE-2: CR

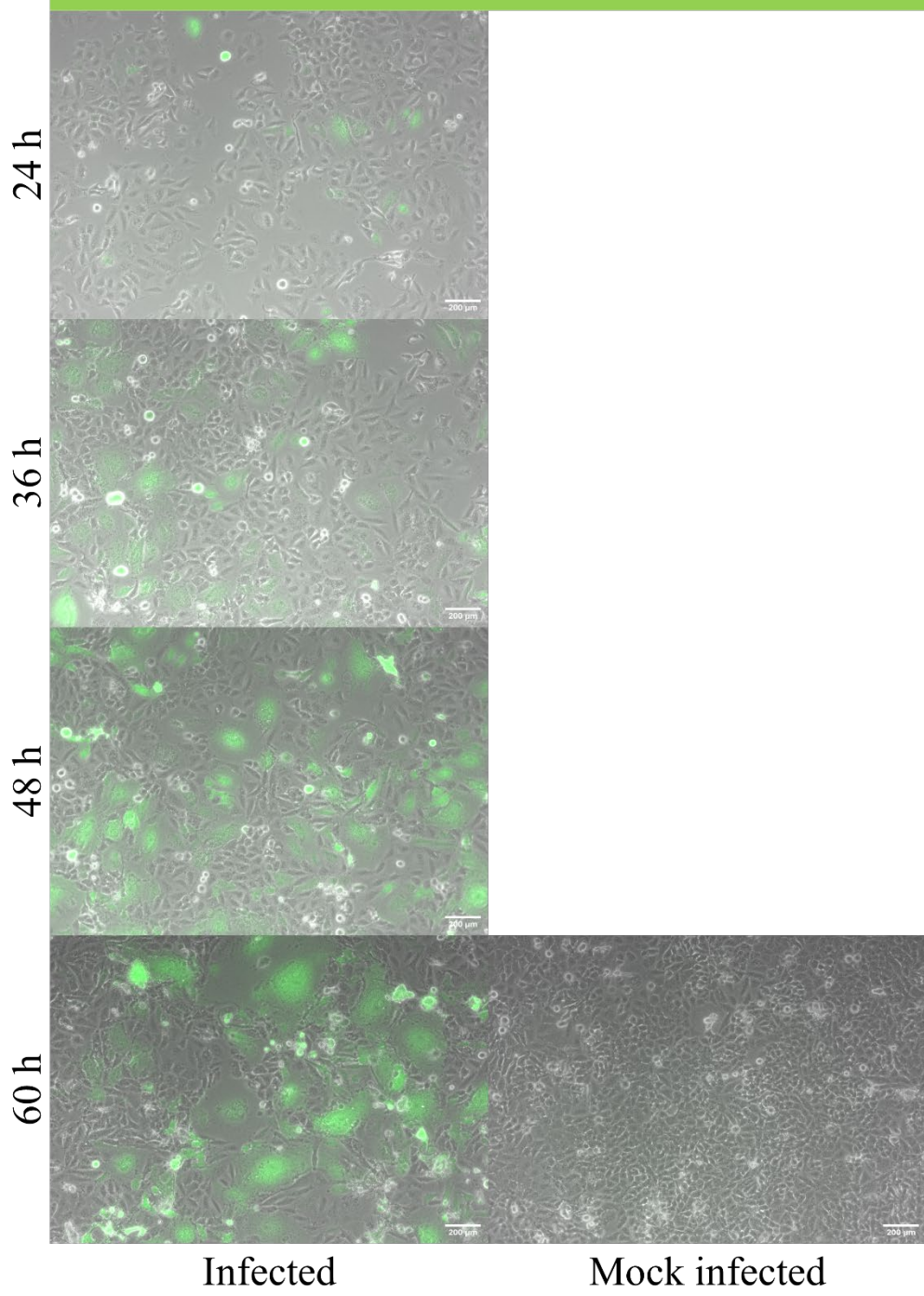


CNE-2: RR

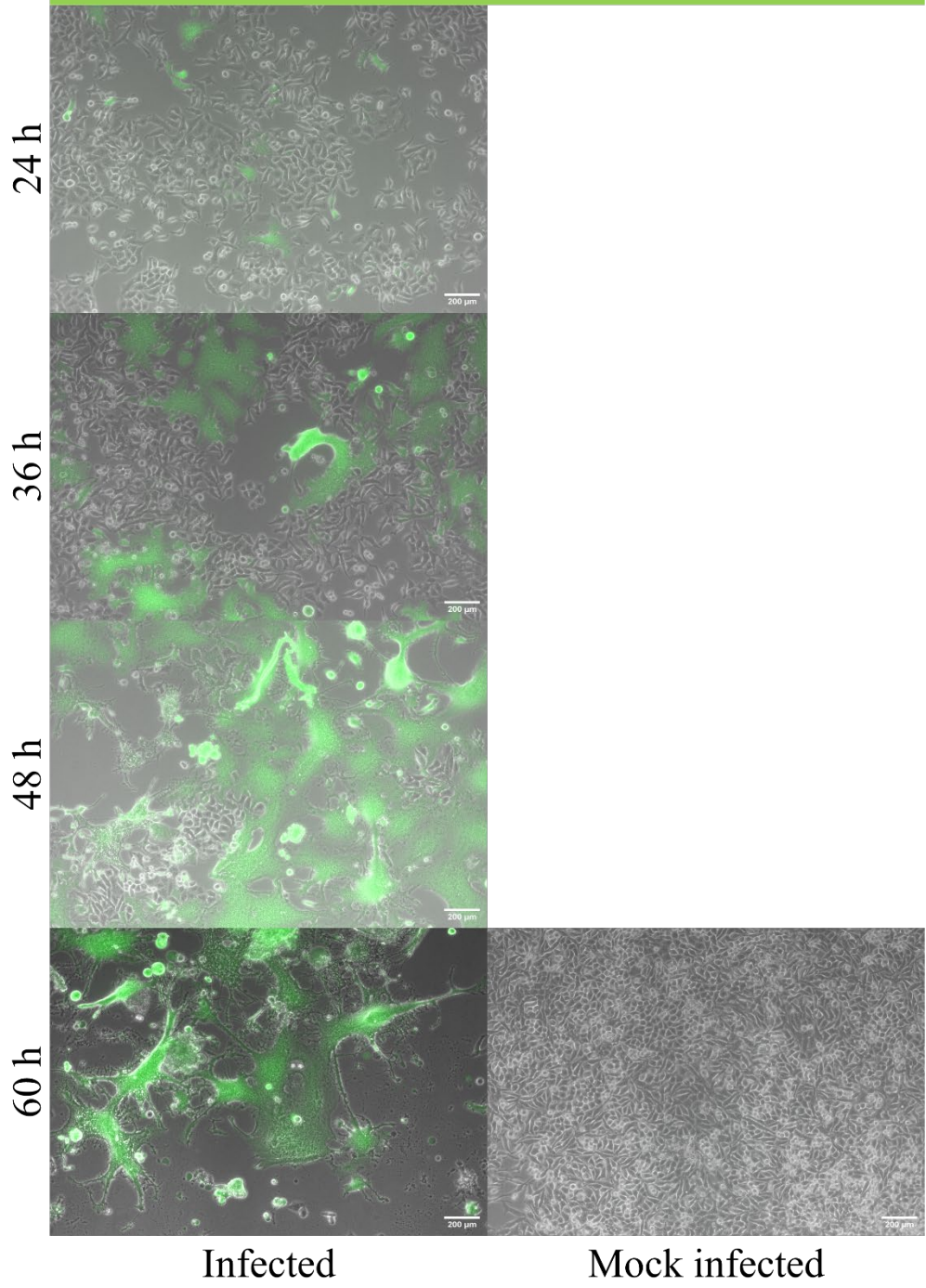


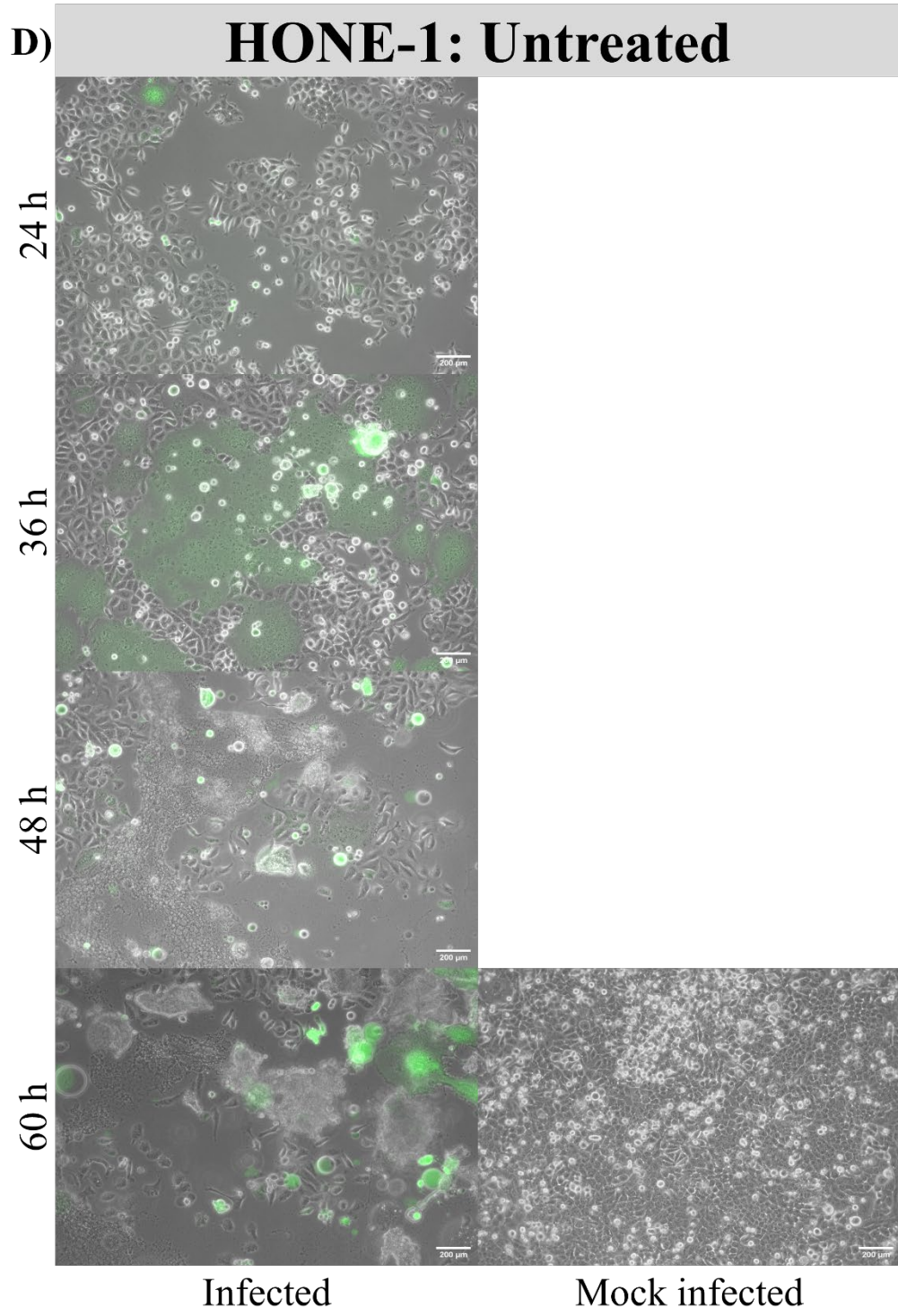


C666-1: CR



C666-1: RR





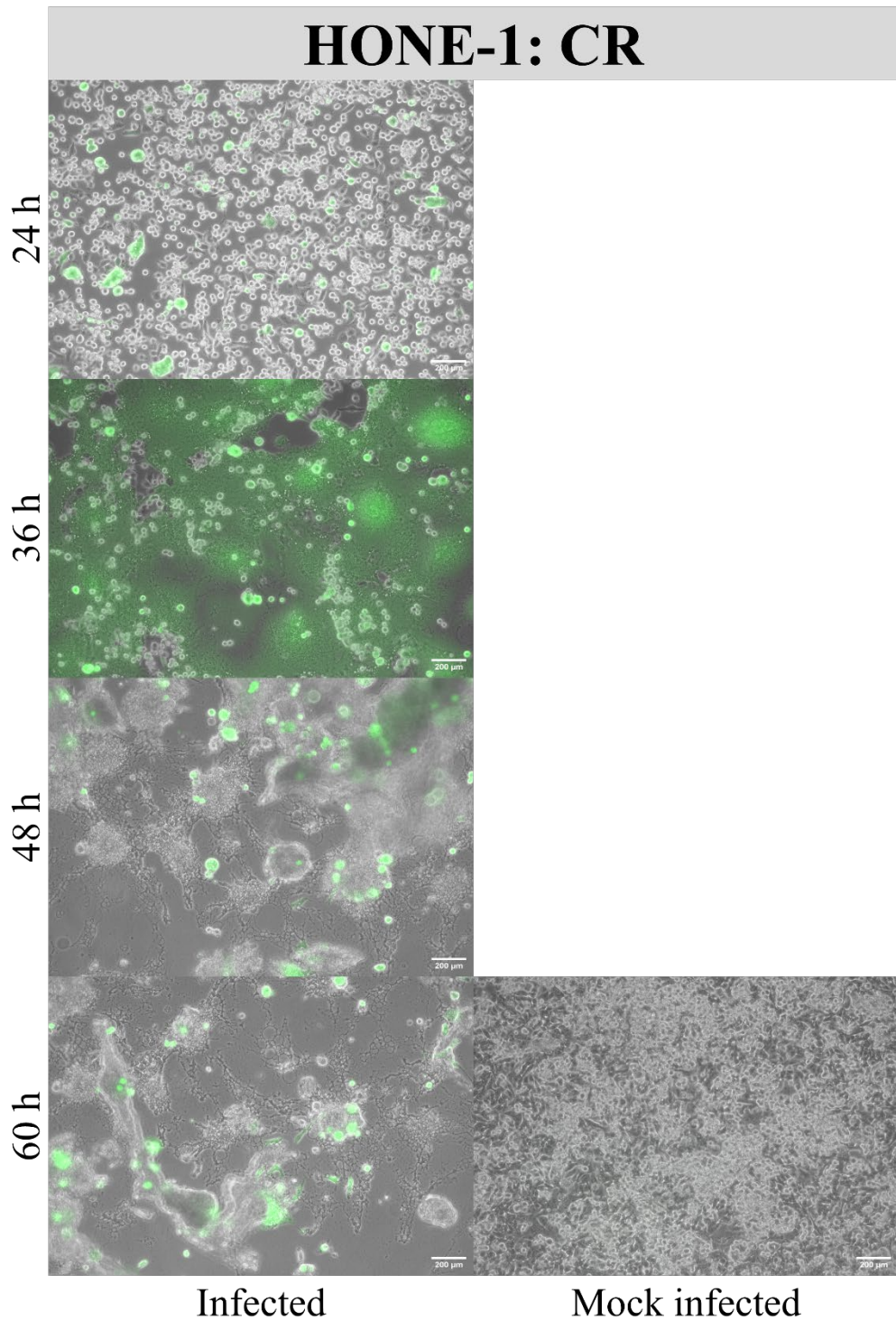
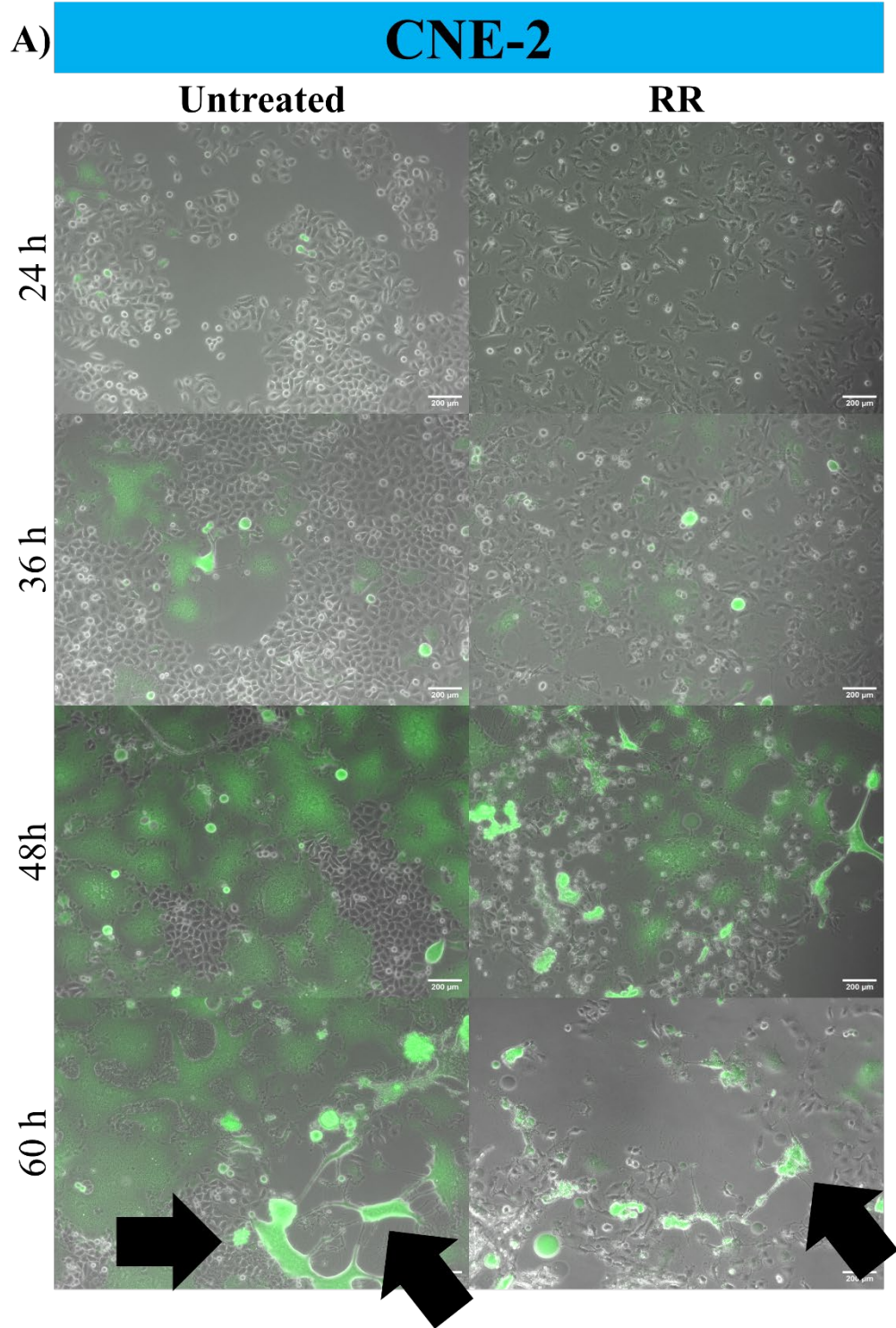


Figure 4.5: The spread of Measles-GFP-NIS infection throughout NPC cells between 36-hours p.i and 60-hours p.i., followed by shrinkage of infected bodies observable at the 60-hours timepoint (Figure 4.6) shows a successful oncolytic event.

CR – chemo-resistant; RR – radioresistant. Inset line represent 200 μ m scale bar.



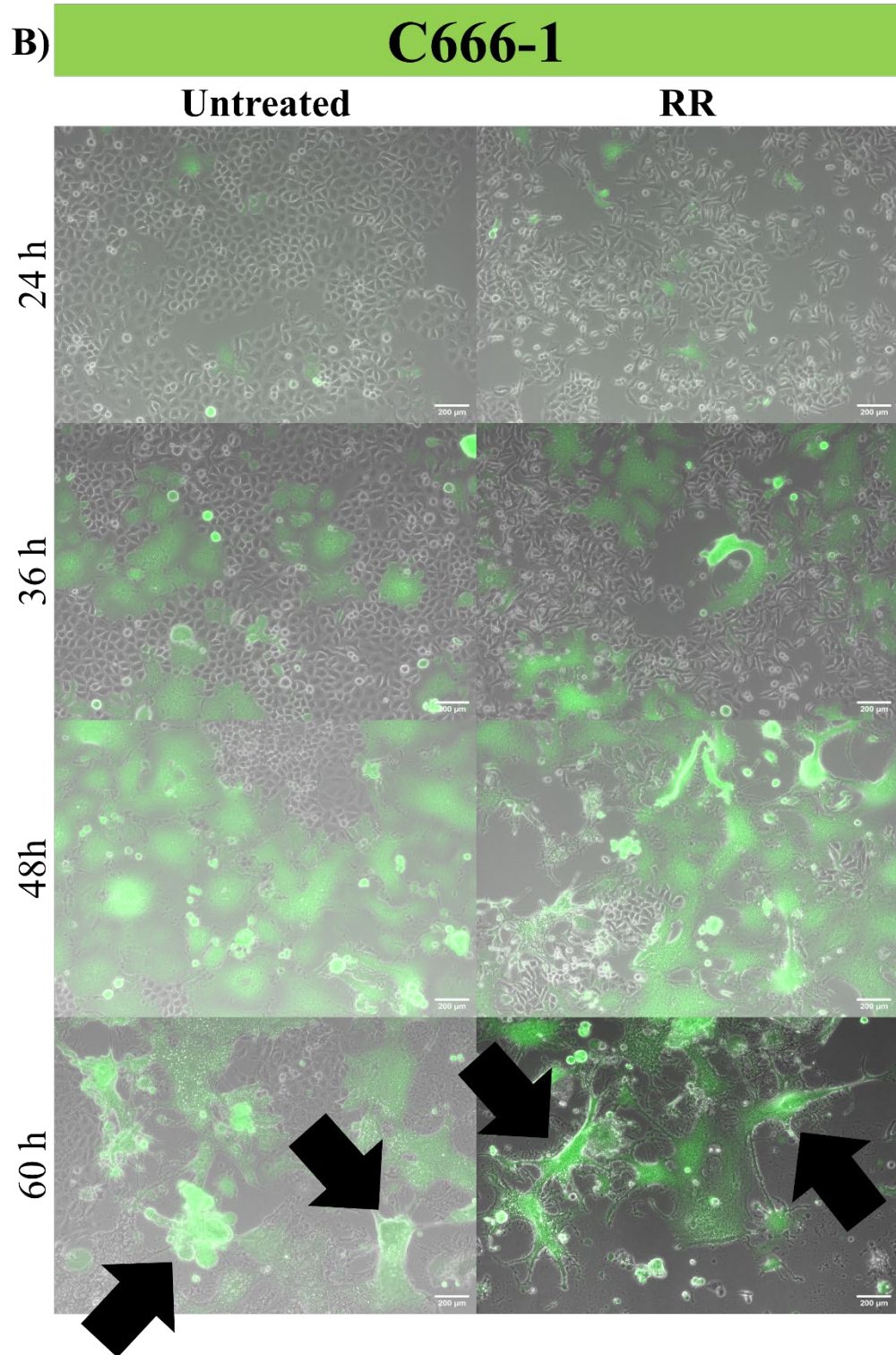


Figure 4.6: Representative fluorescence images showing typical shrinkage of cellular bodies (black arrowhead) in infected (A) CNE-2 and (B) C666-1 observed prominently at 60-hour post-infection.

CR – chemo-resistant; RR – radioresistant. Inset line represent 200 μm scale bar.

With the assumption that the empty spaces seen at 60-hours post-infection were a consequence of cell loss caused by Measles-GFP-NIS infection, presumably cell killing, we evaluated the effectiveness of Measles-GFP-NIS suppression of NPC cells using a tetrazolium-based cell viability assay to quantify viable adherent cells that remained at 60-hours post-infection. In general, at least 59% of cell loss was measured with more cells lost observed in CR- and RR-NPC compared to the untreated NPC (Figure 4.7).

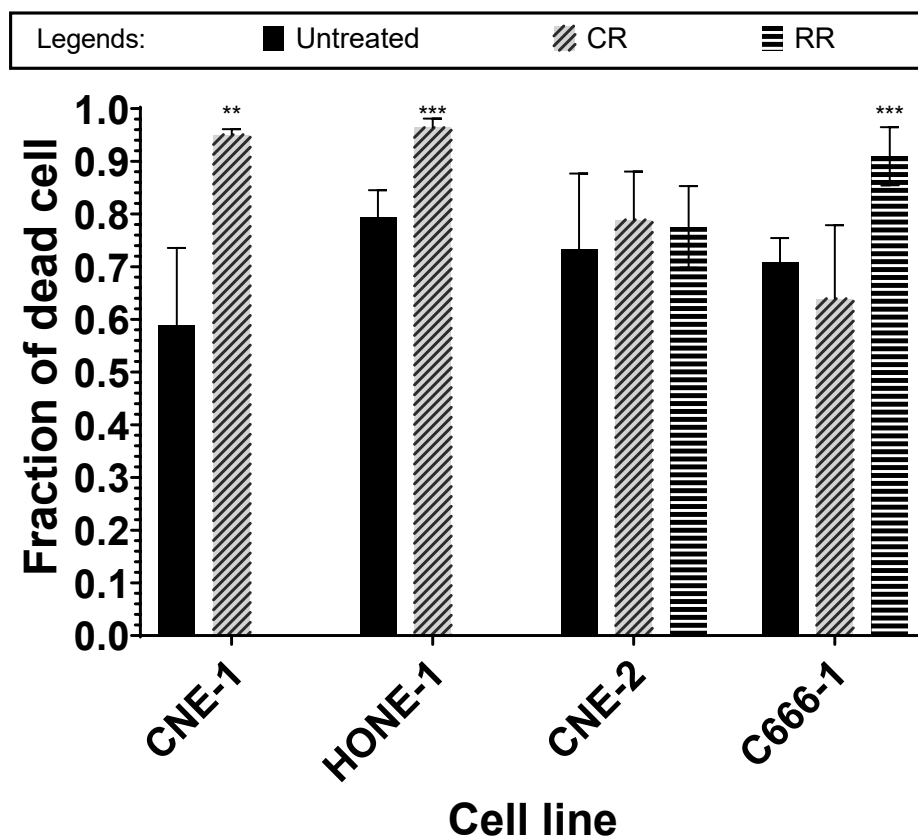


Figure 4.7: CR- and RR-NPC cells exhibit a notable increase in the proportion of dead cells following MV-GFP-NIS infection compared to untreated cells, indicating enhanced susceptibility to infection-induced cell death.

*= $p < 0.05$, **= $p < 0.001$, ***= $p < 0.001$. CR – chemo-resistant; RR – radio-resistant.

4.1.4 Conclusion

In this study, Measles-GFP-NIS successfully infected NPC cell lines expressing CD46 cell surface receptor, able to spread horizontally via the formation of syncytium, and caused more than 59 % cell loss at 60-hours post-infection. In addition, NPC cells exposed to primary cisplatin or radiation treatment were more susceptible to Measles-GFP-NIS infection, suggesting that the existing primary cancer treatments could sensitize NPC cells for oncolytic virotherapy. The infected NPC cell culture developed into “shrunk bodies” with previously occupied spaces now unoccupied appearing as early as 48-hours post-infection. At 60-hours post-infection, cell loss was maximal. Collectively, these results suggested that the oncolytic measles virus can be used to target NPC cells for oncolytic virotherapy.

4.2 Part 2: Evaluation of cell death mechanism induced by Measles-GFP-NIS in NPC cell model

4.2.1 164 genes identified with PeptideShaker tools were differentially regulated throughout 24-, 36-, and 48-hours post-infection

Quantitative proteomics was used to understand the molecular interactions and pathways that led to the death or suppression of the NPC cell line, C666-1, caused by Measles-GFP-NIS infection. The C666-1 cell line was chosen as the model cell line because it constitutively expresses the EBV genome and is biologically closer to actual NPC cells from clinical cancer patients (Cheung et al., 1999; Tsao et al., 2017).

A total of 311 proteins were identified in two sets of biological replicates via peptide spectral matches using PeptideShaker SearchGUI against X!Tandem, OMSSA, Comet, MyriMatch, and MS-GF+ databases (Vaudel et al., 2015). Identified proteins were presented with gene names for bioinformatics analysis. Relative quantification with the PeptideShaker Reporter tool revealed 164 proteins that expressed more than 1.5-fold change (FC) difference or equivalent to $\log_2FC > 0.58$ for upregulated proteins and $\log_2FC < -0.58$ for downregulated proteins (Appendix B - D).

However, the two sets of biological replicates have low overlapping differentially abundance proteins (DAP) across 24-, 36-, and 48-hours post-infection time points (Figure 4.8, Appendix B - D). The low protein overlaps can be attributed to the non-random missing of quantitative data and the inability to control Measles-GFP-NIS life cycle progression and viral dissemination across cells in culture (Luo et al., 2009). The non-random missing of quantitative data is an inherent flaw associated with the limit of detection of

mass spectrometry or due to peptide-level detection or an abundance issue (Luo et al., 2009). Although the density of C666-1 cells seeded and the MOI was fixed, it is impossible to control the rate of Measles-GFP-NIS life cycle progression, the spread of syncytia across the cell population, and to score the number of affected C666-1 cells to harvest for protein extraction. Moreover, the total proteins subjected to quantitative proteomics analysis were extracted from a population of C666-1 cells at different time points after Measles-GFP-NIS infection. The heterogeneity of expression in infected C666-1 cells across the cell population would affect the net abundance level of proteins in each replicate. Despite the flaws, protein abundance in both replicates is still representative of protein changes caused by Measles-GFP-NIS infection. Hence, data from both biological replicates were analysed collectively for downstream bioinformatics analysis to better understand the protein interactions that potentially led to the inhibition and killing of C666-1 cells after Measles-GFP-NIS infection.

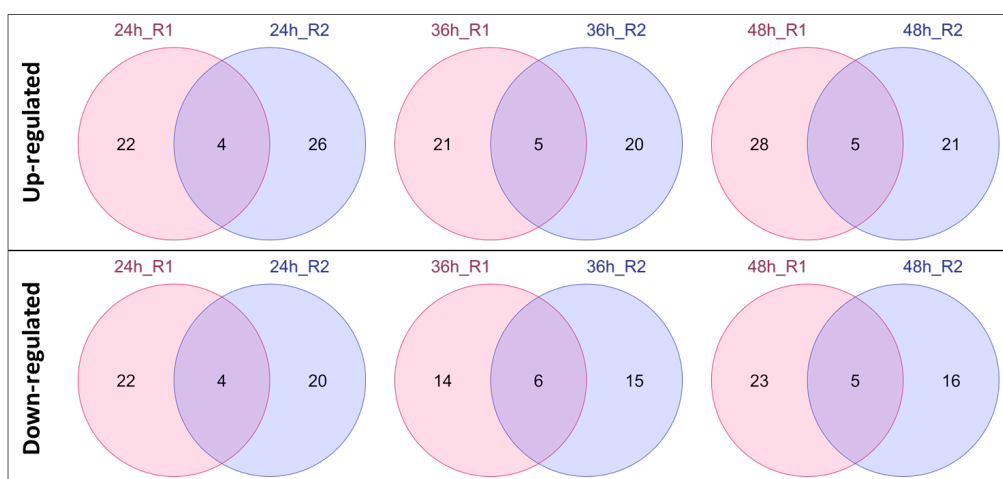


Figure 4.8: Low overlapping of DAPs between two biological replicates (R1 and R2) at 24-,36-, and 48-hours post-infection.

4.2.2 Gene Ontology (GO): cell death-associated DAPs downregulated at 24-hours p.i. but were both up- and downregulated at 48-hours p.i.

Bioinformatic tools were utilized to understand the biological processes and protein-protein interactions among the identified DAPs. GO analysis was performed with the gProfiler tool to identify the biological processes in which the DAPs were involved at each time point post-infection (Table 4.2).

Table 4.2: GO Biological Processes annotation of downregulated and upregulated genes at (A) 24-hours, (B) 36-hours, and (C) 48-hours post-infection.

A) 24-hours p.i.: Top 20 upregulated genes			24-hours p.i.: Top 20 downregulated genes		
GO term ID	GO term name	-log10 (p-value)	GO term ID	GO term name	-log10 (p-value)
GO:0044260	cellular macromolecule metabolic process	4.51	GO:1901564	organonitrogen compound metabolic process	6.22
GO:0006518	peptide metabolic process	4.33	GO:0044248	cellular catabolic process	5.49
GO:0034504	protein localization to nucleus	4.02	GO:0006950	response to stress	5.22
GO:0043603	cellular amide metabolic process	3.78	GO:0019538	protein metabolic process	5.03
GO:0002181	cytoplasmic translation	3.73	GO:0009056	catabolic process	4.81
GO:0006412	translation	3.60	GO:0042981	regulation of apoptotic process	4.52
GO:0043604	amide biosynthetic process	3.58	GO:0033554	cellular response to stress	4.43
GO:0043043	peptide biosynthetic process	3.42	GO:0043067	regulation of programmed cell death	4.40
GO:0140694	non-membrane-bounded organelle assembly	3.23	GO:0000723	telomere maintenance	4.17
GO:0042255	ribosome assembly	3.17	GO:0080134	regulation of response to stress	4.04
GO:0061077	chaperone-mediated protein folding	2.87	GO:0010941	regulation of cell death	3.80
GO:0031647	regulation of protein stability	2.72	GO:0032200	telomere organization	3.64
GO:1900180	regulation of protein localization to nucleus	2.68	GO:0051338	regulation of transferase activity	3.39
GO:0006913	nucleocytoplasmic transport	2.65	GO:0006457	protein folding	3.31
GO:0051169	nuclear transport	2.65	GO:0044093	positive regulation of molecular function	3.19
GO:1900182	positive regulation of protein localization to nucleus	2.33	GO:0043549	regulation of kinase activity	3.12
GO:0051168	nuclear export	2.30	GO:0006996	organelle organization	3.11
GO:1901564	organonitrogen compound metabolic process	2.30	GO:0044260	cellular macromolecule metabolic process	3.10
GO:0044248	cellular catabolic process	2.00	GO:0031347	regulation of defense response	3.06
GO:0006417	regulation of translation	1.99	GO:0019220	regulation of phosphate metabolic process	3.03

36-hours p.i.: Top 20 upregulated genes			36-hours p.i.: Top 20 downregulated genes		
GO term ID	GO term name	-log10 (p-value)	GO term ID	GO term name	-log10 (p-value)
GO:0034504	protein localization to nucleus	8.33	No data available		
GO:0033365	protein localization to organelle	7.61			
GO:1900180	regulation of protein localization to nucleus	5.86			
GO:1900182	positive regulation of protein localization to nucleus	5.73			
GO:0044260	cellular macromolecule metabolic process	5.51			
GO:0006412	translation	5.10			
GO:0043604	amide biosynthetic process	5.06			
GO:0043043	peptide biosynthetic process	4.90			
GO:0000226	microtubule cytoskeleton organization	4.71			
GO:0060341	regulation of cellular localization	4.69			
GO:0051641	cellular localization	4.58			
GO:0006457	protein folding	4.48			
GO:0032880	regulation of protein localization	4.35			
GO:0051246	regulation of protein metabolic process	4.30			
GO:0006404	RNA import into nucleus	4.16			
GO:0006913	nucleocytoplasmic transport	4.16			
GO:0051169	nuclear transport	4.16			
GO:0006996	organelle organization	3.93			
GO:0006518	peptide metabolic process	3.92			
GO:0007017	microtubule-based process	3.89			

48-hours p.i.: Top 20 upregulated genes			48-hours p.i.: Top 20 downregulated genes		
GO term ID	GO term name	-log10 (p-value)	GO term ID	GO term name	-log10 (p-value)
GO:1901564	organonitrogen compound metabolic process	8.97	GO:0006457	protein folding	3.51
GO:0044260	cellular macromolecule metabolic process	6.31	GO:0042981	regulation of apoptotic process	3.21
GO:0043604	amide biosynthetic process	6.18	GO:0043067	regulation of programmed cell death	3.11
GO:0019538	protein metabolic process	5.71	GO:0007005	mitochondrion organization	2.89
GO:0006412	translation	5.32	GO:0010941	regulation of cell death	2.59
GO:0043603	cellular amide metabolic process	5.24	GO:0002491	antigen processing and presentation of endogenous peptide antigen via MHC class II	2.13
GO:1901566	organonitrogen compound biosynthetic process	5.11	GO:0002469	myeloid dendritic cell antigen processing and presentation	2.13
GO:0043043	peptide biosynthetic process	5.11	GO:0065008	regulation of biological quality	2.01
GO:0006518	peptide metabolic process	4.99	GO:0043066	negative regulation of apoptotic process	1.98
GO:0072521	purine-containing compound metabolic process	4.08	GO:0002396	MHC protein complex assembly	1.96
GO:0042981	regulation of apoptotic process	4.02	GO:0002501	peptide antigen assembly with MHC protein complex	1.96
GO:0006457	protein folding	3.98	GO:0043069	negative regulation of programmed cell death	1.89
GO:0043067	regulation of programmed cell death	3.89	GO:0006915	apoptotic process	1.85
GO:0055086	nucleobase-containing small molecule metabolic process	3.78	GO:0009893	positive regulation of metabolic process	1.79
GO:0033554	cellular response to stress	3.70	GO:0006518	peptide metabolic process	1.78
GO:0080134	regulation of response to stress	3.62	GO:0006412	translation	1.73
GO:0044271	cellular nitrogen compound biosynthetic process	3.57	GO:0012501	programmed cell death	1.71
GO:0009150	purine ribonucleotide metabolic process	3.54	GO:0019538	protein metabolic process	1.71
GO:1901576	organic substance biosynthetic process	3.49	GO:0009056	catabolic process	1.60
GO:0051168	nuclear export	3.46	GO:0043043	peptide biosynthetic process	1.59

All identified biological processes were significant ($p < 0.05$).

Biological processes related to metabolism and biosynthesis were consistently upregulated at 24-hours, 36-hours, and 48-hours post-infection (Table 4.2A-C). Genes related to cell death processes were downregulated at 24-hours post-infection (Table 4.2A). This observation is not surprising since oncolytic measles viruses are known to inhibit host cell death to favour viral replication and progenies production at early infection (Cruz et al., 2006; Mao Xia et al., 2014). However, genes related to cell death processes were both upregulated and downregulated at 48-hours post-infection, an observation considered to be unusual (Table 4.2C and Table 4.3).

Table 4.3: Different DAPs related to cell death processes were (A) upregulated and (B) downregulated at 48-hours post-infection.

A) Upregulated DAPs related to cell death processes at 48-hours post-infection

intersecting genes	term id	term name	-log10(p-value)
TFRC HMGB1 ENO1 TOMM22 LGALS1 RUVBL1 ANXA2 H2AFZ SARNP USP14 GANAB PGK1 SF3A1 IDH1 DNAJA1 GLOD4 SERBP1	GO:0042981	regulation of apoptotic process	4.02
TFRC HMGB1 ENO1 TOMM22 LGALS1 RUVBL1 ANXA2 H2AFZ SARNP USP14 GANAB PGK1 SF3A1 IDH1 DNAJA1 GLOD4 SERBP1	GO:0043067	regulation of programmed cell death	3.89
HMGB1 ENO1 RUVBL1 NCL SARNP DLD USP14 GANAB PRDX4 LMNA PGK1 PACSIN2 HSPA8 SF3A1 XRCC6 IDH1 DNAJA1 GLOD4 SERBP1	GO:0033554	cellular response to stress	3.70
HMGB1 ENO1 LGALS1 RUVBL1 MBNL2 NME2 SARNP DLD USP14 GANAB HSPA8 SF3A1 XRCC6 IDH1 GLOD4 SERBP1	GO:0080134	regulation of response to stress	3.62

B) Downregulated DAPs related to cell death processes at 48-hours post-infection

intersecting genes	term id	term name	-log10(p-value)
GPI HSPB1 PHB2 PCBP2 RPS12 BCAP31 HSP90AA1 TIMM44 KRT10 HSPE1 CDC37 UQCRC2 CALR HLA-DRB1	GO:0042981	regulation of apoptotic process	3.21
GPI HSPB1 PHB2 PCBP2 RPS12 BCAP31 HSP90AA1 TIMM44 KRT10 HSPE1 CDC37 UQCRC2 CALR HLA-DRB1	GO:0043067	regulation of programmed cell death	3.11
GPI HSPB1 PHB2 PCBP2 RPS12 BCAP31 HSP90AA1 TIMM44 KRT10 HSPE1 CDC37 UQCRC2 CALR HLA-DRB1	GO:0010941	regulation of cell death	2.59
PSME1 SLC25A5	GO:0002491	antigen processing and presentation of endogenous peptide antigen via MHC class II	2.13
PSME1 SLC25A5	GO:0002469	myeloid dendritic cell antigen processing and presentation	2.13
GPI HSPB1 PHB2 PCBP2 TIMM44 KRT10 HSPE1 CDC37 CALR HLA-DRB1	GO:0043066	negative regulation of apoptotic process	1.98
GPI HSPB1 PHB2 PCBP2 TIMM44 KRT10 HSPE1 CDC37 CALR HLA-DRB1	GO:0043069	negative regulation of programmed cell death	1.89
GPI HSPB1 PHB2 PCBP2 RPS12 BCAP31 HSP90AA1 TIMM44 KRT10 HSPE1 CDC37 UQCRC2 CALR HLA-DRB1	GO:0006915	apoptotic process	1.85
GPI HSPB1 PHB2 PCBP2 RPS12 BCAP31 HSP90AA1 TIMM44 KRT10 HSPE1 CDC37 UQCRC2 CALR HLA-DRB1	GO:0012501	programmed cell death	1.71
GPI HNRNPJ HSPB1 RPL10A PHB2 SYNCRIP PCBP1 HADH RPS12 BCAP31 HSP90AA1 TIMM44 RPS3A SOD2 HSPE1 SND1 KRT19 SUBL1 ALB HLA-DRA MYH9 RPS20 UQCRC2 SLC25A5	GO:0019538	protein metabolic process	1.71
GPI HSPB1 PHB2 PCBP2 TIMM44 KRT10 HSPE1 CDC37 CALR HLA-DRB1	GO:0060548	negative regulation of cell death	1.49
HSPB1 HSP90AA1 KRT10	GO:1902175	regulation of oxidative stress-induced intrinsic apoptotic signaling pathway	1.32
GPI HSPB1 PHB2 PCBP2 RPS12 BCAP31 HSP90AA1 TIMM44 KRT10 HSPE1 CDC37 UQCRC2 CALR HLA-DRB1	GO:0008219	cell death	1.31

All identified biological processes were significant ($p < 0.05$).

Based on the microscopy data in Figure 4.6, the presence of shrunken bodies starts to be observable as early as 48-hours post-infection, indicating the timepoint where the culture potentially started losing cells because of Measles-

GFP-NIS infection. Assuming Measles-GFP-NIS does kill C666-1 cells, essential proteins that drive the signalling cascade in the regulated cell death pathway, for example, caspases for apoptosis or mixed lineage kinase domain-like (MLKL) protein for necroptosis, should be expressed by 48-hours post-infection followed by loss of cells that continues beyond 60-hours post-infection (Tang et al., 2019). However, these pathway-specific essential proteins were not identified in all three post-infection time points within the dataset in this study (Table 4.2, Appendix E - G).

4.2.3 KEGG: pathways not related to regulated cell death were differentially regulated at 48-hours p.i.

KEGG analysis was performed using the gProfiler tool to map all DAP to elucidate pathways that were differentially regulated at 48-hours post-infection. KEGG is the only publicly available bioinformatic database that has mapped the most pathways related to cell death, including pathways in p53 signalling, senescence, apoptosis, necroptosis, ferroptosis, mitophagy, and autophagy. The result revealed that none of the DAPs shortlisted in Table 4.4 matched any of the cell death-related pathways in KEGG (Appendix H and I). In addition, Table 4.4A shows the matching of upregulated proteins at 48-hours post-infection to pathways related to cellular metabolism and biosynthesis, which agreed with the biological processes annotation from GO analysis discussed in the Section 4.2.2 above.

Table 4.4: KEGG analysis showing that pathways related to cellular metabolism and biosynthesis but not regulated cell death were (A) upregulated and (B) downregulated at 48-hours post-infection.

A) 48-hours p.i.: Upregulated DAP

intersecting genes	term id	term name	-log ₁₀ (p-value)
ENO1 DLAT RPS13 MCM5 LMNA	KEGG:00010	Glycolysis / Gluconeogenesis	2.87
ENO1 DLAT RPS13 MCM5 LMNA NPM1	KEGG:01200	Carbon metabolism	2.84
USP14 HSPA8 XRCC6	KEGG:03450	Non-homologous end-joining	2.62
AK2 PACIN2 IDH1 DNAJA1 GLOD4 SERBP1	KEGG:04141	Protein processing in endoplasmic reticulum	1.90
DLAT MCM5 NPM1	KEGG:00020	Citrate cycle (TCA cycle)	1.50
ENO1 RPS13 LMNA NPM1	KEGG:01230	Biosynthesis of amino acids	1.45

B) 48-hours p.i.: Downregulated DAP

intersecting genes	term id	term name	-log ₁₀ (p-value)
BCAP31 ALB MYH9 UQCRC2 SLC25A5	KEGG:04612	Antigen processing and presentation	3.10
RPS3A EEF1A1 MYH9 SLC25A5	KEGG:05150	Staphylococcus aureus infection	1.41

All identified KEGG pathways were significant ($p < 0.05$).

4.2.4 DAP matches protein complexes with protein production and metabolism function

Analysis done in Section 4.2.1 to 4.2.3 focussed on identifying crucial proteins that pre-destined infected C666-1 towards death within small subsets of DAP grouped according to time points. Protein functional analysis with GO biological processes annotation in Section 4.2.2 shows abnormal differential regulation of proteins related to cell death processes. In addition, pathway analysis (Section 4.2.3) on DAP at 48-hours post-infection did not match any pathway in the KEGG database with cell death.

Proteins are known to form multi-protein complexes to serve various signalling and effector functions (Cebecauer et al., 2010). To avoid the possibility of missing out on DAPs that might be involved in forming protein complexes, analysis was performed on two main and larger groupings, upregulated and downregulated DAPs. The MCODE tool was designed to identify potential clusters of proteins that might be functional as protein complexes based on the interaction data mined from bioinformatic repositories (Bader and Hogue, 2003). Subsequently, the shortlisted DAP gene names were matched to the experimentally curated protein complex database, CORUM, to validate the protein complex function identified with the MCODE tool (Giurgiu et al., 2019). The CORUM database was manually searched with keywords related to cell death and any of the regulated cell death mechanisms to ensure that protein complexes related to cell death did exist within the database (Appendix J - P).

The MCODE analysis performed on upregulated DAP identified twenty-eight proteins with a clustering score of 25.333 (Figure 4.9). Based on FunCat annotation, proteins within the identified cluster did not match any protein complexes that play a role in cell death within the CORUM database (Table 4.5). The results in Table 4.5 showed protein complexes that serve protein biosynthesis, signalling and transport. MCODE analysis on downregulated DAP resulted in a cluster of eighteen proteins with a clustering score of 16.824 (Figure 4.10). Annotation from the CORUM database showed that these identified clusters of proteins matched protein complexes that serve protein biosynthesis, metabolism, and signalling (Table 4.6) and did not match any protein complexes that play a role in cell death.

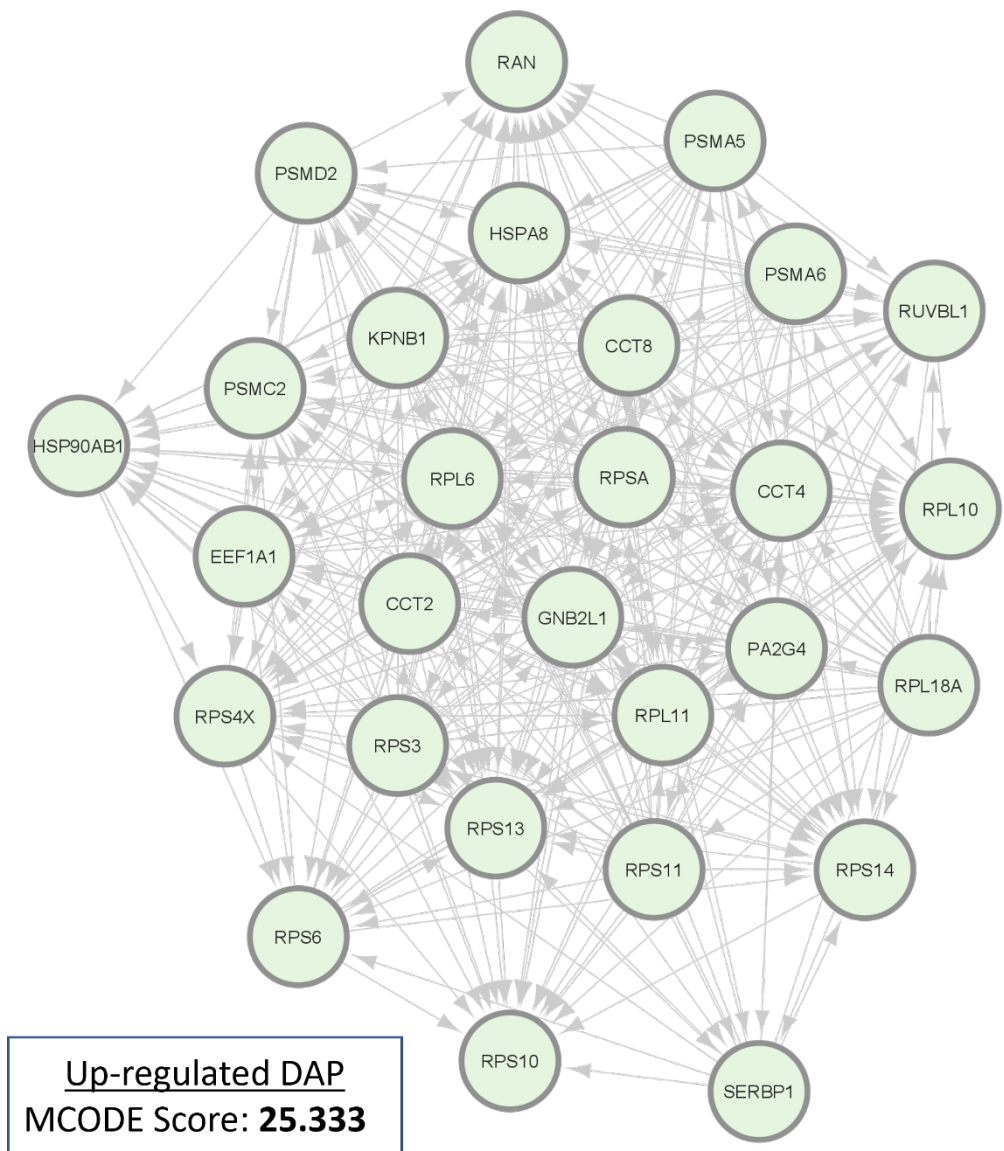


Figure 4.9: Upregulated DAPs cluster identified with MCODE cut-off score ≥ 6.0 .

Table 4.5: Upregulated DAP MCODE clusters validated with the CORUM database.

Intersecting genes	FunCat	CORUM ID	CORUM term name	-log ₁₀ (p-value)
RPL10 RPL11 RPL6 RPS4X RPS14 RPL18A RPS3 RPS11 RPS10 RPS13 RPS6 RPSA	12 PROTEIN SYNTHESIS	CORUM:306	Ribosome, cytoplasmic	11.44
RPS4X RPS14 RPS3 RPS11 RPS10 RPS13 RPS6 RPSA	12 PROTEIN SYNTHESIS	CORUM:338	40S ribosomal subunit, cytoplasmic	8.63
RPS4X RPS14 RPS3 RPS11 RPS10 RPS13 RPS6 RPSA	12 PROTEIN SYNTHESIS	CORUM:305	40S ribosomal subunit, cytoplasmic	8.37
RPL10 RPL11 RPL6 RPS14 RPL18A RPS11 RPS13 RPS6 GNB2L1	12 PROTEIN SYNTHESIS	CORUM:3055	Nop56p-associated pre-rRNA complex	5.71
HSP90AB1 RPL6 RPS11 RPS13	30 CELLULAR COMMUNICATION/SIGNAL TRANSDUCTION MECHANISM	CORUM:5266	TNF-alpha/NF-kappa B signaling complex 6	3.33
CCT8 CCT4 CCT2	14 PROTEIN FATE (folding, modification, destination)	CORUM:126	CCT complex (chaperonin containing TCP1 complex)	2.23
CCT8 CCT4 CCT2	Data not available	CORUM:6247	BBS-chaperonin complex	1.90
SERBP1 RAN	70 SUBCELLULAR LOCALIZATION	CORUM:6143	KPNB1-RAN complex	1.78
PSMD2 EEF1A1 PSMA5 PSMA6	14 PROTEIN FATE (folding, modification, destination)	CORUM:193	PA700-20S-PA28 complex	1.62
SERBP1 RAN	20 CELLULAR TRANSPORT, TRANSPORT FACILITIES AND TRANSPORT ROUTES	CORUM:1554	RANBP1-RAN-KPNB1 complex	1.30

MCODE Cluster score 25.333

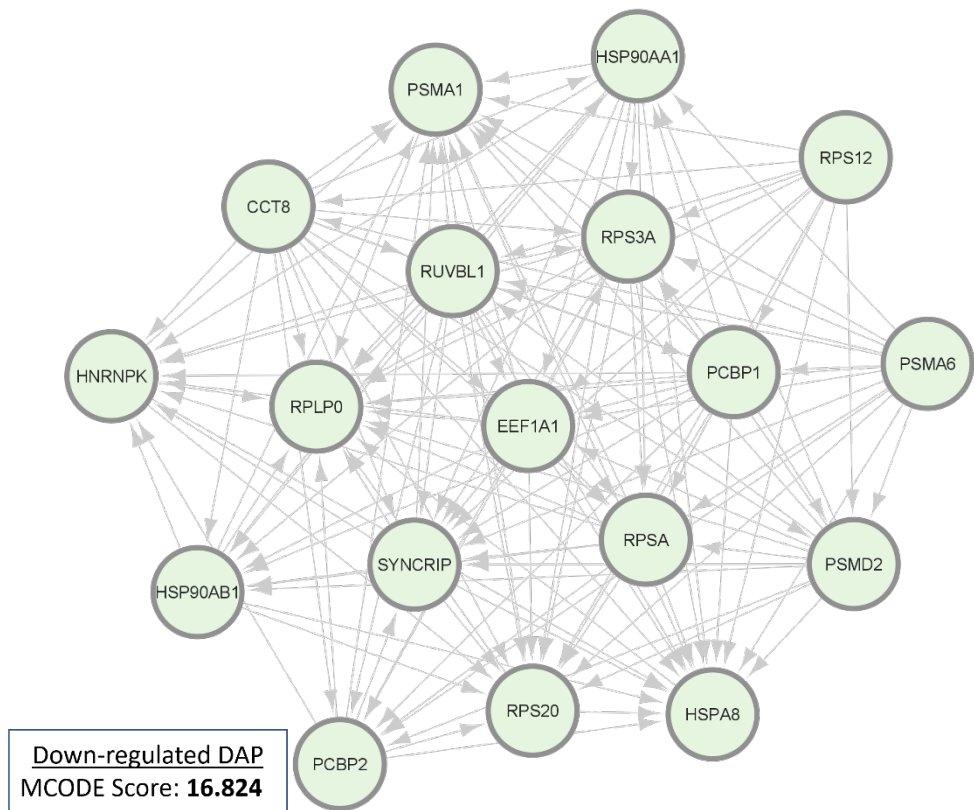


Figure 4.10: Downregulated DAPs cluster identified with MCODE cut-off score ≥ 6.0 .

Table 4.6: Downregulated DAP MCODE cluster validated with CORUM database.

Intersecting genes	FunCat	CORUM ID	CORUM term name	-log10(p-value)
HSP90AA1 HSP90AB1	18 REGULATION OF METABOLISM AND PROTEIN FUNCTION	CORUM:2112	CDC37-HSP90AA1-HSP90AB1-MAP3K11 complex	1.52
RPLP0 RPSA RPS3A PCBP2	12 PROTEIN SYNTHESIS	CORUM:306	Ribosome, cytoplasmic	1.32
SYNCRIP HNRNPK	14 PROTEIN FATE (folding, modification, destination)	CORUM:5209	Ubiquilin-proteasome complex	1.30
HSP90AA1 HSP90AB1	30 CELLULAR COMMUNICATION/SIGNAL TRANSDUCTION MECHANISM	CORUM:5234	IKBKB-CDC37-KIAA1967-HSP90AB1-HSP90AA1 complex	1.30

MCODE Cluster score 16.824

4.2.5 Review of possible anti-cancer effect induced by oncolytic measles virus

Bioinformatics tools were used to elucidate the possible cell death mechanism induced by the oncolytic measles virus. However, data from GO and KEGG analyses did not identify any essential proteins belonging to any of the regulated cell death pathways, while accessory proteins related to cell death processes were unusually up- and downregulated at 48-hours post-infection at the same time. Moreover, protein complex analysis did not identify potential protein clusters that might contribute to cell death signalling and the data agreed with the results from the GO analysis that indicated that the proteins that serve protein synthesis and metabolism functions were generally upregulated across the three post-infection time points. Collectively, the data suggested that regulated cell death pathways were not activated or expressed at 48-hours post-infection although fluorescence microscopy data in Figure 4.5 showed that infected NPC cell cultures started losing cells while the shrunken bodies of cells started to form at 48-hours post-infection.

Experimental observations described in Section 4.1.1 to 4.1.3 showed that Measles-GFP-NIS infection does cause apparent and major cell loss beyond 48-hours post-infection. However, *in silico* bioinformatics analysis of quantitative proteomics results in Sections 4.2.1 to 4.2.4 suggests the possibility that the regulated cell death pathway is not activated at the time point where cell loss becomes observable. Of note, the annotation from GO biological processes did reveal contradicting and unusual differential regulation of proteins that are accessory or non-essential to the regulated cell death pathway, especially at 48-hours post-infection. Results from KEGG, GO, and CORUM protein complex

analysis strengthened the possibility that the usual regulated cell death pathway was not activated in this study. Hence, a more in-depth literature search was conducted.

4.2.5.1 Recent research publication shows that the measles virus does not cause direct death of infected cells

Some viruses are capable of egress without lysing or killing their host cells (Appendix Q) via a secretory autophagosome, exosome, microvesicle, or cell-to-cell contact via protrusion (Owusu et al., 2021). Enveloped viruses, in general, can utilize the host cell's endosomal sorting complexes required for transport (ESCRT) machinery to egress by budding without causing damage to the lipid bilayer membrane of the host cell (Welsch et al., 2007). Of note, the measles virus does not utilize host cell machinery for egress like other enveloped viruses (Appendix R). The interactions between measles matrix (M), ribonucleoprotein (RNP), fusion (F), and haemagglutinin (H) proteins can package virion progeny and egress by budding off the host cell (Gonçalves Carneiro, 2017). This was further supported by two research groups reporting that both wild-type and vaccine strains do not kill infected primary airway epithelial cells (Wen-Hsuan et al., 2021; Hippee et al., 2021).

Hippee et al. (2021) found that human airway epithelial (HAE) cells that were infected with wt-MV did not express caspase 3 after 3-, 7-, 10-, and 14-days post-infection, suggesting that measles virus infection in epithelial cells was non-apoptotic in nature. The author further described that the infection centre or the syncytium progressively detached from the adherent epithelial

layer remained viable after detachment and retained the infectious capacity to initiate secondary infections in macrophages.

Wen-Hsuan et al. (2021) provided microscopic and morphological evidence that the measles virus syncytia developed on infected macaque tracheal epithelial cells remained viable after detachment. The authors further noted that both wt-MV and the vaccine-strain Edmonston-Zagreb measles virus were capable of infecting macaque tracheal epithelial cells from both apical and basolateral surfaces of a tissue layer. However, the apical infection eventually resulted in the shedding of apical cells, while the basolateral infection resulted in the horizontal cell-to-cell spreading of viral particles before the infection spread upward to the apical cell layer. Therefore, both publications provided sufficient evidence that measles virus infection, caused by both wild-type and vaccine strains, does not kill infected epithelial cells.

4.2.5.2 Indirect tumour cell clearance or killing after oMV infection

The effectiveness of oncolytic measles virotherapy has been extensively studied and demonstrated in various clinical trials (Msaouel et al., 2017). Despite several studies that reported killing of cancer cells by variants of oncolytic measles virus, such as Mao Xia et al. (2014), Abdullah et al. (2020), and Wang et al. (2015), the findings by Hippee et al. (2021) and Wen-Hsuan et al. (2021) raised a new question on how oncolytic measles virotherapy was able to clear or remove infected tumour cells *in vivo* without direct killing via the cell death pathway that involves molecular signalling or cascades (Abdullah et al., 2020; Wang et al., 2015; Mao Xia et al., 2014).

Mao Xia and coworkers suggested that oMV possibly kills NSCLC cells via necrosis (Mao Xia et al., 2014). Their work shows that caspase-3, a key effector protein of the caspase pathway responsible for apoptosis, was suppressed in lung cancer cell lines after oncolytic measles virus infection. Their finding shows that mitophagy plays a role in suppressing caspase-3 expression after oMV infection. Their data have shown that inhibitors of receptor-interacting protein kinase 1 (RIPK1), a key regulatory protein that initiates the necroptosis pathway, fail to “kill” the infected lung cancer cells, and concluded oMV does not kill by apoptosis or necroptosis. They do find a correlation between ATP exhaustion and release of high mobility group box 1 (HMGB1), which was associated with necrosis when their publication was published, after 48-hours of post-infection. Hence, Mao Xia and co-workers concluded that oMV kills lung cancer cell lines via necrosis. To date, no methodology can accurately distinguish apoptotic and necrotic phenotypes of presumed dying cells. The commonly adopted method to distinguish necrotic cells is the double-staining phosphatidylserine protein and propidium iodide (Crowley et al., 2016; Hu et al., 2021). Staining of membrane protein phosphatidylserine, which is located intracellularly in healthy cells, is possible only when it is exposed to the extracellular environment due to the process that leads to cell death. Hence, a marker indication death of cells. However, staining of phosphatidylserine alone does not discriminate between necrosis from apoptosis. While necrosis leads to rupture of the lipid bilayer membrane and exposes phosphatidylserine to the extracellular environment, activation of apoptosis leads to activation of scramblase and redistributed phosphatidylserine from the intracellular layer of the lipid bilayer to the extracellular layer too even

though the lipid bilayer membrane is intact during apoptotic event (Blankenberg and Norfray, 2012). The inclusion of the second stain which stains DNA, propidium iodide, is meant to differentiate cell death based on the integrity of the lipid bilayer membrane. Hence, the double-staining method was adopted on the basis that only necrotic cells with ruptured lipid bilayer membrane would be stained with propidium iodide (double positive) while apoptotic cells with intact lipid bilayer membrane will prevent access of propidium iodide to DNA and fail to be stained by propidium iodide. However, this method is not flawless as there is evidence that late-stage apoptotic cells also exhibit ruptured lipid membrane bilayer and will be positively stained by propidium iodide. Hence, it is possible that late-stage apoptotic cells could be misinterpreted as undergoing necrosis (Brauchle et al., 2014). It is still a topic of debate whether the conventionally accepted non-regulated necrosis is still considered a cell death mechanism on its own or has been reclassified as necroptosis that has a regulated molecular signalling pathway (Hu et al., 2021; Galluzzi et al., 2016).

In recent years, it has been well acknowledged that the measles virus can cause immunogenic cell death (ICD) which acts as an indirect secondary tumour cell killing mechanism after the priming of immune cells with tumour antigen released from lysed tumour cells (Donnelly et al., 2013). Accumulating evidence shows that the release of HMGB1 plays an important signalling role in the recruitment of immune cells, typically T-lymphocyte and dendritic cells, to the site of origin to initiate the removal or killing of affected cells (Zhou et al., 2019). Contrary to previous understanding, HMGB1 is not an exclusive molecular marker for cells undergoing necrosis and various forms of stimulation and stressors can lead extracellular release of HMGB1 (Chen et al., 2022). Chen

et al. (2022) thoroughly reviewed how various biological molecules induce either passive, which is highly associated with cell death exhibiting necrotic phenotype, or active release via extracellular vesicles by intact and viable cells in ICD (Appendix S).

Viral infection could induce active HMGB1 release via ROS/RNS or calcium ion signalling pathway (Appendix S) as discussed by Chen et al. (2022). Translocation of nuclear HMGB1 into cytoplasm can be driven by excess intracellular reactive oxygen species (ROS) induced by viral infection (Xiuyan Ding et al., 2021). Expression of measles nucleoprotein (N) does elevate intracellular ROS levels (Bhaskar et al., 2011). For selected viruses, such as the Hepatitis C virus, Human Cytomegalovirus, and Influenza A virus, HMGB1 is essential for viral replication (Xiuyan Ding et al., 2021). A literature search did not reveal any research publication that describes the direct role of HMGB1 in measles virus replication or life cycle, but a relationship between HMGB1 and autophagy has been described. Cytosolic HMGB1 plays a key regulatory role in determining the cell fate between autophagy and apoptosis in inflammation, even without the involvement of pathogenic infection (Zhu et al., 2015). Cytosolic HMGB1 binds to Beclin1 and Atg5 proteins to protect both proteins from calpain-mediated cleavage and result in autophagy activity instead of apoptosis. On this note, MV-Edm requires autophagy for effective viral replication (Rozières et al., 2017; Richetta et al., 2013). MV-Edm induces an early wave of Beclin1-dependent autophagy mediated by the interaction between CD46 and GOPC proteins (Rozières et al., 2017). In addition, measles C proteins can induce a second autophagy wave by interacting with immunity-related GTPase family M protein (IRGM) protein (Rozières et al., 2017). Recent

findings show that IRGM binds with cytosolic HMGB1 and then recruits Beclin1 and forms a protein complex (Tian et al., 2021). Hence, oMV infection could induce and potentially maintain autophagy by two pathways, one by inducing HMGB1 translocation due to ROS generation by measles N protein and the Beclin1-dependent autophagy pathway induced by measles C protein mediated by IRGM.

Mao Xia et al. (2014) demonstrated previously that HMGB1 was detected in cell culture media from two NSCLC cell lines infected with MV-Edm as early as 48-hours post-infection. Recent work by Iankov et al. (2020) has shown that HMGB1 is detected in MV-Edm infected cell culture media at 24-hours post-infection, even earlier than reported by Mao Xia and coworkers (Iankov et al., 2020). Based on the fluorescence microscopic data in Figure 4.5, infected NPC cell cultures started to show cell loss from 48-hours onwards. Moreover, Wen-Hsuan et al. (2021) noted that 60 % of infected cells were shed into media between 24- and 48-hours post-infection. Taken together, it is theoretically possible for viable infected epithelial tumour cells, be it shed or unshed infected cells, to start actively releasing HMGB1 between 24- and 48-hours after being infected by oMV.

In this study, HMGB1 abundance was noted to increase over time in both biological replicates (R1 and R2) across the three post-infection time points studied, with the highest abundance observed at 48-hours post-infection in R1 (Table 4.7). The upregulation trend of HMGB1 from 24- to 48-hours post-infection observed in this study agrees with the finding by Mao Xia et al. (2014) that HMGB1 may be secreted between 24- and 48-hours post-infection. XPO1, the essential protein to translocate nuclear HMGB1 into the cytoplasm for

potential extracellular release, was found to be upregulated in R1 at 48-hours post-infection in line with the upregulation of HMGB1 (Table 4.7).

Table 4.7: Relative abundance of HMGB1 and XPO1 proteins in two biological replicates (R1 and R2).

	PeptideShaker	R1: 24h / Mock	R1: 36h / Mock	R1: 48h / Mock	R2: 24h / Mock	R2: 36h / Mock	R2: 48h / Mock
Gene Name	Confidence [%]	log2 (114/113)	log2 (115/113)	log2 (116/113)	log2 (118/117)	log2 (119/117)	log2 (121/117)
HMGB1	90.98	-0.710	0.000	0.661	-0.894	-1.013	-0.120
XPO1	88.56	1.314	-2.123	1.309	0.000	-0.085	-0.447

log2 (ratio) > 0.58 represent upregulation and log2 (ratio) < -0.58 represent downregulation.

4.2.5.3 Possible mode of active extracellular release of HMGB1 from C666-1 cells infected with Measles-GFP-NIS

Thorburn et al. (2009) previously reported that HMGB1 could be selectively released from the U87MG glioblastoma cell line under the control of autophagy proteins Atg5, Atg7, and Atg12. In the context of oMV infected cells, autophagy is an essential process that enhances viral replication (Rozières et al., 2017; Richetta et al., 2013). Therefore, it is very likely that oMV infection could lead to autophagy-dependent active release of HMGB1.

HMGB1 is known to be released extracellularly through the secretory lysosome by immune cells (Chen et al., 2022). However, there is no clear description that HMGB1 can be actively released via the same channel in non-immune cells, such as epithelial cells and tumour cells (Thorburn et al., 2009; Chen et al., 2022). It was reported that heat shock protein HSP90AA1 facilitate translocation of HMGB1 by stabilizing protein-to-protein interaction between HMGB1 and XPO1 (Kim et al., 2021). Kim and co-workers chemically induced autophagy in immortalized human embryonic kidney (HEK293T) epithelial cells to study the relationship between autophagy and extracellular release of HMGB1 (Kim et al., 2021). Their data demonstrated that HMGB1 was first packaged into autophagosome created from GORASP2-dependent autophagy proteins (Gorasp2, Atg5, Atg7, Atg12, and Atg14), then fused with multiple vesicular bodies and followed by fusion with amphisome before processed by Rab GTPases (Rab8a, Rab11a, and Rab27a) for extracellular release by exosome (Kim et al., 2021). Gorasp2 was reported to play a mediatory role in facilitating the fusion of the autophagosome with lysosome under amino acid starvation conditions (Zhang et al., 2019). The involvement of lysosomes in the

oMV-induced autophagosome requires further investigation since fusion of both vesicles leads to either degradation of cargo for nutrient recycling or autophagic death in normal conditions (Zhang and Chen, 2020). The *gorasp2*, *Atg5*, *Atg7*, *Atg12*, *Atg14*, *Rab8a* and *Rab27a* proteins shortlisted by Kim et al. (2021) were not found in this study. Only *Rab11a* was identified in this study but the expression data available for *Rab11a* protein was lacking for further analysis (Table 4.8). Interestingly, *Rab11a*-associated endosome was implicated in the transportation of measles ribonucleoprotein to the plasma membrane in the presence of measles matrix protein (Nakatsu et al., 2013; Gonçalves Carneiro, 2017). This finding suggests that there could be more molecular interplay between Rab GTPases trafficking activity and biological cargo that has not yet been elucidated, especially under the influence of viral gene product. A comprehensive overview of the autophagy pathway that serves as the foundation for the hypothetical inference of oMV-induced HMGB1 active release has been reviewed elsewhere (Zhang and Chen, 2020; Leonardi et al., 2021).

Table 4.8: Only Rab11a protein shows upregulation at 24- and 36-hours post-infection.

Gene Name	Confidence [%]	R1: 24h / Mock	R1: 36h / Mock	R1: 48h / Mock	R2: 24h / Mock	R2: 36h / Mock	R2: 48h / Mock
		log2 (114/113)	log2 (115/113)	log2 (116/113)	log2 (118/117)	log2 (119/117)	log2 (121/117)
RAB7A	95.39	0.000	0.000	0.000	0.000	-0.250	0.278
RAB1A	83.33	0.000	0.000	0.000	0.000	0.000	0.000
RAB11A	91.73	0.540	0.000	0.000	0.000	1.072	0.000

4.2.6 Conclusion

Literature search and protein expression dataset obtained in this study suggest that the oMV infection observed in this study may not be lytic in nature, and infected cells could possibly be killed and cleared by immune cells *in vivo* via the ICD pathway. One hallmark of measles virus infection is the expression of measles H- and F-protein on the host cell surface, which is responsible for direct contact and fusion with uninfected cells in the vicinity to form syncytia (Engeland and Ungerechts, 2021). Hence, immune cells can recognize the viral proteins that are expressed on infected cells or syncytia for clearance or killing by immune cells, especially the T lymphocytes.

Scientific literature suggests that oMV-induced ICD starts from the active release of HMGB1, between 24- to 48-hours post-infection. This is supported by the HMGB1 expression data from this study. **Figure 4.11** summarizes the hypothetical molecular pathway involved in Measles-GFP-NIS-induced active release of HMGB1 based on data in this study and available literature. Further investigation is required to better understand how oMV infection influences possible means of active HMGB1 release in epithelial tumour cells. Rab11a was identified in this study but not the GORASP2-dependent autophagy proteins (Gorasp2, Atg5, Atg7, Atg12, and Atg14), Rab8a and Rab27a, which were deemed to be essential for autophagy-dependent active exosome released highlighted by Kim et. al (2019). Noting that autophagy is an essentially biological process induced by the measles virus for pro-replicative need, the available evidence to date shows that measles N- and C-proteins can induce autophagy via two separate paths, both mediated by HMGB1, that converge and in turn lead to active release of HMGB1 (Mao Xia et al., 2014).

Moreover, Rab11a protein was reported to be involved in measles virus RNP trafficking to the plasma membrane prior to viral egress by budding (Gonçalves Carneiro, 2017). Hence, the identification of Rab11a protein in this study may not be a coincidence and could be part of the process in active release of HMGB1 by oMV infected cell. However, it is unclear whether oMV infected cells will package and prepare HMGB1 for exosomal release in the same manner as described by Kim et al. (2019) since autophagy in their study was chemically induced and independent of influence from measles virus gene product. Further investigations are necessary to understand the processes from oMV-induced autophagy, Rab GTPases and intracellular vesicle component involved in HMGB1 trafficking, to extracellular secretion.

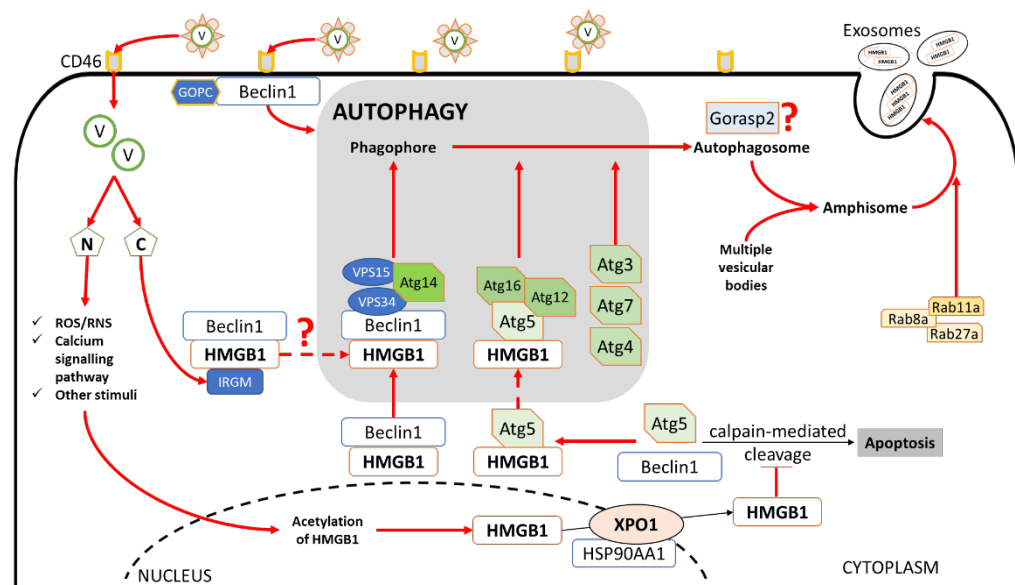


Figure 4.11: Illustration summarizing hypothetical molecular pathway involving Measles-GFP-NIS infection from inducing nuclear-to-cytoplasm translocation of HMGB1 to autophagy-dependent active release of HMGB1 via extracellular vesicle.

V: Measles-GFP-NIS viral particle, N: Measles N protein, dashed arrow: unknown pathway, solid arrow: known pathway from literature, solid line with blunt end: inhibition of process.

CHAPTER 5

CONCLUSION

5.1 Conclusion

In this work, the oMV was shown to be able to effectively infect untreated, CR- and RR-NPC cells regardless of the CD46 expression level. Moreover, CR- and RR-NPC appeared to be more susceptible to Measles-GFP-NIS infection (Figure 4.7). It is not known what the underlying factor that led to an increase in infection susceptibility. However, considering that the CR- and RR-NPC cells survived repeated cycles of cytotoxic treatment, it could be molecular responses towards the cytotoxic insults that enhanced the Measles-GFP-NIS infection susceptibility. This finding suggests that oMV is a potential second-line therapeutic agent that could eliminate resistant and advanced tumour cells which are difficult to eliminate using existing therapeutic regimens.

The bioinformatics analysis of the quantitative proteomics dataset showed that essential proteins belonging to the primary cell-killing pathway were not identified. DAP that belongs to cell death-related biological processes were ambiguous and unusually regulated. KEGG pathway analysis did not match any of the known pathways related to cell death. More importantly, the data did not match any protein complexes known to date that play a role in cell death processes. Thus, the data from this study indicated the possibility that hitherto unknown mechanisms play a part in the cell death caused by oMV infection and more specifically, whether oMV infection led to direct cell death before or after viral egression.

Two recent works by Hippee et al. (2021) and Wen-Hsuan et al. (2021) showed evidence that both wt- and MV-Edm lineages do not kill infected cells, which tally with the finding in this study. Other research publications described 1) the non-apoptotic nature of measles infection, especially infection by the vaccine strain, 2) the essentiality of autophagy for measles virus replication, 3) possible indirect means to kill infected cells via necrosis or ICD, 4) the means of active HMGB1 release in the context of epithelial and tumour cell, and lastly 5) the likely relationship between unconventional autophagy-dependent HMGB1 active release to autophagy-dependent measles life cycle in ICD. Therefore, it appears that MV infections, by both wt- and vaccine strains, are non-lytic in nature and may require induction of ICD for the systemic clearance of infected tumour cells. In summary, the indirect cell killing induced by Measles-GFP-NIS infection could, theoretically, develop in the following sequences. Measles-GFP-NIS may stimulate the upregulation of nuclear HMGB1. Measles virus N protein generates intracellular ROS which in turn stimulates acetylation of nuclear HMGB1 for XPO1-mediated translocation into cytoplasm. Cytoplasmic HMGB1 binds and protects both Beclin1 and Atg5 from degradation and the interaction drives autophagy which is crucial for productive replication of Measles-GFP-NIS. Due to the sustenance of active autophagy activity by the presence of Measles-GFP-NIS gene products, cytoplasmic HMGB1 in turn is subjected to autophagy-dependent processing, packaging, and trafficking destined for extracellular release, resulting in active release of HMGB1.

5.2 Limitation of study

Experiments in this study involving timepoint monitoring of Measles-GFP-NIS infection and spread in cell culture are affected by the inability to control the dynamic of viral replication and the number of NPC cells recruited by the infected cell to form cell-to-cell fusion. These two variables are inherent to viral biology for the former, and dependent on the distribution of infected cells with proximity to uninfected NPC cells in cultures for the latter. The quantitative proteomics study performed captures the net abundance of proteins within the bulk of NPC cells. Hence, the data will be affected by the heterogeneity of viral replication dynamics within each syncytium, the number of syncytia formed per NPC culture, and the proportion of infected cells compared to uninfected cells. In addition, the biological replicate performed for the quantitative proteomics study was limited to two replicates due to the cost constraint of iTRAQ reagents and consumables. iTRAQ kit can only process up to eight samples per kit and we can only perform two biological replicates with four samples collected from different time points in each replicate. The data collected in this study were derived from *in-vitro* experiments and may require an *in-vivo* study for validation.

Due to limitations to time due to the COVID-19 pandemic and resources, the following validations were not performed:

1. Cell line authenticity and EBV positivity were not validated in all NPC cells tested in this study, except C666-1 (Chan et al., 2008; Strong et al., 2014). A PCR targeting EBV's *LMP1* gene (Appendix T) shows C666-1 positive for the gene, partially validating the EBV positive and cell

authenticity of C666-1 which is well known to constitutively expressed EBV genome (Lin et al., 2001; Tso et al., 2013),

2. No primary nasopharyngeal epithelial cell is available to be incorporated into this study as a non-tumour control. Commonly used control cells in other studies, such as NP460 and NP550 were immortalized by exogenous transduction of telomerase reverse transcriptase which causes the cells to partially express pre-tumorous phenotype (Tsang et al., 2012), and
3. Complementary method to validate relative quantitation data derived from mass spectrometry analysis, such as western blot.

This study was conceived and executed with the basis assumption that tumour cells were killed as a direct consequence of infection by oMV and corresponding viral life cycle events. Therefore, alternative conditions that may have led to the natural death of infected cells with time were not investigated.

5.3 Future studies

The findings in this study raise two hypothetical questions, whether oMV is still capable of directly killing infected cells via viral life cycle events given extended time or oMV is not oncolytic in nature and requires ICD for removal of infected cells *in vivo*, otherwise infected cells were kept alive for continuous viral progeny production beyond one viral life cycle under sustainable culture condition.

To address the first hypothetical question, possible conditions that can lead to the natural death of infected cells given extended time under *in vitro* culture and without influence from ICD need to be investigated.

To address the latter hypothetical question, more extensive investigations with an *in vivo* mouse model would be required. Following up on findings by Hippee et al. (2021) and Wen-Hsuan et al. (2021) alongside the molecular finding in this study, the “oncolytic” property of oMV needs to be addressed with a study comparing the infected cell fate with functional and dysfunctional HMGB1 active release, and subsequently, whether the functional active release is a cellular response towards viral infection or influenced by viral life cycle event, for example, viral progeny egress. Interferon assays should be considered as well to investigate the involvement of interferons in oMV-induced ICD both *in vivo* and *in vitro*.

Through the work in this thesis, the ICD caused by oMV infection could be mediated by the unconventional autophagy-dependent active release of HMGB1. Of note, the measles virus can package virions and egress purely by relying on measles viral proteins independent of host machinery like other viruses do. It is crucial to validate that HMGB1 release is indeed an active process that involves viable cells infected by oMV, and not passive release after death or lysis of infected cells. This is another area for further studies to discover possible unique biological processes induced by oMV gene products.

Rab11a was implicated in the active release of HMGB1 by exosome and trafficking of measles virus RNP to host cell membrane as discussed in Section 4.2.5 and 4.2.6. There is a possibility that the active release of HMGB1 could

be an event that accompanies measles virus egress rather than a standalone event. A valuable follow-up to this study would be investigations to clearly define the exact molecular signalling and interaction mechanisms that may involve oMV proteins to substantiate further the novel findings uncovered in this thesis.

Future studies need to acquire non-immortalized primary nasopharyngeal epithelial cells which were recently established in the year 2020 as negative controls for oncolytic measles virus infection studies (Yu et al., 2020).

REFERENCES

- Abdullah, S.A., Al-Shammari, A.M. and Lateef, S.A., 2020. Attenuated measles vaccine strain have potent oncolytic activity against Iraqi patient derived breast cancer cell line. *Saudi Journal of Biological Sciences*, 27(3).
- Adham, M. et al., 2012. Nasopharyngeal carcinoma in indonesia: Epidemiology, incidence, signs, and symptoms at presentation. *Chinese Journal of Cancer*, 31(4).
- Adjemian, S. et al., 2020. Ionizing radiation results in a mixture of cellular outcomes including mitotic catastrophe, senescence, methuosis, and iron-dependent cell death. *Cell Death & Disease* 2020 11:11, 11(11), pp.1–15. Available at: <https://www.nature.com/articles/s41419-020-03209-y> [Accessed: 24 February 2022].
- Advani, S.J., Mezhir, J.J., Roizman, B. and Weichselbaum, R.R., 2006. ReVOLT: radiation-enhanced viral oncolytic therapy. *International Journal of Radiation Oncology Biology Physics*, 66(3).
- Aguilan, J.T., Kulej, K. and Sidoli, S., 2020. Guide for protein fold change and p-value calculation for non-experts in proteomics. *Molecular Omics*, 16(6), pp.573–582. Available at: <https://pubs.rsc.org/en/content/articlehtml/2020/mo/d0mo00087f> [Accessed: 5 January 2023].
- Anand, S. et al., 2017. Label-Based and Label-Free Strategies for Protein Quantitation. *Methods in Molecular Biology*, 1549, pp.31–43. Available at: https://link.springer.com/protocol/10.1007/978-1-4939-6740-7_4 [Accessed: 13 May 2022].
- Anderson, B.D., Nakamura, T., Russell, S.J. and Peng, K.W., 2004. High CD46 receptor density determines preferential killing of tumor cells by oncolytic measles virus. *Cancer Research*, 64(14), pp.4919–4926.
- Ankney, J.A., Muneer, A. and Chen, X., 2016. Relative and Absolute Quantitation in Mass Spectrometry–Based Proteomics. <https://doi.org/10.1146/annurev-anchem-061516-045357>, 11, pp.49–77. Available at: <https://www.annualreviews.org/doi/abs/10.1146/annurev-anchem-061516-045357> [Accessed: 13 May 2022].
- Anon, 2016a. Nasopharyngeal Carcinoma, Keratinizing Type. *Diagnostic Pathology: Head and Neck*, pp.222–223.
- Anon, 2016b. Nasopharyngeal Carcinoma, Nonkeratinizing Types. *Diagnostic Pathology: Head and Neck*, pp.214–221.
- Aref, S. et al., 2020. Type 1 Interferon Responses Underlie Tumor-Selective Replication of Oncolytic Measles Virus. *Molecular Therapy*, 28(4).
- Azizah, A. et al., 2019. Malaysia National cancer registry report (MNCR). *National Cancer Institute, Ministry of Health: Putrajaya, Malaysia*.

- Bachor, R., Waliczek, M., Stefanowicz, P. and Szewczuk, Z., 2019. Trends in the Design of New Isobaric Labeling Reagents for Quantitative Proteomics. *Molecules*, 24(4). Available at: /pmc/articles/PMC6412310/ [Accessed: 26 May 2022].
- Bader, G.D. and Hogue, C.W.V., 2003. An automated method for finding molecular complexes in large protein interaction networks. *BMC Bioinformatics*, 4.
- Bah, E.S. et al., 2020. Retargeted and stealth-modified oncolytic measles viruses for systemic cancer therapy in measles immune patients. *Molecular Cancer Therapeutics*, 19(10).
- Barr, M.P. et al., 2013. Generation and Characterisation of Cisplatin-Resistant Non-Small Cell Lung Cancer Cell Lines Displaying a Stem-Like Signature. *PLoS ONE*, 8(1).
- Barrett, D. et al., 2019. Past and Recent Salted Fish and Preserved Food Intakes Are Weakly Associated with Nasopharyngeal Carcinoma Risk in Adults in Southern China. *The Journal of Nutrition*, 149(9), pp.1596–1605. Available at: <https://doi.org/10.1093/jn/nxz095>.
- Baskar, R. and Itahana, K., 2017. Radiation therapy and cancer control in developing countries: Can we save more lives? *International Journal of Medical Sciences*, 14(1), pp.13–17.
- Bentz, G.L., Shackelford, J. and Pagano, J.S., 2012. Epstein-Barr Virus Latent Membrane Protein 1 Regulates the Function of Interferon Regulatory Factor 7 by Inducing Its Sumoylation. *Journal of Virology*, 86(22).
- Bhaskar, A., Bala, J., Varshney, A. and Yadava, P., 2011. Expression of measles virus nucleoprotein induces apoptosis and modulates diverse functional proteins in cultured mammalian cells. *PLoS ONE*, 6(4).
- Blanchard, P. et al., 2015. Chemotherapy and radiotherapy in nasopharyngeal carcinoma: An update of the MAC-NPC meta-analysis. *The Lancet Oncology*, 16(6).
- Blankenberg, F.G. and Norfray, J.F., 2012. Multimodality Molecular Imaging of Apoptosis in Oncology. <http://dx.doi.org/10.2214/AJR.11.6953>, 197(2), pp.308–317. Available at: www.ajronline.org [Accessed: 1 February 2023].
- Boisgerault, N. et al., 2013. Natural oncolytic activity of live-attenuated measles virus against human lung and colorectal adenocarcinomas. *BioMed Research International*, 2013.
- Bossi, P. et al., 2021. Nasopharyngeal carcinoma: ESMO-EURACAN Clinical Practice Guidelines for diagnosis, treatment and follow-up. *Annals of Oncology*, 32(4).
- Bouleftour, W., Guillot, A. and Magne, N., 2022. The Anti-Nectin 4: A Promising Tumor Cells Target. A Systematic Review. *Molecular Cancer Therapeutics*, 21(4).

- Bovier, F.T. et al., 2021. Inhibition of Measles Viral Fusion Is Enhanced by Targeting Multiple Domains of the Fusion Protein. *ACS Nano*, 15(8), pp.12794–12803. Available at: <https://pubs.acs.org/doi/abs/10.1021/acsnano.1c02057> [Accessed: 3 January 2023].
- Brauchle, E., Thude, S., Brucker, S.Y. and Schenke-Layland, K., 2014. Cell death stages in single apoptotic and necrotic cells monitored by Raman microspectroscopy. *Scientific Reports 2014 4:1*, 4(1), pp.1–9. Available at: <https://www.nature.com/articles/srep04698> [Accessed: 1 February 2023].
- Cao, G.D. et al., 2020. The Oncolytic Virus in Cancer Diagnosis and Treatment. *Frontiers in Oncology*, 10, p.542152.
- Cebecauer, M., Spitaler, M., Sergé, A. and Magee, A.I., 2010. Signalling complexes and clusters: Functional advantages and methodological hurdles. *Journal of Cell Science*, 123(3).
- Chan, A.T.C. et al., 2010. Nasopharyngeal cancer: EHNS–ESMO–ESTRO Clinical Practice Guidelines for diagnosis, treatment and follow-up. *Annals of oncology*, 21(suppl_5), pp.v187–v189.
- Chan, K.C.A., 2014. Plasma Epstein-Barr virus DNA as a biomarker for nasopharyngeal carcinoma. *Chinese journal of cancer*, 33(12), pp.598–603. Available at: <https://pubmed.ncbi.nlm.nih.gov/25418194>.
- Chan, S.Y.Y. et al., 2008. Authentication of nasopharyngeal carcinoma tumor lines. *International Journal of Cancer*, 122(9), pp.2169–2171.
- Chang, E.T. and Adami, H.-O.O., 2006. The Enigmatic Epidemiology of Nasopharyngeal Carcinoma. *Cancer Epidemiology Biomarkers & Prevention*, 15(10), pp.1765 LP – 1777. Available at: <http://cebp.aacrjournals.org/content/15/10/1765.abstract>.
- Chang, E.T., Ye, W., Zeng, Y.X. and Adami, H.O., 2021. The evolving epidemiology of nasopharyngeal carcinoma. *Cancer Epidemiology Biomarkers and Prevention*, 30(6).
- Chatterjee, S., Sinha, S. and Kundu, C.N., 2021. Nectin cell adhesion molecule-4 (NECTIN-4): A potential target for cancer therapy. *European Journal of Pharmacology*, 911.
- Chen, R., Kang, R. and Tang, D., 2022. The mechanism of HMGB1 secretion and release. *Experimental and Molecular Medicine*, 54(2).
- Chen, Y.P. et al., 2021. Chemotherapy in Combination with Radiotherapy for Definitive-Intent Treatment of Stage II-IVA Nasopharyngeal Carcinoma: CSCO and ASCO Guideline. *Journal of Clinical Oncology*, 39(7).
- Chen, Y.-P. et al., 2019. Nasopharyngeal carcinoma. *The Lancet*, 394(10192), pp.64–80. Available at: [https://doi.org/10.1016/S0140-6736\(19\)30956-0](https://doi.org/10.1016/S0140-6736(19)30956-0).
- Cheung, S.T. et al., 1999. Nasopharyngeal carcinoma cell line (C666-1) consistently harbouring Epstein-Barr virus. *International Journal of Cancer*, 83(1).

- Chiang, C.J. et al., 2016. Incidence and survival of adult cancer patients in Taiwan, 2002–2012. *Journal of the Formosan Medical Association*, 115(12).
- Cho, C. et al., 2020. Cancer-associated fibroblasts downregulate type I interferon receptor to stimulate intratumoral stromagenesis. *Oncogene*, 39(38).
- Crowley, L.C., Marfell, B.J., Scott, A.P. and Waterhouse, N.J., 2016. Quantitation of apoptosis and necrosis by annexin V binding, propidium iodide uptake, and flow cytometry. *Cold Spring Harbor Protocols*, 2016(11).
- Cruz, C.D. et al., 2006. Measles Virus V Protein Inhibits p53 Family Member p73. *Journal of Virology*, 80(11), p.5644. Available at: [/pubmed/articles/PMC1472123/](https://pubmed.ncbi.nlm.nih.gov/1472123/) [Accessed: 5 January 2023].
- Dabbagh, A. et al., 2018. Progress Toward Regional Measles Elimination - Worldwide, 2000-2017. *MMWR. Morbidity and mortality weekly report*, 67(47), pp.1323–1329. Available at: <https://pubmed.ncbi.nlm.nih.gov/30496160>.
- D'Arcy, M.S., 2019. Cell death: a review of the major forms of apoptosis, necrosis and autophagy. *Cell Biology International*, 43(6), pp.582–592. Available at: <https://onlinelibrary.wiley.com/doi/full/10.1002/cbin.11137> [Accessed: 17 February 2022].
- Digre, A. and Lindskog, C., 2023. The human protein atlas—Integrated omics for single cell mapping of the human proteome. *Protein Science*, 32(2).
- Ding, Xi et al., 2021. Clinical advances in nasopharyngeal carcinoma surgery and a video demonstration. *Visualized Cancer Medicine*, 2, p.2. Available at: https://vcm.edpsciences.org/articles/vcm/full_html/2021/01/vcm20200010/vcm20200010.html [Accessed: 23 September 2022].
- Ding, Xiuyan, Li, S. and Zhu, L., 2021. Potential effects of HMGB1 on viral replication and virus infection-induced inflammatory responses: A promising therapeutic target for virus infection-induced inflammatory diseases. *Cytokine and Growth Factor Reviews*, 62.
- Doherty, M.R. et al., 2017. Interferon-beta represses cancer stem cell properties in triple-negative breast cancer. *Proceedings of the National Academy of Sciences of the United States of America*, 114(52).
- Donnelly, O.G. et al., 2013. Measles virus causes immunogenic cell death in human melanoma. *Gene Therapy*, 20(1), pp.7–15.
- Dörig, R.E., Marcil, A., Chopra, A. and Richardson, C.D., 1993. The human CD46 molecule is a receptor for measles virus (Edmonston strain). *Cell*, 75(2), pp.295–305.
- Driever, P.H. and Rabkin, S.D., 2001. *Replication-competent viruses for cancer therapy*, Karger Medical and Scientific Publishers.
- Ekburanawat, W. et al., 2010. Evaluation of non-viral risk factors for nasopharyngeal carcinoma in Thailand: Results from a case-control study. *Asian Pacific Journal of Cancer Prevention*, 11(4).

- El-Naggar, A.K. et al., 2017. WHO Classification of Head and Neck Tumours-WHO/IARC Classification of Tumours. *World Health Organization*.
- Elvington, M, Liszewski, M.K. and Atkinson, J.P., 2020. CD46 and Oncologic Interactions: Friendly Fire against Cancer. *Antibodies (Basel)*, 9(4).
- Elvington, Michelle, Liszewski, M.K. and Atkinson, J.P., 2020. CD46 and Oncologic Interactions: Friendly Fire against Cancer. *Antibodies*, 9(4).
- Engeland, C.E. and Ungerechts, G., 2021. Measles virus as an oncolytic immunotherapy. *Cancers*, 13(3).
- Esolen, L.M., Park, S.W., Hardwick, J.M. and Griffin, D.E., 1995. Apoptosis as a Cause of Death in Measles Virus-Infected Cells. *JOURNAL OF VIROLOGY*, 69(6), pp.3955–3958.
- Fang, C.-Y. et al., 2012. The Synergistic Effect of Chemical Carcinogens Enhances Epstein-Barr Virus Reactivation and Tumor Progression of Nasopharyngeal Carcinoma Cells Masucci, M.G., (ed.). *PLoS ONE*, 7(9), p.e44810. Available at: <https://dx.plos.org/10.1371/journal.pone.0044810> [Accessed: 28 July 2020].
- Farag, Y.M., Horro, C., Vaudel, M. and Barsnes, H., 2021. PeptideShaker Online: A User-Friendly Web-Based Framework for the Identification of Mass Spectrometry-Based Proteomics Data. *Journal of Proteome Research*, 20(12).
- Farias, T.P. et al., 2003. Prognostic factors and outcome for nasopharyngeal carcinoma. *Archives of Otolaryngology - Head and Neck Surgery*, 129(7).
- Ferlay, J. et al., 2024, *Global Cancer Observatory: Cancer Today*. [Online]. Available at: <https://gco.iarc.who.int/today/en> [Accessed: 21 February 2024].
- Ferrari, D. et al., 2012. Role of plasma EBV DNA levels in predicting recurrence of nasopharyngeal carcinoma in a western population. *BMC Cancer*, 12.
- Frecha, C. et al., 2008. Stable transduction of quiescent T cells without induction of cycle progression by a novel lentiviral vector pseudotyped with measles virus glycoproteins. *Blood*, 112(13).
- Galluzzi, L. et al., 2018. Molecular mechanisms of cell death: recommendations of the Nomenclature Committee on Cell Death 2018. *Cell Death & Differentiation* 2018 25:3, 25(3), pp.486–541. Available at: <https://www.nature.com/articles/s41418-017-0012-4> [Accessed: 6 April 2022].
- Galluzzi, L., Kepp, O. and Kroemer, G., 2016. Mitochondrial regulation of cell death: A phylogenetically conserved control. *Microbial Cell*, 3(3).
- Gebremeskel, S. and Johnston, B., 2015. Concepts and mechanisms underlying chemotherapy induced immunogenic cell death: impact on clinical studies and considerations for combined therapies. *Oncotarget*, 6(39), p.41600. Available at: [/pmc/articles/PMC4747176/](https://pubmed.ncbi.nlm.nih.gov/2647176/) [Accessed: 10 March 2022].

- Ghosh, G., Tallari, R. and Malviya, A., 2016. Toxicity profile of IMRT vs 3D-CRT in head and neck cancer: A retrospective study. *Journal of Clinical and Diagnostic Research*, 10(9).
- Giancotti, F.G., 2014. Deregulation of cell signaling in cancer. *FEBS Letters*, 588(16), pp.2558–2570.
- Giurgiu, M. et al., 2019. CORUM: The comprehensive resource of mammalian protein complexes - 2019. *Nucleic Acids Research*, 47(D1).
- Gonçalves Carneiro, V.D., 2017. *Molecular mechanisms of measles virus entry and exit*.
- Gooi, Z. et al., 2017. AHNS Series - Do you know your guidelines? Principles of treatment for nasopharyngeal cancer: A review of the National Comprehensive Cancer Network guidelines. *Head & Neck*, 39(2), pp.201–205. Available at: <http://doi.wiley.com/10.1002/hed.24635> [Accessed: 29 July 2020].
- Gordienko, I., Shlapatska, L., Kovalevska, L. and Sidorenko, S.P., 2019. SLAMF1/CD150 in hematologic malignancies: Silent marker or active player? *Clinical Immunology*, 204.
- Green, D.R. and Llambi, F., 2015. Cell Death Signaling. *Cold Spring Harbor Perspectives in Biology*, 7(12). Available at: [/pmc/articles/PMC4665079/](http://pmc/articles/PMC4665079/) [Accessed: 17 February 2022].
- Griffin, D.E., Lin, W.H. and Pan, C.H., 2012. Measles virus, immune control, and persistence. *FEMS Microbiology Reviews*, 36(3).
- Guan, S., Wei, J., Huang, L. and Wu, L., 2020. Chemotherapy and chemoresistance in nasopharyngeal carcinoma. *European Journal of Medicinal Chemistry*, 207, p.112758. Available at: <https://www.sciencedirect.com/science/article/pii/S0223523420307303>.
- Guo, Z. et al., 2021. LncRNA linc00312 suppresses radiotherapy resistance by targeting DNA-PKcs and impairing DNA damage repair in nasopharyngeal carcinoma. *Cell Death and Disease*, 12(1).
- Han, T. et al., 2014. Establishment and characterization of a cisplatin-resistant human osteosarcoma cell line. *Oncology Reports*, 32(3).
- Hannun, Y.A., 1997. Apoptosis and the Dilemma of Cancer Chemotherapy. *Blood*, 89(6), pp.1845–1853. Available at: <https://ashpublications.org/blood/article/89/6/1845/139072/Apoptosis-and-the-Dilemma-of-Cancer-Chemotherapy> [Accessed: 10 March 2022].
- Haralambieva, I. et al., 2007. Engineering oncolytic measles virus to circumvent the intracellular innate immune response. *Molecular Therapy*, 15(3), pp.588–597.
- Harrington, K.J. et al., 2010. Phase I/II study of oncolytic HSVGM-CSF in combination with radiotherapy and cisplatin in untreated stage III/IV squamous cell cancer of the head and neck. *Clinical Cancer Research*, 16(15).

- He, C. et al., 2019. iTRAQ-based phosphoproteomic analysis reveals host cell's specific responses to *Toxoplasma gondii* at the phases of invasion and prior to egress. *Biochimica et Biophysica Acta (BBA) - Proteins and Proteomics*, 1867(3), pp.202–212.
- Heinzerling, L. et al., 2005. Oncolytic measles virus in cutaneous T-cell lymphomas mounts antitumor immune responses in vivo and targets interferon-resistant tumor cells. *Blood*, 106(7), pp.2287–2294. Available at: <https://ashpublications.org/blood/article/106/7/2287/21668/Oncolytic-measles-virus-in-cutaneous-T-cell> [Accessed: 30 January 2023].
- Herschke, F. et al., 2007. Cell-cell fusion induced by measles virus amplifies the type I interferon response. *Journal of Virology*, 81(23), pp.12859–12871.
- Hippee, C.E. et al., 2021. Measles virus exits human airway epithelia within dislodged metabolically active infectious centers. *PLoS Pathogens*, 17(8).
- Ho, S. et al., 2017. Treatment Regret in Long-term Survivors of Nasopharyngeal Carcinoma Treated with Radical Radiotherapy. *Clinical Oncology*, 29(1).
- Hong, J.S. et al., 2015. Quality of life of nasopharyngeal cancer survivors in China. *Current oncology (Toronto, Ont.)*, 22(3), pp.e142–e147. Available at: <http://dx.doi.org/10.3747/co.22.2323>.
- Hotchkiss, R.S., Strasser, A., McDunn, J.E. and Swanson, P.E., 2009. Cell Death in Disease: Mechanisms and Emerging Therapeutic Concepts. *The New England journal of medicine*, 361(16), p.1570. Available at: </pmc/articles/PMC3760419/> [Accessed: 6 April 2022].
- Hsu, E.C. et al., 1998. A Single Amino Acid Change in the Hemagglutinin Protein of Measles Virus Determines Its Ability To Bind CD46 and Reveals Another Receptor on Marmoset B Cells. *Journal of Virology*, 72(4).
- Hu, X.M. et al., 2021. Guidelines for Regulated Cell Death Assays: A Systematic Summary, A Categorical Comparison, A Prospective. *Frontiers in Cell and Developmental Biology*, 9.
- Huang, S.C.M., Tsao, S.W. and Tsang, C.M., 2018. Interplay of Viral Infection, Host Cell Factors and Tumor Microenvironment in the Pathogenesis of Nasopharyngeal Carcinoma. *Cancers*, 10(4), p.106. Available at: <https://pubmed.ncbi.nlm.nih.gov/29617291>.
- Iankov, I.D. et al., 2020. Live Attenuated Measles Virus Vaccine Expressing *Helicobacter pylori* Heat Shock Protein A. *Molecular Therapy - Oncolytics*, 19.
- Janeway, CA; Travers, P; Walport, M., 2001. The complement system and innate immunity - Immunobiology - NCBI Bookshelf. *Immunobiology: The Immune System in Health and Disease.*, 5th Editio.

- Jerrold T. Bushberg, 2020, *RADIATION EXPOSURE AND CONTAMINATION: Focal radiation injury* [Online]. Available at: <https://www.msmanuals.com/professional/injuries-poisoning/radiation-exposure-and-contamination/radiation-exposure-and-contamination#v1113796> [Accessed: 27 January 2022].
- Jia, W.-H. et al., 2010. Traditional Cantonese diet and nasopharyngeal carcinoma risk: a large-scale case-control study in Guangdong, China. *BMC cancer*, 10, p.446. Available at: <http://www.ncbi.nlm.nih.gov/pubmed/20727127> [Accessed: 28 July 2020].
- Johnstone, R.W., Loveland, B.E. and McKenzie, I.F.C., 1993. Identification and quantification of complement regulator CD46 on normal human tissues. *Immunology*, 79(3).
- Karbownik, A. et al., 2012. The physical and chemical stability of cisplatin (Teva) in concentrate and diluted in sodium chloride 0.9%. *Contemporary Oncology*, 16(5), p.435. Available at: </pmc/articles/PMC3687456/> [Accessed: 27 June 2022].
- Kataki, A.C. et al., 2011. Nasopharyngeal carcinoma in the Northeastern states of India. *Chinese Journal of Cancer*, 30(2).
- Kerr, J.F.R., Wyllie, A.H. and Currie, A.R., 1972. Apoptosis: A Basic Biological Phenomenon with Wideranging Implications in Tissue Kinetics. *British Journal of Cancer* 1972 26:4, 26(4), pp.239–257. Available at: <https://www.nature.com/articles/bjc197233> [Accessed: 17 February 2022].
- Kim, Y.H. et al., 2021. Secretory autophagy machinery and vesicular trafficking are involved in HMGB1 secretion. *Autophagy*, 17(9).
- Kit, O.I. et al., 2018. A proteomics analysis of cell signaling pathways in colon cancer. *Journal of Clinical Oncology*, 36(4_suppl).
- Lal, G. and Rajala, M.S., 2019. Combination of oncolytic measles virus armed with BNiP3, a pro-apoptotic gene and paclitaxel induces breast cancer cell death. *Frontiers in Oncology*, 9(JAN), p.676.
- Landgren, O., Devlin, S., Boulad, M. and Mailankody, S., 2016. Role of MRD status in relation to clinical outcomes in newly diagnosed multiple myeloma patients: A meta-analysis. *Bone Marrow Transplantation*, 51(12).
- Lee, H.M., Okuda, K.S., González, F.E. and Patel, V., 2019. Current Perspectives on Nasopharyngeal Carcinoma BT - Human Cell Transformation: Advances in Cell Models for the Study of Cancer and Aging. In: Rhim, J.S., Dritschilo, A. and Kremer, R., (eds.) *Advances in Experimental Medicine and Biology*. Springer International Publishing, Cham, pp. 11–34.
- Lee, N. et al., 2016. Chapter 34 - Nasopharyngeal Carcinoma. In: Gunderson, L.L. and Tepper, J.E.B.T.-C.R.O. (Fourth E., (eds.) Elsevier, Philadelphia, pp. 629-648.e4.
- Lee, N. et al., 2012. Nasopharyngeal Carcinoma. *Clinical Radiation Oncology: Third Edition*, pp.619–638.

- Lei, C., Yang, J., Hu, J. and Sun, X., 2021. On the Calculation of TCID₅₀ for Quantitation of Virus Infectivity. *Virologica Sinica*, 36(1), p.141. Available at: /pmc/articles/PMC7973348/ [Accessed: 28 August 2022].
- Leonardi, L. et al., 2021. Autophagy Modulation by Viral Infections Influences Tumor Development. *Frontiers in Oncology*, 11.
- Leong, K.Y., Azman, M. and Kong, M.H., 2020. Quality of life outcome among nasopharyngeal carcinoma survivors in Kuala Lumpur. *Annals of Nasopharynx Cancer*, 4.
- Li, M.Y. et al., 2017. Radiotherapy induces cell cycle arrest and cell apoptosis in nasopharyngeal carcinoma via the ATM and Smad pathways. *Cancer Biology & Therapy*, 18(9), p.681. Available at: /pmc/articles/PMC5663416/ [Accessed: 3 March 2022].
- Li, N. and Zhan, X., 2019. Signaling pathway network alterations in human ovarian cancers identified with quantitative mitochondrial proteomics. *EPMA Journal*, 10(2).
- Li, S. et al., 2017. Hippo pathway contributes to cisplatin resistant-induced EMT in nasopharyngeal carcinoma cells. *Cell Cycle*, 16(17).
- Lin, D., Shen, Y. and Liang, T., 2023. Oncolytic virotherapy: basic principles, recent advances and future directions. *Signal Transduction and Targeted Therapy*, 8(1).
- Lin, S.Y. et al., 2001. Presence of Epstein-Barr Virus latent membrane protein 1 gene in the nasopharyngeal swabs from patients with nasopharyngeal carcinoma. *Head and Neck*, 23(3).
- Linton, R.E. et al., 2021. Nasopharyngeal carcinoma among the Bidayuh of Sarawak, Malaysia: History and risk factors (Review). *Oncology Letters*, 22(1).
- Liszewski, M.K., Post, T.W. and Atkinson, J.P., 1991. Membrane cofactor protein (MCP or CD46): Newest member of the regulators of complement activation gene cluster. *Annual Review of Immunology*, 9.
- Liu, C. et al., 2007. Combination of Measles Virus Virotherapy and Radiation Therapy Has Synergistic Activity in the Treatment of Glioblastoma Multiforme. *Clinical Cancer Research*, 13(23), pp.7155–7165. Available at: <https://aacrjournals.org/clincancerres/article/13/23/7155/194388/Combination-of-Measles-Virus-Virotherapy-and> [Accessed: 21 July 2022].
- Liu, Y. et al., 2021. Role of Nectin-4 protein in cancer (Review). *International Journal of Oncology*, 59(5).
- Liu, Y.-P. et al., 2014. Ablation of Nectin4 Binding Compromises CD46 Usage by a Hybrid Vesicular Stomatitis Virus/Measles Virus. *Journal of Virology*, 88(4).
- Luo, R., Colangelo, C.M., Sessa, W.C. and Zhao, H., 2009. Bayesian Analysis of iTRAQ Data with Nonrandom Missingness: Identification of Differentially Expressed Proteins. *Statistics in biosciences*, 1(2), p.228. Available at: /pmc/articles/PMC3172970/ [Accessed: 5 January 2023].

- Ma, X. et al., 2018. LncRNA ANCR promotes proliferation and radiation resistance of nasopharyngeal carcinoma by inhibiting PTEN expression. *OncoTargets and Therapy*, 11.
- Macedo, N., Miller, D.M., Haq, R. and Kaufman, H.L., 2020. Clinical landscape of oncolytic virus research in 2020. *Journal for ImmunoTherapy of Cancer*, 8(2).
- MacIejczyk, A. et al., 2011. CD46 expression is an unfavorable prognostic factor in breast cancer cases. *Applied Immunohistochemistry and Molecular Morphology*, 19(6).
- Mahdavifar, N. et al., 2016. Epidemiology and Inequality in the Incidence and Mortality of Nasopharynx Cancer in Asia. *Osong Public Health and Research Perspectives*, 7(6).
- Mailankody, S. et al., 2015. Minimal residual disease in multiple myeloma: Bringing the bench to the bedside. *Nature Reviews Clinical Oncology*, 12(5).
- Mak, H.W. et al., 2015. Clinical Outcome among Nasopharyngeal Cancer Patients in a Multi-Ethnic Society in Singapore Gao, C.-Q., (ed.). *PLOS ONE*, 10(5), p.e0126108. Available at: <https://doi.org/10.1371/journal.pone.0126108> [Accessed: 21 April 2020].
- Makowska, A. et al., 2018. Interferon beta induces apoptosis in nasopharyngeal carcinoma cells via the TRAIL-signaling pathway. *Oncotarget*, 9(18).
- Maltser, S. et al., 2017. A Focused Review of Safety Considerations in Cancer Rehabilitation. *PM and R*, 9(9).
- Mantwill, K. et al., 2021. Concepts in oncolytic adenovirus therapy. *International Journal of Molecular Sciences*, 22(19).
- Martuza, R.L. et al., 1991. Experimental therapy of human glioma by means of a genetically engineered virus mutant. *Science*, 252(5007).
- McDowell, L., Corry, J., Ringash, J. and Rischin, D., 2020. Quality of Life, Toxicity and Unmet Needs in Nasopharyngeal Cancer Survivors. *Frontiers in Oncology*, 10.
- Menon, S.M.P. and Elengoe, A., 2020. Evaluation of the role of kras gene in colon cancer pathway using string and Cytoscape software. *Biomedical Research and Therapy*, 7(6).
- Ministry of Health Malaysia, 2016. Clinical Practice Guideline MANAGEMENT OF NASOPHARYNGEAL CARCINOMA. *Malaysia Health Technology Assessment Section (MaHTAS)*.
- Msaouel, P. et al., 2017. Clinical Trials with Oncolytic Measles Virus: Current Status and Future Prospects. *Current Cancer Drug Targets*, 18(2), pp.177–187.
- Mühlebach, M.D. et al., 2011. Adherens junction protein nectin-4 is the epithelial receptor for measles virus. *Nature*, 480(7378).

- Muñoz-Aliá, M.Á. et al., 2021. MeV-Stealth: A CD46-specific oncolytic measles virus resistant to neutralization by measles-immune human serum. *PLoS pathogens*, 17(2). Available at: <https://pubmed.ncbi.nlm.nih.gov/33534834/> [Accessed: 21 September 2022].
- Myers, R.M. et al., 2007. Preclinical pharmacology and toxicology of intravenous MV-NIS, an oncolytic measles virus administered with or without cyclophosphamide. *Clinical pharmacology and therapeutics*, 82(6), pp.700–10. Available at: <http://www.pubmedcentral.nih.gov/articlerender.fcgi?artid=2769566&tool=pmcentrez&rendertype=abstract>.
- Nakatsu, Y. et al., 2013. Intracellular Transport of the Measles Virus Ribonucleoprotein Complex Is Mediated by Rab11A-Positive Recycling Endosomes and Drives Virus Release from the Apical Membrane of Polarized Epithelial Cells. *Journal of Virology*, 87(8).
- Nicolas Boisgerault, C.A., 2015. Induction of Immunogenic Tumor Cell Death by Attenuated Oncolytic Measles Virus. *Journal of Clinical & Cellular Immunology*, 06(01).
- Nirmala, J.G. and Lopus, M., 2019. Cell death mechanisms in eukaryotes. *Cell Biology and Toxicology 2019 36:2*, 36(2), pp.145–164. Available at: <https://link.springer.com/article/10.1007/s10565-019-09496-2> [Accessed: 17 February 2022].
- Niu, X. et al., 2022. Long-term outcomes of nasopharyngeal carcinoma patients with T1-2 stage in intensity-modulated radiotherapy era. *International Journal of Medical Sciences*, 19(2).
- Noyce, R.S. and Richardson, C.D., 2012. Nectin 4 is the epithelial cell receptor for measles virus. *Trends in Microbiology*, 20(9), pp.429–439. Available at: <http://www.cell.com/article/S0966842X12000960/fulltext> [Accessed: 27 August 2022].
- Onomoto, K., Onoguchi, K. and Yoneyama, M., 2021. Regulation of RIG-I-like receptor-mediated signaling: interaction between host and viral factors. *Cellular & Molecular Immunology 2021 18:3*, 18(3), pp.539–555. Available at: <https://www.nature.com/articles/s41423-020-00602-7> [Accessed: 31 January 2023].
- Oun, R., Moussa, Yvonne E and Wheate, N.J., 2018. The side effects of platinum-based chemotherapy drugs: a review for chemists. *Dalton Transactions*, 47(19), pp.6645–6653.
- Oun, R., Moussa, Yvonne E. and Wheate, N.J., 2018. The side effects of platinum-based chemotherapy drugs: A review for chemists. *Dalton Transactions*, 47(19).
- Owusu, I.A., Quaye, O., Passalacqua, K.D. and Wobus, C.E., 2021. Egress of non-enveloped enteric RNA viruses. *Journal of General Virology*, 102(3).
- Packiriswamy, N. et al., 2020. Oncolytic measles virus therapy enhances tumor antigen-specific T-cell responses in patients with multiple myeloma. *Leukemia*. Available at: <https://doi.org/10.1038/s41375-020-0828-7>.

- Pan, S.T. et al., 2016. Molecular mechanisms for tumour resistance to chemotherapy. *Clinical and Experimental Pharmacology and Physiology*, 43(8), pp.723–737. Available at: <https://onlinelibrary.wiley.com/doi/full/10.1111/1440-1681.12581> [Accessed: 10 March 2022].
- Pan, X. Bin et al., 2017. Concurrent chemoradiotherapy degrades the quality of life of patients with stage II nasopharyngeal carcinoma as compared to radiotherapy. *Oncotarget*, 8(8).
- Pastor, M. et al., 2018. SEOM clinical guideline in nasopharynx cancer (2017). *Clinical and Translational Oncology*, 20(1), pp.84–88. Available at: </pmc/articles/PMC5785612/?report=abstract> [Accessed: 29 July 2020].
- Peng, K.-W. et al., 2004. Oncolytic Measles Virus Selectively Targets CD46 Overexpression on Myeloma Cells. *Blood*, 104(11).
- Perez, C.A. et al., 1969. Cancer of the nasopharynx. Factors influencing prognosis. *Cancer*, 24(1), pp.1–17.
- Perri, F. et al., 2019. Management of recurrent nasopharyngeal carcinoma: Current perspectives. *OncoTargets and Therapy*, 12.
- Pidelaserra-Martí, G. and Engeland, C.E., 2020. Mechanisms of measles virus oncolytic immunotherapy. *Cytokine and Growth Factor Reviews*, 56.
- Pierce, A. et al., 2008. Eight-channel iTRAQ enables comparison of the activity of six leukemogenic tyrosine kinases. *Molecular & cellular proteomics : MCP*, 7(5), pp.853–863. Available at: <https://pubmed.ncbi.nlm.nih.gov/17951628/> [Accessed: 26 May 2022].
- Pignata, C. et al., 1998. Apoptosis as a Mechanism of Peripheral Blood Mononuclear Cell Death after Measles and Varicella-Zoster Virus Infections in Children. *Pediatric Research 1998 43:1*, 43(1), pp.77–83. Available at: <https://www.nature.com/articles/pr199812> [Accessed: 31 March 2022].
- Qiu, Y. et al., 2017. Contamination of Chinese salted fish with volatile N-nitrosamines as determined by QuEChERS and gas chromatography–tandem mass spectrometry. *Food Chemistry*, 232, pp.763–769.
- Qu, S., Liang, Z.G. and Zhu, X.D., 2015. Advances and challenges in intensity-modulated radiotherapy for nasopharyngeal carcinoma. *Asian Pacific Journal of Cancer Prevention*, 16(5), pp.1687–1692. Available at: http://journal.waocp.org/article_30651.html.
- Rahman, M.M. and McFadden, G., 2021. Oncolytic viruses: Newest frontier for cancer immunotherapy. *Cancers*, 13(21).
- Ravindranath, N.M.H. and Shuler, C., 2006. Expression of complement restriction factors (CD46, CD55 & CD59) in head and neck squamous cell carcinomas. *Journal of Oral Pathology and Medicine*, 35(9).
- Reches, A. et al., 2020. Nectin4 is a novel TIGIT ligand which combines checkpoint inhibition and tumor specificity. *Journal for ImmunoTherapy of Cancer*, 8(1).

- Ren, J.T. et al., 2017. Potential factors associated with clinical stage of nasopharyngeal carcinoma at diagnosis: A case-control study. *Chinese Journal of Cancer*, 36(1), pp.1–10. Available at: <https://cancercommun.biomedcentral.com/articles/10.1186/s40880-017-0239-y> [Accessed: 23 September 2022].
- Richetta, C. et al., 2013. Sustained Autophagy Contributes to Measles Virus Infectivity. *PLOS Pathogens*, 9(9), p.e1003599. Available at: <https://journals.plos.org/plospathogens/article?id=10.1371/journal.ppat.1003599> [Accessed: 31 March 2022].
- Rota, J.S., Zhong-De, W., Rota, P.A. and Bellini, W.J., 1994. Comparison of sequences of the H, F, and N coding genes of measles virus vaccine strains. *Virus Research*, 31(3), pp.317–330.
- Roy Chattopadhyay, N., Das, P., Chatterjee, K. and Choudhuri, T., 2017. Higher incidence of nasopharyngeal carcinoma in some regions in the world confers for interplay between genetic factors and external stimuli. *Drug Discoveries & Therapeutics*, 11(4).
- Rozières, A., Viret, C. and Faure, M., 2017. Autophagy in measles virus infection. *Viruses*, 9(12).
- Rudak, P.T., Yao, T., Richardson, C.D. and Mansour Haeryfar, S.M., 2021. Measles Virus Infects and Programs MAIT Cells for Apoptosis. *The Journal of Infectious Diseases*, 223(4), pp.667–672. Available at: <https://academic.oup.com/jid/article/223/4/667/5867532> [Accessed: 21 September 2022].
- Rueda Domínguez, A. et al., 2022. SEOM-TTCC clinical guideline in nasopharynx cancer (2021). *Clinical and Translational Oncology*, 24(4).
- Ruepp, A. et al., 2004. The FunCat, a functional annotation scheme for systematic classification of proteins from whole genomes. *Nucleic Acids Research*, 32(18).
- Russell, S.J. et al., 2014. Remission of disseminated cancer after systemic oncolytic virotherapy. *Mayo Clinic Proceedings*, 89(7), pp.926–933. Available at: <http://dx.doi.org/10.1016/j.mayocp.2014.04.003>.
- Sanders, C. et al., 2022. Nectin-4 is widely expressed in head and neck squamous cell carcinoma. *Oncotarget*, 13(1).
- Sarmiento, M.P.C.B. and Mejia, M.B.A., 2014. Preliminary assessment of nasopharyngeal carcinoma incidence in the Philippines: A second look at published data from four centers. *Chinese Journal of Cancer*, 33(3).
- Schmidt, A., Forne, I. and Imhof, A., 2014. Bioinformatic analysis of proteomics data. *BMC systems biology*, 8.
- Schneider, U., von Messling, V., Devaux, P. and Cattaneo, R., 2002. Efficiency of Measles Virus Entry and Dissemination through Different Receptors. *Journal of Virology*, 76(15), pp.7460–7467.

- Secretan, B. et al., 2009. A review of human carcinogens—Part E: tobacco, areca nut, alcohol, coal smoke, and salted fish. *The Lancet Oncology*, 10(11), pp.1033–1034. Available at: [https://doi.org/10.1016/S1470-2045\(09\)70326-2](https://doi.org/10.1016/S1470-2045(09)70326-2).
- Severa, M., Farina, C., Salvetti, M. and Coccia, E.M., 2020. Three Decades of Interferon- β in Multiple Sclerosis: Can We Repurpose This Information for the Management of SARS-CoV2 Infection? *Frontiers in Immunology*, 11.
- Shahinuzzaman, A.D.A. et al., 2020. Improved in-solution trypsin digestion method for methanol–chloroform precipitated cellular proteomics sample. *Journal of Separation Science*, 43(11), pp.2125–2132. Available at: <https://onlinelibrary.wiley.com/doi/full/10.1002/jssc.201901273> [Accessed: 29 August 2022].
- Shannon, P. et al., 2003. Cytoscape: A software Environment for integrated models of biomolecular interaction networks. *Genome Research*, 13(11).
- Shingai, M. et al., 2005. Wild-Type Measles Virus Infection in Human CD46/CD150-Transgenic Mice: CD11c-Positive Dendritic Cells Establish Systemic Viral Infection. *The Journal of Immunology*, 175(5).
- Sia, J., Szmyd, R., Hau, E. and Gee, H.E., 2020. Molecular Mechanisms of Radiation-Induced Cancer Cell Death: A Primer. *Frontiers in Cell and Developmental Biology*, 8, p.41.
- Simo, R. et al., 2016. Nasopharyngeal carcinoma: United Kingdom National Multidisciplinary Guidelines. *The Journal of laryngology and otology*, 130(S2), pp.S97–S103. Available at: </pmc/articles/PMC4873914/?report=abstract> [Accessed: 29 July 2020].
- Singh, S.A. and Ghosh, S.K., 2019. Metabolic Phase I (CYPs) and Phase II (GSTs) Gene Polymorphisms and Their Interaction with Environmental Factors in Nasopharyngeal Cancer from the Ethnic Population of Northeast India. *Pathology and Oncology Research*, 25(1).
- Stern, L.B., Greenberg, M., Gershoni, J.M. and Rozenblatt, S., 1995. The hemagglutinin envelope protein of canine distemper virus (CDV) confers cell tropism as illustrated by CDV and measles virus complementation analysis. *Journal of Virology*, 69(3).
- Stoffey, R.D., 2012. Head and Neck Imaging, 5th ed. Head and Neck Imaging , 5th ed. By Peter M. Som and Hugh D. Curtin. St. Louis, MO: Mosby, 3080 pp., 2011. \$451.95 hardcover (ISBN: 978-0323053556). *American Journal of Roentgenology*, 199(5), pp.W657–W657.
- Strong, M.J. et al., 2014. Comprehensive High-Throughput RNA Sequencing Analysis Reveals Contamination of Multiple Nasopharyngeal Carcinoma Cell Lines with HeLa Cell Genomes. *Journal of virology*, 88(July), pp.10696–10704. Available at: <http://www.ncbi.nlm.nih.gov/pubmed/24991015>.
- Talamo, G. et al., 2015. Current role of radiation therapy for multiple myeloma. *Frontiers in Oncology*, 5(FEB).

- Tan, C.K. et al., 2018. Gender differences in risk of developing nasopharyngeal cancer (NPC) in one of the highest NPC ethnic in the world. *Annals of Oncology*, 29.
- Tang, D. et al., 2019. The molecular machinery of regulated cell death. *Cell Research*, 29(5).
- Tatsuo, H., Ono, N., Tanaka, K. and Yanagi, Y., 2000. Slam (CDw150) is a cellular receptor for measles virus. *Nature*, 406(6798).
- Thorburn, J. et al., 2009. Autophagy regulates selective HMGB1 release in tumor cells that are destined to die. *Cell Death and Differentiation*, 16(1).
- Tian, L. et al., 2021. IRGM promotes melanoma cell survival through autophagy and is a promising prognostic biomarker for clinical application. *Molecular Therapy - Oncolytics*, 20.
- Tian, W. et al., 2020. Multiple low-frequency and rare HLA-B allelic variants are associated with reduced risk in 1,105 nasopharyngeal carcinoma patients in Hunan province, southern China. *International Journal of Cancer*, 147(5).
- Tsai, W.-L. et al., 2014. Impact of late toxicities on quality of life for survivors of nasopharyngeal carcinoma. *BMC cancer*, 14, p.856. Available at: <https://pubmed.ncbi.nlm.nih.gov/25413127>.
- Tsang, C.M. et al., 2019. Chapter 3 - Pathogenesis of Nasopharyngeal Carcinoma: Histogenesis, Epstein–Barr Virus Infection, and Tumor Microenvironment. In: Lee, A.W.M., Lung, M.L. and Ng, W.T.B.T.-N.C., (eds.) Academic Press, pp. 45–64.
- Tsang, C.M. et al., 2012. Cyclin D1 overexpression supports stable EBV infection in nasopharyngeal epithelial cells. *Proceedings of the National Academy of Sciences of the United States of America*, 109(50).
- Tsao, S.W., Tsang, C.M. and Lo, K.W., 2017. Epstein-barr virus infection and nasopharyngeal carcinoma. *Philosophical Transactions of the Royal Society B: Biological Sciences*, 372(1732).
- Tso, K.K.Y. et al., 2013. Complete genomic sequence of Epstein-Barr virus in nasopharyngeal carcinoma cell line C666-1. *Infectious Agents and Cancer*, 8(1).
- Tu, Z. et al., 2015. BRCC3 acts as a prognostic marker in nasopharyngeal carcinoma patients treated with radiotherapy and mediates radiation resistance in vitro. *Radiation Oncology*, 10(1).
- Unsal, A.A. et al., 2019. Basaloid nasopharyngeal carcinoma: A population-based analysis of a rare tumor. *Laryngoscope*, 129(12).
- Urban, P.L., 2016. Quantitative mass spectrometry: An overview. *Philosophical Transactions of the Royal Society A: Mathematical, Physical and Engineering Sciences*, 374(2079). Available at: <http://dx.doi.org/10.1098/rsta.2015.0382> [Accessed: 12 May 2022].

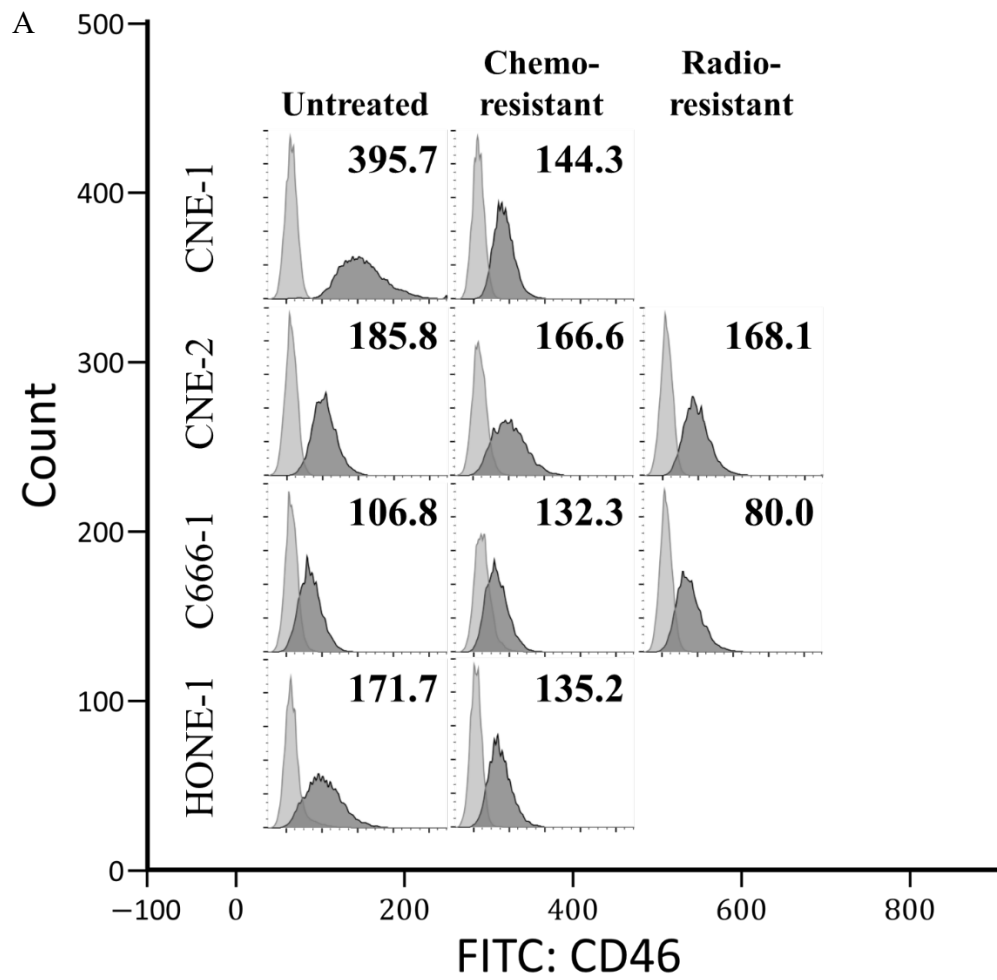
- Vanmeerbeek, I. et al., 2020. Trial watch: chemotherapy-induced immunogenic cell death in immuno-oncology. *Oncoimmunology*, 9(1). Available at: </pmc/articles/PMC6959434/> [Accessed: 10 March 2022].
- Vaudel, M. et al., 2015. PeptideShaker enables reanalysis of MS-derived proteomics data sets: To the editor. *Nature Biotechnology*, 33(1).
- Wah, S. et al., 2014. Etiological factors of nasopharyngeal carcinoma. *Oral Oncology*, 50(5), pp.330–338. Available at: <http://dx.doi.org/10.1016/j.oraloncology.2014.02.006>.
- Wang, B. et al., 2015. Deficiency of caspase 3 in tumor xenograft impairs therapeutic effect of measles virus Edmoston strain. *Oncotarget*, 6(18), pp.16019–16030. Available at: <https://www.oncotarget.com/article/3496/text/> [Accessed: 31 March 2022].
- Wang, H.Y. et al., 2016. A new prognostic histopathologic classification of nasopharyngeal carcinoma. *Chinese journal of cancer*, 35, p.41.
- Wang, N. et al., 2001. CD150 is a member of a family of genes that encode glycoproteins on the surface of hematopoietic cells. *Immunogenetics*, 53(5).
- Wang, P. et al., 2020. Epstein-Barr Virus Early Protein BFRF1 Suppresses IFN- β Activity by Inhibiting the Activation of IRF3. *Frontiers in Immunology*, 11.
- Wang, P. and Wilson, S.R., 2013. Mass spectrometry-based protein identification by integrating de novo sequencing with database searching. *BMC Bioinformatics*, 14(Suppl 2), p.S24. Available at: </pmc/articles/PMC3549845/> [Accessed: 13 May 2022].
- Wang, R. and Kang, M., 2021. Guidelines for radiotherapy of nasopharyngeal carcinoma. *Precision Radiation Oncology*, 5(3).
- Wang, Y., Zhang, Y. and Ma, S., 2013. Racial differences in nasopharyngeal carcinoma in the United States. *Cancer Epidemiology*, 37(6).
- Wei, K. rong et al., 2011. Histopathological classification of nasopharyngeal carcinoma. *Asian Pacific Journal of Cancer Prevention*, 12(5).
- Wei, K.-R. et al., 2017. Nasopharyngeal carcinoma incidence and mortality in China, 2013. *Chinese Journal of Cancer*, 36(1).
- Welsch, S., Müller, B. and Kräusslich, H.G., 2007. More than one door – Budding of enveloped viruses through cellular membranes. *FEBS Letters*, 581(11), pp.2089–2097. Available at: <https://onlinelibrary.wiley.com/doi/full/10.1016/j.febslet.2007.03.060> [Accessed: 1 February 2023].
- Wen-Hsuan, W.L. et al., 2021. Primary differentiated respiratory epithelial cells respond to apical measles virus infection by shedding multinucleated giant cells. *Proceedings of the National Academy of Sciences of the United States of America*, 118(11).

- West, S., Hildesheim, A. and Dosemeci, M., 1993. Non-viral risk factors for nasopharyngeal carcinoma in the philippines: Results from a case-control study. *International Journal of Cancer*, 55(5).
- Wiese, S., Reidegeld, K.A., Meyer, H.E. and Warscheid, B., 2007. Protein labeling by iTRAQ: A new tool for quantitative mass spectrometry in proteome research. *PROTEOMICS*, 7(3), pp.340–350. Available at: <https://onlinelibrary.wiley.com/doi/full/10.1002/pmic.200600422> [Accessed: 13 May 2022].
- Wong, K.C.W. et al., 2021. Nasopharyngeal carcinoma: an evolving paradigm. *Nature Reviews Clinical Oncology*, 18(11).
- Wong, K.Y. et al., 2023. Epidemiology of Nasopharyngeal Carcinoma in Sarawak, East Malaysia. *Asian Pacific Journal of Cancer Prevention*, 24(8).
- Wong, N.H.M., Yuen, K.-S., Chan, C.-P. and Jin, D.-Y., 2017. Suppression of IFN- β production by Epstein-Barr virus lytic transactivator Zta. *The Journal of Immunology*, 198(1 Supplement), p.214.15. Available at: http://www.jimmunol.org/content/198/1_Supplement/214.15.abstract.
- Xia, M. et al., 2014. Mitophagy Enhances Oncolytic Measles Virus Replication by Mitigating DDX58/RIG-I-Like Receptor Signaling. *Journal of Virology*, 88(9), pp.5152–5164.
- Xia, Mao et al., 2014. Mitophagy switches cell death from apoptosis to necrosis in NSCLC cells treated with oncolytic measles virus. *Oncotarget*, 5(11), pp.3907–3918. Available at: <https://www.oncotarget.com/article/2028/text/> [Accessed: 31 March 2022].
- Xie, S.H. et al., 2013. Sex difference in the incidence of nasopharyngeal carcinoma in Hong Kong 1983-2008: Suggestion of a potential protective role of oestrogen. *European Journal of Cancer*, 49(1).
- Xu, C., Sun, L., Liu, W. and Duan, Z., 2018. Latent membrane protein 1 of Epstein-Barr virus promotes RIG-I degradation mediated by proteasome pathway. *Frontiers in Immunology*, 9(JUN), p.1446.
- Yan, G., Elbadawi, M. and Efferth, T., 2020. Multiple cell death modalities and their key features (Review). *World Academy of Sciences Journal*, 2(2), pp.39–48. Available at: <http://www.spandidos-publications.com/10.3892/wasj.2020.40/abstract> [Accessed: 17 February 2022].
- Yeo, G.G., Beh, S.P., Tan, C.K. and Pei Jye, V., 2018. Strong family history of nasopharyngeal carcinoma (NPC) in Bidayuh, a local native group in Sarawak, Malaysia. *Annals of Oncology*, 29.
- Young, L.S. and Dawson, C.W., 2014. Epstein-Barr virus and nasopharyngeal carcinoma. *Chinese Journal of Cancer*, 33(12), pp.581–590.
- Young, Y.-H., 2019. Irradiated ears in nasopharyngeal carcinoma survivors: A review. *The Laryngoscope*, 129(3), pp.637–642. Available at: <https://doi.org/10.1002/lary.27303>.

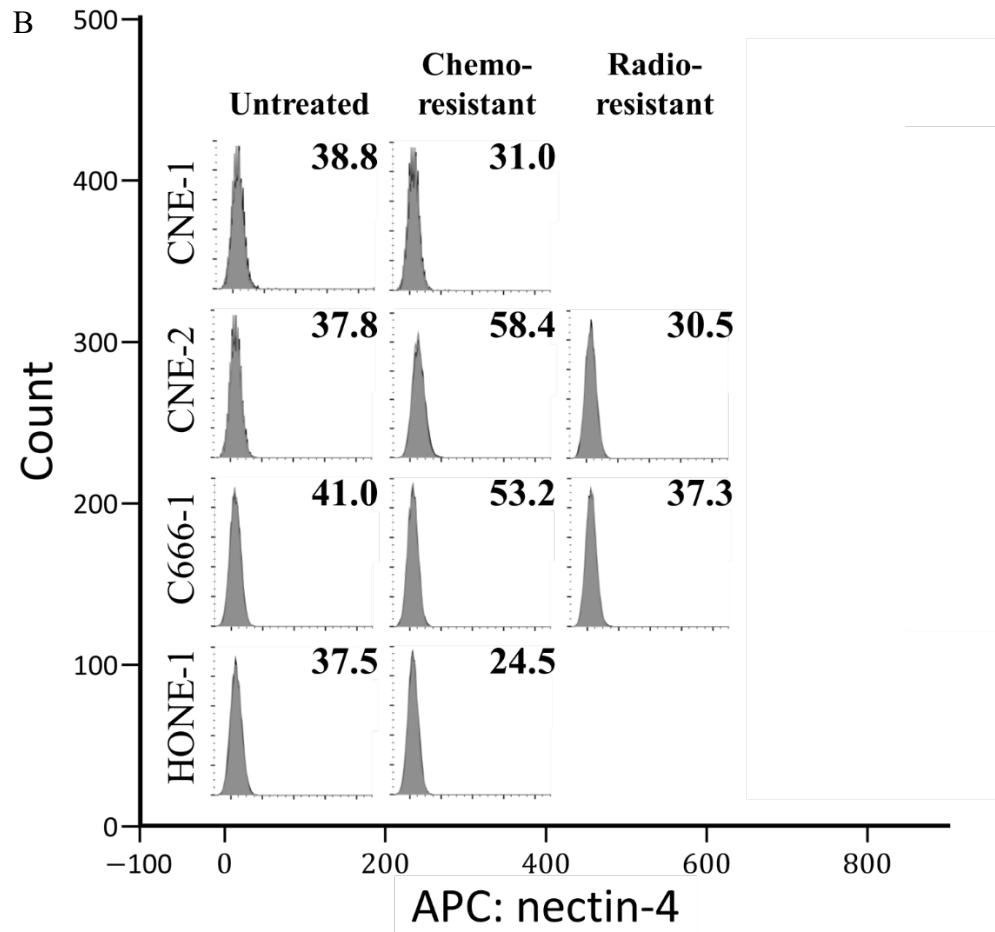
- Yu, F. et al., 2020. Epstein–barr virus infection of pseudostratified nasopharyngeal epithelium disrupts epithelial integrity. *Cancers*, 12(9).
- Yu, M.C. et al., 1988. Preserved foods and nasopharyngeal carcinoma: a case-control study in Guangxi, China. *Cancer research*, 48(7), pp.1954–1959.
- Yuan, J.-M. et al., 2000. Preserved foods in relation to risk of nasopharyngeal carcinoma in Shanghai, China. *International Journal of Cancer*, 85(3), pp.358–363. Available at: [https://doi.org/10.1002/\(SICI\)1097-0215\(20000201\)85:3%3C358::AID-IJC11%3E3.0.CO](https://doi.org/10.1002/(SICI)1097-0215(20000201)85:3%3C358::AID-IJC11%3E3.0.CO).
- Zaoui, K. et al., 2012. Chemovirotherapy for head and neck squamous cell carcinoma with EGFR-targeted and CD/UPRT-armed oncolytic measles virus. *Cancer Gene Therapy*, 19(3).
- Zhang, H. and Chen, Z., 2020. Autophagy and Cell Death: Antitumor Drugs Targeting Autophagy. In: *Programmed Cell Death*.
- Zhang, P. et al., 2014. Epithelial-mesenchymal transition is necessary for acquired resistance to cisplatin and increases the metastatic potential of nasopharyngeal carcinoma cells. *International Journal of Molecular Medicine*, 33(1).
- Zhang, X. et al., 2007. Anti-apoptotic role of TWIST and its association with Akt pathway in mediating taxol resistance in nasopharyngeal carcinoma cells. *International Journal of Cancer*, 120(9).
- Zhang, X. et al., 2019. GORASP2/GRASP55 collaborates with the PtdIns3K UVRAG complex to facilitate autophagosome-lysosome fusion. *Autophagy*, 15(10).
- Zhao, D. et al., 2013. Live attenuated measles virus vaccine induces apoptosis and promotes tumor regression in lung cancer. *Oncology Reports*, 29(1), pp.199–204. Available at: <http://www.spandidos-publications.com/10.3892/or.2012.2109/abstract> [Accessed: 31 March 2022].
- Zhou, J. et al., 2019. Immunogenic cell death in cancer therapy: Present and emerging inducers. *Journal of Cellular and Molecular Medicine*, 23(8), p.4854. Available at: </pmc/articles/PMC6653385/> [Accessed: 6 April 2022].
- Zhu, X. et al., 2015. Cytosolic HMGB1 controls the cellular autophagy/apoptosis checkpoint during inflammation. *Journal of Clinical Investigation*, 125(3).
- Zou, X.N., Lu, S.H. and Liu, B., 1994. Volatile N-nitrosamines and their precursors in chinese salted fish—a possible etiological factor for NPC in China. *International Journal of Cancer*, 59(2), pp.155–158.
- Zuo, Q. et al., 2010. Development of cetuximab-resistant human nasopharyngeal carcinoma cell lines and mechanisms of drug resistance. *Biomedicine and Pharmacotherapy*, 64(8).

APPENDICES

APPENDIX A



APPENDIX A (CONTINUE)



Flow cytometry results show (A) second representative data on CD46 expression and (B) low expression of nectin-4 protein in RR-, CR- and untreated NPC. Light grey: Isotype control, Dark grey: anti-nectin-4 stained. The number inset represents the shift of the MFI signal between the anti-CD46 and -nectin-4 stained and isotype control sample. Data was collected from (A) two and (B) single biological replicates, respectively, without technical repeat in each biological replicate.

APPENDIX B

DAP at 24-hours post-infection time point

Biological Replicate 1					Biological Replicate 2				
Main Accession	Gene Name	Confidence [%]	Validation	log2 (114/113)	Main Accession	Gene Name	Confidence [%]	Validation	log2 (118/117)
P49773	HINT1	90.05	Doubtful	1.981	O75874	IDH1	90.05	Doubtful	1.507
P09104	ENO2	83.77	Confident	1.596	P27635	RPL10	81.52	Confident	0.680
P13645	KRT10	95.39	Confident	0.700	Q02878	RPL6	90.61	Doubtful	0.751
P30048	PRDX3	94.44	Confident	0.969	Q13200	PSMD2	91.68	Doubtful	1.300
Q12907	LMAN2	86.92	Doubtful	0.773	O43615	TIMM44	96.04	Confident	0.609
P62701	RPS4X	84.50	Doubtful	0.667	P49736	MCM2	91.78	Doubtful	0.987
P63000	RAC1	83.33	Doubtful	0.717	P23396	RPS3	96.47	Confident	0.923
O75390	CS	96.48	Doubtful	0.949	Q13162	PRDX4	84.50	Doubtful	1.400
P52292	KPNA2	84.50	Doubtful	0.717	P32119	PRDX2	92.78	Doubtful	0.987
Q16891	IMMT	92.00	Doubtful	0.717	P55084	HADHB	90.05	Doubtful	1.987
P28066	PSMA5	90.13	Doubtful	0.717	P35998	PSMC2	86.98	Doubtful	1.196
O14980	XPO1	88.56	Doubtful	1.314	P10515	DLAT	84.50	Doubtful	0.987
P46783	RPS10	88.56	Doubtful	0.717	P50990	CCT8	98.38	Confident	0.759
P02545	LMNA	90.98	Doubtful	0.894	Q99497	PARK7	98.23	Confident	1.057

APPENDIX B (CONTINUE)

Biological Replicate 1					Biological Replicate 2				
Main Accession	Gene Name	Confidence [%]	Validation	log2 (114/113)	Main Accession	Gene Name	Confidence [%]	Validation	log2 (118/117)
Q15459	SF3A1	90.20	Doubtful	1.433	Q9Y624	F11R	90.05	Doubtful	0.987
P22314	UBA1	98.33	Confident	1.184		CKAP4	98.31	Confident	1.273
P12270	TPR	89.89	Doubtful	2.136	P08727	KRT19	96.11	Confident	0.589
Q9UQ80	PA2G4	81.44	Doubtful	1.449	P06748	NPM1	98.34	Confident	1.197
P19338	NCL	98.29	Confident	0.814	Q9Y617	PSAT1	94.65	Confident	1.157
P38646	HSPA9	98.54	Confident	0.717	P13073	COX4I1	86.92	Doubtful	1.064
P13073	COX4I1	86.92	Doubtful	0.717	P50991	CCT4	94.28	Doubtful	0.987
P62913	RPL11	90.98	Doubtful	0.766	P62913	RPL11	90.98	Doubtful	0.936
Q5VZF2	MBNL2	84.50	Doubtful	1.464	Q5JR59	MTUS2	87.09	Doubtful	0.987
O75131	CPNE3	84.50	Doubtful	1.329	Q9NTK5	OLA1	91.10	Doubtful	1.781
P82979	SARNP	84.50	Doubtful	1.955	P08865	RPSA	98.01	Confident	0.733
P21964	COMT	90.09	Doubtful	0.824	P23526	AHCY	91.63	Doubtful	0.765
P09429	HMGB1	90.98	Confident	-0.710	P53999	SUB1	84.50	Doubtful	1.120
P01911	HLA-DRB1	83.33	Doubtful	-0.962	Q5VZF2	MBNL2	84.50	Doubtful	1.383
P68104	EEF1A1	97.99	Confident	-0.664	O75131	CPNE3	84.50	Doubtful	0.944
Q9NR30	DDX21	95.56	Doubtful	-0.813	O14950	MYL12B	83.33	Doubtful	1.091
Q7KZF4	SND1	96.05	Confident	-1.547	P09429	HMGB1	90.98	Confident	-0.894
O75874	IDH1	90.05	Doubtful	-0.604	P55072	VCP	98.22	Confident	-1.013
Q9UDT6	CLIP2	90.06	Confident	-0.612	Q14697	GANAB	96.13	Doubtful	-1.826

APPENDIX B (CONTINUE)

Biological Replicate 1					Biological Replicate 2				
Main Accession	Gene Name	Confidence [%]	Validation	log2 (114/113)	Main Accession	Gene Name	Confidence [%]	Validation	log2 (118/117)
P08238	HSP90AB1	97.10	Confident	-0.842	P68104	EEF1A1	97.99	Confident	-1.125
P13667	PDIA4	98.32	Confident	-1.487	A1Z651	gag-pol	95.72	Confident	-1.068
Q9Y265	RUVBL1	94.46	Doubtful	-1.027	P20073	ANXA7	91.75	Confident	-0.898
Q99623	PHB2	95.93	Doubtful	-1.174	Q06323	PSME1	98.45	Confident	-1.899
P60900	PSMA6	91.62	Doubtful	-1.182	P30048	PRDX3	94.44	Confident	-0.985
P13010	XRCC5	98.40	Confident	-2.021	Q12907	LMAN2	86.92	Doubtful	-0.586
P09622	DLD	98.38	Confident	-1.125	P0DP23	CALM1	94.28	Confident	-0.776
P02768	ALB	95.57	Confident	-1.403	Q15366	PCBP2	90.11	Confident	-0.856
P62805	H4C16	98.43	Confident	-0.673	P05388	RPLP0	98.45	Confident	-1.456
P07237	P4HB	98.28	Confident	-1.899	P61978	HNRNPK	98.36	Confident	-1.126
P11142	HSPA8	98.53	Confident	-1.468	P07900	HSP90AA1	98.38	Confident	-0.862
Q96C19	EFHD2	86.92	Doubtful	-0.892	P25786	PSMA1	90.09	Doubtful	-1.334
P12236	SLC25A6	83.33	Confident	-2.562	Q00839	HNRNPU	96.63	Confident	-0.616
P68363	TUBA1B	93.87	Confident	-0.903	P00390	GSR	95.76	Confident	-1.935
Q9NTK5	OLA1	91.10	Doubtful	-1.197	O60506	SYNCRIP	90.06	Confident	-1.013
P52209	PGD	93.13	Doubtful	-1.283	Q14103	HNRNPD	91.98	Confident	-11.702
P61247	RPS3A	94.65	Confident	-2.770	P62937	PPIA	98.42	Confident	-1.124
Q07021	C1QBP	98.00	Confident	-1.248	P25398	RPS12	95.58	Confident	-0.675
P05455	SSB	96.07	Confident	-2.262	Q96C19	EFHD2	86.92	Doubtful	-0.823
					P31947	SFN	86.92	Doubtful	-0.730
					P52209	PGD	93.13	Doubtful	-1.506

APPENDIX C

DAP at 36-hours post-infection timepoint

Biological Replicate 1					Biological Replicate 2				
Main Accession	Gene Name	Confidence [%]	Validation	log2 (115/113)	Main Accession	Gene Name	Confidence [%]	Validation	log2 (119/117)
Q02543	RPL18A	90.05	Doubtful	0.624	Q02543	RPL18A	90.05	Doubtful	1.602
P28838	LAP3	89.93	Doubtful	0.605	Q92945	KHSRP	84.50	Doubtful	0.915
P08238	HSP90AB1	97.10	Confident	1.132	P07355	ANXA2	98.31	Confident	0.915
P13667	PDIA4	98.32	Confident	0.616	P13667	PDIA4	98.32	Confident	0.986
Q92499	DDX1	81.60	Doubtful	1.999	P08579	SNRPB2	84.50	Doubtful	0.915
P0DP23	CALM1	94.28	Confident	0.831	P62753	RPS6	90.30	Doubtful	0.915
P23528	CFL1	98.22	Confident	1.003	P62826	RAN	98.00	Confident	0.914
P23396	RPS3	96.47	Confident	1.356	P09622	DLD	98.38	Confident	0.915
P49915	GMPS	84.50	Doubtful	1.224	Q16891	IMMT	92.00	Doubtful	0.714
P35998	PSMC2	86.98	Doubtful	1.901	P02545	LMNA	90.98	Doubtful	0.867
P06744	GPI	94.28	Doubtful	1.429	Q15459	SF3A1	90.20	Doubtful	0.901
O14737	PDCD5	91.73	Doubtful	0.750	P12270	TPR	89.89	Doubtful	1.510
P62805	H4C16	98.43	Confident	0.873	Q9UQ80	PA2G4	81.44	Doubtful	0.697
P23381	WARS1	83.33	Doubtful	1.000	P62263	RPS14	88.07	Doubtful	0.915
Q15459	SF3A1	90.20	Doubtful	0.650	P63244	RACK1	87.11	Doubtful	0.889
P09874	PARP1	96.65	Confident	0.656	P06748	NPM1	98.34	Confident	0.915
P07237	P4HB	98.28	Confident	0.671	P02786	TFRC	92.48	Doubtful	1.397
P19338	NCL	98.29	Confident	0.981	P0C0S5	H2AZ1	90.06	Confident	0.666
P62937	PPIA	98.42	Confident	1.171	P62491	RAB11A	91.73	Doubtful	1.072

APPENDIX C (CONTINUE)

Biological Replicate 1					Biological Replicate 2				
Main Accession	Gene Name	Confidence [%]	Validation	log2 (115/113)	Main Accession	Gene Name	Confidence [%]	Validation	log2 (119/117)
P07437	TUBB	96.45	Confident	1.000	P04406	GAPDH	98.55	Confident	1.368
Q9UNF0	PAC SIN2	91.73	Doubtful	1.160	P14314	PRKCSH	89.01	Doubtful	1.974
P60174	TPI1	98.32	Confident	1.000	Q8WXE9	STON2	86.92	Doubtful	1.059
P02786	TFRC	92.48	Doubtful	0.807	P50395	GDI2	83.33	Doubtful	0.915
P42167	TMPO	90.30	Doubtful	1.313	O75131	CPNE3	84.50	Doubtful	0.591
P04406	GAPDH	98.55	Confident	0.932	B2RXH8	HNRNPCL2	84.50	Doubtful	0.877
P78371	CCT2	98.34	Confident	1.000	P22392	NME2	90.09	Confident	-1.715
P01911	HLA-DRB1	83.33	Doubtful	-0.670	P09429	HMGB1	90.98	Confident	-1.013
Q14697	GANAB	96.13	Doubtful	-2.012	P01911	HLA-DRB1	83.33	Doubtful	-0.625
Q13200	PSMD2	91.68	Doubtful	-1.458	Q14697	GANAB	96.13	Doubtful	-1.085
P30048	PRDX3	94.44	Confident	-1.913	A1Z651	gag-pol	95.72	Confident	-1.431
O43615	TIMM44	96.04	Confident	-1.000	P20073	ANXA7	91.75	Confident	-1.085
P69905	HBA2	96.66	Confident	-1.300	Q9UDT6	CLIP2	90.06	Confident	-10.936
Q9Y265	RUVBL1	94.46	Doubtful	-1.287	P06753	TPM3	92.12	Confident	-0.781
Q99623	PHB2	95.93	Doubtful	-1.027	P30048	PRDX3	94.44	Confident	-1.144
Q13162	PRDX4	84.50	Doubtful	-2.291	P07195	LDHB	98.41	Confident	-1.782
P55084	HADHB	90.05	Doubtful	-16.092	P54819	AK2	92.49	Doubtful	-1.168
P10050	N	83.33	Confident	-0.717	O75390	CS	96.48	Doubtful	-1.080
O14980	XPO1	88.56	Doubtful	-2.123	O60506	SYNCRIP	90.06	Confident	-1.281
P61604	HSPE1	98.45	Confident	-2.127	P62906	RPL10A	96.50	Confident	-2.873

APPENDIX C (CONTINUE)

Biological Replicate 1					Biological Replicate 2				
Main Accession	Gene Name	Confidence [%]	Validation	log2 (115/113)	Main Accession	Gene Name	Confidence [%]	Validation	log2 (119/117)
P25398	RPS12	95.58	Confident	-0.938	P11142	HSPA8	98.53	Confident	-1.972
P0C0S5	H2AZ1	90.06	Confident	-1.000	P25398	RPS12	95.58	Confident	-1.528
P29401	TKT	96.11	Confident	-0.628	P12236	SLC25A6	83.33	Confident	-0.752
P68363	TUBA1B	93.87	Confident	-9.068	P68363	TUBA1B	93.87	Confident	-0.665
P08865	RPSA	98.01	Confident	-1.634	P52209	PGD	93.13	Doubtful	-2.765
P99999	CYCS	96.11	Confident	-2.571	Q96AG4	LRRC59	95.92	Confident	-1.251
O75131	CPNE3	84.50	Doubtful	-1.310	P99999	CYCS	96.11	Confident	-1.107

APPENDIX D

DAP at 48-hours post-infection time point

Biological Replicate 1					Biological Replicate 2				
Main Accession	Gene Name	Confidence [%]	Validation	log2 (116/113)	Main Accession	Gene Name	Confidence [%]	Validation	log2 (121/117)
Q02543	RPL18A	90.05	Doubtful	1.967	P22392	NME2	90.09	Confident	1.216
P09429	HMGB1	90.98	Confident	0.661	P78527	PRKDC	95.37	Doubtful	1.052
Q92945	KHSRP	84.50	Doubtful	1.054	P62277	RPS13	88.56	Doubtful	1.150
Q14697	GANAB	96.13	Doubtful	0.866	P62753	RPS6	90.30	Doubtful	2.036
O75874	IDH1	90.05	Doubtful	1.000	Q9Y265	RUVBL1	94.46	Doubtful	0.594
P07355	ANXA2	98.31	Confident	2.022	P60900	PSMA6	91.62	Doubtful	1.720
Q02878	RPL6	90.61	Doubtful	0.584	P0DP23	CALM1	94.28	Confident	0.689
Q9Y265	RUVBL1	94.46	Doubtful	1.005	Q13162	PRDX4	84.50	Doubtful	1.296
P54819	AK2	92.49	Doubtful	0.850	P54819	AK2	92.49	Doubtful	0.874
P09622	DLD	98.38	Confident	0.613	P63000	RAC1	83.33	Doubtful	1.118
P61326	MAGOH	86.92	Doubtful	1.708	P49915	GMPS	84.50	Doubtful	0.928
Q9HC38	GLOD4	86.98	Doubtful	1.000	P06733	ENO1	98.53	Confident	0.913
P00558	PGK1	98.41	Confident	0.695	P10515	DLAT	84.50	Doubtful	1.568
Q16891	IMMT	92.00	Doubtful	1.196	Q15459	SF3A1	90.20	Doubtful	0.942
O14980	XPO1	88.56	Doubtful	1.309	Q9NS69	TOMM22	95.39	Confident	1.278
P02545	LMNA	90.98	Doubtful	1.181	P07237	P4HB	98.28	Confident	0.928
Q15459	SF3A1	90.20	Doubtful	1.072	P53004	BLVRA	90.34	Doubtful	0.928
P12270	TPR	89.89	Doubtful	1.013	P62937	PPIA	98.42	Confident	1.548
P49411	TUFM	96.06	Confident	1.000	Q9UNF0	PACSIN2	91.73	Doubtful	0.747

APPENDIX D (CONTINUE)

Biological Replicate 1					Biological Replicate 2				
Main Accession	Gene Name	Confidence [%]	Validation	log2 (116/113)	Main Accession	Gene Name	Confidence [%]	Validation	log2 (121/117)
P19338	NCL	98.29	Confident	1.931	P02786	TFRC	92.48	Doubtful	0.928
P38646	HSPA9	98.54	Confident	0.967	P33992	MCM5	88.56	Doubtful	0.928
P63244	RACK1	87.11	Doubtful	0.727	P23526	AHCY	91.63	Doubtful	1.120
P06748	NPM1	98.34	Confident	0.754	P54578	USP14	90.13	Doubtful	0.928
P60174	TPI1	98.32	Confident	2.888	Q8WXE9	STON2	86.92	Doubtful	0.768
P0C0S5	H2AZ1	90.06	Confident	0.648	P31689	DNAJA1	90.98	Doubtful	0.978
P62280	RPS11	83.33	Doubtful	1.011	P82979	SARNP	84.50	Doubtful	0.700
P09382	LGALS1	90.32	Doubtful	1.149	P0C734	BTRF1	84.50	Doubtful	-2.372
P23526	AHCY	91.63	Doubtful	1.266	Q7KZF4	SND1	96.05	Confident	-1.072
Q5VZF2	MBNL2	84.50	Doubtful	2.719	A1Z651	gag-pol	95.72	Confident	-1.011
P82979	SARNP	84.50	Doubtful	2.782	P13645	KRT10	95.39	Confident	-0.705
Q8NC51	SERBP1	90.13	Doubtful	1.000	Q99623	PHB2	95.93	Doubtful	-2.268
O14950	MYL12B	83.33	Doubtful	0.888	P35579	MYH9	98.40	Confident	-0.803
P27797	CALR	98.31	Confident	0.680	P23528	CFL1	98.22	Confident	-0.671
P01911	HLA-DRB1	83.33	Doubtful	-0.751	Q15366	PCBP2	90.11	Confident	-1.166
Q7KZF4	SND1	96.05	Confident	-18.238	P15259	PGAM2	94.65	Doubtful	-0.694
P20073	ANXA7	91.75	Confident	-1.125	P02768	ALB	95.57	Confident	-0.849
P05141	SLC25A5	91.94	Confident	-2.962	P06744	GPI	94.28	Doubtful	-1.584
Q06323	PSME1	98.45	Confident	-1.331	P09874	PARP1	96.65	Confident	-1.072

APPENDIX D (CONTINUE)

Biological Replicate 1					Biological Replicate 2				
Main Accession	Gene Name	Confidence [%]	Validation	log2 (116/113)	Main Accession	Gene Name	Confidence [%]	Validation	log2 (121/117)
O43615	TIMM44	96.04	Confident	-1.119	P01903	HLA-DRA	96.11	Confident	-1.072
P22695	UQCRC2	83.33	Doubtful	-1.193	P19338	NCL	98.29	Confident	-1.253
Q15366	PCBP2	90.11	Confident	-1.180	P61604	HSPE1	98.45	Confident	-1.430
Q13162	PRDX4	84.50	Doubtful	-0.916	P08727	KRT19	96.11	Confident	-0.589
P15259	PGAM2	94.65	Doubtful	-1.023	P12236	SLC25A6	83.33	Confident	-0.607
P07900	HSP90AA1	98.38	Confident	-0.811	P51572	BCAP31	86.92	Doubtful	-1.080
P06744	GPI	94.28	Doubtful	-0.921	Q15365	PCBP1	95.76	Confident	-1.072
Q00839	HNRNPU	96.63	Confident	-1.161	P63104	YWHAZ	96.13	Doubtful	-2.635
O60506	SYNCRIP	90.06	Confident	-0.828	P27797	CALR	98.31	Confident	-1.654
P62805	H4C16	98.43	Confident	-0.791					
P50990	CCT8	98.38	Confident	-2.356					
P62906	RPL10A	96.50	Confident	-1.000					
P62314	SNRPD1	81.57	Doubtful	-1.180					
Q16836	HADH	93.88	Doubtful	-1.174					
P04792	HSPB1	98.42	Confident	-1.000					
P01903	HLA-DRA	96.11	Confident	-1.236					
P25398	RPS12	95.58	Confident	-1.065					
Q96C19	EFHD2	86.92	Doubtful	-0.870					
P04179	SOD2	96.49	Confident	-1.000					
P13073	COX4I1	86.92	Doubtful	-7.819					

APPENDIX D (CONTINUE)

Biological Replicate 1					Biological Replicate 2				
Main Accession	Gene Name	Confidence [%]	Validation	log2 (116/113)	Main Accession	Gene Name	Confidence [%]	Validation	log2 (121/117)
P53999	SUB1	84.50	Doubtful	-0.697					
P61247	RPS3A	94.65	Confident	-16.693					
P60866	RPS20	86.92	Doubtful	-0.885					

APPENDIX E

GO result for DAP upregulated at 24-hour post-infection

intersecting genes	intersection size	precision	recall	term id	term name	-log10 (p-value)
PARK7 RPL6 RPS4X XPO1 PSMD2 DLAT KPNA2 MTUS2 HADHB PSMA5 SARNP NCL SUB1 AHCY RPL10 LMAN2 TPR LMNA RPS3 CCT8 HSPA8 TIMM44 PSAT1 PSMC2 UBA1	25	0.490	0.008	GO:0044260	cellular macromolecule metabolic process	4.51
PARK7 RPL6 RPS4X KPNA2 MTUS2 PSMA5 SARNP AHCY RPL10 LMAN2 LMNA HSPA8 SF3A1 TIMM44	14	0.275	0.015	GO:0006518	peptide metabolic process	4.33
PARK7 XPO1 DLAT RPL10 LMAN2 TPR RPS3 CCT8 HSPA8	9	0.176	0.029	GO:0034504	protein localization to nucleus	4.02
PARK7 RPL6 RPS4X RAC1 KPNA2 MTUS2 PSMA5 SARNP AHCY RPL10 LMAN2 LMNA HSPA8 SF3A1 TIMM44	15	0.294	0.012	GO:0043603	cellular amide metabolic process	3.78
RPL6 RPS4X KPNA2 MTUS2 AHCY RPL10 LMNA	7	0.137	0.044	GO:0002181	cytoplasmic translation	3.73

APPENDIX E (CONTINUE)

intersecting genes	intersection size	precision	recall	term id	term name	-log10 (p-value)
RPL6 RPS4X KPNA2 MTUS2 PSMA5 SARNP AHCY RPL10 LMAN2 LMNA HSPA8 TIMM44	12	0.235	0.016	GO:0006412	translation	3.60
RPL6 RPS4X RAC1 KPNA2 MTUS2 PSMA5 SARNP AHCY RPL10 LMAN2 LMNA HSPA8 TIMM44	13	0.255	0.015	GO:0043604	amide biosynthetic process	3.58
RPL6 RPS4X KPNA2 MTUS2 PSMA5 SARNP AHCY RPL10 LMAN2 LMNA HSPA8 TIMM44	12	0.235	0.016	GO:0043043	peptide biosynthetic process	3.42
RPL6 MTUS2 AHCY RPL10 LMAN2 LMNA HSPA8 CS UBA1	9	0.176	0.023	GO:0140694	non-membrane-bounded organelle assembly	3.23
RPL6 MTUS2 AHCY RPL10 HSPA8	5	0.098	0.082	GO:0042255	ribosome assembly	3.17
RPS3 CCT8 CCT4 HSPA9 UBA1	5	0.098	0.071	GO:0061077	chaperone-mediated protein folding	2.87
PARK7 RPL10 TPR RPS3 CCT8 HSPA9 HSPA8 UBA1	8	0.157	0.025	GO:0031647	regulation of protein stability	2.72

APPENDIX E (CONTINUE)

intersecting genes	intersection size	precision	recall	term id	term name	-log10 (p-value)
PARK7 LMAN2 TPR RPS3 CCT8 HSPA8	6	0.118	0.043	GO:1900180	regulation of protein localization to nucleus	2.68
PARK7 XPO1 DLAT PSMA5 LMAN2 TPR CCT4 HSPA8	8	0.157	0.024	GO:0006913	nucleocytoplasmic transport	2.65
PARK7 XPO1 DLAT PSMA5 LMAN2 TPR CCT4 HSPA8	8	0.157	0.024	GO:0051169	nuclear transport	2.65
PARK7 LMAN2 RPS3 CCT8 HSPA8	5	0.098	0.056	GO:1900182	positive regulation of protein localization to nucleus	2.33
PARK7 XPO1 PSMA5 LMAN2 CCT4 HSPA8	6	0.118	0.037	GO:0051168	nuclear export	2.30
OLA1 PARK7 ENO2 COMT RPL6 RPS4X HINT1 XPO1 PSMD2 RAC1 KPNA2 MTUS2 HADHB PSMA5 SARNP MCM2 AHCY RPL10 MYL12B PRDX2 LMAN2 TPR LMNA HSPA9 HSPA8 SF3A1 TIMM44 PA2G4 KRT19 PSAT1 PSMC2 UBA1	32	0.627	0.005	GO:1901564	organonitrogen compound metabolic process	2.30
PARK7 COMT HINT1 XPO1 PSMD2 CKAP4 HADHB MCM2 RPL10 MYL12B PRDX3 HSPA9 HSPA8 SF3A1 PSAT1 PSMC2 UBA1	17	0.333	0.008	GO:0044248	cellular catabolic process	2.00

APPENDIX E (CONTINUE)

intersecting genes	intersection size	precision	recall	term id	term name	-log10 (p-value)
RPS4X PSMA5 SARNP AHCY LMAN2 LMNA HSPA8 TIMM44	8	0.157	0.020	GO:0006417	regulation of translation	1.99
XPO1 PSMA5 LMAN2 RPS3 CCT8 HSPA8	6	0.118	0.030	GO:0006403	RNA localization	1.81
RPL6 XPO1 MTUS2 AHCY RPL10 HSPA8 TIMM44	7	0.137	0.023	GO:0042254	ribosome biogenesis	1.80
PARK7 F11R RPL6 XPO1 MTUS2 NCL SUB1 AHCY RPL10 MYL12B PRDX4 LMAN2 TPR LMNA RPS3 CCT8 CCT4 HSPA8 IDH1 IMMT CS UBA1	22	0.431	0.006	GO:0006996	organelle organization	1.78
PRDX2 RPS3 CCT8 CCT4 HSPA9 UBA1	6	0.118	0.028	GO:0006457	protein folding	1.67
PARK7 RPL10 RPS3 CCT8 HSPA8 UBA1	6	0.118	0.028	GO:0050821	protein stabilization	1.65
PARK7 RPL6 RPS4X RAC1 KPNA2 MTUS2 PSMA5 SARNP AHCY RPL10 LMAN2 LMNA HSPA8 TIMM44 KRT19	15	0.294	0.008	GO:1901566	organonitrogen compound biosynthetic process	1.64
PARK7 XPO1 LMAN2 CCT4	4	0.078	0.067	GO:0006611	protein export from nucleus	1.61

APPENDIX E (CONTINUE)

intersecting genes	intersection size	precision	recall	term id	term name	-log10 (p-value)
RPS4X PSMA5 SARNP AHCY LMAN2 LMNA HSPA8 TIMM4 4	8	0.157	0.017	GO:0034248	regulation of cellular amide metabolic process	1.56
PARK7 ENO2 COMT HINT1 XPO1 PSMD2 CKAP4 HADHB MC2 RPL10 MYL12B PRDX3 HSPA9 HSPA8 SF3A1 PSAT1 PSMC2 UBA1	18	0.353	0.007	GO:0009056	catabolic process	1.46
LMNA HSPA8 UBA1	3	0.059	0.136	GO:0032069	regulation of nuclease activity	1.43
RPL6 RPS4X KPNA2 MTUS2 PSMA5 SARNP AHCY RPL10 LMAN2 LMNA HSPA8 TIMM44	12	0.235	0.010	GO:0034645	cellular macromolecule biosynthetic process	1.42
RPS4X PSMA5 SARNP AHCY LMAN2 LMNA HSPA8 TIMM4 4	8	0.157	0.016	GO:2000112	regulation of cellular macromolecule biosynthetic process	1.41

APPENDIX E (CONTINUE)

intersecting genes	intersection size	precision	recall	term id	term name	-log10 (p-value)
PARK7 ENO2 COMT HINT1 XPO1 PSMD2 CKAP4 HADHB MCM2 RPL10 HSPA9 HSPA8 SF3A1 PSAT1 PSMC2 UBA1	16	0.314	0.008	GO:1901575	organic substance catabolic process	1.33
CCT4 HSPA9 UBA1	3	0.059	0.125	GO:0042026	protein refolding	1.32

APPENDIX F

GO result for DAP upregulated at 36-hour post-infection

intersecting genes	intersection size	precision	recall	term id	term name	-log10 (p-value)
HSP90AB1 TFRC CSE1L XPO1 KPNA2 CCT2 PARP1 DLD GMPS LMNA SF3A1 PSMC2	12	0.255	0.039	GO:0034504	protein localization to nucleus	8.33
HSP90AB1 TFRC CSE1L GDI2 PDCD5 XPO1 KPNA2 CCT2 PARP1 DLD KPNB1 GMPS LMNA RPS3 SNRNPB2 SF3A1 PA2G4 PSMC2	18	0.383	0.016	GO:0033365	protein localization to organelle	7.61
HSP90AB1 TFRC CCT2 PARP1 GMPS LMNA SF3A1 PSMC2	8	0.170	0.057	GO:1900180	regulation of protein localization to nucleus	5.86
HSP90AB1 TFRC CCT2 PARP1 LMNA SF3A1 PSMC2	7	0.149	0.078	GO:1900182	positive regulation of protein localization to nucleus	5.73
HSP90AB1 TFRC PRKCSH RPS14 XPO1 RPL18A KHSRP KPNA2 CCT2 WARS ANXA2 PARP1 TUBB PDIA4 EEF1A1 LAP3 KPNB1 GMPS LMNA TPR SF3A1 IMMT RAB11A PSMC2 P4HB	25	0.532	0.008	GO:0044260	cellular macromolecule metabolic process	5.51

APPENDIX F (CONTINUE)

intersecting genes	intersection size	precision	recall	term id	term name	-log10 (p-value)
RPS14 RPL18A KHSRP WARS TUBB PDIA4 EEF1A1 LAP3 KPNB1 LMNA TPR SF3A1 IMMT	13	0.277	0.018	GO:0006412	translation	5.10
RPS14 RPL18A KHSRP WARS TUBB PDIA4 EEF1A1 LAP3 PP1A KPNB1 LMNA TPR SF3A1 IMMT	14	0.298	0.016	GO:0043604	amide biosynthetic process	5.06
RPS14 RPL18A KHSRP WARS TUBB PDIA4 EEF1A1 LAP3 KPNB1 LMNA TPR SF3A1 IMMT	13	0.277	0.017	GO:0043043	peptide biosynthetic process	4.90
XPO1 CFL1 H2AFZ LAP3 DLD GMPS LMNA TPR SF3A1 PA2G4 PSMC2 P4HB	12	0.255	0.019	GO:0000226	microtubule cytoskeleton organization	4.71
HSP90AB1 TFRC GDI2 PDCD5 XPO1 CCT2 ANXA2 PARP1 GAPDH GMPS LMNA SNRPB2 SF3A1 PSMC2	14	0.298	0.015	GO:0060341	regulation of cellular localization	4.69
HSP90AB1 TFRC CSE1L GDI2 PDCD5 STON2 XPO1 CFL1 KPNB1 CCT2 ANXA2 PARP1 H2AFZ RPS6 GAPDH DLD KPNB1 GMPS LMNA RPS3 SNRPB2 SF3A1 PA2G4 PSMC2 P4HB	25	0.532	0.007	GO:0051641	cellular localization	4.58
HSP90AB1 PDCD5 CCT2 RPS6 GAPDH SNRPB2 GNB2L1 P4HB	8	0.170	0.038	GO:0006457	protein folding	4.48
HSP90AB1 TFRC GDI2 PDCD5 XPO1 CCT2 PARP1 GAPDH GMPS LMNA SNRPB2 SF3A1 PSMC2	13	0.277	0.015	GO:0032880	regulation of protein localization	4.35

APPENDIX F (CONTINUE)

intersecting genes	intersection size	precision	recall	term id	term name	-log10 (p-value)
GPI HSP90AB1 TFRC PDCD5 RPS14 XPO1 KHSRP WARS ANXA2 PDIA4 EEF1A1 LAP3 GAPDH KPNB1 GMPS LMNA TPR SF3A1 IMMT RAB11A P4HB	21	0.447	0.008	GO:0051246	regulation of protein metabolic process	4.30
DLD LMNA PSMC2	3	0.064	0.750	GO:0006404	RNA import into nucleus	4.16
HSP90AB1 CSE1L XPO1 KPNA2 DLD GMPS LMNA SF3A1 PSMC2	9	0.191	0.027	GO:0006913	nucleocytoplasmic transport	4.16
HSP90AB1 CSE1L XPO1 KPNA2 DLD GMPS LMNA SF3A1 PSMC2	9	0.191	0.027	GO:0051169	nuclear transport	4.16
HSP90AB1 TFRC GDI2 PDCD5 RPS14 XPO1 CFL1 CCT2 ANXA2 PARP1 H2AFZ LAP3 GAPDH DLD KPNB1 GMPS LMNA TPR RPS3 SF3A1 NPM1 PA2G4 PSMC2 P4HB	24	0.511	0.007	GO:0006996	organelle organization	3.93
RPS14 RPL18A KHSRP WARS TUBB PDIA4 EEF1A1 LAP3 KPNB1 LMNA TPR SF3A1 IMMT	13	0.277	0.014	GO:0006518	peptide metabolic process	3.92
XPO1 CFL1 H2AFZ LAP3 DLD GMPS LMNA TPR SNRPB2 SF3A1 PA2G4 PSMC2 P4HB	13	0.277	0.014	GO:0007017	microtubule-based process	3.89
HSP90AB1 CSE1L KPNA2 DLD GMPS LMNA PSMC2	7	0.149	0.042	GO:0006606	protein import into nucleus	3.84
HSP90AB1 CSE1L KPNA2 DLD GMPS LMNA PSMC2	7	0.149	0.041	GO:0051170	import into nucleus	3.77

APPENDIX F (CONTINUE)

intersecting genes	intersection size	precision	recall	term id	term name	-log10 (p-value)
GPI HSP90AB1 TFRC PRKCSH PDCD5 RPS14 XPO1 RPL18A KHSRP TPI1 WARS ANXA2 PARP1 TUBB PDIA4 EEF1A1 NCL LAP3 GAPDH PPIA KPNB1 DDX1 GMPS LMNA TPR SNRPB2 SF3A1 IMMT RAB11A GNB2L1 PSMC2 P4HB	32	0.681	0.005	GO:1901564	organonitrogen compound metabolic process	3.54
HSP90AB1 CSE1L PDCD5 KPNA2 CCT2 DLD GMPS LMNA SNRPB2 PA2G4 PSMC2	11	0.234	0.016	GO:0072594	establishment of protein localization to organelle	3.52
RPS14 RPL18A KHSRP WARS TUBB PDIA4 EEF1A1 LAP3 PPIA KPNB1 LMNA TPR SF3A1 IMMT	14	0.298	0.012	GO:0043603	cellular amide metabolic process	3.47
HSP90AB1 TFRC GDI2 PDCD5 STON2 XPO1 CCT2 ANXA2 PARP1 GAPDH GMPS LMNA RPS3 SNRPB2 SF3A1 PA2G4 PSMC2 P4HB	18	0.383	0.009	GO:0032879	regulation of localization	3.45
HSP90AB1 TFRC CSE1L GDI2 PDCD5 XPO1 KHSRP KPNA2 CCT2 ANXA2 PARP1 RPS6 GAPDH DLD KPNB1 GMPS LMNA RPS3 SNRPB2 SF3A1 PA2G4 PSMC2	22	0.468	0.007	GO:0033036	macromolecule localization	3.42
TFRC PRKCSH GDI2 PDCD5 STON2 XPO1 CFL1 CCT2 WARS ANXA2 PARP1 H2AFZ GMPS LMNA TPR RPS3 SNRPB2 SF3A1 P4HB	19	0.404	0.008	GO:0051128	regulation of cellular component organization	3.40

APPENDIX F (CONTINUE)

intersecting genes	intersection size	precision	recall	term id	term name	-log10 (p-value)
RPS14 KHSRP EEF1A1 LAP3 KPNB1 LMNA TPR SF3A1 IMMT	9	0.191	0.022	GO:0006417	regulation of translation	3.39
GPI HSP90AB1 TFRC PRKCSH PDCD5 RPS14 XPO1 RPL18A KHSRP WARS ANXA2 PARP1 TUBB PDIA4 EEF1A1 NCL LAP3 GAPDH PPIA KPNB1 GMPS LMNA TPR SNRPB2 SF3A1 IMMT RAB11A GNB2L1 P4HB	29	0.617	0.005	GO:0019538	protein metabolic process	3.39
H2AFZ DLD LMNA TPR PA2G4 PSMC2 P4HB	7	0.149	0.035	GO:0007051	spindle organization	3.36
XPO1 KHSRP CCT2 DLD LMNA SF3A1 PSMC2	7	0.149	0.035	GO:0006403	RNA localization	3.34
HSP90AB1 TFRC CFL1 KPNA2 GAPDH SNRPB2 GNB2L1 PSMC2 P4HB	9	0.191	0.022	GO:0016032	viral process	3.34
TFRC PRKCSH GDI2 ANXA2 PARP1 GMPS LMNA RPS3 SNRPB2 SF3A1 P4HB	11	0.234	0.016	GO:0051129	negative regulation of cellular component organization	3.31
HSP90AB1 TFRC CFL1 LAP3 GAPDH SNRPB2 GNB2L1 P4HB	8	0.170	0.027	GO:0044403	biological process involved in symbiotic interaction	3.30

APPENDIX F (CONTINUE)

intersecting genes	intersection size	precision	recall	term id	term name	-log10 (p-value)
HSP90AB1 TFRC CSE1L GDI2 PDCD5 XPO1 KPNA2 CCT2 RPS6 GAPDH DLD GMPS LMNA SNRPB2 SF3A1 PA2G4 PSMC2	17	0.362	0.009	GO:0045184	establishment of protein localization	3.28
XPO1 SF3A1 PSMC2	3	0.064	0.429	GO:0000055	ribosomal large subunit export from nucleus	3.22
H2AFZ DLD LMNA TPR PA2G4 P4HB	6	0.128	0.047	GO:0051225	spindle assembly	3.17
HSP90AB1 TFRC CSE1L GDI2 PDCD5 XPO1 KPNA2 CCT2 PARP1 RPS6 GAPDH DLD KPNB1 GMPS LMNA RPS3 SNRPB2 SF3A1 PA2G4 PSMC2	20	0.426	0.007	GO:0008104	protein localization	3.17
HSP90AB1 TFRC CSE1L GDI2 PDCD5 XPO1 KPNA2 CCT2 PARP1 RPS6 GAPDH DLD KPNB1 GMPS LMNA RPS3 SNRPB2 SF3A1 PA2G4 PSMC2	20	0.426	0.007	GO:0070727	cellular macromolecule localization	3.14
PDCD5 CCT2 RPS6 SNRPB2 P4HB	5	0.106	0.071	GO:0061077	chaperone-mediated protein folding	3.10
GPI TPI1 PARP1 LAP3 PPIA DDX1 SNRPB2 PSMC2 P4HB	9	0.191	0.020	GO:0009150	purine ribonucleotide metabolic process	3.05

APPENDIX F (CONTINUE)

intersecting genes	intersection size	precision	recall	term id	term name	-log10 (p-value)
XPO1 SF3A1 PSMC2	3	0.064	0.375	GO:0000056	ribosomal small subunit export from nucleus	3.02
HSP90AB1 TFRC PDCD5 CCT2 PARP1 GAPDH LMNA SF3A1 PSMC2	9	0.191	0.020	GO:1903829	positive regulation of protein localization	2.96
RPS14 RPL18A KHSRP WARS PARP1 TUBB PDIA4 EEF1A1 LAP3 PPIA KPNB1 DDX1 LMNA TPR SF3A1 IMMT	16	0.340	0.009	GO:1901566	organonitrogen compound biosynthetic process	2.92
GPI TPI1 PARP1 LAP3 PPIA DDX1 SNRPB2 PSMC2 P4HB	9	0.191	0.019	GO:0009259	ribonucleotide metabolic process	2.90
RPS14 KHSRP EEF1A1 LAP3 KPNB1 LMNA TPR SF3A1 IMMT	9	0.191	0.019	GO:0034248	regulation of cellular amide metabolic process	2.90
HSP90AB1 TFRC CSE1L GDI2 PDCD5 XPO1 KPNA2 RPS6 GAPDH DLG1 GMPS LMNA SNRPB2 SF3A1 PA2G4 PSMC2	16	0.340	0.009	GO:0015031	protein transport	2.87

APPENDIX F (CONTINUE)

intersecting genes	intersection size	precision	recall	term id	term name	-log10 (p-value)
GPI TPI1 PARP1 LAP3 PPIA DDX1 SNRPB2 PSMC2 P4HB	9	0.191	0.019	GO:0006163	purine nucleotide metabolic process	2.83
GPI TPI1 PARP1 LAP3 PPIA DDX1 SNRPB2 PSMC2 P4HB	9	0.191	0.019	GO:0019693	ribose phosphate metabolic process	2.83
GPI TFRC PDCD5 WARS ANXA2 EEF1A1 LAP3 KPNB1 GMP S TPR SNRPB2 SF3A1 P4HB	13	0.277	0.011	GO:0010628	positive regulation of gene expression	2.80
GPI TPI1 PARP1 LAP3 SNRPB2 PSMC2 P4HB	7	0.149	0.029	GO:0009205	purine ribonucleoside triphosphate metabolic process	2.77
RPS14 KHSRP EEF1A1 LAP3 KPNB1 LMNA TPR SF3A1 IMMT	9	0.191	0.018	GO:2000112	regulation of cellular macromolecule biosynthetic process	2.72

APPENDIX F (CONTINUE)

intersecting genes	intersection size	precision	recall	term id	term name	-log10 (p-value)
GPI TPI1 PARP1 LAP3 SNRPB2 PSMC2 P4HB	7	0.149	0.028	GO:0009144	purine nucleoside triphosphate metabolic process	2.71
GPI TPI1 PARP1 LAP3 SNRPB2 PSMC2 P4HB	7	0.149	0.028	GO:0009199	ribonucleoside triphosphate metabolic process	2.69
RPS14 RPL18A KHSRP WARS TUBB PDIA4 EEF1A1 LAP3 KPNB1 LMNA TPR SF3A1 IMMT	13	0.277	0.011	GO:0034645	cellular macromolecule biosynthetic process	2.66
GPI TPI1 PARP1 LAP3 PPIA DDX1 SNRPB2 PSMC2 P4HB	9	0.191	0.018	GO:0072521	purine-containing compound metabolic process	2.61
XPO1 KHSRP DLD LMNA SF3A1 PSMC2	6	0.128	0.037	GO:0050658	RNA transport	2.57
XPO1 KHSRP DLD LMNA SF3A1 PSMC2	6	0.128	0.037	GO:0050657	nucleic acid transport	2.57

APPENDIX F (CONTINUE)

intersecting genes	intersection size	precision	recall	term id	term name	-log10 (p-value)
XPO1 KHSRP DLN LMNA SF3A1 PSMC2	6	0.128	0.036	GO:0051236	establishment of RNA localization	2.53
GPI TPI1 PARP1 LAP3 SNRPB2 PSMC2 P4HB	7	0.149	0.026	GO:0009141	nucleoside triphosphate metabolic process	2.50
RPS14 H2AFZ DLN LMNA TPR SF3A1 PA2G4 P4HB	8	0.170	0.021	GO:0140694	non-membrane-bounded organelle assembly	2.49
GPI HSP90AB1 TFRC PDCD5 CFL1 PARP1 TUBB GAPDH GMPS TPR SF3A1 IMMT GNB2L1 P4HB	14	0.298	0.010	GO:0042981	regulation of apoptotic process	2.48
GPI HSP90AB1 KHSRP WARS ANXA2 EEF1A1 LAP3 GAPDH LMNA TPR SF3A1 P4HB	12	0.255	0.012	GO:0051248	negative regulation of protein metabolic process	2.47

APPENDIX F (CONTINUE)

intersecting genes	intersection size	precision	recall	term id	term name	-log10 (p-value)
GPI HSP90AB1 TFRC PDCD5 CFL1 PARP1 TUBB GAPDH GMPS TPR SF3A1 IMMT GNB2L1 P4HB	14	0.298	0.009	GO:0043067	regulation of programmed cell death	2.37
HSP90AB1 TFRC CSE1L GDI2 PDCD5 XPO1 KHSRP KPNA2 RPS6 GAPDH DLD GMPS LMNA SNRPB2 SF3A1 PA2G4 PSMC2	17	0.362	0.008	GO:0071705	nitrogen compound transport	2.25
HSP90AB1 CSE1L PDCD5 XPO1 KPNA2 DLD GMPS LMNA SNRPB2 SF3A1 PA2G4 PSMC2	12	0.255	0.011	GO:0006886	intracellular protein transport	2.22
XPO1 SF3A1 PSMC2	3	0.064	0.200	GO:0033750	ribosome localization	2.11
XPO1 SF3A1 PSMC2	3	0.064	0.200	GO:0000054	ribosomal subunit export from nucleus	2.11
HSP90AB1 CSE1L PDCD5 XPO1 KPNA2 ANXA2 H2AFZ DLD GMPS LMNA SNRPB2 SF3A1 PA2G4 PSMC2 P4HB	15	0.319	0.008	GO:0046907	intracellular transport	2.10
HSP90AB1 CSE1L PDCD5 STON2 XPO1 CFL1 KPNA2 ANXA2 H2AFZ DLD GMPS LMNA SNRPB2 SF3A1 PA2G4 PSMC2 P4HB	17	0.362	0.007	GO:0051649	establishment of localization in cell	2.05
HSP90AB1 TFRC KPNA2 GAPDH SNRPB2 GNB2L1 P4HB	7	0.149	0.022	GO:0019058	viral life cycle	2.04

APPENDIX F (CONTINUE)

intersecting genes	intersection size	precision	recall	term id	term name	-log10 (p-value)
GPI TPI1 PARP1 LAP3 PPIA DDX1 SNRPB2 PSMC2 P4HB	9	0.191	0.015	GO:0009117	nucleotide metabolic process	2.02
GPI TPI1 PARP1 LAP3 PPIA DDX1 SNRPB2 PSMC2 P4HB	9	0.191	0.015	GO:0006753	nucleoside phosphate metabolic process	1.96
HSP90AB1 CCT2 PARP1 DLD KPNB1 GMPS LMNA PA2G4 PSMC2	9	0.191	0.015	GO:0051276	chromosome organization	1.93
HSP90AB1 CCT2 LAP3 GMPS SNRPB2 SF3A1 P4HB	7	0.149	0.022	GO:0031647	regulation of protein stability	1.93
GPI HSP90AB1 TFRC PDCD5 CFL1 PARP1 TUBB GAPDH GMPS TPR SF3A1 IMMT GNB2L1 P4HB	14	0.298	0.009	GO:0010941	regulation of cell death	1.87
HSP90AB1 TFRC CSE1L GDI2 PDCD5 XPO1 KHSRP KPNA2 ANXA2 RPS6 GAPDH DLD GMPS LMNA SNRPB2 SF3A1 PA2G4 PSMC2	18	0.383	0.007	GO:0071702	organic substance transport	1.87
GPI TPI1 PARP1 LAP3 SNRPB2 P4HB	6	0.128	0.028	GO:0046034	ATP metabolic process	1.86
GPI HSP90AB1 TFRC PDCD5 CFL1 PARP1 TUBB LAP3 GAPDH GMPS TPR SF3A1 IMMT GNB2L1 P4HB	15	0.319	0.008	GO:0006915	apoptotic process	1.85

APPENDIX F (CONTINUE)

intersecting genes	intersection size	precision	recall	term id	term name	-log10 (p-value)
CSE1L XPO1 LMNA PSMC2	4	0.085	0.067	GO:0006611	protein export from nucleus	1.79
XPO1 KHSRP DLD LMNA SF3A1 PSMC2	6	0.128	0.027	GO:0015931	nucleobase-containing compound transport	1.76
XPO1 CFL1 H2AFZ TUBB DLD GMPS LMNA TPR SF3A1 PA2G4 PSMC2 P4HB	12	0.255	0.010	GO:0022402	cell cycle process	1.74
GPI HSP90AB1 TFRC PDCD5 CFL1 PARP1 TUBB LAP3 GAPDH GMPS TPR SF3A1 IMMT GNB2L1 P4HB	15	0.319	0.008	GO:0012501	programmed cell death	1.70
DLD LMNA PA2G4 PSMC2 P4HB	5	0.106	0.037	GO:0007052	mitotic spindle organization	1.69
GPI TPI1 PARP1 LAP3 PPIA DDX1 SNRPB2 PSMC2 P4HB	9	0.191	0.013	GO:0055086	nucleobase-containing small molecule metabolic process	1.60
XPO1 CFL1 H2AFZ LAP3 DLD GMPS LMNA TPR RPS3 SF3A1 PA2G4 PSMC2 P4HB	13	0.277	0.009	GO:0007010	cytoskeleton organization	1.60

APPENDIX F (CONTINUE)

intersecting genes	intersection size	precision	recall	term id	term name	-log10 (p-value)
TFRC GDI2 PARP1 GMPS LMNA SF3A1 P4HB	7	0.149	0.019	GO:0010639	negative regulation of organelle organization	1.59
TPR SF3A1 P4HB	3	0.064	0.136	GO:0032069	regulation of nuclease activity	1.59
GPI HSP90AB1 TFRC PRKCSH GDI2 PDCD5 RPS14 KHSRP CFL1 WARS ANXA2 PARP1 TUBB EEF1A1 LAP3 GAPDH GMP S LMNA TPR RPS3 SNRPB2 SF3A1 IMMT P4HB	24	0.511	0.005	GO:0048523	negative regulation of cellular process	1.54
HSP90AB1 CCT2 P4HB	3	0.064	0.130	GO:0051131	chaperone-mediated protein complex assembly	1.53
HSP90AB1 PDCD5 XPO1 CCT2 GAPDH LMNA SNRPB2 PSM C2	8	0.170	0.015	GO:0070201	regulation of establishment of protein localization	1.50

APPENDIX F (CONTINUE)

intersecting genes	intersection size	precision	recall	term id	term name	-log10 (p-value)
GPI HSP90AB1 TFRC CFL1 TUBB GAPDH GMPS SF3A1 IMMT P4HB	10	0.213	0.011	GO:0043066	negative regulation of apoptotic process	1.49
HSP90AB1 TFRC KPNA2 CCT2 PARP1 GMPS TPR SF3A1	8	0.170	0.015	GO:0051052	regulation of DNA metabolic process	1.45
HSP90AB1 TFRC CSE1L GDI2 PDCD5 STON2 XPO1 KHSRP CFL1 KPNA2 CCT2 ANXA2 PARP1 H2AFZ RPS6 GAPDH DLD KPNB1 GMPS LMNA RPS3 SNRNP2 SF3A1 PA2G4 PSMC2 P4HB	26	0.553	0.005	GO:0051179	localization	1.43
HSP90AB1 XPO1 CFL1 H2AFZ TUBB DLD GMPS LMNA TPR SNRNP2 SF3A1 PA2G4 PSMC2 P4HB	14	0.298	0.008	GO:0007049	cell cycle	1.42
GPI HSP90AB1 TFRC PDCD5 KHSRP CFL1 CPNE3 KPNA2 CCT2 WARS ANXA2 PARP1 TUBB EEF1A1 LAP3 GAPDH KPNB1 GMPS LMNA TPR SNRNP2 SF3A1 IMMT PA2G4 RAB11A GNB2L1 PSMC2 P4HB	28	0.596	0.004	GO:0048518	positive regulation of biological process	1.42
GPI HSP90AB1 TFRC CFL1 TUBB GAPDH GMPS SF3A1 IMMT P4HB	10	0.213	0.011	GO:0043069	negative regulation of programmed cell death	1.41

APPENDIX F (CONTINUE)

intersecting genes	intersection size	precision	recall	term id	term name	-log10 (p-value)
DLD LMNA PA2G4 P4HB	4	0.085	0.053	GO:0090307	mitotic spindle assembly	1.39
TFRC GAPDH TPR SF3A1 P4HB	5	0.106	0.032	GO:0051092	positive regulation of NF-kappaB transcription factor activity	1.38
SF3A1 P4HB	2	0.043	0.500	GO:0060699	regulation of endoribonucle ase activity	1.31
GPI HSP90AB1 PDCD5 XPO1 ANXA2 LAP3 TPR RAB11A P4HB	9	0.191	0.012	GO:0030162	regulation of proteolysis	1.31
HSP90AB1 TFRC GDI2 RPS14 XPO1 CCT2 WARS ANXA2 PARP1 H2AFZ TUBB DLD KPNB1 LMNA TPR RPS3 PACSN2 SNRPB2 HSPA8 SF3A1 IMMT PA2G4 PSMC2 P4HB	24	0.511	0.005	GO:0044085	cellular component biogenesis	1.30

APPENDIX G

GO result for DAP upregulated at 48-hour post-infection

intersecting genes	intersection size	precision	recall	term id	term name	-log10 (p-value)
TFRC HMGB1 ENO1 RPL6 XPO1 RPL18A KHSRP MAGOH RUVBL1 DLAT RAC1 RPS11 RPS13 MBNL2 ANXA2 H2AFZ RPS6 NME2 TUFM PSMA6 SARNP MCM5 PPIA DLD BLVRA USP14 AHCY PRKDC AK2 MYL12B GANAB PRDX4 LMNA PACSIN2 HSPA8 SF3A1 XRCC6 NPM1 IDH1 DNAJA1 GLOD4 SERBP1	42	0.792	0.006	GO:1901564	organonitrogen compound metabolic process	8.97
TFRC HMGB1 RPL6 XPO1 RPL18A KHSRP MAGOH RUVBL1 RAC1 RPS11 MBNL2 ANXA2 RPS6 NME2 TUFM PSMA6 NCL DLD USP14 AK2 GANAB PRDX4 HSPA8 SF3A1 XRCC6 GNB2L1 DNAJA1 SERBP1	28	0.528	0.009	GO:0044260	cellular macromolecule metabolic process	6.31
RPL6 RPL18A KHSRP MAGOH DLAT RAC1 RPS11 ANXA2 RPS6 TUFM PSMA6 MCM5 USP14 PRDX4 SF3A1 DNAJA1	16	0.302	0.018	GO:0043604	amide biosynthetic process	6.18
TFRC HMGB1 ENO1 RPL6 XPO1 RPL18A KHSRP MAGOH RUVBL1 RAC1 RPS11 MBNL2 ANXA2 H2AFZ RPS6 NME2 TUFM PSMA6 SARNP MCM5 DLD USP14 AK2 MYL12B GANAB PRDX4 LMNA PACSIN2 HSPA8 SF3A1 XRCC6 IDH1 DNAJA1 GLOD4 SERBP1	35	0.660	0.006	GO:0019538	protein metabolic process	5.71

APPENDIX G (CONTINUE)

intersecting genes	intersection size	precision	recall	term id	term name	-log10 (p-value)
RPL6 RPL18A KHSRP MAGOH RAC1 RPS11 ANXA2 RPS6 TUFM PSMA6 USP14 PRDX4 SF3A1 DNAJA1	14	0.264	0.019	GO:0006412	translation	5.32
RPL6 RPL18A KHSRP MAGOH DLAT RAC1 RPS11 ANXA2 RPS6 TUFM PSMA6 MCM5 USP14 PRDX4 SF3A1 NPM1 DNAJA1	17	0.321	0.014	GO:0043603	cellular amide metabolic process	5.24
ENO1 RPL6 RPL18A KHSRP MAGOH DLAT RAC1 RPS11 ANXA2 H2AFZ RPS6 TUFM PSMA6 MCM5 USP14 AHCY PRKDC PRDX4 SF3A1 DNAJA1	20	0.377	0.011	GO:1901566	organonitrogen compound biosynthetic process	5.11
RPL6 RPL18A KHSRP MAGOH RAC1 RPS11 ANXA2 RPS6 TUFM PSMA6 USP14 PRDX4 SF3A1 DNAJA1	14	0.264	0.018	GO:0043043	peptide biosynthetic process	5.11
RPL6 RPL18A KHSRP MAGOH RAC1 RPS11 ANXA2 RPS6 TUFM PSMA6 USP14 PRDX4 SF3A1 NPM1 DNAJA1	15	0.283	0.016	GO:0006518	peptide metabolic process	4.99
ENO1 DLAT RPS13 H2AFZ MCM5 BLVRA AHCY PRKDC LINA PACSIN2 SERBP1	11	0.208	0.022	GO:0072521	purine-containing compound metabolic process	4.08

APPENDIX G (CONTINUE)

intersecting genes	intersection size	precision	recall	term id	term name	-log10 (p-value)
TFRC HMGB1 ENO1 TOMM22 LGALS1 RUVBL1 ANXA2 H2AFZ SARNP USP14 GANAB PGK1 SF3A1 IDH1 DNAJA1 GLOD4 SERBP1	17	0.321	0.012	GO:0042981	regulation of apoptotic process	4.02
SARNP MYL12B PGK1 PACSIN2 IDH1 DNAJA1 GLOD4 SERBP1	8	0.151	0.038	GO:0006457	protein folding	3.98
TFRC HMGB1 ENO1 TOMM22 LGALS1 RUVBL1 ANXA2 H2AFZ SARNP USP14 GANAB PGK1 SF3A1 IDH1 DNAJA1 GLOD4 SERBP1	17	0.321	0.011	GO:0043067	regulation of programmed cell death	3.89
ENO1 DLAT RPS13 H2AFZ MCM5 BLVRA AHCY PRKDC LMNA PACSIN2 NPM1 SERBP1	12	0.226	0.018	GO:0055086	nucleobase-containing small molecule metabolic process	3.78
HMGB1 ENO1 RUVBL1 NCL SARNP DLA USP14 GANAB PRDX4 LMNA PGK1 PACSIN2 HSPA8 SF3A1 XRCC6 IDH1 DNAJA1 GLOD4 SERBP1	19	0.358	0.010	GO:0033554	cellular response to stress	3.70

APPENDIX G (CONTINUE)

intersecting genes	intersection size	precision	recall	term id	term name	-log10 (p-value)
HMGB1 ENO1 LGALS1 RUVBL1 MBNL2 NME2 SARNP DLD USP14 GANAB HSPA8 SF3A1 XRCC6 IDH1 GLOD4 SERBP1	16	0.302	0.012	GO:0080134	regulation of response to stress	3.62
TFRC HMGB1 ENO1 RPL6 RPL18A KHSRP MAGOH RUVBL1 DLAT RAC1 RPS11 MBNL2 ANXA2 H2AFZ RPS6 NME2 TUFM PSMA6 SARNP MCM5 USP14 AHCY PRKDC PRDX4 PACSIN2 HSPA8 SF3A1 XRCC6 DNAJA1 SERBP1	30	0.566	0.006	GO:0044271	cellular nitrogen compound biosynthetic process	3.57
ENO1 DLAT RPS13 H2AFZ MCM5 AHCY PRKDC LMNA PACSIN2 SERBP1	10	0.189	0.022	GO:0009150	purine ribonucleotide metabolic process	3.54
TFRC HMGB1 ENO1 RPL6 RPL18A KHSRP MAGOH RUVBL1 DLAT RAC1 RPS11 RPS13 MBNL2 ANXA2 H2AFZ RPS6 NME2 TUFM PSMA6 SARNP MCM5 USP14 AHCY PRKDC PRDX4 LMNA PACSIN2 HSPA8 SF3A1 XRCC6 NPM1 DNAJA1 SERBP1	33	0.623	0.006	GO:1901576	organic substance biosynthetic process	3.49
XPO1 MAGOH PSMA6 PRDX4 PGK1 SF3A1 DNAJA1	7	0.132	0.043	GO:0051168	nuclear export	3.46

APPENDIX G (CONTINUE)

intersecting genes	intersection size	precision	recall	term id	term name	-log10 (p-value)
ENO1 DLAT RPS13 H2AFZ MCM5 AHCY PRKDC LMNA PAC SIN2 SERBP1	10	0.189	0.021	GO:0009259	ribonucleotide metabolic process	3.38
ENO1 DLAT RPS13 H2AFZ MCM5 AHCY PRKDC LMNA PAC SIN2 NPM1 SERBP1	11	0.208	0.018	GO:0009117	nucleotide metabolic process	3.35
TFRC HMGB1 ENO1 RPL6 RPL18A KHSRP MAGOH RUVBL1 DLAT RAC1 RPS11 RPS13 MBNL2 ANXA2 H2AFZ RPS6 NME2 TUFM PSMA6 SARNP MCM5 USP14 AHCY PRKDC PRDX4 LMNA PACSIN2 HSPA8 SF3A1 XRCC6 NPM1 DNAJA1 SERBP1	33	0.623	0.006	GO:0009058	biosynthetic process	3.33
ENO1 DLAT RPS13 H2AFZ MCM5 AHCY PRKDC LMNA PAC SIN2 SERBP1	10	0.189	0.021	GO:0006163	purine nucleotide metabolic process	3.30
ENO1 DLAT RPS13 H2AFZ MCM5 AHCY PRKDC LMNA PAC SIN2 SERBP1	10	0.189	0.021	GO:0009693	ribose phosphate metabolic process	3.30

APPENDIX G (CONTINUE)

intersecting genes	intersection size	precision	recall	term id	term name	-log10 (p-value)
ENO1 DLAT RPS13 H2AFZ MCM5 AHCY PRKDC LMNA PAC SIN2 NPM1 SERBP1	11	0.208	0.018	GO:000 6753	nucleoside phosphate metabolic process	3.28
TFRC HMGB1 ENO1 TOMM22 LGALS1 RUVBL1 ANXA2 H2 AFZ SARNP USP14 GANAB PGK1 SF3A1 IDH1 DNAJA1 GLO D4 SERBP1	17	0.321	0.010	GO:001 0941	regulation of cell death	3.27
MAGOH RPS11 TPI1 TUFM PACSIN2 SF3A1 SERBP1	7	0.132	0.038	GO:004 3484	regulation of RNA splicing	3.16
PGK1 PACSIN2 IDH1 SERBP1	4	0.075	0.167	GO:004 2026	protein refolding	3.14
TFRC HMGB1 ENO1 RPL6 RPL18A KHSRP MAGOH RUVBL1 DLAT RAC1 RPS11 RPS13 MBNL2 ANXA2 H2AFZ RPS6 NM E2 TUFM PSMA6 SARNP MCM5 USP14 AHCY PRKDC PRDX 4 PACSIN2 HSPA8 SF3A1 XRCC6 NPM1 DNAJA1 SERBP1	32	0.604	0.006	GO:004 4249	cellular biosynthetic process	3.00
TFRC HMGB1 ENO1 LGALS1 RUVBL1 MBNL2 NME2 NCL S ARNP DLD BLVRA USP14 MYL12B GANAB PRDX4 LMNA P GK1 PACSIN2 HSPA8 SF3A1 XRCC6 NPM1 IDH1 DNAJA1 GL OD4 SERBP1	26	0.491	0.007	GO:000 6950	response to stress	2.99

APPENDIX G (CONTINUE)

intersecting genes	intersection size	precision	recall	term id	term name	-log10 (p-value)
TFRC ENO1 BLVRA USP14 GANAB PRDX4 LMNA HSPA8 SF3A1 XRCC6 IDH1 DNAJA1 GLOD4 SERBP1	14	0.264	0.012	GO:0009628	response to abiotic stimulus	2.96
XPO1 KHSRP MAGOH RUVBL1 PSMA6 PRDX4 SF3A1	7	0.132	0.035	GO:0006403	RNA localization	2.89
RPL6 RPL18A KHSRP MAGOH RAC1 RPS11 ANXA2 RPS6 TUFM PSMA6 USP14 PRDX4 SF3A1 DNAJA1	14	0.264	0.012	GO:0034645	cellular macromolecule biosynthetic process	2.72
TFRC HMGB1 ENO1 RPL6 RPL18A KHSRP MAGOH RUVBL1 DLAT RAC1 RPS11 RPS13 TPI1 MBNL2 ANXA2 H2AFZ RPS6 NME2 TUFM PSMA6 NCL SARNP MCM5 PPIA BLVRA USP14 AHCY PRKDC GANAB PRDX4 LMNA PACSIN2 HSPA9 HSPA8 SF3A1 XRCC6 NPM1 GNB2L1 DNAJA1 SERBP1	40	0.755	0.004	GO:0034641	cellular nitrogen compound metabolic process	2.70

APPENDIX G (CONTINUE)

intersecting genes	intersection size	precision	recall	term id	term name	-log10 (p-value)
TFRC HMGB1 ENO1 RPL6 KHSRP MAGOH RUVBL1 RPS11 TPI1 MBNL2 H2AFZ NME2 TUFM PSMA6 NCL SARNP USP14 GANAB PRDX4 PACSIN2 HSPA8 SF3A1 XRCC6 GNB2L1 DNAJA1 SERBP1	26	0.491	0.006	GO:0019219	regulation of nucleobase-containing compound metabolic process	2.66
XPO1 MAGOH PSMA6 GANAB PRDX4 PGK1 SF3A1 DNAJA1	8	0.151	0.024	GO:0006913	nucleocytoplasmic transport	2.49
XPO1 MAGOH PSMA6 GANAB PRDX4 PGK1 SF3A1 DNAJA1	8	0.151	0.024	GO:0051169	nuclear transport	2.49
TFRC HMGB1 ENO1 XPO1 KHSRP MAGOH MBNL2 TUFM PSMA6 SARNP DLA USP14 GANAB PRDX4 HSPA8 SF3A1 XRCC6 IDH1 DNAJA1 SERBP1	20	0.377	0.008	GO:0051246	regulation of protein metabolic process	2.46
TFRC HMGB1 ENO1 TOMM22 LGALS1 RUVBL1 ANXA2 H2AFZ SARNP USP14 GANAB PGK1 SF3A1 IDH1 DNAJA1 GLOD4 SERBP1	17	0.321	0.009	GO:0006915	apoptotic process	2.40

APPENDIX G (CONTINUE)

intersecting genes	intersection size	precision	recall	term id	term name	-log10 (p-value)
ENO1 XPO1 KHSRP MAGOH RPS13 MBNL2 NME2 MCM5 PP1A DLDBLVRA LMNA PACSIN2 SF3A1 NPM1 GNB2L1 DNAJA1 SERBP1	18	0.340	0.008	GO:1901575	organic substance catabolic process	2.35
ENO1 RPS13 H2AFZ PRKDC LMNA PACSIN2 SERBP1	7	0.132	0.029	GO:0009205	purine ribonucleoside triphosphate metabolic process	2.33
ENO1 RPS13 H2AFZ PRKDC LMNA PACSIN2 SERBP1	7	0.132	0.028	GO:0009144	purine nucleoside triphosphate metabolic process	2.27

APPENDIX G (CONTINUE)

intersecting genes	intersection size	precision	recall	term id	term name	-log10 (p-value)
ENO1 RPS13 H2AFZ PRKDC LMNA PACSIN2 SERBP1	7	0.132	0.028	GO:0009199	ribonucleoside triphosphate metabolic process	2.24
TFRC HMGB1 ENO1 TOMM22 LGALS1 RUVBL1 ANXA2 H2AFZ SARNP USP14 GANAB PGK1 SF3A1 IDH1 DNAJA1 GLOD4 SERBP1	17	0.321	0.009	GO:0012501	programmed cell death	2.23
XPO1 KHSRP MAGOH PSMA6 PRDX4 SF3A1	6	0.113	0.037	GO:0050658	RNA transport	2.18
XPO1 KHSRP MAGOH PSMA6 PRDX4 SF3A1	6	0.113	0.037	GO:0050657	nucleic acid transport	2.18
XPO1 KHSRP MAGOH PSMA6 PRDX4 SF3A1	6	0.113	0.036	GO:0051236	establishment of RNA localization	2.13

APPENDIX G (CONTINUE)

intersecting genes	intersection size	precision	recall	term id	term name	-log10 (p-value)
TFRC HMGB1 ENO1 RPL6 KHSRP MAGOH RUVBL1 RPS11 TPI1 MBNL2 H2AFZ NME2 TUFM PSMA6 SARNP USP14 PRDX4 PACSIN2 HSPA8 SF3A1 XRCC6 GNB2L1 DNAJA1 SERBP1	24	0.453	0.006	GO:0051252	regulation of RNA metabolic process	2.11
TFRC HMGB1 ENO1 RPL6 XPO1 KHSRP MAGOH RUVBL1 RPS11 TPI1 MBNL2 H2AFZ NME2 TUFM PSMA6 NCL SARNP DLD USP14 GANAB PRDX4 PACSIN2 HSPA8 SF3A1 XRCC6 NPM1 IDH1 GNB2L1 DNAJA1 SERBP1	30	0.566	0.005	GO:0031323	regulation of cellular metabolic process	2.06
ENO1 RPS13 H2AFZ PRKDC LMNA PACSIN2 SERBP1	7	0.132	0.026	GO:0009141	nucleoside triphosphate metabolic process	2.06
TFRC HMGB1 ENO1 RPL6 XPO1 RPL18A KHSRP MAGOH RUVBL1 DLAT RAC1 RPS11 RPS13 TPI1 MBNL2 ANXA2 H2AFZ RPS6 NME2 TUFM PSMA6 NCL SARNP MCM5 PPIA DLD BLVRA USP14 AHCY PRKDC AK2 MYL12B GANAB PRDX4 LMNA PGK1 PACSIN2 HSPA9 HSPA8 SF3A1 XRCC6 NPM1 IDH1 GNB2L1 DNAJA1 SERBP1	46	0.868	0.004	GO:0044237	cellular metabolic process	2.03

APPENDIX G (CONTINUE)

intersecting genes	intersection size	precision	recall	term id	term name	-log10 (p-value)
HMGB1 ENO1 KHSRP RPS11 MBNL2 TUFM PSMA6 SARNP DLD USP14 PRDX4 PACSIN2 HSPA8 SF3A1 XRCC6 IDH1 DNAJA1 SERBP1	18	0.340	0.008	GO:0031324	negative regulation of cellular metabolic process	2.01
HMGB1 RUVBL1 NCL HSPA8 XRCC6	5	0.094	0.050	GO:0032392	DNA geometric change	1.98
TFRC HMGB1 ENO1 RPL6 XPO1 RPL18A KHSRP MAGOH RUVBL1 DLAT RAC1 RPS11 RPS13 TPI1 MBNL2 ANXA2 H2AFZ RPS6 NME2 TUFM PSMA6 NCL SARNP MCM5 PPIA DLD BLVRA USP14 AHCY PRKDC AK2 MYL12B GANAB PRDX4 LMNA PACSIN2 HSPA9 HSPA8 SF3A1 XRCC6 NPM1 IDH1 GNB2L1 DNAJA1 GLOD4 SERBP1	46	0.868	0.004	GO:0006807	nitrogen compound metabolic process	1.98
TFRC HMGB1 ENO1 RPL6 KHSRP MAGOH RUVBL1 DLAT RPS11 RPS13 TPI1 MBNL2 ANXA2 H2AFZ NME2 TUFM PSMA6 NCL SARNP MCM5 PPIA BLVRA USP14 AHCY PRKDC GANAB PRDX4 LMNA PACSIN2 HSPA9 HSPA8 SF3A1 XRCC6 NPM1 GNB2L1 DNAJA1 SERBP1	37	0.698	0.004	GO:0046483	heterocycle metabolic process	1.92

APPENDIX G (CONTINUE)

intersecting genes	intersection size	precision	recall	term id	term name	-log10 (p-value)
TFRC HMGB1 ENO1 RPL6 KHSRP MAGOH RUVBL1 DLAT RPS11 RPS13 TPI1 MBNL2 ANXA2 H2AFZ NME2 TUFM PSMA6 NCL SARNP MCM5 PPIA BLVRA USP14 AHCY PRKDC GANAB PRDX4 LMNA PACSIN2 HSPA9 HSPA8 SF3A1 XRCC6 NPM1 GNB2L1 DNAJA1 SERBP1	37	0.698	0.004	GO:0006725	cellular aromatic compound metabolic process	1.83
KHSRP MAGOH TUFM PSMA6 USP14 PRDX4 SF3A1 DNAJA1	8	0.151	0.020	GO:0006417	regulation of translation	1.83
HMGB1 RUVBL1 NCL HSPA8 XRCC6	5	0.094	0.046	GO:0071103	DNA conformation change	1.82
ENO1 DLAT RPS13 MCM5 LMNA	5	0.094	0.046	GO:0006090	pyruvate metabolic process	1.80
ENO1 RPS13 LMNA	3	0.057	0.188	GO:0061718	glucose catabolic process to pyruvate	1.79
ENO1 RPS13 LMNA	3	0.057	0.188	GO:0006735	NADH regeneration	1.79
ENO1 RPS13 LMNA	3	0.057	0.188	GO:0061621	canonical glycolysis	1.79

APPENDIX G (CONTINUE)

intersecting genes	intersection size	precision	recall	term id	term name	-log10 (p-value)
TFRC HMGB1 MBNL2 GANAB PRDX4 TPR PACSIN2 SF3A1 XRCC6 SERBP1	10	0.189	0.014	GO:0051129	negative regulation of cellular component organization	1.78
MAGOH TPI1 TUFM PACSIN2 SF3A1	5	0.094	0.045	GO:0048024	regulation of mRNA splicing, via spliceosome	1.78
HMGB1 ENO1 XPO1 KHSRP MAGOH RPS13 MBNL2 NME2 MCM5 PPIA DLD BLVRA LMNA PACSIN2 SF3A1 NPM1 GNB2L1 DNAJA1 SERBP1	19	0.358	0.007	GO:0009056	catabolic process	1.77
TFRC HMGB1 ENO1 TOMM22 LGALS1 RUVBL1 ANXA2 H2AFZ SARNP USP14 GANAB PGK1 SF3A1 IDH1 DNAJA1 GLOD4 SERBP1	17	0.321	0.008	GO:0008219	cell death	1.75
HMGB1 ENO1 RUVBL1 SARNP DLD USP14 SF3A1 IDH1 GLOD4 SERBP1	10	0.189	0.014	GO:0080135	regulation of cellular response to stress	1.72

APPENDIX G (CONTINUE)

intersecting genes	intersection size	precision	recall	term id	term name	-log10 (p-value)
TFRC ENO1 ANXA2 H2AFZ SARNP USP14 GANAB PGK1 SF3A1 IDH1 SERBP1	11	0.208	0.012	GO:0043066	negative regulation of apoptotic process	1.71
HMGB1 XPO1 KHSRP MAGOH RPS13 MBNL2 NME2 MCM5 PPIA DLD BLVRA PACSIN2 SF3A1 NPM1 GNB2L1 DNAJA1 SERBP1	17	0.321	0.008	GO:0044248	cellular catabolic process	1.71
TFRC HMGB1 ENO1 RPL6 XPO1 KHSRP MAGOH RUVBL1 RPS11 TPI1 MBNL2 H2AFZ NME2 TUFM PSMA6 NCL SARNP DLD USP14 GANAB PRDX4 PACSIN2 HSPA8 SF3A1 XRCC6 NPM1 IDH1 GNB2L1 DNAJA1 SERBP1	30	0.566	0.005	GO:0080090	regulation of primary metabolic process	1.70
KHSRP MAGOH TPI1 TUFM PACSIN2 SF3A1 GNB2L1	7	0.132	0.023	GO:1903311	regulation of mRNA metabolic process	1.69
HMGB1 ENO1 KHSRP RPS11 MBNL2 TUFM PSMA6 SARNP DLD USP14 PRDX4 PACSIN2 HSPA8 SF3A1 XRCC6 IDH1 DNAJA1 SERBP1	18	0.340	0.008	GO:0051172	negative regulation of nitrogen compound metabolic process	1.63

APPENDIX G (CONTINUE)

intersecting genes	intersection size	precision	recall	term id	term name	-log10 (p-value)
TFRC ENO1 ANXA2 H2AFZ SARNP USP14 GANAB PGK1 SF3A1 IDH1 SERBP1	11	0.208	0.012	GO:0043069	negative regulation of programmed cell death	1.63
ENO1 RPS13 LMNA	3	0.057	0.167	GO:0061620	glycolytic process through glucose-6-phosphate	1.62
TFRC HMGB1 ENO1 RPL6 KHSRP MAGOH RUVBL1 DLAT RPS11 RPS13 TPI1 MBNL2 ANXA2 H2AFZ NME2 TUFM PSMA6 NCL SARNP MCM5 BLVRA USP14 AHCY PRKDC GANAB PRDX4 LMNA PACSIN2 HSPA9 HSPA8 SF3A1 XRCC6 NPM1 GNB2L1 DNAJA1 SERBP1	36	0.679	0.004	GO:0006139	nucleobase-containing compound metabolic process	1.61
TFRC HMGB1 ENO1 RPL6 KHSRP RUVBL1 DLAT MBNL2 H2AFZ NME2 TUFM PSMA6 SARNP MCM5 USP14 AHCY PRKDC PRDX4 PACSIN2 HSPA8 SF3A1 XRCC6 DNAJA1 SERBP1	24	0.453	0.006	GO:0034654	nucleobase-containing compound biosynthetic process	1.57

APPENDIX G (CONTINUE)

intersecting genes	intersection size	precision	recall	term id	term name	-log10 (p-value)
ENO1 DLAT RPS13 H2AFZ MCM5 BLVRA AHCY PRKDC AK2 LMNA PACSIN2 SERBP1	12	0.226	0.011	GO:1901135	carbohydrate derivative metabolic process	1.56
ENO1 RPS13 LMNA	3	0.057	0.158	GO:0061615	glycolytic process through fructose-6-phosphate	1.55
TFRC HMGB1 ENO1 RPL6 KHSRP MAGOH RUVBL1 DLAT RPS11 RPS13 TPI1 MBNL2 ANXA2 H2AFZ NME2 TUFM PSMA6 NCL SARNP MCM5 PPIA BLVRA USP14 AHCY PRKDC GANAB PRDX4 LMNA PACSIN2 HSPA9 HSPA8 SF3A1 XRCC6 NPM1 GNB2L1 DNAJA1 SERBP1	37	0.698	0.004	GO:1901360	organic cyclic compound metabolic process	1.51
XPO1 PRDX4 PGK1 DNAJA1	4	0.075	0.067	GO:0006611	protein export from nucleus	1.51
RUVBL1 USP14 GANAB PACSIN2 SF3A1 DNAJA1 SERBP1	7	0.132	0.022	GO:0031647	regulation of protein stability	1.50
TFRC HMGB1 RUVBL1 NCL USP14 HSPA8 XRCC6	7	0.132	0.021	GO:0006310	DNA recombination	1.48

APPENDIX G (CONTINUE)

intersecting genes	intersection size	precision	recall	term id	term name	-log10 (p-value)
RPL6 USP14 SF3A1 XRCC6	4	0.075	0.066	GO:0042255	ribosome assembly	1.48
ENO1 RPS13 PRKDC LMNA PACSIN2 SERBP1	6	0.113	0.028	GO:0046034	ATP metabolic process	1.47
HMGB1 USP14 HSPA8 XRCC6	4	0.075	0.065	GO:0002218	activation of innate immune response	1.45
ENO1 DLAT H2AFZ MCM5 AHCY PRKDC	6	0.113	0.027	GO:0009152	purine ribonucleotide biosynthetic process	1.45
TFRC HMGB1 ENO1 RPL6 KHSRP RUVBL1 DLAT MBNL2 H2AFZ NME2 TUFM PSMA6 SARNP MCM5 USP14 AHCY PRKDC PRDX4 PACSIN2 HSPA8 SF3A1 XRCC6 DNAJA1 SERBP1	24	0.453	0.006	GO:0018130	heterocycle biosynthetic process	1.43
USP14 XRCC6	2	0.038	0.667	GO:0034462	small-subunit processome assembly	1.43
XPO1 KHSRP MAGOH PSMA6 PRDX4	5	0.094	0.038	GO:0051028	mRNA transport	1.43

APPENDIX G (CONTINUE)

intersecting genes	intersection size	precision	recall	term id	term name	-log10 (p-value)
TFRC HMGB1 ENO1 RPL6 XPO1 KHSRP MAGOH RUVBL1 RPS11 TPI1 MBNL2 H2AFZ NME2 TUFM PSMA6 NCL SARNP DLD USP14 GANAB PRDX4 PACSIN2 HSPA8 SF3A1 XRCC6 IDH1 GNB2L1 DNAJA1 SERBP1	29	0.547	0.005	GO:0051171	regulation of nitrogen compound metabolic process	1.42
TFRC HMGB1 ENO1 RPL6 KHSRP RUVBL1 DLAT MBNL2 H2AFZ NME2 TUFM PSMA6 SARNP MCM5 USP14 AHCY PRKDC PRDX4 PACSIN2 HSPA8 SF3A1 XRCC6 DNAJA1 SERBP1	24	0.453	0.006	GO:0019438	aromatic compound biosynthetic process	1.41
KHSRP MAGOH TUFM PSMA6 USP14 PRDX4 SF3A1 DNAJA1	8	0.151	0.017	GO:0034248	regulation of cellular amide metabolic process	1.40
XPO1 KHSRP MAGOH PSMA6 PRDX4 SF3A1	6	0.113	0.027	GO:0015931	nucleobase-containing compound transport	1.37
HMGB1 SF3A1 SERBP1	3	0.057	0.136	GO:0032069	regulation of nuclease activity	1.35

APPENDIX G (CONTINUE)

intersecting genes	intersection size	precision	recall	term id	term name	-log10 (p-value)
ENO1 RPS13 H2AFZ PRKDC LMNA	5	0.094	0.037	GO:0009132	nucleoside diphosphate metabolic process	1.35
HMGB1 XPO1 KHSRP MAGOH MBNL2 DLD SF3A1 NPM1 GNB2L1 SERBP1	10	0.189	0.013	GO:0031329	regulation of cellular catabolic process	1.35
TFRC HMGB1 ENO1 RPL6 RPL18A KHSRP MAGOH RUVBL1 RAC1 RPS11 MBNL2 ANXA2 H2AFZ RPS6 NME2 TUFM PSMA6 SARNP USP14 PRDX4 PACSIN2 HSPA8 SF3A1 XRCC6 DNAJA1 SERBP1	26	0.491	0.005	GO:0009059	macromolecule biosynthetic process	1.32
HMGB1 USP14 HSPA8 XRCC6	4	0.075	0.060	GO:0006303	double-strand break repair via nonhomologous end joining	1.31
ENO1 DLAT H2AFZ MCM5 AHCY PRKDC	6	0.113	0.026	GO:0009260	ribonucleotide biosynthetic process	1.31

APPENDIX H

KEGG analysis results for DAP upregulated at 48-hours post-infection

Intersecting genes	Intersection size	Precision	Recall	Term id	Term name	-log10 (p-value)
ENO1 DLAT RPS13 MCM5 LMNA	5	0.125	0.075	KEGG:00010	Glycolysis / Gluconeogenesis	2.87
ENO1 DLAT RPS13 MCM5 LMNA NPM1	6	0.150	0.052	KEGG:01200	Carbon metabolism	2.84
USP14 HSPA8 XRCC6	3	0.075	0.231	KEGG:03450	Non-homologous end-joining	2.62
AK2 PACSIN2 IDH1 DNAJA1 GLOD4 SERBP1	6	0.150	0.036	KEGG:04141	Protein processing in endoplasmic reticulum	1.90
DLAT MCM5 NPM1	3	0.075	0.100	KEGG:00020	Citrate cycle (TCA cycle)	1.50
ENO1 RPS13 LMNA NPM1	4	0.100	0.054	KEGG:01230	Biosynthesis of amino acids	1.45

APPENDIX I

KEGG analysis results for DAP downregulated at 48-hours post-infection

intersecting genes	intersection size	precision	recall	term id	term name	-log10 (p-value)
BCAP31 ALB MYH9 UQCRC2 SLC25A5	5	0.143	0.072	KEGG:04612	Antigen processing and presentation	3.10
RPS3A EEF1A1 MYH9 SLC25A5	4	0.114	0.046	KEGG:05150	Staphylococcus aureus infection	1.41

APPENDIX J

Protein complexes related to cell death identified in CORUM database

Complex ID	Complex Name	GO Identifier	GO Description	FunCat Identifier	FunCat Remarks	Protein match
999	p23 protein complex	GO:0005515; GO:0043067	protein binding; regulation of programmed cell death	16.01; 40.10.02.04	protein binding; regulation of apoptosis	PDCD6; HNRNPA2B1; PTGES3
1163	ING1-PCNA complex	GO:0006974; GO:0009314; GO:0008219; GO:0005694	cellular response to DNA damage stimulus; response to radiation; cell death; chromosome	32.01.09; 32.01.13; 40.10; 70.10.03	DNA damage response; electromagnetic waves stress response (e.g. UV, X-ray); cell death; chromosome	PCNA; ING1
1243	Ubiquitin E3 ligase (SPOP, DAXX, CUL3)	GO:2001141; GO:0006355; GO:0016567; GO:0043161; GO:0006511; GO:0043067; GO:0005634	regulation of RNA biosynthetic process; regulation of DNA-templated transcription; protein ubiquitination; proteasome-mediated ubiquitin-dependent protein catabolic process; ubiquitin-dependent protein catabolic process; regulation of programmed cell death; nucleus	11.02.03.04; 14.07.05; 14.13.01.01; 40.10.02.04; 70.10	transcriptional control; modification by ubiquitination, deubiquitination; proteasomal degradation (ubiquitin/proteasomal pathway); regulation of apoptosis; nucleus	SPOP; CUL3; DAXX

APPENDIX J (CONTINUE)

Complex ID	Complex Name	GO Identifier	GO Description	FunCat Identifier	FunCat Remarks	Protein match
2962	CRK-BCAR1-DOCK1 complex	GO:0007229; GO:0006909; GO:0043067	integrin-mediated signaling pathway; phagocytosis; regulation of programmed cell death	30.05.02.26; 36.25.16.01.0 3; 40.10.02.04	integrin receptor signalling pathway; phagocyte response (e.g. macrophages, dendritic cells, granulocytes); regulation of apoptosis	CRK; BCAR1; DOCK1
3335	NAIP homotetramer complex	GO:0043067	regulation of programmed cell death	40.10.02.04	regulation of apoptosis	NAIP
4158	HSP90-FKBP38-CAM-Ca(2+) complex	GO:0043067	regulation of programmed cell death	40.10.02.04	regulation of apoptosis	HSP90AA1; CALM1; FKBP8
5317	LATS1-HTRA2-BIRC4 complex	GO:0008219	cell death	40.1	cell death	HTRA2; LATS1; XIAP

APPENDIX J (CONTINUE)

Complex ID	Complex Name	GO Identifier	GO Description	FunCat Identifier	FunCat Remarks	Protein match
5526	BCL2 - CALM1-FKBP38 complex	GO:0005509; GO:0030234; GO:0050790; GO:0043067; GO:0006915	calcium ion binding; enzyme regulator activity; regulation of catalytic activity; regulation of programmed cell death; apoptotic process	16.17.01; 18.02.01; 40.10.02.04; 40.10.02	calcium binding; enzymatic activity regulation / enzyme regulator; regulation of apoptosis; apoptosis (type I programmed cell death)	CALM1; BCL2; FKBP8
5749	MRIT complex	GO:0006919; GO:0008219; GO:0089720	activation of cysteine-type endopeptidase activity involved in apoptotic process; cell death; caspase binding	40.10.02.02.0 2; 40.10	caspase activation; cell death	CFLAR; BCL2L1; CASP8
5798	Death induced signaling complex II (CASP8, CFLAR, FADD), cytosolic, CD95L induced	GO:0089720; GO:0008219	caspase binding; cell death	40.1	cell death	CFLAR; FADD; CASP8

APPENDIX J (CONTINUE)

Complex ID	Complex Name	GO Identifier	GO Description	FunCat Identifier	FunCat Remarks	Protein match
5823	MCL1-BAK1 complex	GO:0043067; GO:0005741	regulation of programmed cell death; mitochondrial outer membrane	40.10.02.04; 70.16.01	regulation of apoptosis; mitochondrial outer membrane	MCL1; BAK1
6056	APP-TNFRSF21 complex	GO:0016322; GO:0070997	neuron remodeling; neuron death	None	None	TNFRSF21; APP
6178	LUBAC complex	GO:0050727; GO:0043122; GO:0010941; GO:0097039; GO:0032434; GO:0039535; GO:0045087	regulation of inflammatory response; regulation of I-kappaB kinase/NF-kappaB signaling; regulation of cell death; protein linear polyubiquitination; regulation of proteasomal ubiquitin-dependent protein catabolic process; regulation of RIG-I signaling pathway; innate immune response	36.25.16.01	innate immune response (invertebrates and vertebrates)	RNF31; RBCK1; SHARPIN

APPENDIX J (CONTINUE)

Complex ID	Complex Name	GO Identifier	GO Description	FunCat Identifier	FunCat Remarks	Protein match
7524	Ubiquitin E3 ligase (CUL3, KLHL20, RBX1)	GO:0031461; GO:1904093; GO:0043161	cullin-RING ubiquitin ligase complex; negative regulation of autophagic cell death; proteasome-mediated ubiquitin-dependent protein catabolic process	14.13.01.01	proteasomal degradation (ubiquitin/proteasomal pathway)	RBX1; CUL3; KLHL20
7529	APP-Abeta42-VDAC1 complex	GO:0005739; GO:0045121; GO:0008308; GO:0008219	mitochondrion; membrane raft; voltage-gated anion channel activity; cell death	70.16; 40.10	mitochondrion; cell death	APP; APP; VDAC1
7587	APP(AI CD)-FOXO3 complex	GO:0005737; GO:0008219; GO:0006979; GO:0005634; GO:0006915	cytoplasm; cell death; response to oxidative stress; nucleus; apoptotic process	70.03; 40.10; 32.01.01; 70.10; 40.10.02	cytoplasm; cell death; oxidative stress response; nucleus; apoptosis (type I programmed cell death)	FOXO3; APP
7588	APP(AI CD)-FOXO1 complex	GO:0008219; GO:0005737; GO:0006915	cell death; cytoplasm; apoptotic process	40.10; 70.03; 40.10.02	cell death; cytoplasm; apoptosis (type I programmed cell death)	APP; FOXO1

APPENDIX J (CONTINUE)

Complex ID	Complex Name	GO Identifier	GO Description	FunCat Identifier	FunCat Remarks	Protein match
7589	APP(AI CD)-FOXO4 complex	GO:0008219; GO:0005737; GO:0006915	cell death; cytoplasm; apoptotic process	40.10; 70.03; 40.10.02	cell death; cytoplasm; apoptosis (type I programmed cell death)	APP; FOXO4
7685	ERN1-MAP3K5-TRAF2 complex	GO:0007254; GO:0043068; GO:0034976	JNK cascade; positive regulation of programmed cell death; response to endoplasmic reticulum stress	30.01.05.01.0 2	JNK cascade	ERN1; TRAF2; MAP3K5
7819	MLKL-PGAM5-RIPK1-RIPK3 complex	GO:0070265; GO:0031966	necrotic cell death; mitochondrial membrane	None	None	RIPK1; MLKL; PGAM5; RIPK3
8059	LYN-PAG1-STAT3 complex	GO:0045121; GO:0008219	membrane raft; cell death	40.1	cell death	LYN; STAT3; PAG1
8079	CABLES1-TP53-TP73 complex	GO:0008219; GO:0051726	cell death; regulation of cell cycle	40.10; 10.03.01	cell death; mitotic cell cycle and cell cycle control	TP73; TP53; CABLES1

APPENDIX J (CONTINUE)

Complex ID	Complex Name	GO Identifier	GO Description	FunCat Identifier	FunCat Remarks	Protein match
8205	PAWR-PRKCZ-SQSTM1 complex	GO:0043067; GO:0043122	regulation of programmed cell death; regulation of I-kappaB kinase/NF-kappaB signaling	40.10.02.04	regulation of apoptosis	PRKCZ; SQSTM1; PAWR
8286	TNFR1-signaling complex I, membrane-bound	GO:0033209; GO:0005886; GO:0051092; GO:0050727; GO:0060548; GO:0043066	tumor necrosis factor-mediated signaling pathway; plasma membrane; positive regulation of NF-kappaB transcription factor activity; regulation of inflammatory response; negative regulation of cell death; negative regulation of apoptotic process	70.02; 40.10.02.01	eukaryotic plasma membrane / membrane attached; anti-apoptosis	TNFRSF1A; TRAF2; BIRC2; RIPK1; TRADD

APPENDIX J (CONTINUE)

Complex ID	Complex Name	GO Identifier	GO Description	FunCat Identifier	FunCat Remarks	Protein match
8294	PANoptosome	GO:0045087; GO:0002221; GO:0051607; GO:0042742; GO:0061702; GO:0050727; GO:0042981; GO:0043067	innate immune response; pattern recognition receptor signaling pathway; defense response to virus; defense response to bacterium; inflammasome complex; regulation of inflammatory response; regulation of apoptotic process; regulation of programmed cell death	36.25.16.01; 40.10.02.04	innate immune response (invertebrates and vertebrates); regulation of apoptosis	FADD; RIPK1; CASP8; NLRP3; ZBP1; PYCARD; RIPK3
8296	RIPK3-ZBP1 complex	GO:0045087; GO:0051607; GO:0043067; GO:0002221; GO:0051092; GO:0032481; GO:0097300; GO:1990784	innate immune response; defense response to virus; regulation of programmed cell death; pattern recognition receptor signaling pathway; positive regulation of NF-kappaB transcription factor activity; positive regulation of type I interferon production; programmed necrotic cell death; response to dsDNA	36.25.16.01; 40.10.02.04	innate immune response (invertebrates and vertebrates); regulation of apoptosis	ZBP1; RIPK3

APPENDIX J (CONTINUE)

Complex ID	Complex Name	GO Identifier	GO Description	FunCat Identifier	FunCat Remarks	Protein match
8561	TNFR1 signaling complex, TNF-induced	GO:0016567; GO:0010803; GO:0060548; GO:0050727; GO:0034612	protein ubiquitination; regulation of tumor necrosis factor-mediated signaling pathway; negative regulation of cell death; regulation of inflammatory response; response to tumor necrosis factor	14.07.05	modification by ubiquitination, deubiquitination	IKBKB; CHUK; MAP3K7; HTRA2; TNF; TNFRSF1A; TNFAIP3; TRAF2; BIRC3; BIRC2; RIPK1; IKBKE; TNIP1; TRADD; TNIP2; TANK; RNF31; RBCK1; SHARPIN; CYLD; TAB2; TBK1; SPATA2; IKBKG

APPENDIX J (CONTINUE)

Complex ID	Complex Name	GO Identifier	GO Description	FunCat Identifier	FunCat Remarks	Protein match
8562	LUBAC- SPATA2 -CYLD complex	GO:0032434; GO:0097039; GO:0010941; GO:0043122; GO:0010803; GO:0070432	regulation of proteasomal ubiquitin-dependent protein catabolic process; protein linear polyubiquitination; regulation of cell death; regulation of I-kappaB kinase/NF-kappaB signaling; regulation of tumor necrosis factor-mediated signaling pathway; regulation of nucleotide-binding oligomerization domain containing 2 signaling pathway	None	None	RNF31; RBCK1; SHARPIN; CYLD; SPATA2
8699	CASP8- FADD- RIPK1- RIPK3 complex	GO:0097300; GO:0034612	programmed necrotic cell death; response to tumor necrosis factor	None	None	FADD; RIPK1; CASP8; RIPK3

APPENDIX J (CONTINUE)

Complex ID	Complex Name	GO Identifier	GO Description	FunCat Identifier	FunCat Remarks	Protein match
8760	MAP2K1-WWOX complex	GO:0012501; GO:0005764	programmed cell death; lysosome	40.10.90; 70.25	other programmed cell death; vacuole or lysosome	MAP2K1; WWOX
8761	HYAL2-WWOX complex	GO:0005634; GO:0008219	nucleus; cell death	70.10; 40.10	nucleus; cell death	HYAL2; WWOX
8763	HYAL2-SMAD4-WWOX complex	GO:0008219; GO:0045893; GO:0005634	cell death; positive regulation of DNA-templated transcription; nucleus	40.10; 11.02.03.04.0 1; 70.10	cell death; transcription activation; nucleus	HYAL2; SMAD4; WWOX

APPENDIX K

Protein complexes related to pyroptosis identified in CORUM database

Complex ID	Complex Name	GO Identifier	GO Description	FunCat Identifier	FunCat Remarks	Protein match
7880	DHX9-NLRP9-PYCARD complex	GO:0051607; GO:0006954; GO:0045087; GO:0032741; GO:0070269	defense response to virus; inflammatory response; innate immune response; positive regulation of interleukin-18 production; pyroptosis	36.25.16.0 7; 36.25.16.0 1	inflammatory response; innate immune response (invertebrates and vertebrates)	DHX9; NLRP9; PYCARD
7889	AIM2 inflammasome	GO:0061702; GO:0051607; GO:0045087; GO:1990784; GO:0042742; GO:0002221; GO:0032731; GO:0140447; GO:0140639	inflammasome complex; defense response to virus; innate immune response; response to dsDNA; defense response to bacterium; pattern recognition receptor signaling pathway; positive regulation of interleukin-1 beta production; cytokine precursor processing; positive regulation of pyroptosis	36.25.16.0 1	innate immune response (invertebrates and vertebrates)	AIM2; CASP1; PYCARD

APPENDIX K (CONTINUE)

Complex ID	Complex Name	GO Identifier	GO Description	FunCat Identifier	FunCat Remarks	Protein match
7905	NAIP-NLRC4 inflammasome	GO:0061702; GO:0045087; GO:0002221; GO:0042742; GO:0032731; GO:0050727; GO:0140639	inflammasome complex; innate immune response; pattern recognition receptor signaling pathway; defense response to bacterium; positive regulation of interleukin-1 beta production; regulation of inflammatory response; positive regulation of pyroptosis	36.25.16.0 1	innate immune response (invertebrates and vertebrates)	CASP1; NAIP; NLRC4
7909	NLRP12 inflammasome	GO:0061702; GO:0070269; GO:0002221; GO:0045087; GO:0050729; GO:0032731; GO:0051092; GO:0006952; GO:0140447	inflammasome complex; pyroptosis; pattern recognition receptor signaling pathway; innate immune response; positive regulation of inflammatory response; positive regulation of interleukin-1 beta production; positive regulation of NF-kappaB transcription factor activity; defense response; cytokine precursor processing	36.25.16.0 1	innate immune response (invertebrates and vertebrates)	CASP1; NLRP12; PYCARD

APPENDIX K (CONTINUE)

Complex ID	Complex Name	GO Identifier	GO Description	FunCat Identifier	FunCat Remarks	Protein match
8593	NLRP1 inflamma some	GO:0051607; GO:0045087; GO:0072558; GO:0002221; GO:0050729; GO:0032731; GO:0032496; GO:0042742; GO:0061702; GO:0140639; GO:0140447	defense response to virus; innate immune response; NLRP1 inflammasome complex; pattern recognition receptor signaling pathway; positive regulation of inflammatory response; positive regulation of interleukin-1 beta production; response to lipopolysaccharide; defense response to bacterium; inflammasome complex; positive regulation of pyroptosis; cytokine precursor processing	36.25.16.0 1	innate immune response (invertebrates and vertebrates)	CASP1; NLRP1; PYCARD

APPENDIX L

Protein complexes related to p53 signalling identified in CORUM database

Complex ID	Complex Name	GO Identifier	GO Description	FunCat Identifier	FunCat Remarks	Protein match
8465	ESR1-MAGEA2-TP53 complex	GO:0005634; GO:0033148; GO:0072331	nucleus; positive regulation of intracellular estrogen receptor signaling pathway; signal transduction by p53 class mediator	70.1	nucleus	ESR1; TP53; MAGEA2

APPENDIX M

Protein complexes related to necroptosis identified in CORUM database

Complex ID	Complex Name	GO Identifier	GO Description	FunCat Identifier	FunCat Remarks	Protein match
8698	RIPK1-RIPK3 complex	GO:0034612; GO:0051607; GO:0006955; GO:0032481; GO:1990784; GO:0032088; GO:0045087; GO:0060544; GO:0019048	response to tumor necrosis factor; defense response to virus; immune response; positive regulation of type I interferon production; response to dsDNA; negative regulation of NF-kappaB transcription factor activity; innate immune response; regulation of necroptotic process; modulation by virus of host process	36.25.16; 36.25.16.01	immune response; innate immune response (invertebrates and vertebrates)	RIPK1; RIPK3

APPENDIX N

Protein complexes related to autophagy identified in CORUM database

Complex ID	Complex Name	GO Identifier	GO Description	FunCat Identifier	FunCat Remarks	Protein match
5213	AAA\u2013013ATPase complex, peroxisomal	GO:0007031; GO:0005777; GO:0000425; GO:0030242	peroxisome organization; peroxisome; pexophagy; autophagy of peroxisome	42.19; 70.19	peroxisome; peroxisome	PEX1; PEX6; PEX26
6192	CHDH-SQSTM1-MAP1LC3 complex	GO:1904925	positive regulation of autophagy of mitochondrion in response to mitochondrial depolarization	None	None	SQSTM1; CHDH; MAP1LC3A
6229	ATG13-RB1CC1-ULK1 complex	GO:1905037; GO:0006914	autophagosome organization; autophagy	None	None	ATG13; ULK1; RB1CC1
6230	ATG13-RB1CC1-ULK2 complex	GO:0006914; GO:1905037	autophagy; autophagosome organization	None	None	ATG13; ULK2; RB1CC1

APPENDIX N (CONTINUE)

Complex ID	Complex Name	GO Identifier	GO Description	FunCat Identifier	FunCat Remarks	Protein match
6232	ATG101-ATG13-RB1CC1-ULK1 complex	GO:0006914	autophagy	None	None	ATG13; ULK1; RB1CC1; ATG101
6754	KICSTOR complex	GO:0032418; GO:1904262; GO:0010506	lysosome localization; negative regulation of TORC1 signaling; regulation of autophagy	None	None	SZT2; ITFG2; KICS2; KPTN
6816	ULK1-ATG13-ATG14-PIK3C3 complex	GO:0000045; GO:0010506	autophagosome assembly; regulation of autophagy	None	None	ATG13; ULK1; ATG14; PIK3C3
7063	C9orf72-SMCR8-WDR41 complex	GO:0006914; GO:0000139	autophagy; Golgi membrane	None	None	SMCR8; C9orf72; WDR41
7064	C9orf72-SMCR8 complex	GO:0006914; GO:0000139	autophagy; Golgi membrane	None	None	SMCR8; C9orf72

APPENDIX N (CONTINUE)

Complex ID	Complex Name	GO Identifier	GO Description	FunCat Identifier	FunCat Remarks	Protein match
7065	WDR41-(C9orf72 - SMCR8) - (FIP200-ULK1-ATG13-ATG101) complex	GO:0006914; GO:0000139	autophagy; Golgi membrane	None	None	ATG13; ULK1; RB1CC1; SMCR8; C9orf72; ATG101; WDR41
7275	BCL2-CISD2 complex	GO:0006914; GO:0005783	autophagy; endoplasmic reticulum	70.07	endoplasmic reticulum	BCL2; CISD2
7667	Vps34 Complex I	GO:0016239	positive regulation of macroautophagy	None	None	BECN1; ATG14; PIK3C3; NRBF2; PIK3R4

APPENDIX N (CONTINUE)

Complex ID	Complex Name	GO Identifier	GO Description	FunCat Identifier	FunCat Remarks	Protein match
7825	CCZ1-MON1A - MON1B-RMC1 complex	GO:0016236	macroautophagy	None	None	CCZ1; MON1B; MON1A; RMC1
7954	BIF1-UVRAG-Beclin1 complex	GO:0006914; GO:0000045; GO:0042594	autophagy; autophagosome assembly; response to starvation	32.01.11	nutrient starvation response	BECN1; UVRAG; SH3GLB1
8355	AP2-PICALM adaptor complex	GO:0006914; GO:0072583; GO:0030119; GO:0038024	autophagy; clathrin-dependent endocytosis; AP-type membrane coat adaptor complex; cargo receptor activity	None	None	AP2A1; AP2B1; PICALM; AP2M1

APPENDIX N (CONTINUE)

Complex ID	Complex Name	GO Identifier	GO Description	FunCat Identifier	FunCat Remarks	Protein match
8613	TRAPP III complex	GO:0034976; GO:0006915; GO:0006914	response to endoplasmic reticulum stress; apoptotic process; autophagy	40.10.02	apoptosis (type I programmed cell death)	TRAPPC13; TRAPPC3; TRAPPC6A; TRAPPC2; TRAPPC11; TRAPPC6B; TRAPPC5; TRAPPC12; TRAPPC2L; TRAPPC4; TRAPPC8; TRAPPC1
8616	SRI complex	GO:0009407; GO:0006914	toxin catabolic process; autophagy	None	None	WDR11; C17orf75

APPENDIX O

Protein complexes related to senescence identified in CORUM database

Complex ID	Complex Name	GO Identifier	GO Description	FunCat Identifier	FunCat Remarks	Protein match
723	MORF4L1-MRFAP1-RB1 complex	GO:0045893; GO:0005634; GO:0090398	positive regulation of DNA-templated transcription; nucleus; cellular senescence	11.02.03.04.01; 70.10	transcription activation; nucleus	RB1; MORF4L1; MRFAP1
724	MAF2 complex	GO:0045893; GO:0006473; GO:0005634; GO:0090398	positive regulation of DNA-templated transcription; protein acetylation; nucleus; cellular senescence	11.02.03.04.01; 14.07.04; 70.10	transcription activation; modification by acetylation, deacetylation; nucleus	KAT8; MORF4L1
729	Ubiquitin E3 ligase (FBXO31, SKP1A, CUL1, RBX1)	GO:0000278; GO:0016567; GO:0030163; GO:0006511; GO:0090398	mitotic cell cycle; protein ubiquitination; protein catabolic process; ubiquitin-dependent protein catabolic process; cellular senescence	10.03.01.01; 14.07.05; 14.13; 14.13.01.01	mitotic cell cycle; modification by ubiquitination, deubiquitination; protein/peptide degradation; proteasomal degradation (ubiquitin/proteasomal pathway)	RBX1; SKP1; CUL1; FBXO31

APPENDIX O (CONTINUE)

Complex ID	Complex Name	GO Identifier	GO Description	FunCat Identifier	FunCat Remarks	Protein match
1217	WRN-TRF2 complex	GO:0004386; GO:0032204; GO:0005634; GO:0090398	helicase activity; regulation of telomere maintenance; nucleus; cellular senescence	70.1	nucleus	WRN; TERF2
1218	BLM-TRF2 complex	GO:0090398; GO:0032204; GO:0005634	cellular senescence; regulation of telomere maintenance; nucleus	70.1	nucleus	BLM; TERF2
7383	OGT-HIRA complex	GO:0006334; GO:2000772	nucleosome assembly; regulation of cellular senescence	None	None	OGT; HIRA; UBN1; CABIN1
8447	ASXL2-BAP1 complex	GO:0016579; GO:0090398	protein deubiquitination; cellular senescence	14.07.05	modification by ubiquitination, deubiquitination	ASXL2; BAP1

APPENDIX P

Protein complexes related to apoptosis identified in CORUM database

Complex ID	Complex Name	GO Identifier	GO Description	FunCat Identifier	FunCat Remarks	Protein match
129	PIDDsome complex	GO:0006919; GO:0006915	activation of cysteine-type endopeptidase activity involved in apoptotic process; apoptotic process	40.10.02.02.02; 40.10.02	caspase activation; apoptosis (type I programmed cell death)	CASP2; CRADD; PIDD1
525	TIP60 histone acetylase complex	GO:0006281; GO:0006915; GO:0003677	DNA repair; apoptotic process; DNA binding	10.01.05.01; 40.10.02; 16.03.01	DNA repair; apoptosis (type I programmed cell death); DNA binding	ACTL6A; KAT5; RUVBL2; RUVBL1; TRRAP
761	Apoptosis- and splicing-associated protein complex (SAP18, RNPS1, Acinus-S)	GO:0000398; GO:0006397; GO:0006915; GO:0005634	mRNA splicing, via spliceosome; mRNA processing; apoptotic process; nucleus	11.04.03; 40.10.02; 70.10	mRNA processing (splicing, 5'-, 3'-end processing); apoptosis (type I programmed cell death); nucleus	SAP18; RNPS1; ACIN1

APPENDIX P (CONTINUE)

Complex ID	Complex Name	GO Identifier	GO Description	FunCat Identifier	FunCat Remarks	Protein match
1039	PCNA-PAF complex	GO:0006281; GO:0007049; GO:0006915; GO:0005634; GO:0005739	DNA repair; cell cycle; apoptotic process; nucleus; mitochondrion	10.01.05.01; 10.03; 40.10.02; 70.10; 70.16	DNA repair; cell cycle; apoptosis (type I programmed cell death); nucleus; mitochondrion	PCNA; PCLAF
1040	p33ING1b-PCNA complex	GO:0006281; GO:0007049; GO:0006915; GO:0005634; GO:0005739	DNA repair; cell cycle; apoptotic process; nucleus; mitochondrion	10.01.05.01; 10.03; 40.10.02; 70.10; 70.16	DNA repair; cell cycle; apoptosis (type I programmed cell death); nucleus; mitochondrion	PCLAF; ING1
1062	BAR-BCL2-CASP8 complex	GO:0006915	apoptotic process	40.10.02	apoptosis (type I programmed cell death)	BCL2; CASP8; BFAR
1248	Apoptosome	GO:0006915; GO:0005737	apoptotic process; cytoplasm	40.10.02; 70.03	apoptosis (type I programmed cell death); cytoplasm	APAF1; CYCS
1795	SORT1-NGFR-NGFB complex	GO:0006915	apoptotic process	40.10.02	apoptosis (type I programmed cell death)	NGF; NGFR; SORT1

APPENDIX P (CONTINUE)

Complex ID	Complex Name	GO Identifier	GO Description	FunCat Identifier	FunCat Remarks	Protein match
2321	ITGA6-ITGB4-FYN complex	GO:0005515; GO:0006921	protein binding; cellular component disassembly involved in execution phase of apoptosis	16.01; 40.10.02.02.03	protein binding; disassembly of cell structures	FYN; ITGB4; ITGA6
2489	NCR3-CD247 complex	GO:0006915	apoptotic process	40.10.02	apoptosis (type I programmed cell death)	NCR3; CD247
2580	Survivin homodimer complex	GO:0000279; GO:0051225; GO:0007098; GO:0043066; GO:0000226; GO:0015630; GO:0000278	M phase; spindle assembly; centrosome cycle; negative regulation of apoptotic process; microtubule cytoskeleton organization; microtubule cytoskeleton; mitotic cell cycle	10.03.01.01.11; 10.03.05.01; 40.10.02.01; 42.04.05; 70.04.05; 10.03.01.01	M phase; spindle pole body/centrosome and microtubule cycle; anti-apoptosis; microtubule cytoskeleton; microtubule cytoskeleton; mitotic cell cycle	BIRC5

APPENDIX P (CONTINUE)

Complex ID	Complex Name	GO Identifier	GO Description	FunCat Identifier	FunCat Remarks	Protein match
2593	FOXO3-SIRT1 complex, oxidative stress stimulated	GO:2001141; GO:0006355; GO:0000302; GO:0006979; GO:0043066; GO:0005634	regulation of RNA biosynthetic process; regulation of DNA-templated transcription; response to reactive oxygen species; response to oxidative stress; negative regulation of apoptotic process; nucleus	11.02.03.04; 32.01.01; 40.10.02.01; 70.10	transcriptional control; oxidative stress response; anti-apoptosis; nucleus	FOXO3; SIRT1
2754	JUND-FOSB-SMAD3-SMAD4 complex	GO:2001141; GO:0006355; GO:0007167; GO:0006915; GO:0005634	regulation of RNA biosynthetic process; regulation of DNA-templated transcription; enzyme-linked receptor protein signaling pathway; apoptotic process; nucleus	11.02.03.04; 30.05.01; 40.10.02; 70.10	transcriptional control; receptor enzyme mediated signalling; apoptosis (type I programmed cell death); nucleus	JUND; FOSB; SMAD3; SMAD4

APPENDIX P (CONTINUE)

Complex ID	Complex Name	GO Identifier	GO Description	FunCat Identifier	FunCat Remarks	Protein match
2842	DAXX-Axin-p53-HIPK2 complex	GO:2001141; GO:0006355; GO:0006468; GO:0009314; GO:0006915; GO:0005634	regulation of RNA biosynthetic process; regulation of DNA-templated transcription; protein phosphorylation; response to radiation; apoptotic process; nucleus	11.02.03.04; 14.07.03; 32.01.13; 40.10.02; 70.10	transcriptional control; modification by phosphorylation, dephosphorylation, autophosphorylation; electromagnetic waves stress response (e.g. UV, X-ray); apoptosis (type I programmed cell death); nucleus	AXIN1; TP53; HIPK2; DAXX
2844	Axin-p53-HIPK2 complex	GO:2001141; GO:0006355; GO:0009314; GO:0006915; GO:0005634	regulation of RNA biosynthetic process; regulation of DNA-templated transcription; response to radiation; apoptotic process; nucleus	11.02.03.04; 32.01.13; 40.10.02; 70.10	transcriptional control; electromagnetic waves stress response (e.g. UV, X-ray); apoptosis (type I programmed cell death); nucleus	AXIN1; TP53; HIPK2

APPENDIX P (CONTINUE)

Complex ID	Complex Name	GO Identifier	GO Description	FunCat Identifier	FunCat Remarks	Protein match
2851	ING2 complex	GO:0006265; GO:0000278; GO:0051726; GO:0006473; GO:0006476; GO:0006915; GO:0001525; GO:0051276; GO:0005634	DNA topological change; mitotic cell cycle; regulation of cell cycle; protein acetylation; protein deacetylation; apoptotic process; angiogenesis; chromosome organization; nucleus	10.01.09.05; 10.03.01.01; 10.03.01; 14.07.04; 40.10.02; 41.05.16; 42.10.03; 70.10	DNA conformation modification (e.g. chromatin); mitotic cell cycle; mitotic cell cycle and cell cycle control; modification by acetylation, deacetylation; apoptosis (type I programmed cell death); angiogenesis; organization of chromosome structure; nucleus	SAP30; ARID4A; RBBP4; HDAC1; RBBP7; ARID4B; BRMS1L; HDAC2; SIN3A; SAP130; ING2; SUDS3; BRMS1

APPENDIX P (CONTINUE)

Complex ID	Complex Name	GO Identifier	GO Description	FunCat Identifier	FunCat Remarks	Protein match
2856	NuA4/Tip60 HAT complex	GO:0051276; GO:0006281; GO:0006265; GO:0000278; GO:0051726; GO:0003677; GO:0006915; GO:0005634; GO:0016573	chromosome organization; DNA repair; DNA topological change; mitotic cell cycle; regulation of cell cycle; DNA binding; apoptotic process; nucleus; histone acetylation	42.10.03; 10.01.05.01; 10.01.09.05; 10.03.01.01; 10.03.01; 16.03.01; 40.10.02; 70.10	organization of chromosome structure; DNA repair; DNA conformation modification (e.g. chromatin); mitotic cell cycle; mitotic cell cycle and cell cycle control; DNA binding; apoptosis (type I programmed cell death); nucleus	ACTL6A; KAT5; EP400; BRD8; EPC1; DMAP1; ING3; MORF4L1; RUVBL1; TRRAP
2857	NuA4/Tip60 HAT complex	GO:0051276; GO:0006281; GO:0006265; GO:0000278; GO:0051726; GO:0003677; GO:0006915; GO:0005634; GO:0016573	chromosome organization; DNA repair; DNA topological change; mitotic cell cycle; regulation of cell cycle; DNA binding; apoptotic process; nucleus; histone acetylation	42.10.03; 10.01.05.01; 10.01.09.05; 10.03.01.01; 10.03.01; 16.03.01; 40.10.02; 70.10	organization of chromosome structure; DNA repair; DNA conformation modification (e.g. chromatin); mitotic cell cycle; mitotic cell cycle and cell cycle control; DNA binding; apoptosis (type I programmed cell death); nucleus	YEATS4; ACTL6A; EPC2; KAT5; EP400; BRD8; EPC1; MEAF6; DMAP1; ING3; MORF4L1; RUVBL2; RUVBL1; TRRAP

APPENDIX P (CONTINUE)

Complex ID	Complex Name	GO Identifier	GO Description	FunCat Identifier	FunCat Remarks	Protein match
2858	ING5 complex (ING5, JADE1, KAT7, MEAF6)	GO:0000278; GO:0051726; GO:0006915	mitotic cell cycle; regulation of cell cycle; apoptotic process	10.03.01.01; 10.03.01; 40.10.02	mitotic cell cycle; mitotic cell cycle and cell cycle control; apoptosis (type I programmed cell death)	KAT7; JADE1; ING5; MEAF6
2859	ING5 (BRPF1, MOZ, MORF) complex	GO:0000278; GO:0051726; GO:0006915	mitotic cell cycle; regulation of cell cycle; apoptotic process	10.03.01.01; 10.03.01; 40.10.02	mitotic cell cycle; mitotic cell cycle and cell cycle control; apoptosis (type I programmed cell death)	BRPF1; KAT6B; ING5; KAT6A; MEAF6

APPENDIX P (CONTINUE)

Complex ID	Complex Name	GO Identifier	GO Description	FunCat Identifier	FunCat Remarks	Protein match
2944	Notch1-p56lck-PI3K complex	GO:0045893; GO:0007219; GO:0043066; GO:0030217	positive regulation of DNA-templated transcription; Notch signaling pathway; negative regulation of apoptotic process; T cell differentiation	11.02.03.04.01; 30.05.02.14; 40.10.02.01; 43.03.07.02.01.02	transcription activation; Notch-receptor signalling pathway; anti-apoptosis; T-cell	LCK; PIK3R1; NOTCH1
3046	hs4 enhancer complex (slow migrating complex)	GO:2001141; GO:0006355; GO:0003677; GO:0007249; GO:0043066; GO:0030183; GO:0005634	regulation of RNA biosynthetic process; regulation of DNA-templated transcription; DNA binding; I-kappaB kinase/NF-kappaB signaling; negative regulation of apoptotic process; B cell differentiation; nucleus	11.02.03.04; 16.03.01; 30.01.05.01.04; 40.10.02.01; 43.03.07.02.01.01; 70.10	transcriptional control; DNA binding; NIK-I-kappaB/NF-kappaB cascade; anti-apoptosis; B-cell; nucleus	YY1; RELB

APPENDIX P (CONTINUE)

Complex ID	Complex Name	GO Identifier	GO Description	FunCat Identifier	FunCat Remarks	Protein match
3168	DAXX-AXIN complex	GO:0005515; GO:0019209; GO:0051090; GO:0009314; GO:0006915	protein binding; kinase activator activity; regulation of DNA-binding transcription factor activity; response to radiation; apoptotic process	16.01; 18.02.01.01.05; 18.02.09; 32.01.13; 40.10.02	protein binding; kinase activator; regulator of transcription factor; electromagnetic waves stress response (e.g. UV, X-ray); apoptosis (type I programmed cell death)	AXIN1; DAXX
3170	Daxx-Axin-p53 complex	GO:2001141; GO:0006355; GO:0009314; GO:0006915; GO:0005634	regulation of RNA biosynthetic process; regulation of DNA-templated transcription; response to radiation; apoptotic process; nucleus	11.02.03.04; 32.01.13; 40.10.02; 70.10	transcriptional control; electromagnetic waves stress response (e.g. UV, X-ray); apoptosis (type I programmed cell death); nucleus	AXIN1; TP53; DAXX

APPENDIX P (CONTINUE)

Complex ID	Complex Name	GO Identifier	GO Description	FunCat Identifier	FunCat Remarks	Protein match
3492	BAX homo-oligomer complex	GO:0006915; GO:0005739	apoptotic process; mitochondrion	40.10.02; 70.16	apoptosis (type I programmed cell death); mitochondrion	BAX
3900	GABP(gamma)1-E2F1-DP1 complex	GO:0000082; GO:0045893; GO:0003677; GO:0006915; GO:0005634	G1/S transition of mitotic cell cycle; positive regulation of DNA-templated transcription; DNA binding; apoptotic process; nucleus	10.03.01.01.03; 11.02.03.04.01; 16.03.01; 40.10.02; 70.10	G1/S transition of mitotic cell cycle; transcription activation; DNA binding; apoptosis (type I programmed cell death); nucleus	E2F1; TFDP1; GABPB2
5288	P53-BARD1-KU70 complex	GO:0006915; GO:0042325	apoptotic process; regulation of phosphorylation	40.10.02	apoptosis (type I programmed cell death)	TP53; XRCC6; BARD1

APPENDIX P (CONTINUE)

Complex ID	Complex Name	GO Identifier	GO Description	FunCat Identifier	FunCat Remarks	Protein match
5473	DISC complex (FAS, FADD, CASP8)	GO:0006915; GO:0097191	apoptotic process; extrinsic apoptotic signaling pathway	40.10.02	apoptosis (type I programmed cell death)	FAS; FADD; CASP8
5526	BCL2 -CALM1-FKBP38 complex	GO:0005509; GO:0030234; GO:0050790; GO:0043067; GO:0006915	calcium ion binding; enzyme regulator activity; regulation of catalytic activity; regulation of programmed cell death; apoptotic process	16.17.01; 18.02.01; 40.10.02.04; 40.10.02	calcium binding; enzymatic activity regulation / enzyme regulator; regulation of apoptosis; apoptosis (type I programmed cell death)	CALM1; BCL2; FKBP8
5529	BIRC2-TRAF2 complex	GO:0016567; GO:0006915; GO:0005783	protein ubiquitination; apoptotic process; endoplasmic reticulum	14.07.05; 40.10.02; 70.07	modification by ubiquitination, deubiquitination; apoptosis (type I programmed cell death); endoplasmic reticulum	TRAF2; BIRC2

APPENDIX P (CONTINUE)

Complex ID	Complex Name	GO Identifier	GO Description	FunCat Identifier	FunCat Remarks	Protein match
5531	TNFR1-TRADD-TRAF2-cIAP1 complex	GO:0023052; GO:0006915	signaling; apoptotic process	30.01; 40.10.02	cellular signalling; apoptosis (type I programmed cell death)	TNFRSF1A; TRAF2; BIRC2; TRADD
5540	TRAF2-TRADD complex	GO:0006915	apoptotic process	40.10.02	apoptosis (type I programmed cell death)	TRAF2; TRADD
5541	FADD-TRADD-TRAF2 complex	GO:0006915	apoptotic process	40.10.02	apoptosis (type I programmed cell death)	TRAF2; FADD; TRADD
5749	MRIT complex	GO:0006919; GO:0008219; GO:0089720	activation of cysteine-type endopeptidase activity involved in apoptotic process; cell death; caspase binding	40.10.02.02.02; 40.10	caspase activation; cell death	CFLAR; BCL2L1; CASP8

APPENDIX P (CONTINUE)

Complex ID	Complex Name	GO Identifier	GO Description	FunCat Identifier	FunCat Remarks	Protein match
5799	DISC complex (FAS, FADD, CASP8, CFLAR), membrane-associated, CD95L induced	GO:0097190	apoptotic signaling pathway	40.10.02.03.01	induction of apoptosis by extracellular signals	CFLAR; FAS; FADD; CASP8
5800	DISC complex (FAS, FADD, CASP8)	GO:0006915; GO:0005886; GO:0097191	apoptotic process; plasma membrane; extrinsic apoptotic signaling pathway	40.10.02; 70.02	apoptosis (type I programmed cell death); eukaryotic plasma membrane / membrane attached	FAS; FADD; CASP8
5808	DISC complex (CD95, FADD, CASP8)	GO:0097190	apoptotic signaling pathway	40.10.02.03.01	induction of apoptosis by extracellular signals	FADD; CASP8; CD95
5811	p53-BCL2 complex	GO:0006915; GO:0005739	apoptotic process; mitochondrion	40.10.02; 70.16	apoptosis (type I programmed cell death); mitochondrion	TP53; BCL2
5812	p53-BCL2 complex	GO:0006915; GO:0005739	apoptotic process; mitochondrion	40.10.02; 70.16	apoptosis (type I programmed cell death); mitochondrion	TP53; BCL2L1

APPENDIX P (CONTINUE)

Complex ID	Complex Name	GO Identifier	GO Description	FunCat Identifier	FunCat Remarks	Protein match
5816	Apoptosome, 700 kDa	GO:0006915; GO:0005737	apoptotic process; cytoplasm	40.10.02; 70.03	apoptosis (type I programmed cell death); cytoplasm	APAF1; CASP9; CYCS
5843	AIF-CYPA-DNA complex	GO:0006915; GO:0005634	apoptotic process; nucleus	40.10.02; 70.10	apoptosis (type I programmed cell death); nucleus	AIFM1; PPIA
5856	AK2-FADD-caspase-10 (AFAC10) complex	GO:0097193	intrinsic apoptotic signaling pathway	40.10.02.03.02	induction of apoptosis by intracellular signals	AK2; FADD; CASP10
5859	FAS-FADD-CASP8-CASP10 complex	GO:0006915	apoptotic process	40.10.02	apoptosis (type I programmed cell death)	FAS; FADD; CASP8; CASP10
5860	DISC complex (FAS, FADD, CASP8)	GO:0006915	apoptotic process	40.10.02	apoptosis (type I programmed cell death)	FAS; FADD; CASP8
5861	FAS-FADD-CASP10 complex	GO:0006915	apoptotic process	40.10.02	apoptosis (type I programmed cell death)	FAS; FADD; CASP10
5991	LRRK2-FADD-CASP8 complex	GO:0006915	apoptotic process	40.10.02	apoptosis (type I programmed cell death)	FADD; CASP8; LRRK2

APPENDIX P (CONTINUE)

Complex ID	Complex Name	GO Identifier	GO Description	FunCat Identifier	FunCat Remarks	Protein match
6158	TRIAL-DR5 complex	GO:0006915	apoptotic process	40.10.02	apoptosis (type I programmed cell death)	TNFRSF10B; TNFSF10
6193	ADAM12-alphaVbeta3-integrin-MMP-14 complex	GO:0042981	regulation of apoptotic process	None	None	ADAM12; ITGB3; ITGAV; MMP14
6289	prohibitin 2 complex, mitochondrial	GO:0006915; GO:0008637	apoptotic process; apoptotic mitochondrial changes	40.10.02; 40.10.02.02.01	apoptosis (type I programmed cell death); apoptotic mitochondrial changes	HAX1; SLC25A5; PHB1; VDAC2; PHB2
6292	HAX-1-XIAP complex	GO:0006915; GO:1902915	apoptotic process; negative regulation of protein polyubiquitination	40.10.02	apoptosis (type I programmed cell death)	HAX1; XIAP

APPENDIX P (CONTINUE)

Complex ID	Complex Name	GO Identifier	GO Description	FunCat Identifier	FunCat Remarks	Protein match
6344	TNFR1 signaling complex, native	GO:0006954; GO:0016567; GO:0051092; GO:0046328; GO:0042981; GO:0010803	inflammatory response; protein ubiquitination; positive regulation of NF-kappaB transcription factor activity; regulation of JNK cascade; regulation of apoptotic process; regulation of tumor necrosis factor-mediated signaling pathway	36.25.16.07; 14.07.05	inflammatory response; modification by ubiquitination, deubiquitination	IKBKB; CHUK; MAP3K7; TNF; TNFRSF1A; TRAF2; BIRC3; RIPK1; TNIP1; TRADD; TAB1; RNF31; RBCK1; TAB2; IKBKG NPHP1; PKD1
6600	NPHP1-PKD1 complex	GO:0006915; GO:0060271	apoptotic process; cilium assembly	40.10.02	apoptosis (type I programmed cell death)	

APPENDIX P (CONTINUE)

Complex ID	Complex Name	GO Identifier	GO Description	FunCat Identifier	FunCat Remarks	Protein match
6794	LPAR2-TRIP6-NHERF2 complex, LPA stimulated	GO:0043066	negative regulation of apoptotic process	40.10.02.01	anti-apoptosis	SLC9A3R2; TRIP6; LPAR2
6795	LPAR2-SIVA1 complex	GO:0042981	regulation of apoptotic process	None	None	SIVA1; LPAR2
6797	LPAR2-SIVA1 complex	GO:0042981	regulation of apoptotic process	None	None	SIVA1; LPAR2
6846	DBC1-SIRT1 complex	GO:0090311; GO:0043065	regulation of protein deacetylation; positive regulation of apoptotic process	None	None	CCAR2; SIRT1
6848	IRF2BP2-IRF2BP1-IRF2BPL complex	GO:0045892; GO:0042981	negative regulation of DNA-templated transcription; regulation of apoptotic process	11.02.03.04.03	transcription repression	IRF2BP2; IRF2BP1; IRF2BPL

APPENDIX P (CONTINUE)

Complex ID	Complex Name	GO Identifier	GO Description	FunCat Identifier	FunCat Remarks	Protein match
6900	Ubiquitin E3 ligase (CUL1, FBXO10, SKP1)	GO:0043065; GO:0006511	positive regulation of apoptotic process; ubiquitin-dependent protein catabolic process	14.13.01.01	proteasomal degradation (ubiquitin/proteasomal pathway)	SKP1; CUL1; FBXO10
6919	ILK-LIMS1-PARVA complex	GO:0016477; GO:0006915; GO:0008360; GO:0007160	cell migration; apoptotic process; regulation of cell shape; cell-matrix adhesion	34.05.01; 40.10.02; 34.07.02	cell migration; apoptosis (type I programmed cell death); cell-matrix adhesion	LIMS1; ILK; PARVA
6984	ProTalpha C2 complex	GO:0043066; GO:0008283	negative regulation of apoptotic process; cell population proliferation	40.10.02.01	anti-apoptosis	PTMA; MARCKSL1; ACTB; SET
6987	ProTalpha C7 complex	GO:0043066; GO:0008283	negative regulation of apoptotic process; cell population proliferation	40.10.02.01	anti-apoptosis	PTMA; ANP32A; ANP32B
6988	ProTalpha C8 complex	GO:0043066; GO:0008283	negative regulation of apoptotic process; cell population proliferation	40.10.02.01	anti-apoptosis	PTMA; ANP32A; RAB11A; ANP32B
6989	ProTalpha C9 complex	GO:0043066; GO:0008283	negative regulation of apoptotic process; cell population proliferation	40.10.02.01	anti-apoptosis	PTMA; SET

APPENDIX P (CONTINUE)

Complex ID	Complex Name	GO Identifier	GO Description	FunCat Identifier	FunCat Remarks	Protein match
7252	ING5 (BRPF2, MOZ, MORF) complex	GO:0006915; GO:0000278; GO:0051726	apoptotic process; mitotic cell cycle; regulation of cell cycle	40.10.02; 10.03.01.01; 10.03.01	apoptosis (type I programmed cell death); mitotic cell cycle; mitotic cell cycle and cell cycle control	BRD1; KAT6B; ING5; KAT6A; MEAF6
7253	ING5 (BRPF3, MOZ, MORF) complex	GO:0006915; GO:0000278; GO:0051726	apoptotic process; mitotic cell cycle; regulation of cell cycle	40.10.02; 10.03.01.01; 10.03.01	apoptosis (type I programmed cell death); mitotic cell cycle; mitotic cell cycle and cell cycle control	KAT6B; ING5; KAT6A; MEAF6; BRPF3
7254	ING5 complex (ING5, JADE2, KAT7, MEAF6)	GO:0006915; GO:0000278; GO:0051726	apoptotic process; mitotic cell cycle; regulation of cell cycle	40.10.02; 10.03.01.01; 10.03.01	apoptosis (type I programmed cell death); mitotic cell cycle; mitotic cell cycle and cell cycle control	KAT7; ING5; MEAF6; JADE2

APPENDIX P (CONTINUE)

Complex ID	Complex Name	GO Identifier	GO Description	FunCat Identifier	FunCat Remarks	Protein match
7255	ING5 complex (ING5, JADE3, KAT7, MEAF6)	GO:0006915; GO:0000278; GO:0051726	apoptotic process; mitotic cell cycle; regulation of cell cycle	40.10.02; 10.03.01.01; 10.03.01	apoptosis (type I programmed cell death); mitotic cell cycle; mitotic cell cycle and cell cycle control	KAT7; ING5; JADE3; MEAF6
7298	ACTB-ANP32A- C1QBP-PSMA1- PTMA-PSMA1 complex	GO:0008283; GO:0043066; GO:0046902	cell population proliferation; negative regulation of apoptotic process; regulation of mitochondrial membrane permeability	40.10.02.01	anti-apoptosis	PTMA; PSMA1; ANP32A; ACTB; SLC25A3; C1QBP
7299	ANP32A- ANP32B- PSMA3-PTMA- SLC25A5 complex	GO:0008283; GO:0043066; GO:0046902	cell population proliferation; negative regulation of apoptotic process; regulation of mitochondrial membrane permeability	40.10.02.01	anti-apoptosis	SLC25A5; PTMA; PSMA3; ANP32A; ANP32B
7324	HINT1-TIP60 complex	GO:0045893; GO:0042981	positive regulation of DNA- templated transcription; regulation of apoptotic process	11.02.03.04.01	transcription activation	HINT1; KAT5

APPENDIX P (CONTINUE)

Complex ID	Complex Name	GO Identifier	GO Description	FunCat Identifier	FunCat Remarks	Protein match
7421	TSPY1-TSPYL5-USP7 complex	GO:0051726; GO:0042981	regulation of cell cycle; regulation of apoptotic process	10.03.01	mitotic cell cycle and cell cycle control	TSPY1; TSPYL5; USP7
7587	APP(AICD)-FOXO3 complex	GO:0005737; GO:0008219; GO:0006979; GO:0005634; GO:0006915	cytoplasm; cell death; response to oxidative stress; nucleus; apoptotic process	70.03; 40.10; 32.01.01; 70.10; 40.10.02	cytoplasm; cell death; oxidative stress response; nucleus; apoptosis (type I programmed cell death)	FOXO3; APP
7588	APP(AICD)-FOXO1 complex	GO:0008219; GO:0005737; GO:0006915	cell death; cytoplasm; apoptotic process	40.10; 70.03; 40.10.02	cell death; cytoplasm; apoptosis (type I programmed cell death)	APP; FOXO1
7589	APP(AICD)-FOXO4 complex	GO:0008219; GO:0005737; GO:0006915	cell death; cytoplasm; apoptotic process	40.10; 70.03; 40.10.02	cell death; cytoplasm; apoptosis (type I programmed cell death)	APP; FOXO4

APPENDIX P (CONTINUE)

Complex ID	Complex Name	GO Identifier	GO Description	FunCat Identifier	FunCat Remarks	Protein match
7590	CASP2(S isoform)-SPTAN1 complex	GO:0043066; GO:1904171	negative regulation of apoptotic process; negative regulation of bleb assembly	40.10.02.01	anti-apoptosis	CASP2; SPTAN1
7591	Del133-p53beta-RHOB complex	GO:0043066	negative regulation of apoptotic process	40.10.02.01	anti-apoptosis	TP53; RHOB
7625	IFI1-IFI2-IFI3 complex	GO:0006915; GO:0005737	apoptotic process; cytoplasm	40.10.02; 70.03	apoptosis (type I programmed cell death); cytoplasm	IFIT3; IFIT2; IFIT1
7879	NLRP3-NLRC4 inflammasome	GO:0042742; GO:0002221; GO:0061702; GO:0045087; GO:0050727; GO:0032731; GO:0042981; GO:0140447	defense response to bacterium; pattern recognition receptor signaling pathway; inflammasome complex; innate immune response; regulation of inflammatory response; positive regulation of interleukin-1 beta production; regulation of apoptotic process; cytokine precursor processing	36.25.16.01	innate immune response (invertebrates and vertebrates)	CASP1; CASP8; NLRP3; NLRC4; PYCARD

APPENDIX P (CONTINUE)

Complex ID	Complex Name	GO Identifier	GO Description	FunCat Identifier	FunCat Remarks	Protein match
7883	MIF-NME1 complex	GO:0042981; GO:0051726	regulation of apoptotic process; regulation of cell cycle	10.03.01	mitotic cell cycle and cell cycle control	MIF; NME1
7884	ANP32A-APEX1-HMG2-NME1-SET complex	GO:0006915; GO:0006304	apoptotic process; DNA modification	40.10.02; 10.01.09	apoptosis (type I programmed cell death); DNA restriction or modification	NME1; HMGB2; APEX1; ANP32A; SET
7892	AIM2 inflammasome (CASP8)	GO:0045087; GO:0005829; GO:0042742; GO:0002221; GO:0061702; GO:0050727; GO:0032731; GO:0042981; GO:1990784; GO:0140447	innate immune response; cytosol; defense response to bacterium; pattern recognition receptor signaling pathway; inflammasome complex; regulation of inflammatory response; positive regulation of interleukin-1 beta production; regulation of apoptotic process; response to dsDNA; cytokine precursor processing	36.25.16.01	innate immune response (invertebrates and vertebrates)	AIM2; CASP8; PYCARD

APPENDIX P (CONTINUE)

Complex ID	Complex Name	GO Identifier	GO Description	FunCat Identifier	FunCat Remarks	Protein match
7957	CASP8-CASP10-FADD-FLIP(S)-RIPK1 complex	GO:0006915	apoptotic process	40.10.02	apoptosis (type I programmed cell death)	CFLAR; FADD; RIPK1; CASP8; CASP10
7990	NPM1-PA2G4 complex	GO:0042981; GO:0042127	regulation of apoptotic process; regulation of cell population proliferation	None	None	NPM1; PA2G4
8000	BAX-BCL2L11-PACS2-TNFRSF10B-TNFSF10 complex	GO:0006915; GO:0005764	apoptotic process; lysosome	40.10.02; 70.25	apoptosis (type I programmed cell death); vacuole or lysosome	TNFRSF10B; BCL2L11; TNFSF10; BAX; PACS2
8006	CTBP1-EP300-FOXO3 complex	GO:0006355; GO:0042981	regulation of DNA-templated transcription; regulation of apoptotic process	11.02.03.04	transcriptional control	FOXO3; EP300; CTBP1
8159	Aposome complex	GO:0006915	apoptotic process	40.10.02	apoptosis (type I programmed cell death)	APAF1; CASP3; CASP7; CASP9
8160	Microaposome complex	GO:0006915	apoptotic process	40.10.02	apoptosis (type I programmed cell death)	CASP3; CASP7

APPENDIX P (CONTINUE)

Complex ID	Complex Name	GO Identifier	GO Description	FunCat Identifier	FunCat Remarks	Protein match
8161	Procaspase 7-APAF1 complex	GO:0006915	apoptotic process	40.10.02	apoptosis (type I programmed cell death)	APAF1; CASP7
8240	BIRC5-XIAP complex	GO:0042981; GO:0010498	regulation of apoptotic process; proteasomal protein catabolic process	None	None	BIRC5; XIAP
8280	AIM2 PANoptosome complex	GO:0061702; GO:0042742; GO:0051607; GO:0045087; GO:0002221; GO:0050727; GO:0042981; GO:1990784	inflammasome complex; defense response to bacterium; defense response to virus; innate immune response; pattern recognition receptor signaling pathway; regulation of inflammatory response; regulation of apoptotic process; response to dsDNA	36.25.16.01	innate immune response (invertebrates and vertebrates)	AIM2; MEFV; CASP1; FADD; RIPK1; CASP8; ZBP1; PYCARD; RIPK3
8281	CASP8-FLIP(L) complex	GO:0006915	apoptotic process	40.10.02	apoptosis (type I programmed cell death)	CFLAR; CASP8

APPENDIX P (CONTINUE)

Complex ID	Complex Name	GO Identifier	GO Description	FunCat Identifier	FunCat Remarks	Protein match
8286	TNFR1-signaling complex I, membrane-bound	GO:0033209; GO:0005886; GO:0051092; GO:0050727; GO:0060548; GO:0043066	tumor necrosis factor-mediated signaling pathway; plasma membrane; positive regulation of NF-kappaB transcription factor activity; regulation of inflammatory response; negative regulation of cell death; negative regulation of apoptotic process	70.02; 40.10.02.01	eukaryotic plasma membrane / membrane attached; anti-apoptosis	TNFRSF1A; TRAF2; BIRC2; RIPK1; TRADD
8288	Pro-death complex II, cytosolic	GO:0006915; GO:0033209; GO:0050727; GO:0005737	apoptotic process; tumor necrosis factor-mediated signaling pathway; regulation of inflammatory response; cytoplasm	40.10.02; 70.03	apoptosis (type I programmed cell death); cytoplasm	TRAF2; FADD; BIRC2; RIPK1; CASP8; TRADD

APPENDIX P (CONTINUE)

Complex ID	Complex Name	GO Identifier	GO Description	FunCat Identifier	FunCat Remarks	Protein match
8294	PANoptosome	GO:0045087; GO:0002221; GO:0051607; GO:0042742; GO:0061702; GO:0050727; GO:0042981; GO:0043067	innate immune response; pattern recognition receptor signaling pathway; defense response to virus; defense response to bacterium; inflammasome complex; regulation of inflammatory response; regulation of apoptotic process; regulation of programmed cell death	36.25.16.01; 40.10.02.04	innate immune response (invertebrates and vertebrates); regulation of apoptosis	FADD; RIPK1; CASP8; NLRP3; ZBP1; PYCARD; RIPK3
8455	EP300-TP53 complex	GO:0010468; GO:0010659	regulation of gene expression; cardiac muscle cell apoptotic process	None	None	TP53; EP300
8611	SUG1-NLRC4- CASP8 complex	GO:0016567; GO:0043065	protein ubiquitination; positive regulation of apoptotic process	14.07.05	modification by ubiquitination, deubiquitination	PSMC5; CASP8; NLRC4

APPENDIX P (CONTINUE)

Complex ID	Complex Name	GO Identifier	GO Description	FunCat Identifier	FunCat Remarks	Protein match
8613	TRAPP III complex	GO:0034976; GO:0006915; GO:0006914	response to endoplasmic reticulum stress; apoptotic process; autophagy	40.10.02	apoptosis (type I programmed cell death)	TRAPPC13; TRAPPC3; TRAPPC6A; TRAPPC2; TRAPPC11; TRAPPC6B; TRAPPC5; TRAPPC12; TRAPPC2L; TRAPPC4; TRAPPC8; TRAPPC1
8622	Apoptosis- and splicing-associated protein complex (SAP18, RNPS1, Acinus-L)	GO:0006915; GO:0006397; GO:0000398; GO:0005634	apoptotic process; mRNA processing; mRNA splicing, via spliceosome; nucleus	40.10.02; 11.04.03; 70.10	apoptosis (type I programmed cell death); mRNA processing (splicing, 5'-, 3'-end processing); nucleus	SAP18; RNPS1; ACIN1

APPENDIX P (CONTINUE)

Complex ID	Complex Name	GO Identifier	GO Description	FunCat Identifier	FunCat Remarks	Protein match
8677	TLR3-associated signaling complex	GO:0045087; GO:0002221; GO:0002224; GO:0034138; GO:0051607; GO:0042981	innate immune response; pattern recognition receptor signaling pathway; toll-like receptor signaling pathway; toll-like receptor 3 signaling pathway; defense response to virus; regulation of apoptotic process	36.25.16.01	innate immune response (invertebrates and vertebrates)	TLR3; CFLAR; CFLAR; FADD; RIPK1; CASP8; TICAM1
8678	TLR3 death-signaling complex	GO:0043331; GO:0034138; GO:0045087; GO:0002221; GO:0002224; GO:0043065; GO:0006952	response to dsRNA; toll-like receptor 3 signaling pathway; innate immune response; pattern recognition receptor signaling pathway; toll-like receptor signaling pathway; positive regulation of apoptotic process; defense response	36.25.16.01	innate immune response (invertebrates and vertebrates)	TLR3; CFLAR; FADD; RIPK1; CASP8; TICAM1; CASP10

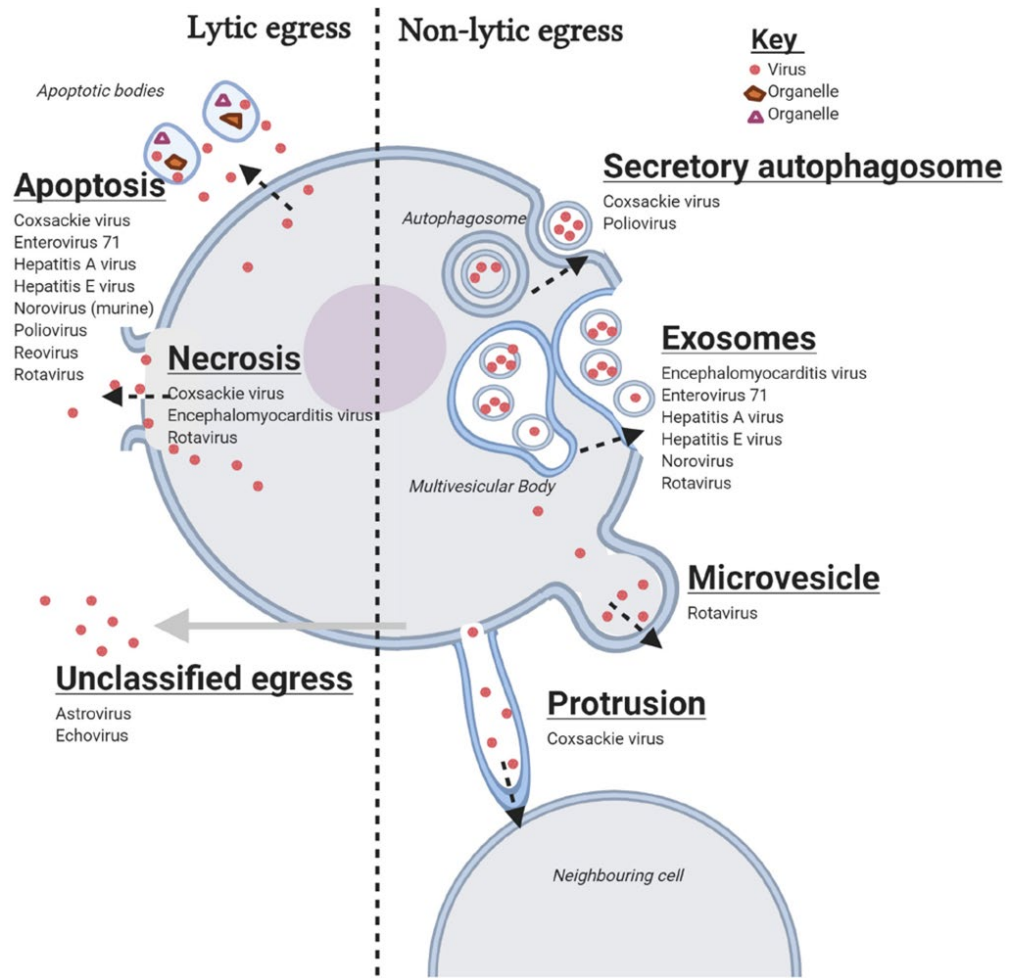
APPENDIX P (CONTINUE)

Complex ID	Complex Name	GO Identifier	GO Description	FunCat Identifier	FunCat Remarks	Protein match
8679	TLR3-DISC complex, atypical	GO:0006915; GO:0002224; GO:0002221; GO:0045087; GO:0051607; GO:0034138	apoptotic process; toll-like receptor signaling pathway; pattern recognition receptor signaling pathway; innate immune response; defense response to virus; toll-like receptor 3 signaling pathway	40.10.02; 36.25.16.01	apoptosis (type I programmed cell death); innate immune response (invertebrates and vertebrates)	TLR3; FADD; RIPK1; CASP8; TICAM1
8730	BAX-HSP90-IRF3-TOMM70 complex	GO:0016032; GO:0005741; GO:0006915; GO:0140374	viral process; mitochondrial outer membrane; apoptotic process; antiviral innate immune response	70.16.01; 40.10.02	mitochondrial outer membrane; apoptosis (type I programmed cell death)	TOMM70; HSP90AA1; BAX; IRF3
8731	BAX-IRF3 complex	GO:0016032; GO:0045087; GO:0006915	viral process; innate immune response; apoptotic process	36.25.16.01; 40.10.02	innate immune response (invertebrates and vertebrates); apoptosis (type I programmed cell death)	BAX; IRF3

APPENDIX P (CONTINUE)

Complex ID	Complex Name	GO Identifier	GO Description	FunCat Identifier	FunCat Remarks	Protein match
8734	HSP90-IRF3-MAVS-TBK1-TOMM70 complex	GO:0005741; GO:0016032; GO:0006915; GO:0140374	mitochondrial outer membrane; viral process; apoptotic process; antiviral innate immune response	70.16.01; 40.10.02	mitochondrial outer membrane; apoptosis (type I programmed cell death)	TOMM70; HSP90AA1; IRF3; MAVS; TBK1
8766	NFKB1-RELA-UXT complex	GO:0005634; GO:0006355; GO:0006915	nucleus; regulation of DNA-templated transcription; apoptotic process	70.10; 11.02.03.04; 40.10.02	nucleus; transcriptional control; apoptosis (type I programmed cell death)	NFKB1; RELA; UXT

APPENDIX Q



Summary of lytic and non-lytic egress utilized by non-enveloped RNA viruses for egress adapted from Owusu et al. (2021).

APPENDIX R

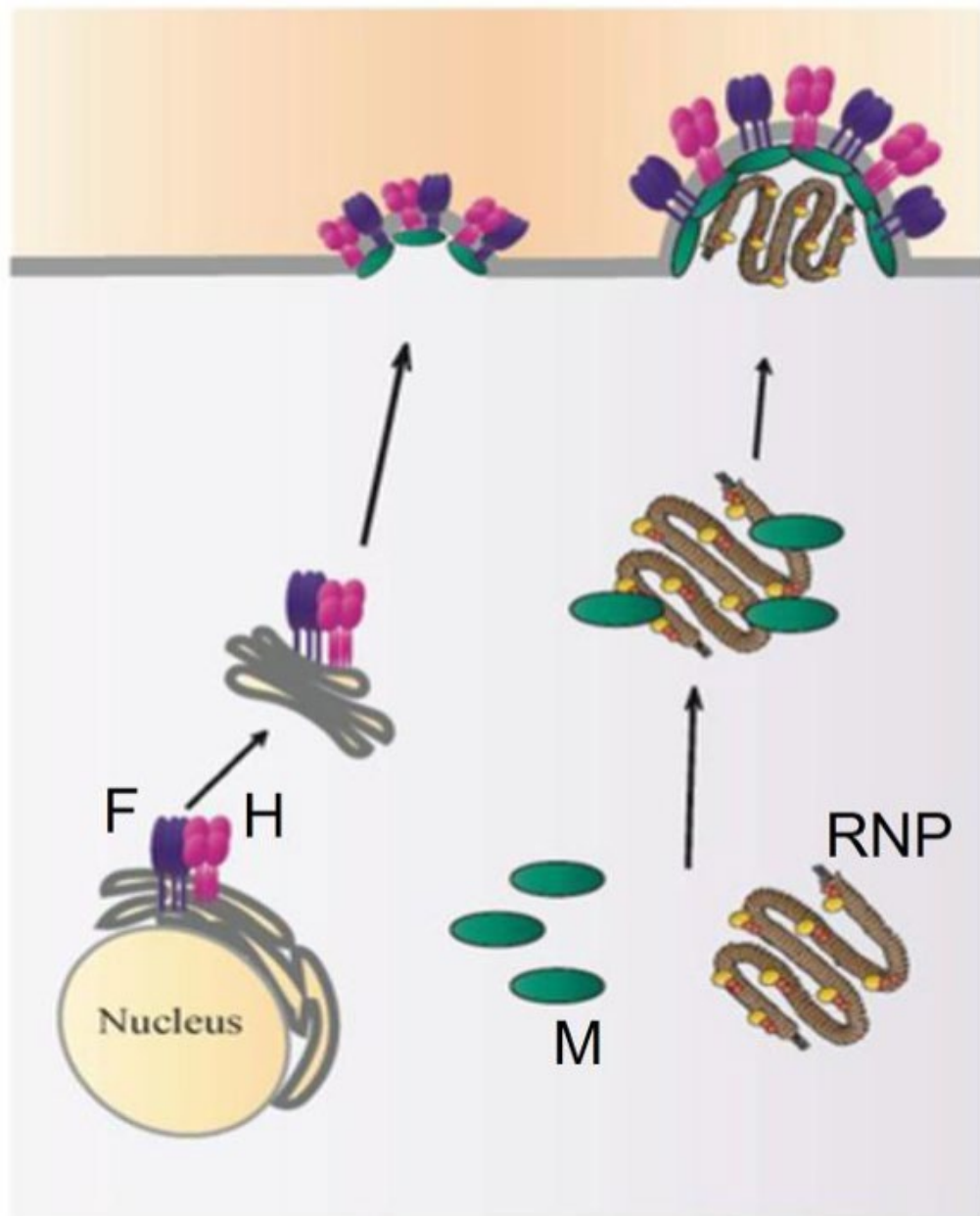


Illustration adapted from Gonçalves Carneiro (2017) summarizing how measles proteins conduct packaging of viral progeny independent of host cell machinery.

APPENDIX S

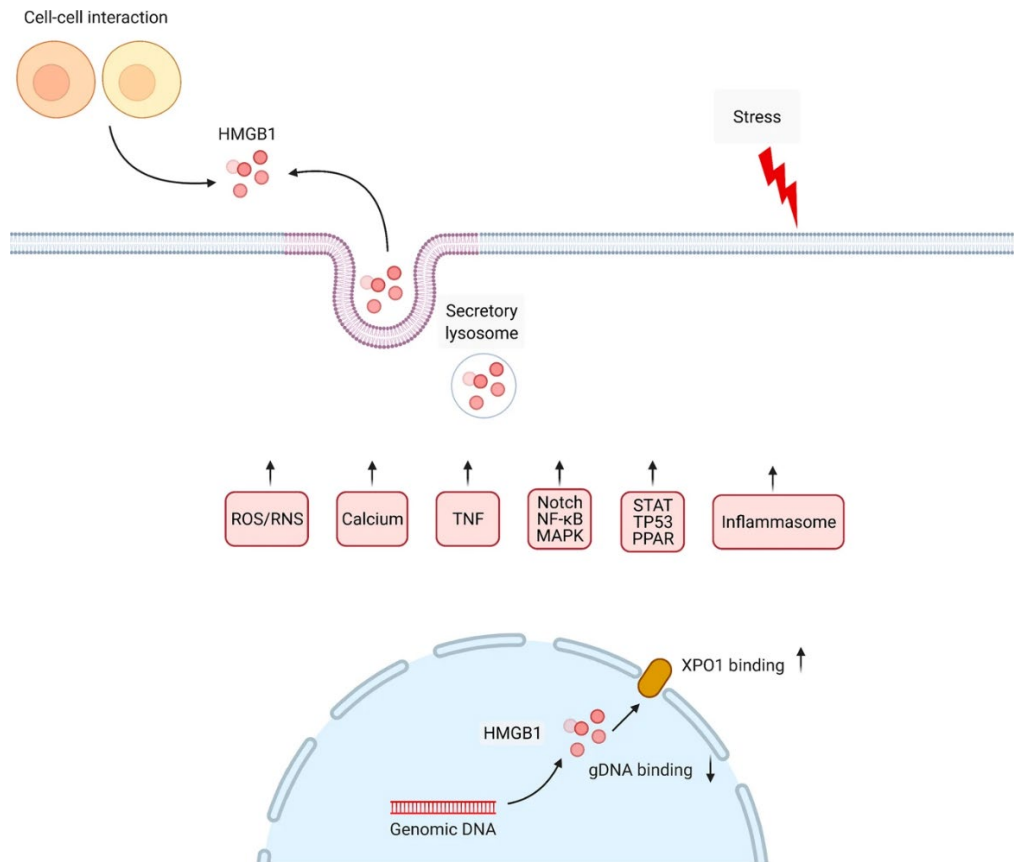
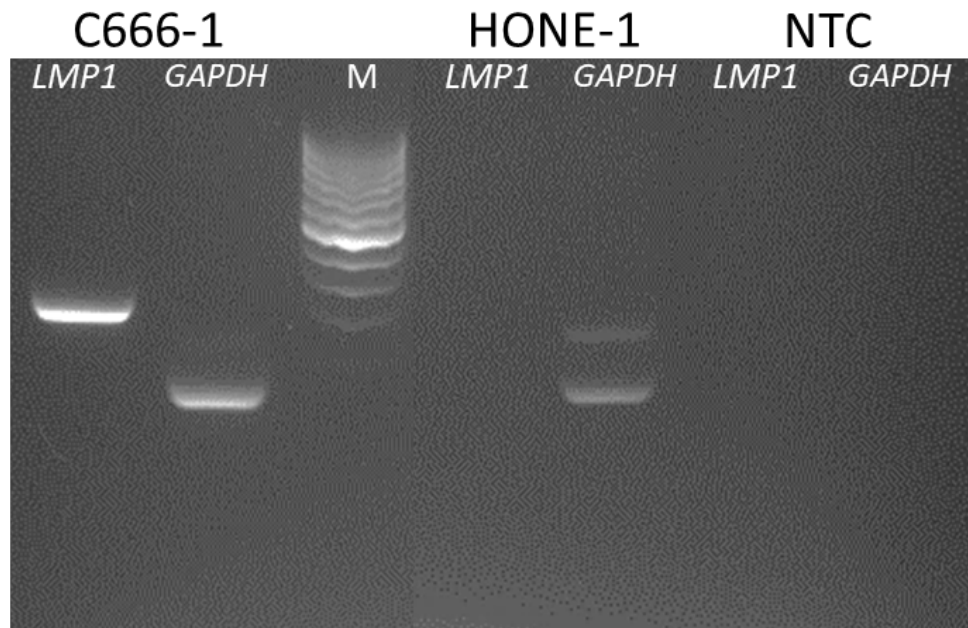


Illustration adapted from Chen et al. (2022) showing several molecular drivers of active HMGB1 release and nuclear-to-cytoplasm translocation of HMGB1 aided by the XPO1 protein.

APPENDIX T



Agarose gel electrophoresis (2 %) image showing C666-1 expresses *LMP1* genome using BN1 (5'-AGCGACTCTGCTGGAAATGAT-3') and BN2 (5'-TGATTAGCTAAGGCATTCCCA-3') primers (Lin et al., 2001). Total PCR cycle: 32, NTC: no template control (water only), M: 1000bp DNA size marker, *GAPDH*: Glyceraldehyde 3-phosphate dehydrogenase gene, PCR master mix and protocol: TopTaq 2x PCR master mix kit (Qiagen N.V., Germany).